UTS UNIVERSITY OF TECHNOLOGY SYDNEY

Carboxymethyl Cellulose and Titania Composites as Adsorbents

by Dinushi Munasingha Mudiyanselage

Thesis submitted in fulfilment of the requirements for the degree of

Doctor of Philosophy

under the supervision of Prof Steven J Langford
Dr Sujeewa De Silva
Dr Francois Malherbe

University of Technology Sydney
Faculty of Science

August, 2023

CERTIFICATE OF ORIGINAL AUTHORSHIP

I, Dinushi Munasingha Mudiyanselage declare that this thesis, is submitted in fulfilment of the requirements for the award of Doctor of Philosophy, in the School of Mathematical and Physical Sciences at the University of Technology Sydney.

This thesis is wholly my own work unless otherwise referenced or acknowledged. In addition, I certify that all information sources and literature used are indicated in the thesis.

This document has not been submitted for qualifications at any other academic institution.

This research is supported by the Australian Government Research Training Program.

Signature: Production Note:
Signature removed prior to publication.

Date: 19/01/2024

ACKNOWLEDGEMENT

I am delighted to extend my gratitude to those who have contributed to the completion of this thesis. First and foremost, I wish to express my heartfelt appreciation to my supervisor, Professor Steven Langford. His invaluable guidance, beginning from the project's commencement to its end, has enabled me to grasp the project's essence. His clear instructions and continuous support not only enriched my project but also extended to understanding the emotional aspects of my time at both Swinburne University of Technology, Hawthorn (SUT) and University of Technology, Sydney (UTS). I am indebted to him for his care since my arrival in a foreign country. Without his motivation, enthusiasm, extensive knowledge, and helping hand, the completion of this project would have been an insurmountable challenge. His constructive feedback during the research process, comprehensive review, constructive criticism, and excellent advice during thesis preparation have inspired me to excel academically.

I extend my heartfelt gratitude to my co-supervisor, Dr. Francois Malherbe, of Swinburne University of Technology, Hawthorn, for guiding my research efforts and generously granting access to their equipment. I would also like to acknowledge the immense support of my co-supervisor, Dr. Sujeewa De Silva, from the University of Technology, Sydney. Her attention, facilitation, consideration of research project needs, and emotional support have been invaluable throughout this journey in an unfamiliar city.

My appreciation extends to my colleagues and group members – Glenn, Mohammed, Salman, Pradnya, Desi, and Lauren – whose support during my research work has been indispensable. A heartfelt thank you to the lab technicians at both SUT and UTS, and all other lab assistants, for their assistance whenever I needed during my lab work. I am also grateful to Dr. Nazrul Islam for facilitating XPS analysis at the University of Wollongong.

I extend my profound gratitude to my parents and brother for their unwavering support throughout this journey. Their encouragement has been the driving force behind my achievements. To my dear friends – Didula, Sudithya, Hasitha, Lakshani, Rasanjana, and Chanaka – your unfaltering support, belief in me during challenging times, and being my family away from home have been invaluable. Without your encouragement and understanding, completing this work would have been an impossible task.

Finally, I extend my regards and blessings to all those who have directly or indirectly supported and assisted me during the completion of this project. I am grateful for the financial support provided by both Swinburne University of Technology and the University of Technology Sydney.

In closing, this journey has been made possible by the collective efforts, guidance, and support of these remarkable individuals and institutions.

August 2023

Dinushi

COVID-19 IMPACT ON THE PROJECT

The unexpected arrival of the COVID-19 pandemic in my second year at Swinburne University of Technology, Hawthorn, introduced a series of challenges that profoundly influenced my PhD journey. The global crisis disrupted not only our daily lives but also the very fabric of academic pursuits, reshaping the way we approached research and learning. The closure of research facilities and laboratories in response to lockdown measures meant that I lost complete access to the lab for an extended period of approximately one year. This interruption was not only frustrating but also significantly hindered the progression of my research. The limited hours granted subsequently as restrictions eased proved insufficient to make up for the lost time, and I encountered unexpected setbacks.

Beyond the research setbacks, the pandemic's impact extended to the very core of my personal life. Being stuck in a compact apartment throughout extended lockdowns, the isolation the isolation took a toll on my mental well-being. The inability to visit my parents for three years weighed heavily on my heart, intensifying the emotional strain of the situation. Moreover, contracting COVID-19 as soon as moving to Sydney, added a new layer of complexity to an already challenging scenario.

The disruptions caused by the pandemic definitely affected my capacity to complete the planned tasks within the expected time. Nonetheless, I take comfort in the unexpected accomplishments that arose despite these challenges. With the unwavering support of my supervisors, I managed to achieve more than I had initially set out to accomplish in this condensed period. As I move forward, I am reminded that while the pandemic may have disrupted my plans, it did not diminish my determination.

ABSTRACT

Water, being an irreplaceable resource and primary source of life and energy on Earth, is under immense stress due to pollution caused by rapid industrialization and urbanization. This has led to an alarming shortage of fresh water for millions of people. Contaminants such as organic pollutants, and pathogens threaten human health and ecosystems. To address this global concern, wastewater treatment methods have gained increasing attention in the 20th century, aiming to remove pollutants and ensure water safety. Conventional water purification methods have limitations in treating diverse pollutants efficiently. Among various techniques, photocatalytic oxidation (PCO) has emerged as an effective and eco-friendly method, utilizing semiconductor photocatalysts like TiO_2 to degrade water pollutants.

This thesis focuses on the synthesis of a multifunctional, environmentally-friendly and cost-effective adsorbent material for wastewater treatment by combining the environmentally friendly biopolymer carboxymethylcellulose (CMC) with TiO_2. Two protocols were used to incorporate TiO_2 into CMC, resulting in stable and processable materials. The first method involved direct incorporation of TiO_2 powder into CMC to create a foam, while the second method utilized in-situ synthesis of TiO_2 on CMC. The prepared composites demonstrated excellent adsorption and photocatalytic activity.

Chapter 2 presents a comprehensive literature review, including the research gap and where this research fits in. Moreover, the chapter highlights the adsorption and photocatalytic mechanisms, as well as the chemical capabilities of the raw materials. Chapter 3 focuses on the synthesis of CMC/TiO_2 foam, with the direct incorporation of TiO_2 powder (P25). The synthesised foam exhibits an excellent stability and degradation efficiency of methylene blue (MB) dye under UV. The chapter ends with identifying a major drawback as the TiO_2 is leaching from the composite.

Chapter 4 presents the successful synthesis of CMC/TiO_2 composites through an *in-situ* TiO_2 synthesis method, aiming to immobilise TiO_2 within the polymer system (CTTIP). The combined sol-gel/hydrothermal method was utilized to improve the efficiency of the synthesis process, resulting in the successful formation of anatase at a relatively low temperature (110°C). Anatase was present in all the synthesized samples, including the synthesized TiO_2 powder. The CTTIP composites and synthesized TiO_2 exhibited a reduced band gap, leading to excellent photocatalytic activity for both cationic (methylene blue) and anionic (methyl

orange) dyes under direct sunlight. Furthermore, the CTTIP composites showed promising potential in degrading phenol. Chapter 5 superficially investigates the degradation of anionic batik dyes under UV light, demonstrating the prepared composites' potential capability to effectively degrade them. The conclusion in Chapter 5 emphasizes the significance of CMC/TiO_2 composites as potent candidates for wastewater treatment. Their exceptional properties, such as low toxicity, environmental friendliness, and cost-effectiveness, make them promising materials for addressing water pollution challenges. We conclude with a brief overview of future work, including how understanding the structure-property relationship, investigating batik wastes, and evaluating antibacterial properties could lead to commercially viable products. Further exploration of heavy metal and ionic solvent removal is planned to expand the composites' applications.

In summary, this thesis presents a novel approach to synthesize environmentally friendly, cost-effective, and versatile CMC/TiO_2 composites for effective wastewater treatment. Continued research in this direction promises to contribute significantly to sustainable water purification solutions.

TABLE OF CONTENT

LIST OF FIGURES

LIST OF TABLES

LIST OF EQUATIONS

LIST OF ABBREVIATION

ATR- FTIR	Attenuated Reflectance Fourier Transform Infrared
BET	Brunauer, Emmett and Teller
BOD	Biochemical oxygen demanding
CB	Conduction band
CFU	Colony forming units
CKT	Carboxymethyl cellulose -potassium bromide – titanium dioxide
CMC	Carboxymethyl cellulose
CO	Carbon monoxide
CO_2	Carbon dioxide
COD	Chemical oxygen demanding
CTTIP	Carboxymethyl cellulose – titanium isopropoxide
CVD	Chemical vapor deposition
DRS	Diffuse reflectance spectroscopy
DS	Degree of substitution
DSC	Dye sensitised solar cells
DSP	Dye sensitise photocatalysis
ED	Electrodialysis
EDX	Energy dispersive X-ray
HEC	Hydroxyethyl cellulose
HOMO	Highest occupied molecular orbital
HPLC	High performance liquid chromatography
HQ	Hydroquinone
LC-MS	Liquid chromatography – mass spectroscopy
LUMO	Lowest unoccupied molecular orbital
MB	Methylene blue
MEUF	Micelle enhanced ultrafiltration
MF	Micro filtration
MO	Molecular orbital
MO	Methyl orange
MOF	Metal organic framework
NF	Nanofiltration
OD	Optical density
PAA	Poly acrylic acid
PC	Photocatalyst
PCO	Photocatalytic oxidation
PEFU	Polymer enhanced ultrafiltration
Ph	Phenol
PVA	Polyvinyl alcohol
PZC	Point of zero charge
Rh B	Rhodamine B
RO	Reverse osmosis
SDS	Sodium dodecyl sulphate

SEM	Scanning electron microscopy
TBO	Titanium butoxide
TBOT	Tetrabutyl titanate
TEO	Titanium ethoxide
TGA	Thermal gravimetric analysis
TTIP	Titanium isopropoxide
UF	Ultra filtration
UV-Vis	Ultra violet – Visible
VB	Valence band
VOC	Volatile organic compounds
WHO	World Health Organisation
XPS	X-ray photoelectron spectroscopy
XRD	X-ray diffraction

CHAPTER 1

INTRODUCTION

1.1 Overview of Water Pollution

Water, the most irreplaceable liquid on the earth, is a primary source of life and energy, yet millions of people are suffering from a lack of access to fresh water. Water coverage of the Earth's surface is about 71% by area and yet there is only about 3% that is fresh water. Out of that 3%, only 0.5% is available to living beings.[1] Due to rapid industrialisation and urbanisation, water pollution has now become a major environmental issue, as it seriously effects both human health and the ecosystem we live in. Fresh water resources are under a huge stress, as everyday these resources are polluted with domestic, agricultural, industrial and natural wastes. As examples for the ways of polluting water, marine dumping,[2] oil leakage,[3] industrial wastage,[4] global warming, deforestation,[5] and rubbish and faecal water dumping,[6] agricultural and livestock farming[7] can be highly considered.[8] These sources release enormous quantities of different types of pollutants such as organic pollutants, heavy metals, fuel, biological effluents, pesticides and pharmaceuticals to water.[9] Different sources have documented diverse classifications of water pollutants. Figure 1.1 shows a categorisation of water pollutants based on the prevailing published data.[10] It is reported that nearly 72 types of chemicals released from textile and dye industries and more than 30 of them are irreversible.[11] As examples, the gold mining in Venezuela has released a high concentration of Hg has been reported in some rivers,[12] in Australia, enormous fish kills were seen in the early 2000's due to low chemical oxygen demand (COD) caused by pollutants in water,[13,14] in Romania a major fish kill had been taken place in January,2000 due to a cyanide leaching and this event is considered as the worst disaster since Chernobyl[15]and in Bangladesh, Arsenic from the Himalaya's provides challenges for potable drinking water from bores.[16]

According to World Health Organization (WHO) records, more than 2 billion people consume polluted water. More than 140 million of people across 50 countries usually drink water with higher arsenic concentration, which is higher than the WHO standard limit (10μg/L).[9] These pollutants can cause striking water borne diseases such as diarrhoea, cholera, polio, typhoid and dysentery. Over 485,000 death are usually recorded due to diarrhoea caused by polluted water. It has also been reported that nearly 70-80% of the diseases caused by polluted water

occur in the developing countries.[17] The problem is only set to get worse as according to the United Nations in 2000, the global water demand is expected to increase by 55% to 2050.[18] This alarming global situation has awakened the urge for the large-scale purification of water.

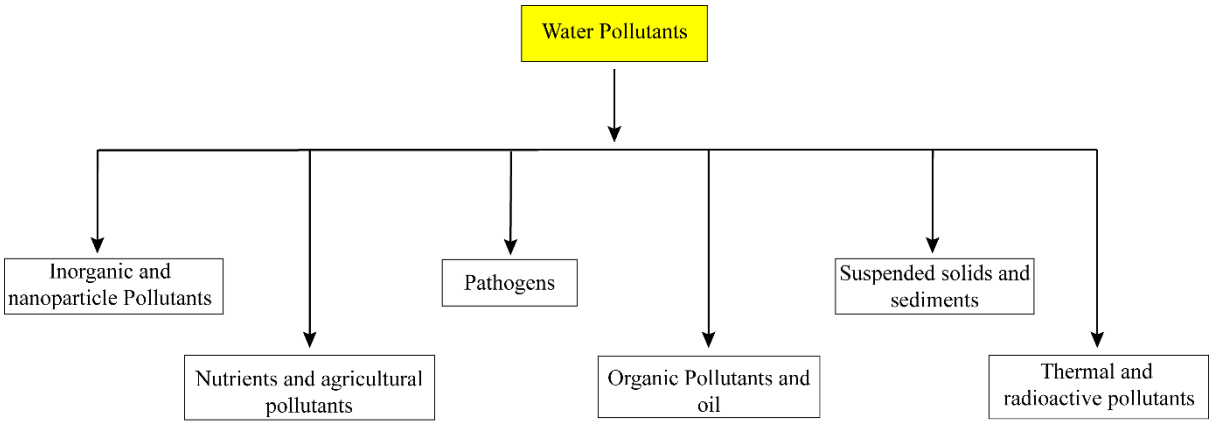

Figure 1.1 Classification of water pollutants.[10]

The very first wastewater treatment plant had been in built in London in mid 1800s, utilizing a combination of all physical, chemical and biological treatment methods.[19] Throughout the 20th century, wastewater treatment methods have become increasingly attractive. Adelaide, Australia is known to have the very first sewerage system in Australia which helped in reducing 40% of deaths in Adelaide due to typhoid, a water-borne disease.[20] A proper treatment for wastewater should completely remove the pollutants in water or minimise those pollutants to a safer limit. Moreover, a wastewater treatment protocol should consider all the technical, economic and environmental aspects.[21]

1.2 Wastewater Treatment Methods

There are number of conventional water purification methods, including filtration, adsorption, photocatalytic oxidation, plasma filtration, ozonisation to name a few under the four main categories of physical, chemical, mechanical and biological treatment methods.[22] The majority of published methods have been designed to target only one pollutant; however, there are a few number of reports that describe techniques capable of removing multiple types of pollutants. For instance, adsorption is suitable for all types of pollutants including organics, inorganics, oil and pathogens.[23] When looking at out day-today water treatment processes, municipal water purification in Australia uses three distinct steps as follows:

1. Primary treatment – This step removes large and suspended solids through screening and sedimentation. Moreover, grit removal is employed to remove small and heavy particles like sand. It can employ a bioremediation approach.
2. Secondary treatment – This step includes a biological treatment method which breaks down the organic matters and the nutrients with the help of microorganisms introduced along with the sludge to the water.
3. Tertiary treatment – This stage is a combination of physical, chemical and/or biological methods to remove remaining impurities and nutrients in the water. Additionally, this step includes disinfection using ultra-violet light or chlorine.[24]

Figure 1.2 shows a visual representation of filtration section, sedimentation tanks and chemical treatment columns implemented at Sydney Water.

Figure 1.2: Visual representation of water treatment implemented at Sydney Water.

Among various water treatment techniques employed across industries and diverse applications, photocatalytic oxidation (PCO) has gained a significant attention as one of the most effective and environmentally friendly methods. Photocatalysis occurs in the case where a semiconductor such as TiO_2 and ZnO (both of which are white powders) are irradiated with UV light. When the photocatalyst is irradiated at 240-360 nm, it can generate highly reactive

radicals such as hydroxyl and superoxide radicals which can react and degrade all types of water pollutants.[25] TiO_2 is a cheap and extensively used photocatalyst due to its promising characteristics such as high photocatalytic ability, low toxicity, chemical inertness, UV shielding properties, semiconducting properties, and antibacterial activity.[26] Titanium dioxide can be found in three main polymorphs - anatase, rutile and brookite. Evonik Aeroxide P25 (Degussa P25) is a type of commercial titania nanoparticle which contains ~85% anatase, ~15% rutile and small amounts of amorphous titania. It has been reported that P25 has the highest photocatalytic activity and also is relatively inexpensive[27], able to be prepared in a variety of forms including as a nanocrystalline powder with high surface area. TiO_2 is generally used in many industries such as paint, dyes, pigments, paper, coatings, adhesives, semiconductor materials, cosmetics and personal care products including suns cream, toothpaste and whitening cream.[28,29,30]

All most all the purification methods are with their own limitations, as they can be expensive, prone to rapid saturation, and may produce potentially harmful by-products (e.g. in ozonisation). Additionally, generation of by-products that serve as secondary pollutants is a common challenge associated with any purification method. However, as reported in the literature, this issue can be effectively controlled or inhibited in PCO by incorporating the appropriate materials, such as noble metals, semiconducting materials, MOFS, and C based materials including polymers.[31,32,33]Also high amount of oxygen has been found to promote the completion of the PCO reaction.[34]

1.3 Materials Used For Wastewater Treatments.

To produce an effective water treatment method, a diverse range of materials have been employed including carbon nanotubes, graphene oxide,[35] metal organic frames (MOFs),[36] synthetic polymers like polyacrylonitrile, polyacryloamides[37] and natural polymers like cellulose,[38] soy protein, gelatin.[39] Most of these materials fulfil the basic properties of a filter material such as high surface area, high adsorption capacity and high porosity, while some of the materials inherit a very limited chemical functionality, causing insufficient interactions with pollutants.[40] Out of these currently used materials for wastewater treatment, natural polymers have emerged as a promising candidate as they are rich in functional groups, highly abundant in the nature, sustainable replacement for synthetic polymers, biodegradable, cost effective, high adsorption capacity, high degree of crystallinity and broad possibility of surface modification.[41] Considering all these factors, this project aims to prepare an **environmentally-**

friendly, inexpensive and **multifunctional** adsorbent material for wastewater treatment with the use of an environmentally friendly biopolymer, carboxymethylcellulose (CMC) and TiO_2. The term 'multifunctional' here refers to the design of a material which is capable of removing different types of water pollutants including dyes, phenols and pathogens, and by combining CMC and TiO_2 to reduce the band gap, enabling it to absorb visible light as a supramolecular effect - an effect different to the sum of the individual properties. CMC is a cellulose derivative with excellent properties; rich in functional groups, biocompatibility, soluble in water, low cost, and non-toxic. As a result, CMC is widely used in food, cosmetic and pharmaceutical industries. Previous data on CMC indicated that it has high adsorption capacity.[42]

Batik, an ancient fabric dyeing process, is widely practiced in Asian countries and results in vibrant and colorful products. However, this technique consumes a substantial amount of water and involves the use of various dyes and chemicals, leading to significant water pollution due to inadequate waste management. The majority of individuals engaged in batik operate home-based businesses, facing challenges related to waste control and lack of support from relevant authorities. Having a background in the batik industry, I have personally witnessed the environmental threats posed by batik waste. As a chemistry researcher, I feel a responsibility and have set a goal to develop an environmentally-friendly, cost-effective, and versatile material to address the issue of batik waste. By doing so, I aim to support the preservation and global spread of this traditional technique in an environmentally-conscious manner. In this thesis, two different protocols have been used to incorporate TiO_2 onto CMC.

1. Direct incorporation of TiO_2 powder to CMC and then make a high surface area foam;
2. *In-situ* synthesis of TiO_2 on CMC.

The photocatalytic properties of the prepared composites have been analysed for wastewater treatment using all cationic, anionic dyes, phenols and batik dyes which are textile dyes common in Asian countries.

There are a couple of questions and hypotheses that have been investigated during this research progress:

1. Can TiO_2 and CMC form a stable and processable material?
2. What are differences between two preparation methods?
3. Can the prepared composites be activated using natural sunlight?
4. Do the prepared composites possess antibacterial properties?

5. Is the prepared composite capable of removing both cationic and anionic textile dyes?
6. What are the by-products attained from the PCO treatment.
7. Cultural preservation through scientific innovation in batik dye removal.

CHAPTER 2

LITERATURE REVIEW

2.1 An Overview of Water Pollution

With the change of dramatic changes in people's lifestyles, rapid increases in both urbanization and industrialization have started affecting nature in a deleterious way. Due to technological development, beginning with the industrial revolution, both human and machine activity has become the major source of water pollution, which is one of the major global concerns leading to an immense risk in human and ecosystem health and also an increase of global water demand.[43] In a world which considers the access to the safe water is a human right, many populous countries are suffering with polluted water. According to the reports by Indian government, about 600 million individuals have been impacted by extreme to high levels of water stress.[44] Pakistan Council of Research in Water Resources has reported that the water quality of 80-90% of the sources is below the required standard. Similarly, China also undergoes the same problem with their natural water resources and 25% of their lakes are full of nutrients and algae leading to a concerning eutrophic issues. Moreover, some rivers in various countries including Indonesia, USA, Brazil and Philippines have been identified as having among the most polluted rivers globally.[45] It can be clearly seen that all the aforementioned nations are highly populated and industrialised and that exhibits an evident acceleration of water pollution.

Natural water resources are subjected to pollution in number of different ways, such as release of industrial waste (heavy metals, toxic chemicals and textile dyes), agricultural runoff, release of domestic waste and natural disasters such as volcanic eruptions. These sources can be categorised based on two main criteria. The first approach is to distinguish them between natural and anthropogenic sources. Volcanic eruptions, flooding and weathering of rocks can be identified as natural sources while agricultural practices, industrial discharges, urban runoff and domestic sewage have been classified under anthropogenic sources which originate from human activities.[9] The second approach involves categorising them into point and non-point sources. Point source pollution is where the source is specific and clearly identified, such as industrial zones, water treatment plants, and municipal discharge pipes. Non-point sources, on the other hand are diffused, scattered and the exact location is really difficult to pinpoint and agricultural discharges and natural causes like flooding can be considered as examples for nonpoint sources.[46]

Irrespective of the type of pollution source, enormous amounts of pollutants are being introduced daily to the water ways escalating the global water pollution crisis with the time. As discussed in Chapter 1, there are many ways to classify the water pollutants, and in here one common classification has been brought up as follow, considering a number of published reports.

1. Organic pollutants – Phenolic compounds, dyes, petroleum, pharmaceuticals. These organic pollutants can be categorised into four groups; polyaromatic hydrocarbons (PAH), polychlorinated dibenzo-p-dioxins (PCDDS), polychlorinated biphenyls (PCB) and γ-hexachlorocyclohexane (γ-HCH).[47]

2. Inorganic and nanoparticle pollutants – heavy metals, trace elements, sulphates, cyanides, mineral acids, inorganic salts, metals and metal complexes. They are incapable of degradation.[48]

3. Nanoparticle pollutants - These have emerged as a new class of water contaminant. Nanoparticles can be categorised in to natural and synthetic nanoparticles. As to the researches carried out, both types of nanoparticles can be found in water resources as the small size of nanoparticles has made them possess a high mobility, easy to aggregate, and high reactivity.[49]

4. Nutrients and agricultural pollutants – This category consists of a broad spectrum of pollutants including nitrates, phosphorous compounds, heavy metals, and organic compounds which are from fertilizers, herbicides and pesticides. They find their own way to water streams through agricultural runoff.[50]

5. Pathogens – Sources like slaughterhouses, biological labs and hospitals contribute to this group with viruses, bacteria and other pathogenic microorganisms.[51]

6. Solids and sediments – Sand and silts.

7. Thermal and radioactive pollutants – Thermal pollutant refers to the discharge of heated water from industrial processes. Radioactive pollutants can originate naturally within the earth crust or anthropogenically through nuclear plants.[52]

Among the aforementioned types of water pollutants, dyes and heavy metals have become the most alarming and critical concerns. When examining real life scenarios, the textile industry

releases nearly 200,000 tons of dyes per year to water streams.[53] It has been reported that in India which is home for 1.3 billion people, 15-135 L of wastewater is generated per person for a day.[44] Moreover, countries like Brazil, India and China which are heavily engaged in agricultural activities have faced a concerning issue with high concentration of glyphosate in water streams.[54] Recent research have been able to determine alarming concentrations of pharmaceutical chemicals such as metoprolol, and anti-inflammatory drugs in rivers and lakes in countries including Mexico, Switzerland, Japan and USA.[55] Furthermore, it has been reported that approximately 40% of the lakes and rivers in the world are being polluted by heavy metals. The annual release of mercury as a result of mining operations is approximately 65-1000 tons.[12]

The presence of these pollutants can increase the oxygen demand in water leading to adverse effects onto the ecosystem. Moreover, they have been identified as the potential causes for striking waterborne diseases like diarrhoea, cholera, polio, typhoid and dysentery. In addition to that, dyes and heavy metals are known carcinogenic contaminants and on the other hand they can create health issues like skin, kidney and liver diseases and also, impairments of human physiological functioning. Continuous intake of high fluoride level, can disrupt the calcium and phosphorous metabolism in the body, leading to a calcium deficiency and skeletal fluorosis.[56] Research findings indicate that diarrhea causes deaths of nearly 300,000 of children under the age of five. Polluted water also accounts for 15-30% of gastrointestinal diseases globally.[2] Therefore, it is necessary to develop effective strategies, materials and technologies to protect and conserve our valuable water resources and to minimise this global crisis.

The literature review in this scientific thesis comprehensively examines contemporary methodologies employed for the removal of water pollutants and the diverse array of materials utilized in such treatment processes. Critical analysis of existing methods underscores their limitations, thereby clarifying the importance of the methods and materials proposed within this thesis to address these gaps and contribute to bridging the identified gaps in water pollutant removal techniques.

2.2 Methods of Water Purification

A wide range of water treatment technologies are currently employed in the industry, while numerous methods are under extensive research. In this section, some of the treatment methods will be discussed in brief.

2.2.1 Membrane Filtration

This pressure-driven process involves a semi-permeable membrane which acts as a physical barrier to segregate impurities and contaminants from water. Membrane filtration can be classified in to four different types based on their pore sizes; ultrafiltration (UF), microfiltration (MF), nanofiltration (NF) and reverse osmosis (RO) as illustrated in Figure 2.1.[57]

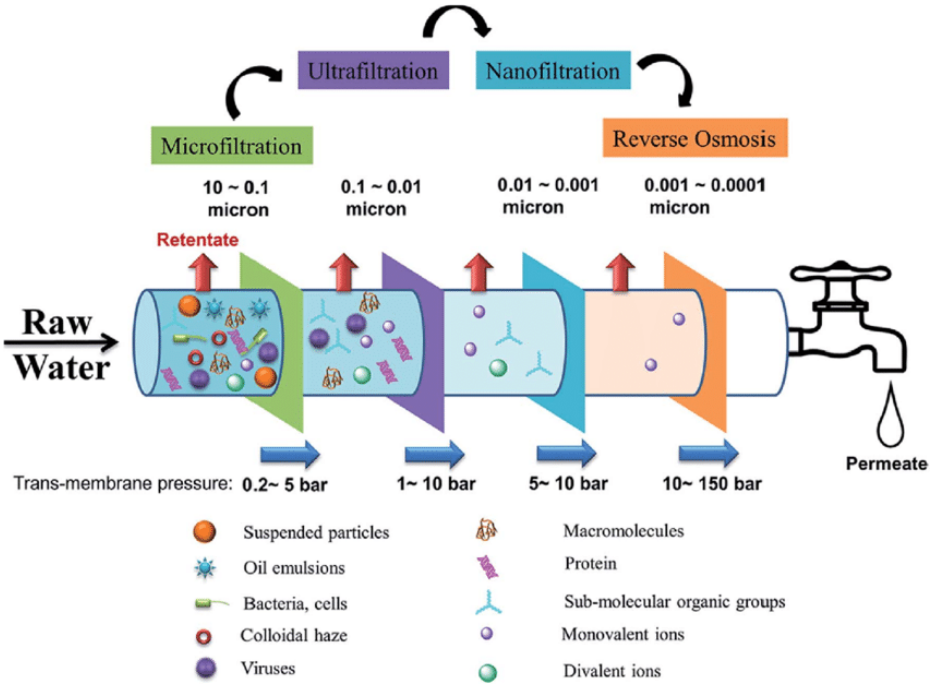

Figure 2.1 A schematic diagram of pressure driven membrane processes and the pore sizes of the membranes used for each process[57]

MF is a pressure driven water purification techniques which uses the membranes with 0.1-10 microns to remove suspended solids and some bacteria in water. UF involves membranes with pore sizes of 0.001-0.1 microns. Two types of techniques could be identified in UFs; first one is micelle enhanced ultrafiltration (MEUF) which uses surfactants to form micelles around the target contaminants, increasing their sizes and that helps in separating the water pollutants. This is effective in removing metal ions, heavy metals and some organic compounds. The other popular techniques under UF is polymer enhanced ultrafiltration (PEUF), which is used primarily for the removal of contaminants like colloidal particles, organic matters and proteins. In this technique, polymers can interact with the contaminants and form larger complexes

which can be easily retained by the membrane. Interestingly, it has been reported that UF has potential in removing some viruses and bacteria in water.[58]

NF has been recognised as a technique with a higher selectivity as it is used a membrane with the pore size of 0.0001-0.001 microns. This is commonly used in removing microorganisms, turbidity, some salts which makes water hard. The final pressure driven UF technique the RO in which water is passed through a membrane with the lowest pore size values (less than 0.001 microns) to segregate salts, ions, some viruses and organic molecules to produce ultrapure water for household drinking water, pharmaceutical and electronic industries.[59]

Electrodialysis (ED) is also considered as a membrane filtration method, developed for desalination. This method utilizes an electric field to pass the ions through a semi-permeable membrane and it is highly used for the removal of dissolved salts and other ionised particles.[8]

Overall, membrane filtration offers several advantages such as simplicity, efficient and rapid technique even at high concentrations, low solid waste generation, produces high-quality-treated effluent, effective for a wide range of real applications, and minimal space required. Contrary, it is important to understand some disadvantages associated with this technique; high energy consumptions, high maintenance and operation costs, limited flow rates and a potential issue of membrane clogging.[60]

2.2.2 Chemical Precipitation

This is a conventional water treatment technique, used to remove metal ions and other ionic constituents in water. In this process a precipitation agent such as hydroxyl ions, iron salts, and aluminium salts are being used to precipitate the metal wastes as to the following chemical equation. Chemical precipitation is always followed by some other water treatment process such as filtration to remove the formed precipitate.

$$M^{n+} + n(OH^-) \longrightarrow M(OH)_n$$

Chemical precipitation presents numerous advantages as it is highly effective in removing metal ions and inorganic contaminants, the process is simple and cost effective, and it is suitable for high pollutant concentrations. However there are some disadvantages to consider such as high chemical consumption, elevated sludge production and requirement of a second method to remove the precipitation, ineffective at a low concentration and low removal of arsenic.[61]

2.2.3 Ion Exchange Method

This is one of the oldest and most effective methods to remove heavy metals from water. In this reversible process, an aqueous ion will be exchanged stoichiometrically to a similar charged ion attached to a solid material added to the water. A synthetic or natural resin with an immobile and insoluble acidic/basic group and a mobile ion is used as the ion carrier. Examples for typical cation and anion exchanges have been given below.

$2NaR + CaCl_2 \rightleftharpoons 2NaCl + CaR_2$ (Cationic exchange)

$2RCl + Na_2SO_4 \rightleftharpoons 2NaCl + R_2SO_4$ (Anionic exchange)

Ion exchanging is highly used in water softening and removing of heavy metals as this simple and rapid method is highly effective even at a low concentration, but a few disadvantages could be identified in this, such as quick saturation, degradation of the matrix, column beads can be blocked with organic materials and particulate matters and a possible issue of reactor clogging.[62]

2.2.4 Ion Flotation

This is a promising technique which uses a synthetic or a natural surfactant with the opposite charges to the target ions in the water. The added surfactants can form a surfactant complex which are being collected at the solution-vapour interface by passing gas bubbles through the solution. Surfactants like sodium oleate, sodium dodecyl sulfate (SDS), and silica nanoparticles are among the most highly used synthetic surfactants or collectors, yet it has been found that bio-surfactants are a more significant alternative to synthetic surfactants.[63] Ion flotation is a simple and rapid process which requires a limited space and it is effective in removing heavy metals and specially to segregate target ions selectively from a mixed solution. However, as the disadvantages of this process, it is important to consider the initial cost and the maintenance and the operation costs.[64] Figure 2.2 illustrates a diagrammatic representation of the setup of an ion flotation column.[65]

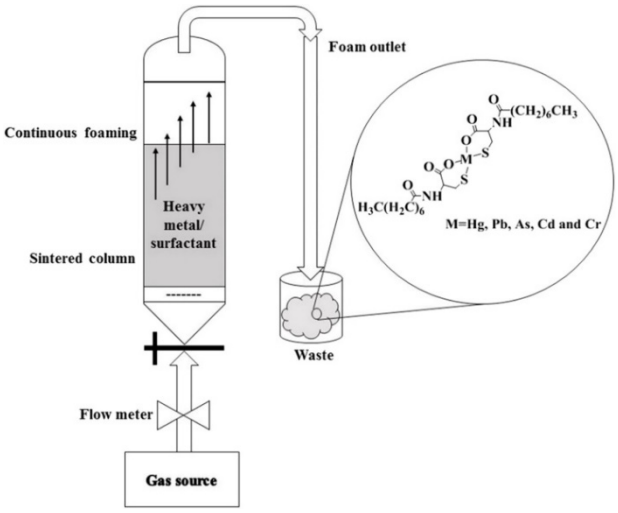

Figure 2.2 Schematic diagram of ion flotation column setup to remove heavy metals using surfactants.[65]

2.2.5 Ozone Oxidation

Since the 1990's, the gas ozone, has been used as a water purification source, especially for degradation of toxic pollutants and disinfection due to its powerful oxidative properties. However, the efficiency of ozonisation is very low, resulting incomplete removal of contaminants and production of harmful secondary pollutants. Ozone oxidation could also produce harmful intermediates such as aldehydes and organic acids which are unable to further react with ozone. [66]. Moreover, the low solubility of ozone in water can elevate the operation cost due to the low efficiency. However, using a catalyst like hydrogen peroxide, carbon-based materials and metal oxides can overcome the above-mentioned drawbacks up to a certain extent. Ozonisation can be used to degrade and remove contaminants such as phenols, dyes, pharmaceuticals and other organic pollutants.[67]

2.2.6 Biological Wastewater Treatment

A centuries old process which uses different types of microorganisms to breakdown and degrade the organic matters. This process can be classified in to two different categories; anaerobic digestion which uses microorganisms in the absence of oxygen and aerobic digestion with both microorganisms and oxygen.

In anaerobic digestion process, a mixture of acidogenic, acetogenic, and methanogenic bacteria are used to break down the monomers in to volatile acids and then the volatile acids in to simple molecules like carbon dioxide, methane, hydrogen and acetic acid via four main steps

hydrolysis, acidogenesis, acetogenesis, and methanogenesis. Nonetheless, anaerobic digestion process is comparatively slow.[68] For aerobic process, a mixture of heterotrophic microorganisms which utilises organic carbon compounds as the carbon source and autotrophic bacteria that uses inorganic carbon (CO_2) as their carbon source. Conventional biological nitrogen removal process utilises nitrification and denitrification via aerobic digestion. Generally, in industrial plants both processes are in use (anaerobic followed by aerobic) due to the high oxygen demand and process time required by aerobic digestion. Moreover, biological wastewater treatment methods can be disadvantageous due to the fact that these processes are able to produce some unwanted microorganisms in the medium, the process can change the physiochemical properties of water and also the cost to create a suitable environment for the process.[69]

2.2.7 Electrochemical Oxidation Method

Among electrochemical-based processes including electrocoagulation, electrochemical membrane filtration, electro-Fenton reaction and to name a few, electrochemical oxidation method is considered as one of the most efficient removal methods, though high energy involving electrons transfer reactions which can be either electrooxidation or electroreduction.[70] This involves two electrodes, serving as an anode and cathode, connected to a power supply in the presence of an energy input and an appropriate supporting electrolyte (Figure 2.3). This setup facilitates the efficient generation of powerful oxidizing species (hydroxyl radical, superoxide radical, etc), which oxidise or reduce the pollutants at the electrodes.[71] The mechanism of electrochemical oxidation can be primarily categorized into direct oxidation and indirect oxidation. Direct oxidation involves the direct transfer of electrons, leading to the oxidation of pollutants at the anode. On the other hand, indirect oxidation involves the creation of active species during the electrolytic reaction, and these species subsequently act upon the pollutants.[72] This process is suitable for the removal of metal ions, as well as to remove complex organic matters via ring opening. In this regard, non-biocompatible organic matters can be converted in to biocompatible organic, and then after a biological process is usually employed to degrade the produced biocompatible organics. However, this method exhibits certain drawbacks that need to be addressed. The primary concern is its high cost, and there is also the possibility of sludge deposition on the electrodes,

which can significantly reduce the electrode's lifespan and result in elevated energy consumption.[62,73]

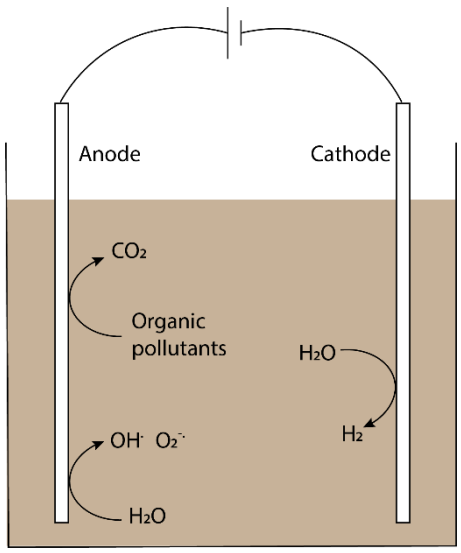

Figure 2.3 Schematic diagram of electrochemical oxidation setup.

2.2.8 Adsorption

Adsorption process have gained a widespread use in wastewater treatment due to its high efficiency, simplicity and cost effectiveness. This is a surface phenomenon in which a particular material (adsorbate) in the form of a solid/liquid or gas gets attached on to a solid (adsorbent) via a physical or a chemical bond. Therefore, adsorption process can be categorised in to two main groups; physisorption and chemisorption. In physisorption, the binding between the adsorbate and the adsorbent is governed by van der Waal's forces where as in chemisorption it is the ionic or covalent bonds. Charged contaminants tend to get adsorbed on to the oppositely charged adsorbents through electrostatic forces while heavy metals, dyes and other organic pollutants exhibit a strong affinity towards surface hydroxyl groups or other functional groups, which facilitate the adsorption.[74]

Adsorption process typically involve three distinct, sequential steps; transportation of the pollutant material to the adsorbent surface from the bulk solution, adsorption on to the solid surface and the transport within the adsorbent material (Figure 2.4). The porosity, pore sizes, the surface area of the adsorbent material and other physical properties of both adsorbent and the adsorbate can control the adsorption of the adsorbate molecules. Moreover, temperature, pH, contact time, concentrations of both adsorbates and adsorbents and presence of other pollutants can affect the adsorption process.[75] In many instances, adsorption is a reversible

process followed by desorption where adsorbate molecules detach from the adsorbent surface, which makes an adsorbent to be regenerated and reused multiple times. This characteristic makes adsorption, a cost-effective method.[76]

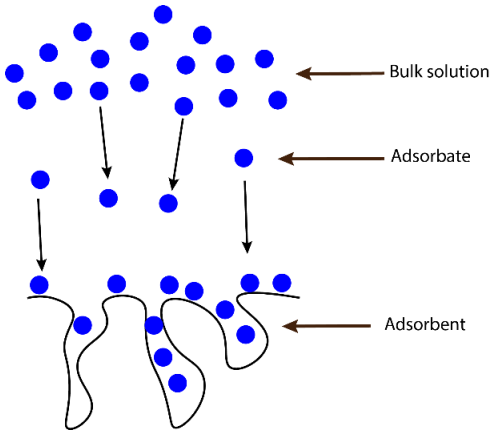

Figure 2.4 Major steps of an adsorption mechanism.

To evaluate the interactions between the adsorbate and adsorbent at equilibrium at a constant temperature, a set of mathematical formula; isotherms have been defined such as Freundlich, Langmuir, Temkin, Sips, Flory-Huggins, and others.[77] There are two mainly used isotherms; the Langmuir isotherm, which describes the monolayer adsorption and the Freundlich isotherm, which is based on multi-layer adsorption as depicted in Figure 2.5. By analysing the data obtained from these models, the adsorption mechanism can be determined.[78] Moreover, intra-particle diffusion mechanism is used to understand the adsorption process, investigating the diffusion and mass transfer steps. In adsorption, adsorbent material plays a major role. Materials with high surface and/or with high functional groups/active sites are generally used as adsorbents to retain contaminants on the surface. The most commonly used conventional adsorbent materials are activated carbon, zeolites, silica gel, activated alumina, mineral clay, and some polymers such as chitosan, cellulose, and polyaniline.[79]

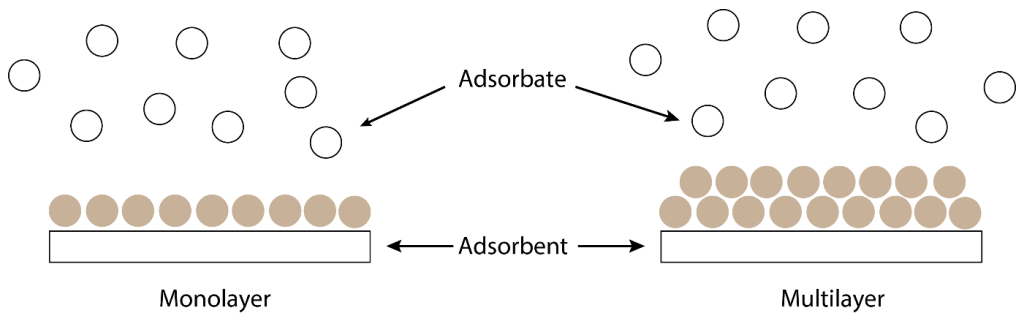

Figure 2.5 A schematic diagram representing monolayer and multilayer adsorption.

Furthermore, not only for the wastewater treatments, but this method has also been identified as one of the best methods to remove general indoor VOC pollutants and toxic gases. As an example, activated carbon has been used for indoor heating, ventilation and air-conditioning systems.[80] But same material in 'filtration', means the adsorption can saturate quickly and then the adsorbent becomes a place for harmful pathogens to grow. The adsorbents need to be replaced frequently as a result. Also, not all pollutants are adsorbed and adsorbed VOC can generate secondary pollutants by reacting with ozone.[22, 81]

2.2.9 Photocatalytic Oxidation

Photocatalytic oxidation (PCO) has become one of the promising water treatment technologies due to its ability to completely decompose a wide variety of water pollutants. Moreover, this process has gained a huge attraction of the research world as it is being simple, identified as a green and environmentally-friendly procedure, no formation of sludge, no or less formation of by-products and being able to perform at room temperature.[25] PCO encompasses a semiconductor like TiO_2, ZnO, CdS and ZnS and a light source producing free radicals which can break down and degrade toxic pollutants and pathogens in water.[82] The mechanism of PCO could be explained as below.

This mechanism operates through a series of oxidative and reductive reactions taking place on the surface of the photocatalyst (PC). Semiconductors consist of highest occupied molecular orbital (HOMO) which is equivalent to the valence band in MO theory and lowest unoccupied molecular orbital (LUMO) which is the conduction band. The energy gap between these two orbitals is known as the band gap. Upon irradiating the semiconductor/catalyst with light, the catalyst can absorb photons with energy similar to or higher than that of band gap which will facilitate electrons to excite from the valence band to the conduction band, creating holes on the valence band and electrons on the conduction band. Subsequently, the formed electron-hole pairs will migrate to the catalyst surface, engaging in variety of oxidation-reduction reactions as shown below. Photogenerated holes will oxidise water to form hydroxyl radicals as in the given reactions, while electrons reduce the oxygen molecules, yielding superoxide radicals. Due to the high oxidizable nature of these radicals, they can react with pollutants and mineralise the organic pollutants, degrade other toxic contaminants and kill pathogens in water (Figure 2.6).[83]

$$PC + h\mu \longrightarrow e^- + h^+$$

$$e^- + O_2 \longrightarrow {}^{\cdot}O_2^-$$

$${}^{\cdot}O_2^- + H^+ \longrightarrow {}^{\cdot}OOH$$

$$2\ {}^{\cdot}OOH \longrightarrow O_2 + H_2O_2$$

$$H_2O_2 + {}^{\cdot}O_2^- \longrightarrow OH^- + {}^{\cdot}OH + O_2$$

$$H_2O_2 + h\mu \longrightarrow 2\ {}^{\cdot}OH$$

$$h^+ + H_2O \longrightarrow {}^{\cdot}OH + H^+$$

$$h^+ + OH^- \longrightarrow {}^{\cdot}OH$$

$$\text{Pollutants} + ({}^{\cdot}OH/\ e^-/\ h^+/\ {}^{\cdot}OOH/\ {}^{\cdot}O_2^-) \longrightarrow \text{degradation products}$$

During this process, the highly reactive electron-hole pairs with a short lifetime can undergo recombination, impeding the efficiency of photocatalytic rate.[84] However, this issue can be addressed by implementing necessary protocols such as incorporating a suitable material to the photocatalyst and this will be further discussed in subsequent sections of this chapter.

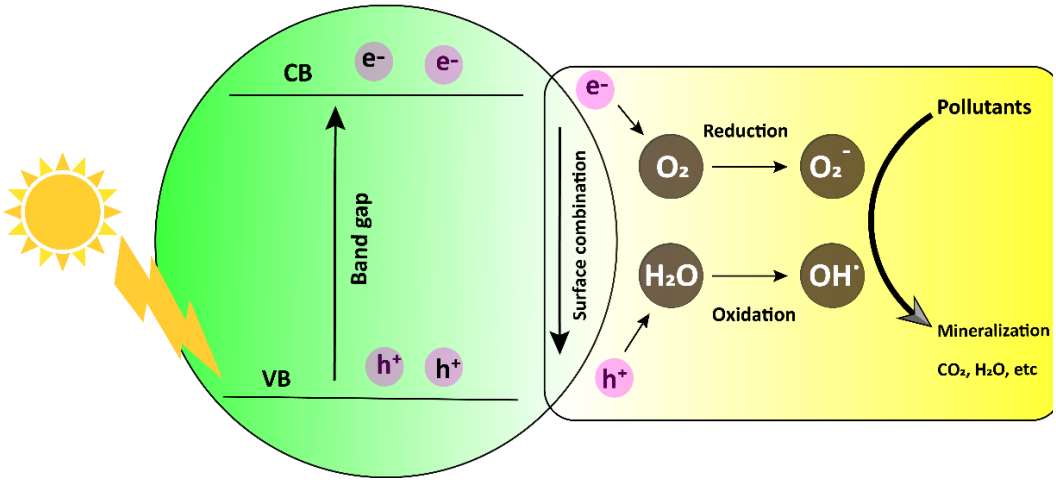

Figure 2.6 General mechanism of removing air pollutants using PCO.

2.2.10 Combined Systems

In order to address the issues with a wide variety of pollutants, researches have been developing combined systems to enhance the removal efficiency.[85] Several of these systems include plasma-catalytic hybrid systems, biological process-photocatalytic oxidation hybrid systems, adsorption-photocatalysis hybrid systems and biological process-adsorption hybrid systems.

Among these, adsorption-photocatalysis hybrid systems have emerged as one of the most efficient systems as this coupling can enhance the physiochemical properties of the combined system, boosting the pollutant removal efficiency. [86] In this scenario, the adsorbent can retain pollutants on the surface while the photocatalyst can degrade the pollutants. Table 2.1 provides a summary of various hybrid systems reported in the literature.

2.3 Adsorbent Materials

In numerous separation processes, the effectiveness of separation mainly relies on the presence of a mass separating agent which is commonly known as an adsorbent. Adsorption is recognised as one of the most effective separation methods in wastewater treatment. Therefore, the quality of the adsorbent directly affects the performance of the adsorption process. In this regard, the initial and the most crucial step is towards an efficient adsorption is to explore and identify the most suitable adsorbent which possesses a high selectivity, adsorption capacity, and functional groups.[87]

Table 2.1 Examples of hybrid systems and their target pollutant applications

Hybrid system used	**Targeted pollutants**
Plasma-catalytic hybrid system	Phenol[88], Oxytetracycline[89],
Photocatalytic-biological process hybrid system	2,4-dinitrotoluene[90], Phenol[91], Reactive Black 5 and Reactive Yellow 86[92], C16 alkane[93]
Ultrasound-adsorption-membrane ultrafiltration hybrid system	Diclofenac, Carbamazepine, Amoxicillin[94]
Bio-ozone hybrid system	Pharmaceuticals stock solution consists of caffeine, carbamazepine, diclofenac, gemfibrozil, ibuprofen, metoprolol, naproxen, sulfamethoxazole and trimethoprim[95]
Electro-coagulation-forward osmosis hybrid system	Oil[96]
Electrochemical-photocatalytic hybrid system	Eriochrome Black T dye[97]
Electrocoagulation-photocatalytic hybrid system	Petrolium[98]
Bio-electrochemical hybrid system	Congo red[99], Reduction of Nitrobenzene to Aniline[100], Methyl orange[101]
Adsorptive photocatalytic hybrid system	Methylene Blue[102,103], Pathogens,[104] Tetracycline[105,106], Crystal violet[107], Methyl orange[108]

When selecting an adsorbent material, it is essential to have a comprehensive knowledge of its chemical structure and properties of the material, types of the pollutants to be targeted and as well as the potential mechanism involved. Moreover, there are other important properties of an adsorbent to be considered. [109]

1. Environmentally friendliness,
2. Cost effectiveness,
3. Being readily available,
4. Being able to withstand in critical conditions (higher humidity, higher temperature),
5. Limited degradability, and
6. Absence of any health effects or discomforts.

Taking above mentioned properties into account, a number of materials have been introduced as adsorbents for wastewater treatment - polymeric substances, carbon-based materials, metal oxides, nanomaterials and metal organic frameworks (MOFs) as some examples.[110] Table 2.2 Examples for common adsorbent materials and their properties Table 2.2 provides a list of examples of adsorbent materials and their respective properties.

Table 2.2 Examples for common adsorbent materials and their properties

Adsorbent material	**Properties**	**References**
Carbon nanotubes	High surface area, adsorption capacity, tensile strength, hydrophobicity-excellent candidate for humid environment, easy to modify.	[111,112,113]
Graphene oxide	Rich oxygen containing groups, high surface area, low density. Able to form strong interactions with polar substances, being a versatile material, owning fast kinetics	[114,115,116]
Activated carbon	High surface area, porosity, adsorption capacity, easy to synthesise from abundant carbonaceous sources like wood, coal, and various agricultural wastes	[117,118]

Metal-organic frameworks (MOF's)	Having a highly porous structure, high thermal and chemical stability, rich in functional groups, easy to fabricate.	[119,120,121]
Synthetic polymers (eg: polyacrylonitrile, polyacrylamide, polyvinylacetate)	stable chemical and thermal properties, controllable fluid properties, long durability, easy to fabricate, rich in functional groups.	[122,123]
Natural polymers (eg: cellulose, chitosan, gelatin, soy protein etc)	Rich in functional groups, highly abundant in the nature, sustainable replacement for synthetic polymers, biodegradable, cost effective, high adsorption capacity, high degree of crystallinity and broad possibility of surface modification.	[124,125]

Most industrial water adsorbents are made of low environmental-friendly, chemically synthesised or petroleum-based materials[110, 126] In addition to that some materials require a high temperature, energy and pre-treatments steps to synthesize which elevates the cost of the process along with the price of the adsorbents. Some synthetic processes cause serious safety issues.[124] Therefore, new approaches that help develop new materials to overcome these limitations are desirable to the industry. On the other hand, recent research has proven that natural adsorbents including polymers have become a prominent alternative to synthesised adsorbents.[40, 127]

Nowadays, several natural polymers including cellulose, chitosan,[128] gelatin,[129] starch, alginate to name a few are being used as adsorbents.. Even if cellulose is the most abundant natural polymer, it faces challenges due to its limited water solubility and low adsorption capacity. Therefore, recent researches have been more focused on enhancing the properties of cellulose by introducing diverse functional groups like carboxyl groups, amine groups and amide groups to it and incorporating various materials.[130] But some processes employed for this can leave unreacted monomers and initiators which are toxic in the system. Therefore, synthesis of CMC has gained a significant attention as it is easy and cost effective.[131]

2.3.1 Carboxymethyl Cellulose

Cellulose is a macromolecule with linked anhydroglucose units by β-1,4-glycosidic bonds.[132] When cellulose is converted to CMC, free hydroxyl groups are completely or partially substituted by carboxymethyl groups, represented by OR in Figure 2.7. This replacement leads to loss the possibility of having a sheet like structure in CMC because of steric and electrostatic interactions. However, CMC, being a cellulose derivative, contains the properties of its main structure such as, orientation of the bigger constituent groups in the equatorial plane, rigidity of glucose units and impossible to rotate about C−O−C bond.[133]

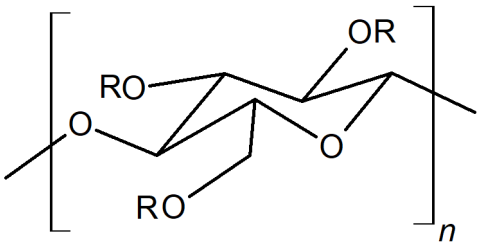

Figure 2.7 CMC monomer (R stands for −H for cellulose; R = $-CH_2CO_2Na$ for CMC).

Carboxymethylation is one of the simplest and most attractive ways of modifying polysaccharides as the final products will have numerous promising properties, including being a polyelectrolyte. Carboxymethylation is usually achieved via a Williamson ether synthesis with the use of aqueous alkali hydroxide (mostly NaOH) for the alkali cellulose treatment as the first step and monochloroacetic acid or its sodium salt for esterification step which is the second step as illustrated in Figure 2.8.[42] CMC was initially synthesised in 1918, and was synthesised commercially for the first time in 1935 at IG Farbenindustrie AG in Germany.[42, 134] CMC can be synthesised from many plant materials, bacteria that produce cellulose and many waste materials. For example, synthesised CMC using sago waste produced from the oil palm industry in SE Asia,[135] while Haleem *et. al* have used cotton gin waste to produce CMC.[136] Moreover, materials like alpha-cellulose, cavendish banana pseudo stem, Boaobab fruit shell and rice stubble have been reported as raw materials for synthesising CMC.[137, 138]

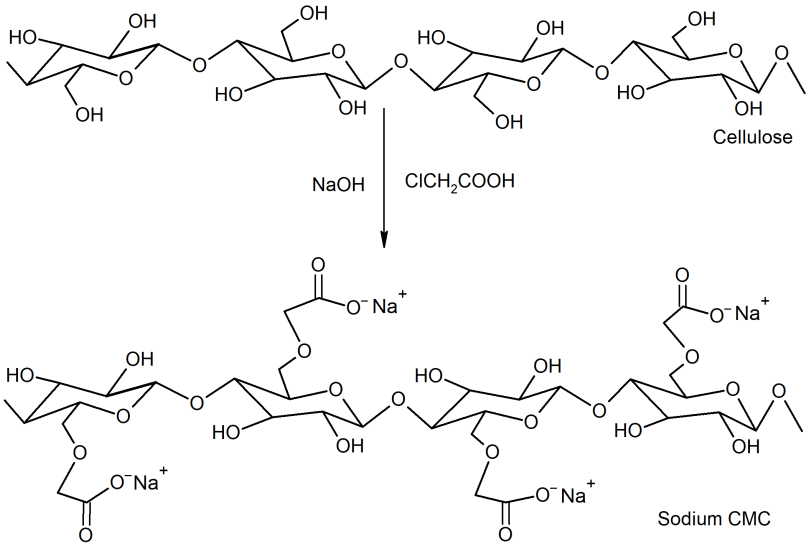

Figure 2.8 Conversion of cellulose in to sodium CMC.

The amount of substitution is defined by the term 'Degree of Substitution' (DS). DS represents the average number of hydroxyls that have been replaced per monomer unit. The range of DS values typically varies from 0-3. For instance, when all free hydroxyl groups are substituted, the DS reaches its maximum, three.[139] However, it has been found that DS usually doesn't usually exceed two because the CH_2COOH groups distribute randomly along the polymer chain and as the substitution increases steric hinderance starts to play a dominant role in shaping the structure. The DS is making CMC available in a range of molecular weight spanning from 90,000 to 200,000 g/mol. The degree of uniformity of the derivatisation is one of the main important facts that explains the behaviour of CMC in solution. Therefore, this non-uniformity of the distribution of $-CH_2COOH$ groups causes CMC to have a thixotropic behaviour in solution.[140] When DS $\leq$ 0.3, CMC is not water soluble and alkaline solutions can be used as solvent. When DS is from 0.3- 0.6, CMC is partially soluble in water and DS from 0.7-1.0, completely soluble in water. That indicates, higher carboxymethyl groups substituted, higher the solubility in water, lower the viscosity.[141] Wang *et al*. have identified that CMC has a helical structure in both bulk and water through simulation studies and in water that helical structure is more stretched (Figure 2.9).[142]

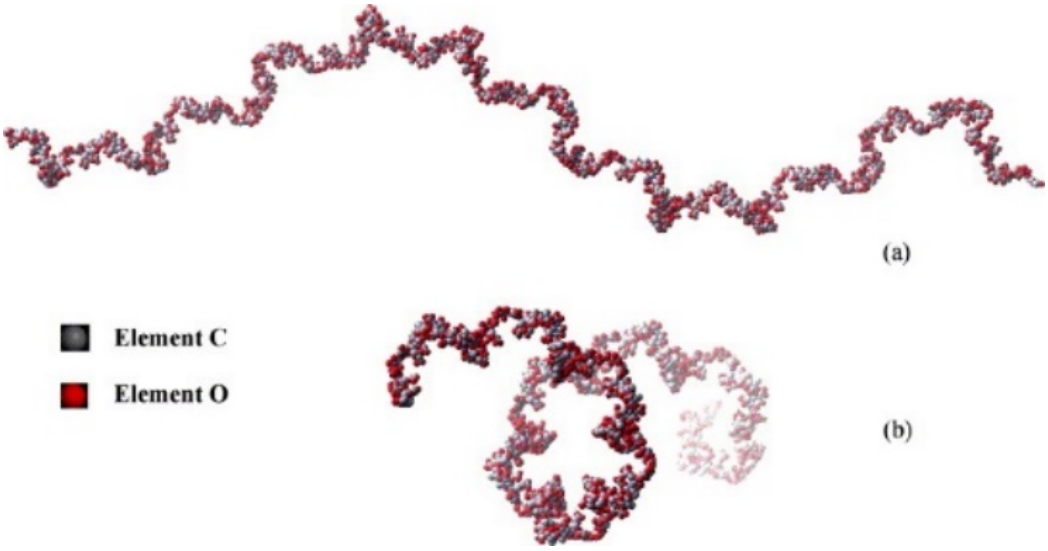

Figure 2.9 Computer simulated structure of CMC in aqueous environment (a) latitudinal view (b) longitudinal view of CMC molecule in aqueous solution.

The solubility of CMC is also influenced by its nature as a polyelectrolyte including its characteristics such as, the charge density and the electric properties. Moreover, the properties of CMC depend on other various factors like average chain length, molecular weight, degree of substitution and concentration of counter ions etc.[134] Majority of the commercial CMC is in the form of sodium salt and its general chemical formula is as given below:

$$[C_6H_7O(OH)_x(OCH_2COOH)_y]_n$$

Where: 'x' is the number of remaining free hydroxyl groups

'y' is the degree of substitution

'n' is the degree of polymerization

As each glucose monomer contains three free OH groups available, (x+y) = 3.[134]

2.3.1.1 Applications of CMC

CMC possess salient properties of: (i) biocompatibility; (ii) non-toxicity; (iii) biodegradability; (iv) hydrophilic properties; (v) low cost; (vi) renewable/recyclable; (vii) protection for proteins exposed to acids and heat;[143] (viii) film forming properties; (ix) high efficiency with a low dosage; (x) ability to form gels with metal cations; (xi) easy to synthesise; (xii) rich in functional groups; (xiii) tuneable hydrophilicity and many more.[144,145] These versatile

properties have made CMC a promising candidate in many applications such as drug delivery, paper industry, as an adhesive/binder, detergent, paint industry, textile industry and particularly the food industry.[146] The applications of CMC mainly depend on the factors such as purity, degree of substitution, degree of polymerisation and uniformity as these factors significantly effect on the properties of end products. Different types of CMC are generally distinguished in to three main categories; food grade, pharmaceutical grade and industrial grade based on their purity levels and degree of substitution.[147]

In the food industry, CMC is used as an auxiliary agent in various food products such as pet foods, protein foods, beverages, frozen desserts and syrups due to its excellent properties including tasteless, noncaloric, odourless and physiologically inert which are important factors to consider in food industry.[148] The cosmetics industry is using CMC as a rheological modifier in shampoo and conditioners, an emulsifier in lotions facial masks, a delivery matrix if suns cream and a denature adhesive for denaturing treatments in dental cases.[147] Moreover, its lower susceptibility towards microbial contaminations compared to other polymeric gelling agents means CMC has a long shelf life, which is an important property to develop self-care formulations.[149]

CMC plays a vital role in drug delivery in pharmaceutical industry, especially for slow-releasing drugs.[150] It has been recognised as a highly reliable carrier for anti-cancer chemotherapy drugs. Not only that, CMC is used in ointments, syrups, tablet binders and wound dressing.[134] Additionally, CMC is a potential candidate in 3D bioprinting in tissue engineering.[141] Another important application of CMC is wastewater treatment which will be discussed later in this Chapter.

Despite the above-mentioned advantageous properties of CMC, there are certain drawbacks to consider. For instance, the hygroscopic nature of CMC results in reducing the mechanical strength, biostability and shelf life. Furthermore, CMC shows a low adsorption capacity. To overcome these drawbacks, researches have explored several physical and chemical modifications including incorporating suitable materials in to CMC. Table 2.3 provides examples of modifications of CMC by grafting other chemicals.

Table 2.3 Examples for modification of CMC and their properties and applications.

Modification	**Properties**	**Applications**
Graphene oxide	Strong ability to adsorb metal ions, can be used as a catalyst, high adsorption capacity, high reusability, biodegradability, cost effective	Removal of metal ions, heavy metals, organic liquids, dyes and developing of memory devices [151,130,152,153]
ZnO	Formation of a hydrogel, high swelling rate, good antibacterial properties,	Drug delivery, wound dressing, Fruit storage [146,154]
Carbon nanotubes	Formation of an aerogel, high mechanical properties, high adsorption capacity	Removal of oil, electronical applications [155,156]
Epichlorohydrin crosslinked	High adsorption properties	Dye removal [157]
Sodium alginate	Barrier properties against UV light, effective antibacterial properties, high mechanical strength	Cosmetics and pharmaceutical applications [158]
CuO	High surface area, better photocatalytic and antimicrobial activity, high reusability	Wastewater treatment [159]
Silk fibroin/ graphene oxide	High thermal stability, cost effective	Packaging industry [160]
MOF-5	High adsorption capacity and reusability	Removal of Lead[161]
Polyethylene glycol	Biocompatibility, wound healing efficacy	Wound dressing [162]
Dextran sulfate	High adsorption capacity, reusable, eco-friendly	Removal of MB [163]
Polyethylene glycol/ montmorillonite clay	High thermal stability, adsorption properties	Wastewater treatment and pharmaceutical industry[164]

In addition to above mentioned materials, and critical to this thesis, TiO_2 is another candidate that can be incorporated to enhance the properties of CMC. However, as to our knowledge limited research has been conducted specifically on the composites of CMC and TiO_2. Since this project focuses solely on developing composite using CMC and TiO_2 only, the structure and properties of TiO_2 will be discussed in the coming subsections.

2.4 TiO_2

With the discovery of titanium dioxide in 1791 by William Gregor in the black magnetic sand found in Cornwall and the isolation of the titanium oxide from the rutile mineral in 1795 by M.H. Klaproth in Hungary, TiO_2 has become the most studied metal oxide semiconductor and photocatalyst.[165] This metal oxide naturally exists in three main polymorphs, identified as anatase, rutile and brookite which are based on their crystalline arrangements (Figure 2.10).[166] Both anatase and rutile show tetragonal crystal forms while brookite owns a rhombohedral crystal form. All these forms of TiO_2 have been made up of distorted TiO_6 octahedral building blocks in which Ti^{4+} is surrounded by 6 oxygen atoms, therefore, Ti-O bond plays a vital role in the properties of different TiO_2 forms. The formation of anatase takes place via sharing of corners of TiO_6 octahedral unit, while rutile is formed through sharing of edges and in brookite, both edges and corners are shared.[167]

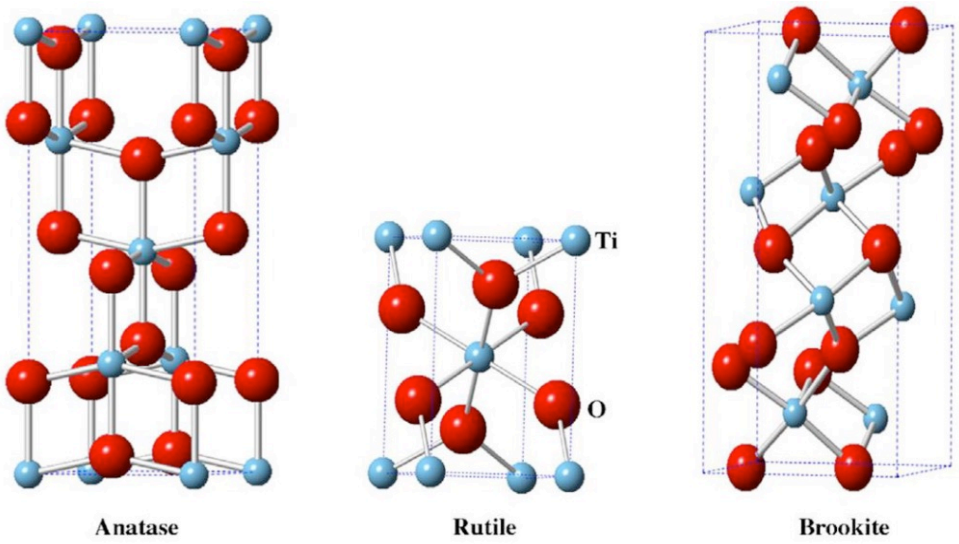

Figure 2.10 Crystal structures of the polymorphs of TiO_2.[168]

Of the polymorphs of TiO_2, rutile is the thermodynamically most stable and naturally abundant polymorph while the other two are metastable and readily transform to the rutile form upon heating. However, in the nanoscale range, anatase and brookite are more stable due to the low surface area and transformation to rutile is possible only after reaching a certain 'nano-size'.[26, 169,170] Anatase is the most active polymorph in both photocatalysis and photoelectrochemical studies. The main reason behind this can likely be attributed to the higher fermi levels of anatase compared to rutile. Anatase shows a very low electron-hole recombination due to having an indirect band gap and high concentration of oxygen vacancies compared to other two

polymorphs.[171] Moreover, the surface area of anatase is higher than rutile, creating more active sites on nanocrystals, and also the larger band gap of anatase makes its redox capability a slightly higher than that of rutile.[172]

Evonik Aeroxide P25 (Degussa P25) is a type of commercial titania nanoparticle which is synthesized through a pyrolysis process using $TiCl_4$. Aeroxide was first synthesized in early 1980's and it is a multiphasic nanostructured titania which contains 80-90% of anatase, small amount of rutile and some amorphous titania. Aeroxide is widely used as a photocatalyst, catalyst supporter and a heat stabilizer due to its unique properties such as high quantum efficiency and photocatalytic activity, high chemical purity, relatively broad light absorption, low aggregation and excellent dispersion especially in liquid media.[173, 174] Based on experimental analysis, many structures have been proposed for Degussa p25 (Figure 2.11). The first image box (A) in Figure 2.7 shows that according to the results from transition electron microscopy (TEM) anatase and rutile remain separated without forming a heterojunction between them. However, as in the second image box (B), some researchers have observed mixed particles, in the structure of P25; mostly anatase covered from a thin layer of rutile. Further, some research outputs indicate that anatase and rutile in Degussa p25 have inter-particle contact as in image box C.[173, 175]

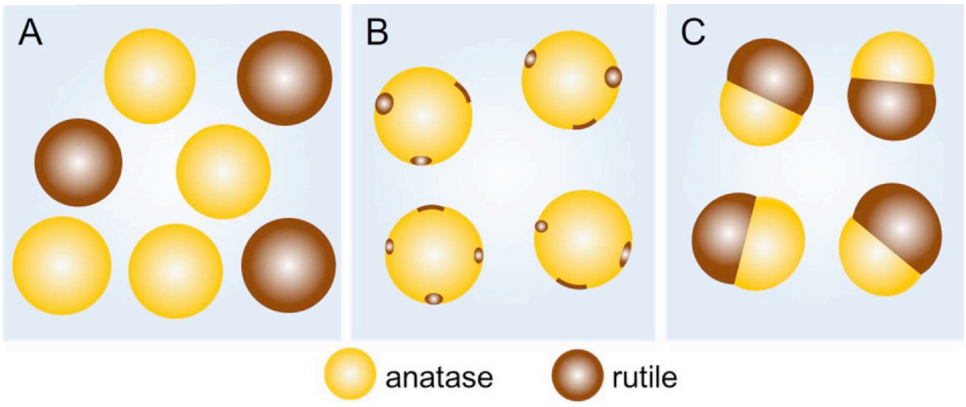

Figure 2.11 The possible microstructures in p25[173]

2.4.1 Synthesis of TiO_2

Various types of synthesis methods including sol-gel, sol, hydrothermal, solvothermal, sonochemical, microwave, chemical vapour deposition (CVD) and solid state reactions, have been employed to synthesis TiO_2 nanoparticles depending on the desired properties such as the

particle size, morphology, purity, and the applications.[176] All these methods use a titanium precursor, such as titanium tetrachloride, titanium butoxide and titanium isopropoxide, as the starting material.[177] This section will provide a brief overview of some common methods used in TiO_2 synthesis.

1. **Sol-gel method** – This method involves hydrolysis of a titanium precursor followed by formation of a gel and subsequently that gel will be dried and calcinated to achieve crystallinity. Sol-gel method has been identified as a simple process which is able to synthesise a diverse range of products such as fibres, powders and coatings with a good chemical homogeneity and high purity.[178] However, there are some restrictions can be recognised in this method; formation of agglomerations which increases the particle size and possible formation of secondary pollutants.[179]

2. **Hydrothermal and solvothermal methods** – These are two processes which share many similarities, except the fact that hydrothermal method utilises aqueous solvents while solvothermal method employs non-aqueous solvents. Both processes involve a reaction at a considerable pressure and temperature in an isolated system or autoclave.[180] These processes are known as versatile methods to prepare highly crystalline TiO_2 nanoparticles with high purity and less agglomeration. Moreover, these methods are able to save processing time, energy and cost as these are one step synthesis processes and post-synthesis calcination/sintering process is not required.[181] Hydrothermal and solvothermal processes have traditionally been recognised as high temperature, high pressure, energy-intensive and costly processes, however, recently researches have done many experiments to synthesise TiO_2 at a low temperature using these two methods. Additionally, these are potential methods to synthesise TiO_2 with different structures, morphologies, and compositions by changing the synthesis parameters. Among these two methods, hydrothermal process has gained the priority as it uses water as the solvent.[182]

3. **Microwave-assisted method** – This novel method has a gained a considerable attraction due to its simplicity as the reaction can be conducted at atmospheric pressure in a domestic microwave oven which results in a high yield of the product with a high crystallinity, a high purity and less aggregation within a short period of time.[183] In this process, microwave energy serves as a catalyst in promoting the nucleation and crystal growth of TiO_2, leading to a more controlled synthesis process compared to

conventional methods. This method contains the ability to achieve the desired particle sizes and morphologies.[184] Despite the above-mentioned advantages, some drawbacks are there in this method; possible temperature variations and even heating can affect the growth of TiO_2 nanoparticles and not being able to scale up the production with microwave-assisted synthesis.[185]

4. **Chemical-vapour deposition (CVD)** - This method uses volatile precursors which will undergo a thermal decomposition or react in vacuum chamber. The properties of the product can be alternated by changing the temperature, pressure, and the composition of the reactant gas mixture.[186] CVD is well known for the ability of getting a homogeneous film on various substrates, controlling the thickness of the film, and potential for the large-scale production. In contrast, it has some limitations, such as highly costly and high temperature and specialised instruments required.[187]

5. **Sonochemical synthesis** – This method utilises ultrasound waves in the range of 20-100 kHz that promotes the rapid nucleation and growth of TiO_2 particles via acoustic cavitation which implies the formation, growth and subsequent collapse of a bubble in the liquid. This abrupt collapse generates extreme conditions such as high pressure and temperature, shockwaves and microjets causing the breakage of chemical bonds.[188] This method presents some notable advantages such as being able to carry out the process at a low temperature without any harsh chemicals, having a homogeneous distribution, rapid and efficient reaction kinetics and less agglomeration. However, sonochemical method requires careful optimisation of the necessary parameters.[28,189]

2.4.1.1 Combined Methods

As discussed in Section 2.2.3, combined systems can be developed to minimise the drawbacks arouse from a single method and to improve the efficiency of the synthetic process. Report suggest that combining sol-gel method with other methods like hydrothermal, solvothermal and microwave assisted method, could possess high surface area and also enhance the photocatalytic activity even under visible light range.[190] Yang *et. al.* have successfully synthesised amorphous-mesoporous TiO_2 with a high surface area using integrated sol-gel/solvothermal for the removal of Sb(III) in aqueous solution.[191] Imoisili *et. al.* have combined microwave assisted synthesis method with sol-gel method to produce V and Ag co-doped TiO_2 which shows an amazing photocatalytic activity in removal of both MO and MB dyes within 60 minutes.[185] Moreover, it has been evident that these combined systems can

minimise the aggregation between particles, lower the working temperature and increase the crystallinity.[192,193] Furthermore, a solvothermal-pyrolysis system has been developed to synthesise ZnO-biochar composite for the removal of perrhenate and pertechnetate in radioactive effluents.[194] Netarajan and his group have used sol-gel/hydrothermal combined system to develop bismuth doped TiO_2 nanotubes for the degradation of rhodamine B dye under sunlight.[195] In addition to that, a system of sol-gel/ pyrolysis has been used to synthesise $(MnFe_2)_4$/magnetic biochar composite to remove diclofenac sodium.[196] In this thesis, for the second part sol-gel/hydrothermal integrated system was used to immobilise TiO_2 in CMC polymer matrix.

2.4.2 TiO_2 as a Photocatalyst

With the discovery made by Fujishima and Honda in 1972 on the photolysis of water on TiO_2 electrodes, titania has gained a greater awareness in various applications.[197, 198] Titania's high surface area with higher density of localised states leads to a better photocatalytic activity. Titania has a wide band gap and the radiation is normally in the UV region (290-380 nm). The general photocatalysis mechanism of titania is as same as what has been discussed in Section 2.2.2.

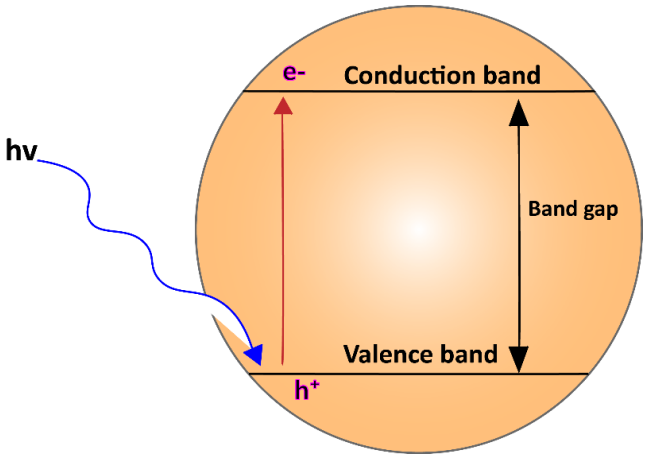

Figure 2.12 Schematic diagram of the bands of TiO_2 with UV irradiation.

Once titania is irradiated with a suitable wavelength as it can exceed the band gap, photoexcitation can take place and photogenerated holes can facilitate the oxidation reaction while electrons facilitate the reduction. This reaction involves many steps including charge carrier generation, separation, recombination, and surface capturing of photogenerated electrons and hole pairs. The following chemical equations depict the reactions of TiO_2 involved in photocatalysis:

$TiO_2 + h\nu \longrightarrow TiO_2 (e^-, h^+)$

$TiO_2 (h^+) + RX_{ads} \longrightarrow TiO_2 + RX_{ads}^{\cdot +}$

$TiO_2 (h^+) + H_2O_{ads} \longrightarrow TiO_2 + OH_{ads}^{\cdot} + H^+$

$TiO_2 (h^+) + OH_{ads}^- \longrightarrow TiO_2 + OH_{ads}^{\cdot}$

$TiO_2 (e^-) + O_{2,ads} \longrightarrow TiO_2 + O_2^{\cdot -}$

$TiO_2 (e^-) + H_2O_{2,ads} \longrightarrow TiO_2 + OH^- + OH_{ads}^{\cdot}$

Various reactions can take place during photocatalysis including oxidative cleavages, substitutions, polymerisations, oxidations, condensations, reductions, geometric and valence isomerisations.[26, 197, 199]

The charge separation of TiO_2 takes place promptly after the generation upon light irradiation. In anatase, generated electrons transfer to the 101 face which acts as the reduction face while the generated holes move to 001 face on which the oxidation sites are located.[200] However, approximately 90% of the generated electrons and holes recombine immediately after their separation. Consequently, the remaining separated electrons and holes can be effectively used in the photocatalysis process.[201] In addition to that, charge trapping can take place in the photocatalysis process, especially during electron relaxation. In here, the charges can be trapped in different trap sites such as the surface, defects, impurities, and other localised energy levels which makes charges immobilise. These phenomena hinder the overall efficiency of TiO_2.[202]

The physicochemical properties of TiO_2, which are influenced by a number of factors including morphology, porosity, surface area, preparation technique, particle size, and ratio of polymorphs have a considerable impact on its applications.[203] Out of the three major polymorphs of titania, anatase has the largest band gap and the highest photocatalytic activity (Anatase 3.2 eV, Rutile 3.0 eV, Brukite 2.96 eV) as mentioned in Section 2.4.[204] However, there are some significant drawbacks of titania which can restrict its role as a photocatalyst. These advantages include a wide band gap, poor sunlight absorption and considerably high electron-hole recombination. As a result, extensive research is being conducted to address these issues and narrow the band gap of titania to upgrade its performance in visible range.[205]

2.4.3 Modification Strategies of TiO_2

To overcome the above-mentioned disadvantages of TiO_2, a number of strategies have been experimented and implemented according to the requirements of the applications.

2.4.3.1 Doping

This technique involves introducing a foreign material like metals and non-metals to the TiO_2 lattice by chemical or physical means to improve the electronic and optical properties of TiO_2. These foreign materials can enhance the properties of TiO_2 in three ways;

I. Narrowing the band gap by inducing an impurity state/mid-gap state within the band gap. This helps to extend the photocatalytic activity of TiO_2 towards the visible light range.[199]

II. Improving the charge carrier separation by increasing the mobility of charge carriers and reducing the charge trapping. This improves the conductivity of TiO_2 through increasing the mobility of charge carriers.[206]

III. Increasing the surface area and active sites for the adsorbents.[207]

Dopants are categorised into metals and non-metals and metals into transition metals, noble metals and rare earth metals. The commonly used dopants under the afore-mentioned categories are shown in Figure 2.13.[208,209,210,83,211]

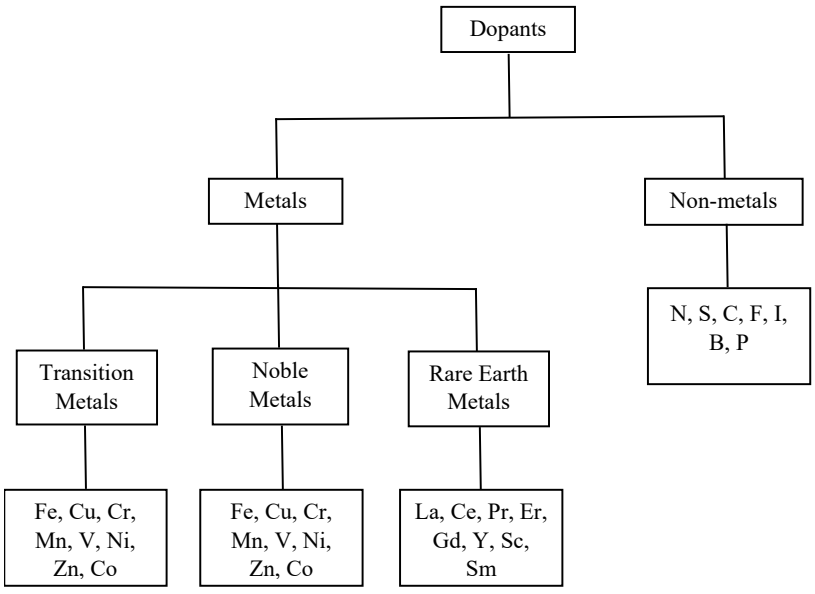

Figure 2.13 Classification of dopants for TiO_2.

Figure 2.14 illustrates the molecular orbital diagram of anatase. Metal dopants can downward shift in the conduction band while non-metals are able to increase the valence band which is called *upward shifting*. The shift occurs as the energy levels of the dopants can create alternative pathways for electrons to transfer. As a result, the fermi levels of the doped TiO_2 experience a downward or an upward shift.[212,213]

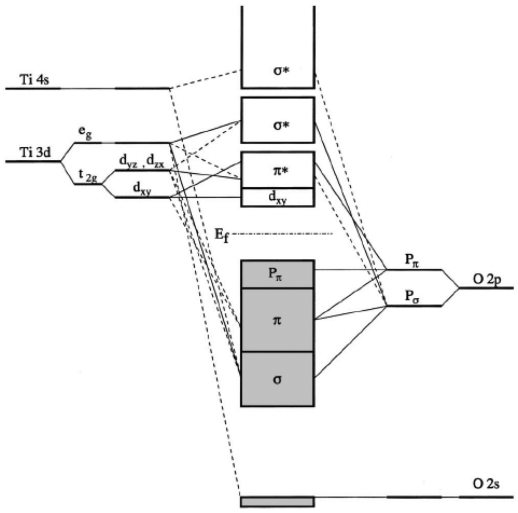

Figure 2.14 Molecular-orbital bonding diagram of anatase.[214]

When incorporating rare earth metals, partially filled 4*f* orbitals of rare earth metals can interact with the electronic states of TiO_2. These 4*f* orbitals possess energy levels which fall within TiO_2 band gap, resulting in band gaps known as *mid-gap/impurity states*. Figure 2.15 depicts band gap changes with dopants.[83,215]

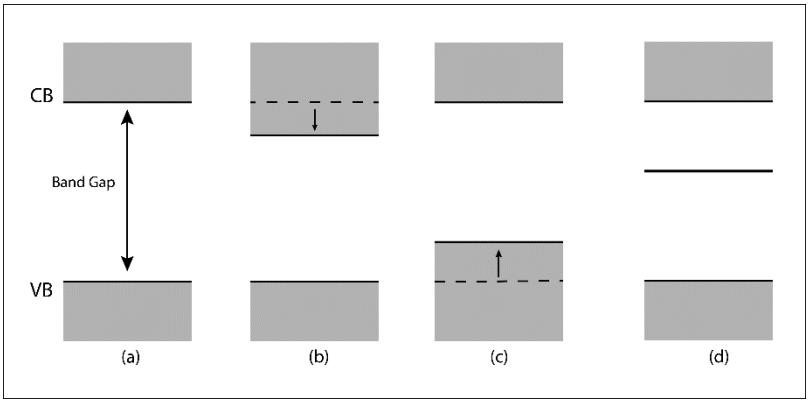

Figure 2.15 Schematic diagram of changes of TiO_2 band gap with the dopants (a) Undoped TiO_2, (b) downward shift (c) upward shift (d) mid-states.

Various doping combinations such as metal/metal, non-metal/non-metal and metal/non-metal have been discovered to enhance the properties of TiO_2.[216] Table 2.4 summarises some of previous research outcomes that employed doping techniques to modify TiO_2.

2.4.3.2 Semiconductor-TiO_2 Heterojunctions

Creating heterojunctions has emerged as a highly promising technique to enhance the photocatalytic performances of TiO_2 based materials as it is believed that a well-defined junction facilitates efficient charge transfer and suppress the recombination of photogenerated electrons and pairs.[217] In this scenario, electrons-holes pairs are generated both TiO_2 and incorporated semiconductor through photo excitation. There are three types of heterojunctions have been identified between TiO_2 and the other semiconductor (Figure 2.16):[218]

I. Type I – The two semiconductors should be either p-type or n-type. The conduction band of the second semiconductor should be higher than that of the first semiconductor while the valence band should be lower than that of the first semiconductor resulting both electrons and holes transfer from second semiconductor to the first one.

II. Type II – In this setup, electrons will transfer from second semiconductor to the first one while the holes will transfer from the first one to second one.

III. Type III – The electrons and holes transferring is similar to type II but a large gap between CB and VB can be identified. This requires a large driving force for the generated charges to transfer.

Table 2.4 Examples for different TiO_2 dopants and applications of the final composite

Photocatalyst	**Application**	**References**
Cu^{2+}, Cu^{+} - TiO_2	Solar applications	[219]
F-TiO_2	Bio imaging, energy and environmental cleaning	[220]
N, S-TiO_2	MB degradation under visible light	[221]
W-TiO_2	Degradation of resazurin redox dye under visible light	[222]
Ta-TiO_2	Photoanodes for sunlight-driven photoelectrochemical water-splitting	[223]

In-TiO_2	Photocatalytic reduction of CO_2	224
Zn-TiO_2	Photovolatic and photocatalytic applications	225
Cr, N- TiO_2	An alternative method of reducing power losses and threshold voltage	226
Cu, F-TiO_2	Degradation of MO under visible light	227
Pr, Fe-TiO_2	Degradation of Acid Orange 7 azo dye and phenol under visible light	228
Co, Zn – TiO_2	Degradation of Rhodamine B dye under visible light	229
C, N – TiO_2	Degradation of MB under visible light	230
B, N, F – TiO_2	Reduction of Cr(IV) and oxidation of benzoic acid	231

Semiconductors such as CdS, WO_3, ZnO, MoS_2, NiO, CeO_2 are frequently used to develop semiconductor-TiO_2 heterojunction.[232] Li *et al.* have synthesised a CdS-TiO_2 heterostructure composite which can be activated under visible light and this composite is a potential candidate to degrade tetracycline hydrochloride.[233] Moreover, $BiVO_4$ is a promising semiconductor material to construct a heterojunction with TiO_2 in order to extend titania's activity to visible light spectrum. These $BiVO_4$-TiO_2 composites have shown a great potential for applications like degradation of methylene blue degradation and Rh B dye[234], as well as in photovoltaics and sensing applications.[235]

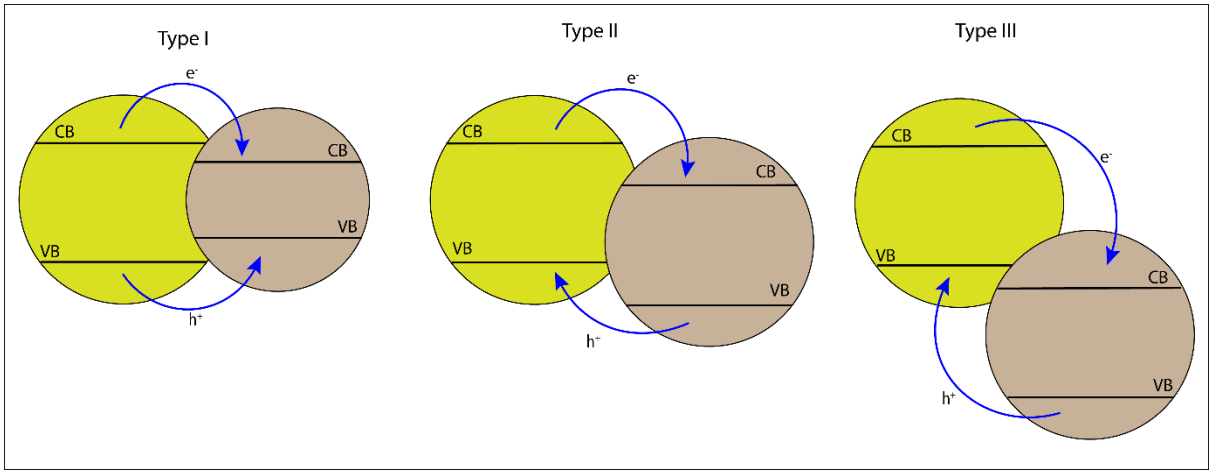

Figure 2.16 Different types of semiconductor heterojunctions.

2.4.3.3 Dye Sensitisation

The use of organic dyes which can absorb visible light has become a promising strategy to narrow the band gap of TiO_2. During this process, dye molecules are initially adsorbed on to the surface of TiO_2 and then upon irradiation electrons of the dye molecules are transferred to the conduction band of TiO_2. This phenomena helps to separate the photogenerated charges, thus increase the photocatalytic activity of TiO_2.[236] To be considered as a suitable candidate as a dye sensitisation, a dye should possess some specific characteristics such as having effective anchoring groups (phosphonic acids, carboxylic acids, esters, and ethers, etc.) to form strong interactions with TiO_2 and energy levels and the redox potentials in the ground state of the dye should be well aligned with those of TiO_2.[232]

There are two main approaches where dye-sensitised TiO_2 is used; dye-sensitised solar cells (DSC) and dye-sensitised photocatalysis (DSP). In DSC, a photovoltage is generated upon photoexcitation of the anchored dye and then subsequently charges are being transferred as discussed above.[237] Cho *et al*. studied the degradation of carbon tetrachloride using a dye-sensitised TiO_2 under visible light using a *tris*(4,4′-dicarboxy-2,2′-bipyridyl) ruthenium(II) dye complex to modify TiO_2.[238] There is some research which has used natural pigments for the dye sensitisation process. Patterson *et al.* had used 22 different tropical plants to extract the natural pigments and then use those pigments to modify TiO_2 for the removal ibuprofen, famotidine, warfarin, trimethoprim, and metoprolol. Out of those 22 natural pigments, the Begonia extraction had given the best results as an outstanding dye for sensitisation processes.[239] Other strategies including cocatalysts, surface modification and defect formation have been used to modify the properties of TiO_2.[240]

2.4.4 TiO_2 with Biopolymers

As discussed in section 2.4.3, the properties of a support material for TiO_2 is highly important to enhance applications. Biochar, biopolymers, silicates, clays, and glass plates are commonly used supporting agents with different photocatalysts to develop hybrid materials.[241] Among commonly used supports, the use of biopolymers to enhance the properties of TiO_2 has emerged as an outstanding technique as the biopolymers including starch, cellulose, alginate, CMC and chitosan provide numerous advantageous such as being biocompatible, cost-effective, highly abundant, and able to engineer the TiO_2 band gap easily.[242, 243] Moreover, another major reason for the attraction towards TiO_2-biopolymer combination is the synergistic effect from both chemical and physical interactions between inorganic and organic materials.[244]

Goudarzi *et al.* have synthesised an ecofriendly, UV shielding material with the use of starch and TiO_2[245] and recently extended the technology to a photo-producible and photo-degradable starch-TiO_2 bionanocomposite.[243] Other research has studied the photo-degradable properties of alginate-TiO_2 bionanocomposites and were able to discover a fast, convenient and environmental-friendly method to recover the photocatalyst used and this composite can be used in waste water treatment.[246] Moreover, there is some literature on the excellent antibacterial and heavy metal adsorption properties of cellulose-TiO_2 bionanocomposites.[247]

In the aqueous media, TiO_2 exists as the Lewis acid $Ti(OH)_4$ and the hydroxyl groups can interact to the hydroxyl groups of cellulose by forming H bonds.[248] On drying or dehydration, permanent covalent bonds can be formed between Ti and O and cellulose as shown in Figure 2.17.[248, 249] CMC can also react with TiO_2 through the carboxyl groups in many ways (Figure 2.18) including bidentate chelating, monodentate through CO, monodentate ester type and so on.[250]

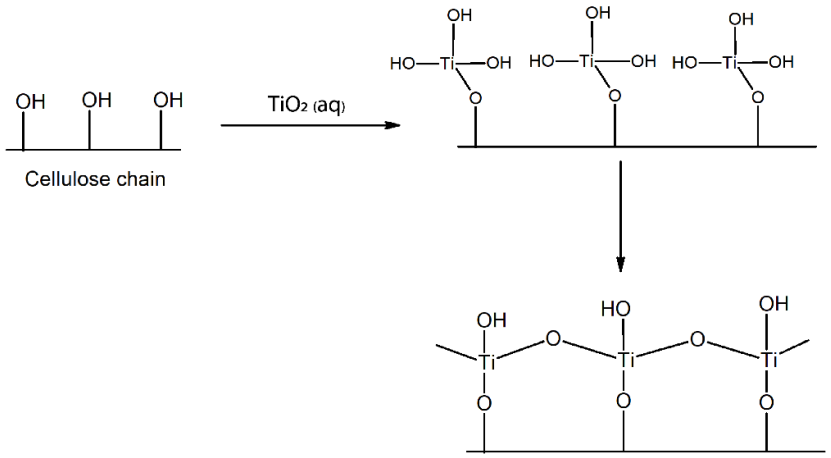

Figure 2.17 Formation of TiO_2 on cellulose chain.

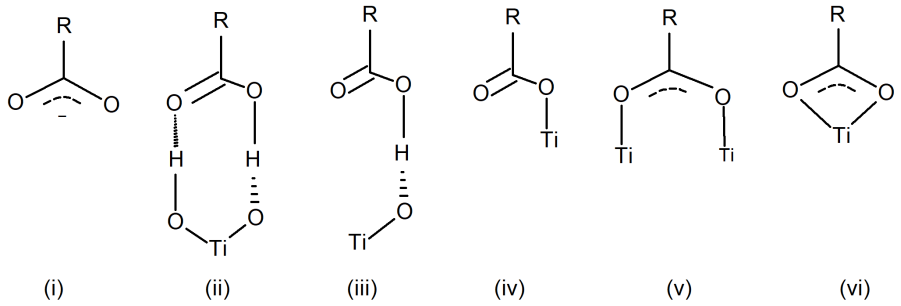

Figure 2.18 Possible binding modes of carboxylic group and TiO_2: (i) electrostatic interactions; (ii) and (iii) H bonding; (iv) ester-like linkage; (v) bidentate bridging; (vi) bidentate chelating.

For this project CMC was chosen to combine with TiO_2, considering the exceptional properties of CMC, discussed in Section 2.3.1. In addition, CMC's properties as a widely recognised surfactant and demonstrated use in synthesizing nanoparticles to have a homogeneous distribution by alleviating aggregation, appealed to this theses approach.[251] Table 2.5 provides some examples for CMC-TiO_2 bionanocomposites.

2.4.5 TiO_2 in Wastewater Treatment

With the rising global effect due to the polluted water, a number of water treatment methods have emerged during past few decades. Among those methods, heterogeneous photocatalysis has been recognised as one of the most effective and environmentally-friendly methods as outlined in Chapter 1. This section will discuss the two main aspects of TiO_2 as a potential material for wastewater treatment.

Table 2.5 Examples for CMC-TiO_2 bio nanocomposites, their properties and applications.

TiO_2 composite	**Properties and application**	**Reference**
CMC/Ag/gelatin – TiO_2	High stability and photocatalytic activity. Degradation of ammonia, ethanol and benzene	[252]
CMC - TiO_2	Transport and deposition of anatase nanoparticles on environmental surfaces, Lower the TiO2 band gap	[253]
CMC/ HEC- TiO_2	Hydrogel, high photocatalytic activity, enhanced properties to degrade methylene blue.	[254]
CMC/ polyaniline - TiO_2	High surface area, reusability up to five cycles without a significant change in adsorption capacity, a potential candidate for the removal of congo red dye.	[255]
CMC	UV shield, filtering visible light, prevent fogging	[256]
CMC/ Miswak (*Salvadora persica L.*) extract	High antibacterial properties, blocking UV	[257]
Ag, CMC, laser induced graphene electrode– TiO_2	Improved hydrophilicity of the electrode. For a sensor to detect chloramphenicol in water	[258]
CMC, sodium montmorillonite – TiO_2	Potential of UV blocking, high mechanical strength, suitable for biodegradable packaging	[259]
Cu, CMC – TiO_2	Strong antibacterial properties under visible light, able to delay banana browning, suitable for food packaging	[260]
CMC, PVA – TiO_2	Possess antimicrobial properties, suitable for develop textile fabrics like cotton with antibacterial properties	[261]

2.4.5.1 TiO_2 as an antimicrobial agent

Metal oxide antimicrobial agents including Ag, Ti, Cu and Zn have been utilised in the applications of antimicrobial activity. However, many of them face challenges in their performances like a limited spectrum of activity, potential toxicity concerns and negative impacts on the environment.[262,263] Out of those metal oxides, TiO_2 has gained a special attention due to its promising properties in terms of antimicrobial performance such as biocompatibility, chemical stability and durability, low risk of microbial resistance development, broad spectrum antimicrobial activity, being able to incorporate into many other materials easily and cost effectiveness.[264] The antimicrobial properties of TiO_2 were first reported by Matsunaga and co-workers, with the observation TiO_2-Pt killed microbial cells in water when the catalyst was exposed to UV light.[265]

Heterogeneous photocatalysis of TiO_2 results in formation of many reactive oxygen species such as peroxide radicals, superoxide and hydroxyl radicals ($O_2^{\cdot-}$ and $^{\cdot}OH$) which possess the ability to either kill microbes or supress their growth.[266] It has been also been proposed several methods for biocidal activity of photocatalyst since the anti-microbial mechanism via photocatalytic pathways are still not well understood. When TiO_2 makes the first contact with the intact cell at the beginning of the process, photocatalytic oxidative damage takes place on the cell wall. This leads to the efflux of intracellular components which will cause the cell death. With the degradation of the outer membrane, the underlying cytoplasmic membrane also starts to experience oxidative damage. As well, peroxidation of polyunsaturated phospholipids in the cell membrane can be initiated by ROS.[267] Both the hydroxyl free radical ($^{\cdot}OH$) and hydrogen peroxide (H_2O_2) can penetrate the cell walls and since $^{\cdot}OH$ is highly reactive, non-selective and short-lived, it can break DNA strands leading to apoptosis. Both superoxide anion ($^{\cdot}O_2^-$) and H_2O_2 can act as precursors to form $^{\cdot}OH$. Once the H_2O_2 penetrates the cell wall, it gets activated by ferrous ion (Fe^{2+}) via the Fenton reaction as described in the following equations:[265]

$$TiO_2\ (e^-) + Fe^{3+} \longrightarrow Fe^{2+}$$

$$Fe^{3+} + {}^{\cdot}O_2^- \longrightarrow Fe^{2+} + O_2$$

$$Fe^{2+} + H_2O_2 \longrightarrow Fe^{3+} + {}^{\cdot}OH + OH^-$$

It has been reported that TiO_2 has the ability to withstand harsh conditions like humidity. In a study by Khaiboullina *et al*., it was demonstrated that TiO_2 nanoparticles maintain their ability to deactivate viruses even under extremely high humidity conditions. This finding suggests that TiO_2 nanoparticles are suitable for coatings on outdoor surfaces. The research provided evidence that surfaces coated with TiO_2 exhibit viral inactivation properties, even when exposed to dried virus droplets.[268] Furthermore, higher antibacterial properties in polyethylene-TiO_2 composites have been observed by Yage *et al*.[269] Successful antibacterial properties of TiO_2 and graphene oxide have also been investigated by Wanag *et al.* and the composite could be activated under artificial solar light.[270] Also they have found the negative charge of TiO_2 surface has changed into positive when incorporating with graphene oxide which improves the contact between TiO_2 surface and *E. coli* surface, leading the compound to own higher anti-microbial properties. Additionally, TiO_2 modification using various chemicals such as Ag_2O, BTO and Au to enhance the antibacterial properties have also been reported.[199] There are several some other factors that affect the antibacterial effectiveness of TiO_2. These factors include the specific type of TiO_2, crystallinity, particle size, surface area, the concentration of TiO_2 used, properties of the supporting agent of TiO_2, and the intensity of the UV lamp used.[271]

2.4.5.2 Degradation of Dyes

The utilisation of dyes in industries like textiles, papermaking, photographic, cosmetics, plastics, pharmaceuticals and other chemical industries have become a great concern as they create a major environmental problem by releasing the dyes to the environment. Even a small quantity of dyes, (as low as <1 part per million) in water can be easily detected by the naked eye, making them a significant type of pollutant in wastewater. These dyes can result in a range of health issues like harm to organs, allergic reactions, reproductive problems and potential carcinogenic effects.[272]

A compound can exhibit a colour, if only it can absorb light from the visible region. There are two main structural components of an organic dye which help to produce the colour:[273]

I. **Chromophore** – This is considered as the active part of the dye, which can absorb light in the visible region. A Chromophore consists of an unsaturated group and it must be a part of a conjugated system. The common chromophore groups found in the dye molecules have been listed below. Nitro (−NO_2), azo (−N=N−), nitroso (−N=O), thiocarbonyl (−C=S), carbonyl (−C=O), aromatics and alkanes (−C=C−).[274]

II. **Auxochrome** – This is the saturated group attached to the chromopore. An auxochrome can modify an enhance the properties of the chromophore, like intensifying the colour. These groups are generally electron donors and some common auxochrome groups are $-OH$, $-NH_2$, $-NO_2$, $-NR_2$, $-COOH$ and $-SO_3$. They can be either acidic or basic.[273,275]

Dyes can be categorised based on different factors such as their synthesis method, chemical structure, colour index, charges on the molecule, and the industrial application. The following chart in Figure 2.19 on dye classification was created based on literature reports.[11] In addition to that dyes can be classified as anionic, cationic and non-ionic dyes, based on their general structure and charges on the molecules.[276]

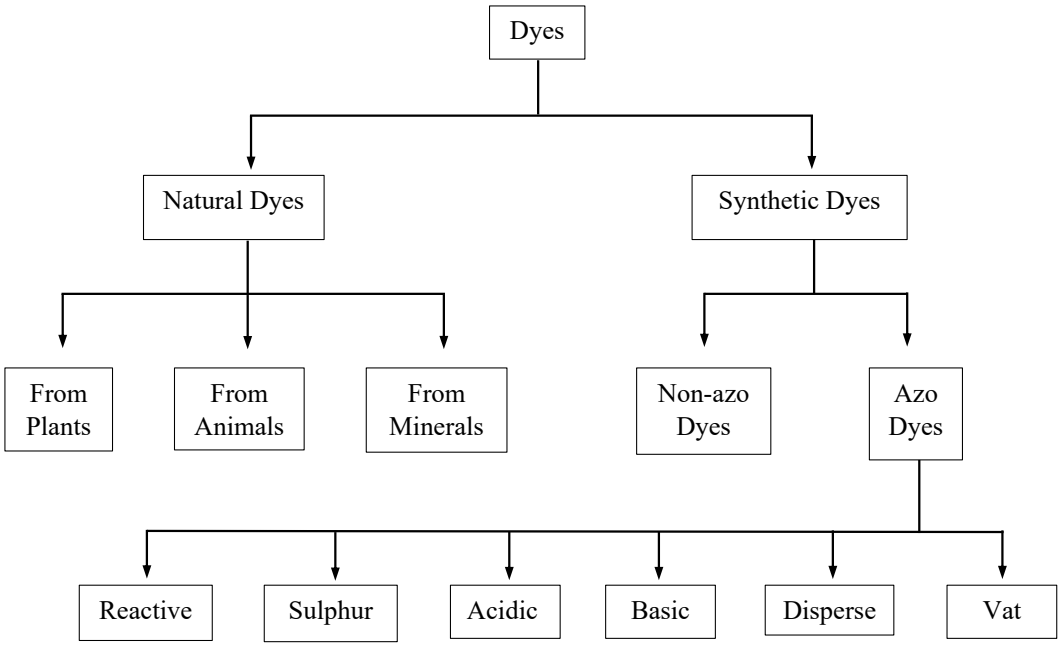

Figure 2.19 A classification of dyestuffs.

As the use of dyes, particularly in the textile industry, continues to increase over time, it creates a significant global threat. Therefore, the removal of dyes becomes crucial for the preservation of the ecosystem. With that regard, heterogeneous photocatalysis has been proven as the most important method of removing dye because it is highly effective and environmental-friendly. This also extends to self-cleaning textiles, where stains can be removed by an activated textile.[277, 278] Removal of dyes via photocatalysis can be classified in to four main groups depending on their final photocatalysis products:[11]

1. **Photodecolourisation** – This involves photocatalytic oxidation or photoreduction, simply to remove the colour of the dye but dye has the ability to revert back to its original colour through reduction or oxidation.[279]
2. **Photodegradation** – This pathway decomposes dye into some stable products.[280]
3. **Photomineralisation** – This involves in breaking down the dye molecules into simple compounds like H_2O, CO_2, N_2, etc. This should be the ultimate goal of photocatalysis.
4. **Photodecomposition** – Different researchers may have varying interpretations of the term, as it can refer to both photodegradation and mineralization in different situations. However, decolorization is generally not considered a part of its definition.[281]

In this project methylene blue (MB) dye, methyl orange (MO) dye and reactive batik dyes (Reactive Red) were used (Figure 2.20) to investigate the photocatalytic properties of the prepared CMC-TiO_2 composites. MB is a cationic dye with a thiazine chromophore group and it is one of the widely used dyes because it is safe to handle, easy to prepare and store and readily available.[282] Methyl orange is an anionic azo dye.

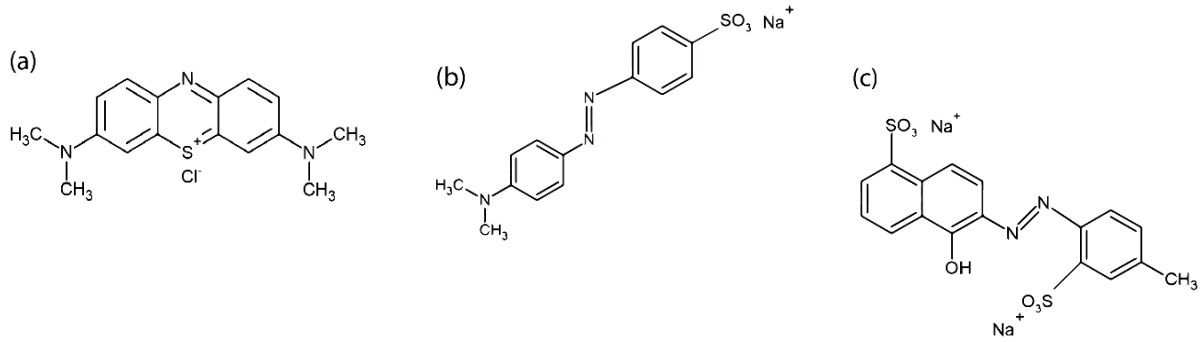

Figure 2.20 Chemical structures of (a) MB (b) MO (c) Scarlet red – GN.

2.5 Aims and Objectives

The use of CMC and TiO_2 as a composite has not been reported much in the literature. When it comes to *in-situ* synthesis of TiO_2 on biopolymers, to our knowledge, no record was found on this strategy on immobilising TiO_2. The aim of this project was to develop a multifunctional, adsorbent with photocatalytic activity for wastewater treatment using carboxymethyl cellulose and TiO_2. The specific objectives of this research project are given below:

I. To synthesize a CMC-TiO_2 foam composite using CMC and TiO_2 powder directly and evaluate its adsorption capacity and photocatalytic activity for wastewater treatment.

II. To perform *in-situ* synthesis of TiO_2 on CMC for improved stability and effectiveness, and evaluate the resulting CMC-CTTIP composite focusing on its photocatalytic activity in degrading dyes and phenol.

III. To assess the effectiveness of the synthesized CMC/TiO2 composites in degrading three specific batik dyes obtained from Sri Lanka, by measuring the photocatalytic degradation.

CHAPTER 3

Preparation of a Foam Composite Between CMC and TiO_2 Powder for Wastewater Treatment

3.1 Introduction

This chapter examines the synthesis of a foam for wastewater treatment using a straightforward method that directly employs carboxymethyl cellulose and TiO_2 powder. The synthesis process outlined herein aspires to be both environmentally sustainable and cost-effective.

Water pollution is one of the chronic issues in the world. Out of the many water pollutants known, organic dyes have become one of the most threatening issues as they are difficult to degrade due their complex and stable organic structures.[283] One area in which this problem is prevalent, is in the textile industry. As mentioned in Chapter 1, the over-pollution of waterways throughout much of the known world as a result of textile dyes has resulted in detrimental impacts on both ecosystems and human health. For example, based on a study focusing on the characterization of textile effluent, the average concentrations of COD and BOD in the last decade were found to be within the ranges of (150-30,000) mg L^{-1} and (80–6000) mg L^{-1}, respectively. Such high levels of pollutants could lead to adverse effects on both the environment and human health.[284] Furthermore, a study conducted on German painters by Myslak *et al*. revealed that prolonged exposure to azo dyes increases the risk of developing bladder tumours in individuals.[285]

Figure 3.1 depicts the global damage caused by textile dyes all over the world.[286] Thus, removal of textile dyes from water has gained a considerable attention of the research world.[48] As outlined in Chapter 2, diverse materials and methodologies have been applied in this treatment process. Notably, there has been a shift towards environmentally friendly and cost-effective materials, particularly biopolymers, drawing an increased attention in recent studies.

Carboxymethyl cellulose (CMC) is a cellulose derivative with outstanding properties such as water solubility, eco-friendliness, biocompatibility, non-toxicity, high adsorption capacity and cost effectiveness. Most importantly due to being both hydrophilic and rich in function groups, CMC has become a highly used material in wastewater treatments.

Figure 3.1 Three examples of water pollution caused by textile dyes impacting natural and runoff waterways.[286]

Table 3.1 provides examples for using CMC for wastewater treatments highlighting its successful capacity and diverse applications within this domain. This rationalises the choice to use CMC in the current research. Furthermore, TiO_2 is one of the most studied candidates in wastewater treatments for its photocatalytic, non-toxic and environmentally friendly nature.[131] One of the major drawbacks in TiO_2 with regards to wastewater treatment is its low adsorption capacity.[287]

Table 3.1 Examples of using CMC for wastewater treatments

Composite	**Application**
CMC/bentonite	Removal of crystal violet and Cd(II) ions [288]
CMC/PAA	Removal of MB [131]
CMC/PDA@ZIF-8/PTFE	Removal of oil in water [289]
CMC/acrylic acid/itaconic acid	Removal of Safranin-O [290]
CMC/PAA/activated C	Removal of Cu ions and MB in water [291]
CMC/ graphene composite aerogel beads	Removal of MB [292]
CMC/ polyacrylamide	Removal of Cu, Pb and Cd ions in water [293]

In this study TiO_2 was incorporated into CMC to increase the active sites and surface area of the composite which is in an important factor in wastewater treatments. In the synthesised composite, we hypothesise that CMC acts as the matrix to adsorb the waste and TiO_2 acts as the photocatalyst to break them down. Since CMC is an anionic polymer thanks to its carboxylic acid/carboxylate groups, methylene blue, a cationic dye, was chosen as the model dye.[163] Another significance of this study was to find a simple method to prepare the composite as the literature often shows complicated methods used to modify CMC with TiO_2. The synergistic nature between CMC and TiO_2 has successfully resulted a significant candidate for MB dye removal with photocatalytic properties. Therefore, this study supports our first objective of synthesising a foam directly using CMC and TiO_2 powder via an environmentally friendly and cost-effective method to enhance wastewater treatment.

3.2 Experimental

3.2.1 Materials and Reagents

Sodium carboxymethyl cellulose (degree of substitution = 0.7, average Mw = 250,000) and titanium(IV) oxide (Degussa P25 aeroxide, particle size ~ 21nm) were purchased from Sigma Aldrich, Australia and used as is.

3.2.2 Preparation of TiO_2 suspension

KBr (0.01 g, 0.084 mmol) was dissolved in distilled water (20 ml) and TiO_2 powder (0.05 g, 0.63 mmol) was added to it. The resulting suspension was ultra-sonicated for 1h then stirred using a magnetic stirrer for an additional hour.

3.2.3 Preparation of CMC-TiO_2 suspension

CMC powder (0.2 g) was dissolved in distilled water (20 ml) at room temperature for 3 h until the CMC powder completely dissolved. A portion of the TiO_2 suspension above (5 ml) was added to the CMC solution dropwise while stirring. The mixture was allowed to stir for another 4.5 h at room temperature.

3.2.4 Preparation of the Foam Composite

The CMC-TiO_2 suspension was poured into a Teflon tube with 10 mm of internal diameter and 50 mm of length. One end of the tube was covered using a copper sheet hung in a Styrofoam cup using a copper wire as shown in the Figure 3.2. The Styrofoam cup was placed in a Styrofoam bowl and then the cup was filled with liquid N_2 to the point that half of the tube was covered. When the liquid N_2 evaporated, the suspension underwent unidirectional freezing.

Once the suspension solidified, it was taken out from the Teflon tube and placed in a freeze dry vessel and the samples were freeze-dried for 48 h. Two controls were prepared; one only with CMC in water and the one with CMC and KBr in water.

Figure 3.2 Unidirectional freezing apparatus used to prepare the foam samples.

3.2.5 Characterisation of Samples

The selected techniques were employed to characterise the synthesised sample, as they are instrumental in identifying key structural properties such as crystallinity, surface area, bonding nature, elemental distribution, and material charge. These properties play a crucial role in determining the adsorption and photocatalytic capabilities of the compound.

3.2.5.1 X-Ray Diffraction (XRD)

A Bruker X-ray diffractometer (XRD) D8 advance with a CuKα sealed tube (λ = 1.5406 nm) and Lynxeye detector was used for XRD analysis. The samples were scanned between 5° and 90°. The tube current and voltage were 40 mA and 40 kV, respectively. Samples

3.2.5.2 Brunauer-Emmett-Teller (BET) Analysis

Surface area and pores size measurements were conducted by BET N_2 adsorption-desorption analysis. These measurements were made using a Smart VacPrep station (degas) and TriStar II Plus (BET) SI apparatus with N_2 as the sorbate at 77 K. The samples were degassed at 110°C under vacuum (1×10^{-2} Torr) for 12 h prior to analysis. The total specific surface areas were determined by multipoint BET methods,while the specific total pore volume was evaluated from N_2 uptake at a relative pressure of $P/P_0 = 0.99$.

3.2.5.3 Attenuated Reflectance Fourier Transform Infrared (ATR FTIR) Spectroscopy

ATR-FTIR spectrum of the prepared samples (approx. 5-10 mg) were recorded using a Thermoscientific Nicolet iD5 spectrophotometer. The functional groups of the samples were identified by spectroscopic analysis in transmission mode with the detection range from 800 to 4000 cm^{-1}.

3.2.5.4 X-Ray Photoelectron Spectroscopy

The elemental compositions of the fabricated materials were examined through X-ray photoelectron spectroscopy (XPS) spectra using Kratos AXIS NOVA spectrometer (Kratos Analytical, Inc., Manchester, UK) instrument. The X-ray source used was Al Kα. Subsequently, the acquired data was subjected to analysis through the casaXPS software.

3.2.5.5 Thermogravimetric Analysis (TGA)

The thermal stability of the materials prepared were investigated using a Q500-0341 TGA instrument. The TG curve recorded represents the evolution of the mass as a function of the temperature. The sample was heated from room temperature to 1000°C under a nitrogen atmosphere at a heating rate of 10°C/min.

3.2.5.6 Scanning Electron Microscopy (SEM) and Energy Dispersive X-ray (EDX) Analysis

A Hitachi S-4800 scanning electron microscope with a field emission gun was used to analyse the surface morphology and structure of prepared samples. Working distance for EDX was 10 mm. These samples were gold coated using a sputter coater before observation. All images include scale bars.

3.2.5.7 Zeta Potential Analyser

Zeta potential analysis of TiO_2 suspensions, TiO_2 with KBr suspensions and CMC-TiO_2 suspensions (prepared CMC-TiO_2 foam in water) were carried out using a Malvern Zetasizer Ultra zeta potential instrument. Measurements were performed on a dilute suspension at native pH.

3.2.6 Photocatalytic Activity

A 3 mg/L methylene blue (MB) solution was used as the prototypical dye product and its concentration in water was monitored by a Shimadzu UV Visible spectrometer. A 50 mL volume of the MB solution with 0.47 g/L of the CKT foam was exposed to the light source UV

over 4 h, under stirring. Samples were taken every 15 min. The suspension was centrifuged using an Eppendorf Minispin Centrifuge at 14,000 rpm for 15 min. The supernatant was transferred to a disposable cuvette and measured for absorbance at 665 nm.

In detail, two parallel experiments were conducted; one in dark and the other under UVA, at 366 nm. Initially, absorbance readings of MB solutions (without TiO_2) were taken. Subsequent readings were taken as soon as adsorbent was added to both the solutions as T = 0 min. Then both MB-sample mixtures were kept in the dark for 75 mins until they reach their adsorption-desorption equilibrium. Once reached, one of the samples was irradiated with UV and other was kept in the dark. The same method was followed with TiO_2 powder (9 mg) and CMC powder (36 mg). These masses were obtained by a back calculation. pH of solution was varied using 0.1M NaOH and 0.1M HCl as needed. The effect of catalyst dosage was carried out varying the amount catalyst used for MB test.

3.2.7 Anti-Bacterial Testing

Anti-microbial properties of the prepared samples were investigated against *E. coli* and *S. aureus* using UV A (wavelength – 365 nm) light. The sample amounts used for this experiment are given in Table 3.2.

Table 3.2 Samples and their amounts used for anti-bacterial testing.

Sample	**Amount (mg)**
Sample A (CMC foam)	40
Sample B (CMC/KBr foam)	40
Sample C (CMC/KBr/TiO_2 foam)	40
TiO_2 powder	10

Before the experiment, the bacteria were inoculated into LB broth and incubated in a shaker at 37^{o}C and 220 rpm overnight. Then the optical density (OD) of the bacteria culture was determined using a Shimadzu UV Visible spectrometer and adjusted to 10^6 using saline solution. Samples were placed in a nine well plate and 1 mL of bacteria solution (OD adjusted) was suspended on to each sample. In addition, 1 mL from bacteria solution was added to one of the wells without any samples as a positive control test. The well plates were kept under UV lamp in biosafety cabinet for 3 h after which, the samples with a bacteria solution which had

become a suspension were taken out and each sample was diluted up to 10^6 using saline solution. Then 0.1 ml of each dilution was dispersed into an agar plate and the plates were incubated at 37°C for 16 h. After the certain period of time, plates were taken out and number of colonies in the agar plates were counted and colony forming units for 1 mL (CFU/mL) was determined using the following equation.

$$CFU\ (mL) = \frac{Number\ of\ colonies \times Dilution\ factor}{Volume\ plated\ in\ mL} \qquad \text{Equation 3.1}$$

In all experiments, a negative control test was conducted in the dark, without UV light, simultaneously.

3.3 Results and Discussion

3.3.1 Preparation of the solutions

Five different types of foams were successfully prepared for this study by varying different parameters as in Table 3.3. In the context of abbreviations, 'C' denotes CMC, 'K' represents KBr, and 'T' stands for TiO_2. Additionally, the quantity of TiO_2 used is mentioned after 'T', followed by the stirring duration. For instance, CKT0.05_4.5h signifies a foam concocted using CMC, KBr, and 0.05 g of TiO_2, stirred for 4.5 hours.

The observations could be well explained as follows. CMC was easily dissolved in water, resulting a quite viscous solution due to CMC's known hydrogel properties.[142] Preparation of TiO_2 suspensions, required some deviation from a simple mix. Preparing a suspension indicates breaking and dispersing the nanoparticle clusters in an aqueous solution with subsequent stabilization. But titania tends to agglomerate very easily due to Van der Waals attractions among the particles.[294] In the process used for this project, steps were taken to minimize agglomeration. In aqueous solution TiO_2 binds with water molecules and takes its hydrated form $Ti(OH)_4$. Having a strong electrolyte (such as KBr) in the solution, can hamper the phase transformation of $Ti(OH)_4$ into TiO_2 clusters by shielding the effect of attractive electrical force from solid particles. At the same time, an electrolyte can enhance the adsorption of OH^- and H^+ on TiO_2 particles.[295] The second strategy to impede agglomeration was ultrasonication. The generated shocked wave from the ultra-sonic bath can create collisions among agglomerated particles, thus separating them. This also enhances the formation of the TiO_2 suspension.[294] Samples C-E were prepared by varying the amount of TiO_2 under different timeframes and the viscosity trend appeared to be as: A < B < C < D < E.

Table 3.3 Prepared samples and their compositions.

Sample	CMC (g)	KBr (g)	TiO_2 (g)	Stirring time after adding TiO_2
C_4.5h (A)	0.2			4.5 h
CK_4.5h (B)	0.2	0.01		4.5 h
CKT0.05_4.5h (C)	0.2	0.01	0.05	4.5 h
CKT0.3_4.5h (D)	0.2	0.01	0.3	4.5 h
CKT0.05_7d (E)	0.2	0.01	0.05	7 d

Sample B in Table 3.3 contains only CMC powder and KBr powder. Since KBr is a strong electrolyte it dissociates completely. The resulting monovalent cations can form bridges/crosslinks among the polymer chains as shown in Figure 3.3, causing a small change in the viscosity. This will also hold true for samples C-E.

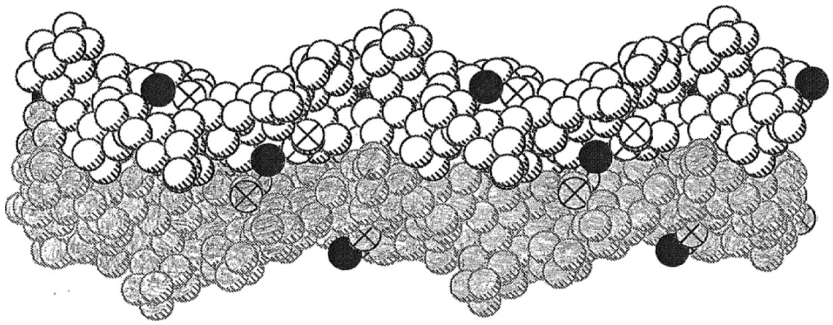

Figure 3.3 The formation of salt bridges among polymer chains by K+ ions (black circles). The white circles with crosses symbolise oxygen atoms of carboxylate groups [296]

The above viscosity results indicate that higher the amount of TiO_2 and the stirring time, higher the viscosity and it can be rationalised through the crosslinking capabilities of TiO_2. Since titania is oxophilic, it can coordinate strongly to carboxylates within the chain, leading to both more rigid, but also larger super structures leading to enhanced viscosity.[297]

3.3.2 Preparation of Foams

In the initial phase of this project, we decided to produce foams by using CMC and TiO_2. This choice was based on the well-documented exceptional characteristics of foams, including a high surface area, a three-dimensional porous structure, and excellent permeability, all of which are essential attributes for an effective adsorbent.[298,299]

The foams were prepared by unidirectional freezing of the solution followed by freeze drying. As mentioned in the method, unidirectional freezing allows to transfer heat through the solution

in the Teflon tubes only from bottom to top as Teflon tubes prevent heat transferring from side walls (Figure 3.4). Consequently, the freezing process generates a thermal gradient in a single direction, resulting in the formation of aligned pores within the material.[300] Furthermore, as documented in the literature, unidirectional freezing allows for better control over the size and distribution of pores by minimizing ice entanglements during the freezing process.[301] Therefore, for the preparation of an adsorbent, unidirectional freezing offers more advantages compared to radial freezing.[302]

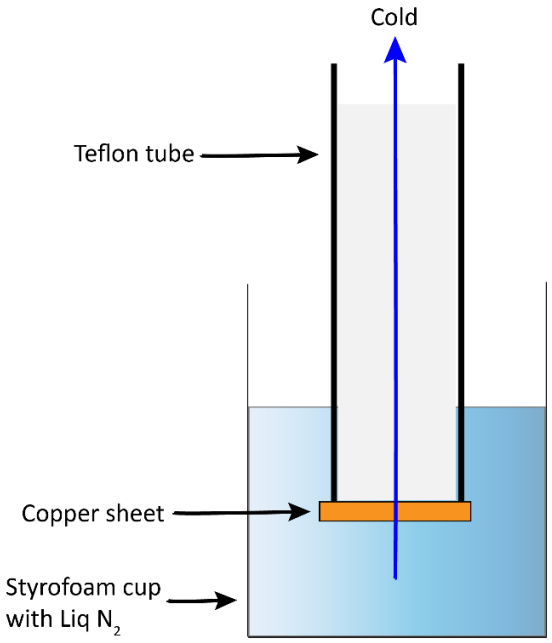

Figure 3.4 Schematic diagram of the apparatus used to gain unidirectional freezing of the samples.

Figure 3.5, illustrates the white, opaque, soft in texture and low density of prepared foams caused by the freeze-drying method. When freeze drying, the frozen water is removed via sublimation and it generates a very low volume shrinkage, resulting a low density of the foams.[303]

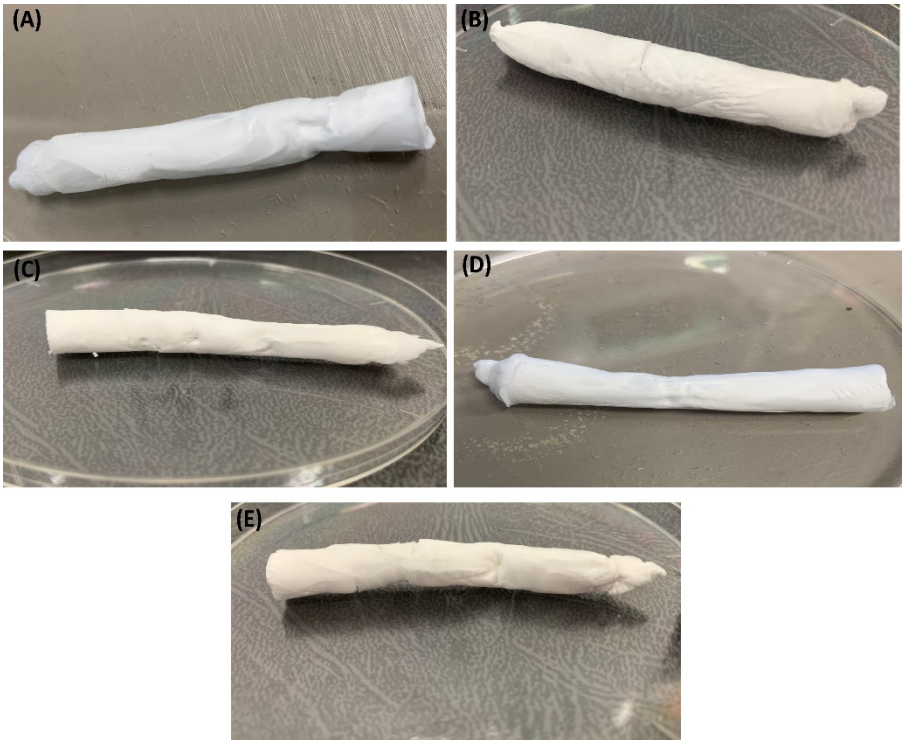

Figure 3.5 Prepared foams (9 x1 cm) varying amount of TiO_2 and stirring time. (A) C_4.5h; (B) CK_4.5h, (C) CKT0.05_4.5h, (D) CKT0.3_4.5h, and (E) CKT0.05_7d.

3.3.3 Material Characterization of Foams

3.3.3.1 X-ray Diffraction

XRD is a technique that provides information on crystal composition and molecular connectivity including phases, crystal orientation, level of crystallinity, average grain size and crystal defects. This investigation anticipates using X-ray diffraction (XRD) analysis to identify the crystalline structure of the final compound. Consequently, this method will enable the identification and characterization of material phases within the samples under study. XRD profiles of all raw materials and samples prepared are shown in Figure 3.6. The broad diffraction peak at approx. $2\theta = 22^0$ in all CMC profiles is attributed to the amorphous nature of CMC.[278] The P25 (TiO_2) XRD profile shows crystalline phases peaks can be attributed to anatase, rutile and amorphous titania as P25 is known to be a mixture of all TiO_2 phases. Therefore, 2θ peaks at 25.5, 38.1, 48.1, 54.35, 55.4, 62.75 are corresponded to the crystal planes of 101, 004, 200, 201, 211, 204 for anatase, respectively, and the peak at 27.05 (110) strongly supports the additional rutile phase.[257,27,253] Moreover, in samples contain KBr, sharp peaks at 24.05, 27.05, 38.75, 39.25, 48.35, 55.65, 63.04, 70.05 were given by the reflections from (111), (200), (220), (222), (400), (420) and (422) planes of KBr.[304]

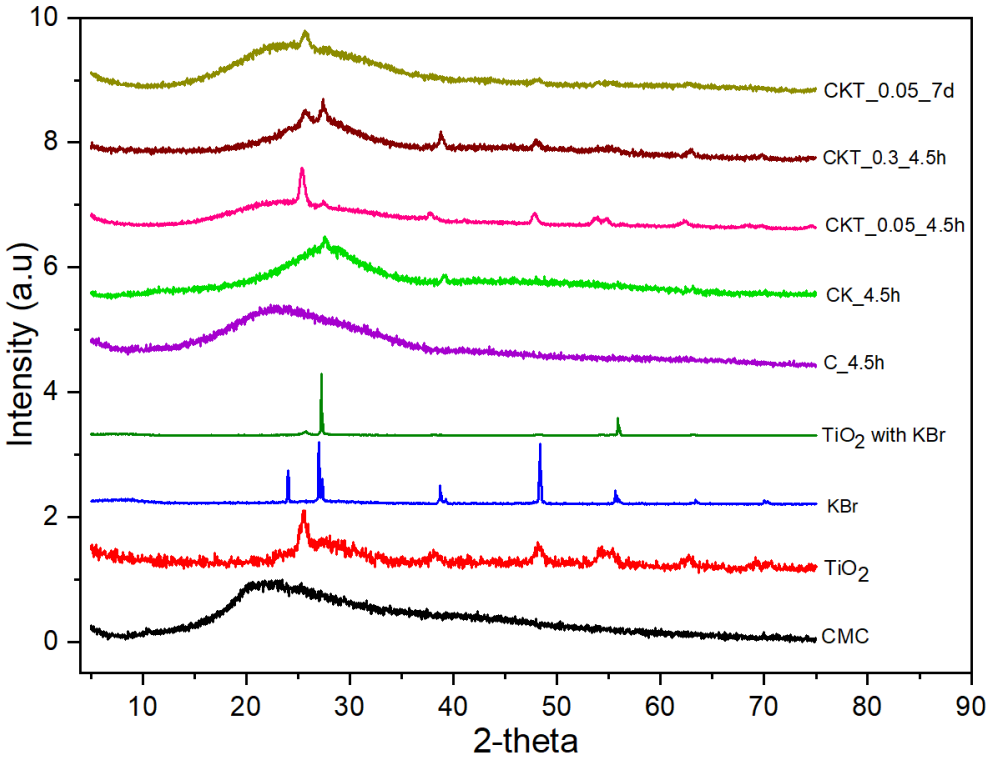

Figure 3.6 XRD patterns of precursors and prepared foams.

In the spectra of samples containing a combination of CMC, KBr, and titania composites, distinct peaks corresponding to CMC, KBr, and TiO_2 are readily observable, affirming the successful formation of the composite composition. However, no difference of the peak positions could be observed between the peaks in raw materials and composites, indicating either TiO_2 has not bound to carboxymethyl cellulose[255] or the amount of TiO_2 is not sufficient as the instrument can detect. In XRD graph of sample E, the intensities of TiO_2 and KBr peaks are very low compared to sample C and D. It can be assumed that stirring for a longer period (7 days) might allow CMC and TiO_2 react well together.

3.3.3.2 Attenuated Reflectance Fourier Transform Infrared (ATR FTIR) Spectroscopy

IR is a technique that allows to determine the structural information of a molecule through the motions (vibration, stretching, bending, scissoring) of the bonds after absorbing the energy in the IR region. This study aims to utilize ATR FTIR analysis to distinguish the emergence of new bond formations within the resultant compound, as well as to observe changes in the existing bonds resulting from the incorporation of CMC and TiO_2.

Figure 3.7 shows the FTIR spectrum of CMC with DS 0.7. The absorption band at 3314 cm^{-1} is assigned mainly to the stretching of —OH groups though a small amount of water may also

contribute. The band at 2885 cm^{-1} is due to C—H stretching vibrations within the polysaccharide backbone. Presence of carboxymethyl substituents are represented by the peaks at 1618 and 1417 cm^{-1} because carboxylic groups in its salts form have wavenumbers typically paired at 1600-1640 cm^{-1} and 1400-1450 cm^{-1}. The band at 1324 cm^{-1} is attributed to —CH_2 scissoring motion. The band at 1023 cm^{-1} is given by CH-O-CH stretching at the β-glycosidic bonds.[137,162]

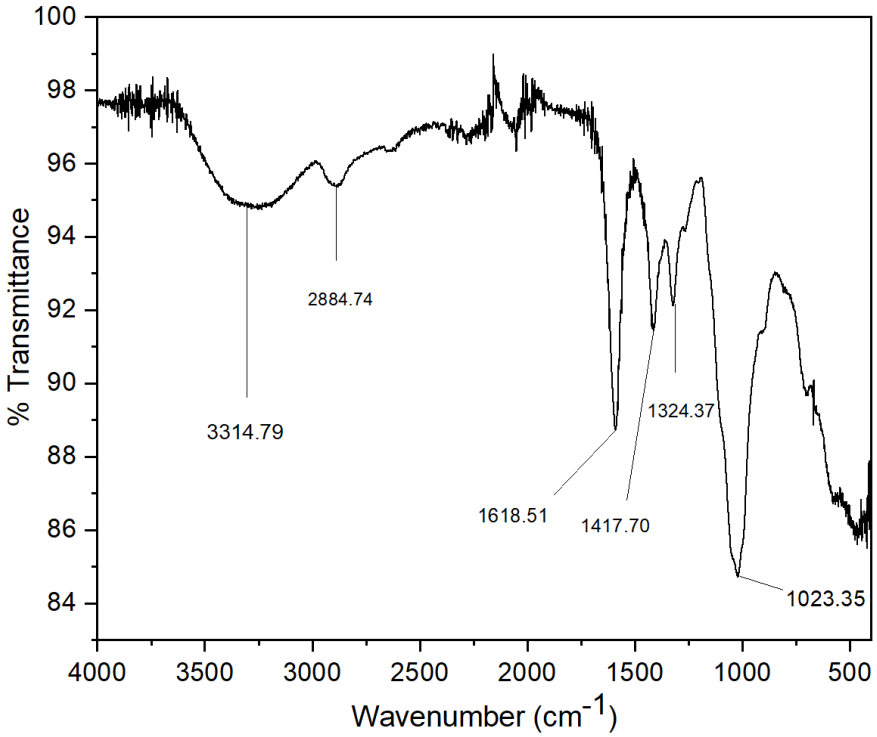

Figure 3.7 ATR-FTIR spectrum of CMC powder.

Figure 3.8 shows the ATR FTIR results of our composite materials. As reported in literature, peaks from 400-800 cm^{-1} are attributed to asymmetric, symmetric stretching and bonding modes of Ti-O-Ti bonds.[305] The weak peak at 480-500 cm^{-1} is due to the presence of Ti-O-Ti bond and the peak at 440 cm^{-1} is given by the stretching vibrations of Ti-O-Ti and Ti-O peaks.[306] Even if these peaks cannot be seen clearly in Figure 1.7, the weak peak at 500 cm^{-1} firmly suggests the presence of Ti-O-Ti bonds in the samples C-E, but no significant shift could be observed in peak positions between the sample prepared and CMC powder. Even there was a small change of shifts, it could not consider as it is within the % error region. This could be due to the small amount of TiO_2 loaded in the composite.[257]

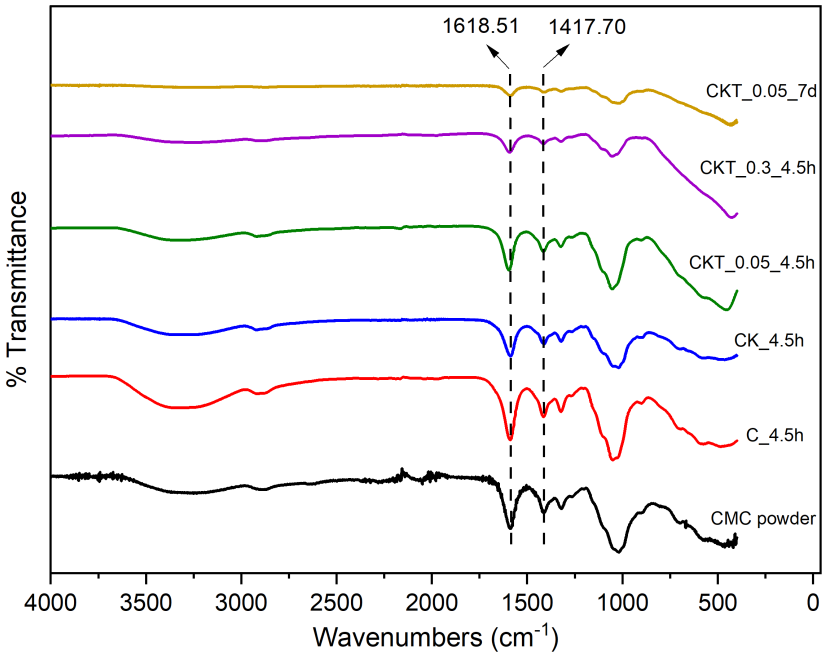

Figure 3.8 ATR-FTIR spectra of CMC powder and prepared samples.

3.3.3.3 X-ray Photoelectron Spectroscopy (XPS)

XPS serves as a quantitative spectroscopic method employed to examine a materials surface chemistry. It specifically assesses the elemental composition, establishes the empirical formula, scrutinizes the chemical state, and explores the electronic state of the constituent elements within the material. The acquisition of XPS spectra involves subjecting a material to X-ray irradiation and concurrently measuring the kinetic energy and the quantity of electrons emitted from the uppermost 1-10 nm of the material under analysis.[307] This study aims to employ XPS analysis to discover the elemental composition of CKT foam, emphasizing the electronic states of each significant constituent. Furthermore, this analysis aims to identify the formation of novel bonds between CMC and TiO_2, particularly for its relevance in enhancing the material's photocatalytic activity.

According to the C1s elemental analysis, five peaks could be identified at 284.7 eV (C-C bond), 286.3eV (C-OH bond), 288.1eV (C=O bond), which are typical functional groups in CMC, 285.4eV (C-O-Ti bond) and 293.0eV (π-π* shake up satellite peak).[308] Satellite peaks arise when a core electron is removed by photoionization. With respect to O1s elemental analysis, five peaks could be observed at 529.3eV (Ti-O-C), 531.1eV (C=O), 532.5eV (C-O/ O-C=O), 533.3eV (C-O-C) and 535.8eV (Na auger peak).[307] As in Figure 3.9, the high resolution XPS

Ti 2p spectra could be fitted considering the peaks at 458.1eV and 463.6 which are attributed to Ti $2p_{3/2}$ and Ti $2p_{1/2}$ spin orbitals splitting photoelectrons in the state of Ti^{4+}.[308] XPS results reveal that Ti has bound to CMC but in contrast the low intensity of Ti peaks in C1s and O1s can be due to the low amount of TiO_2 used compared to CMC.

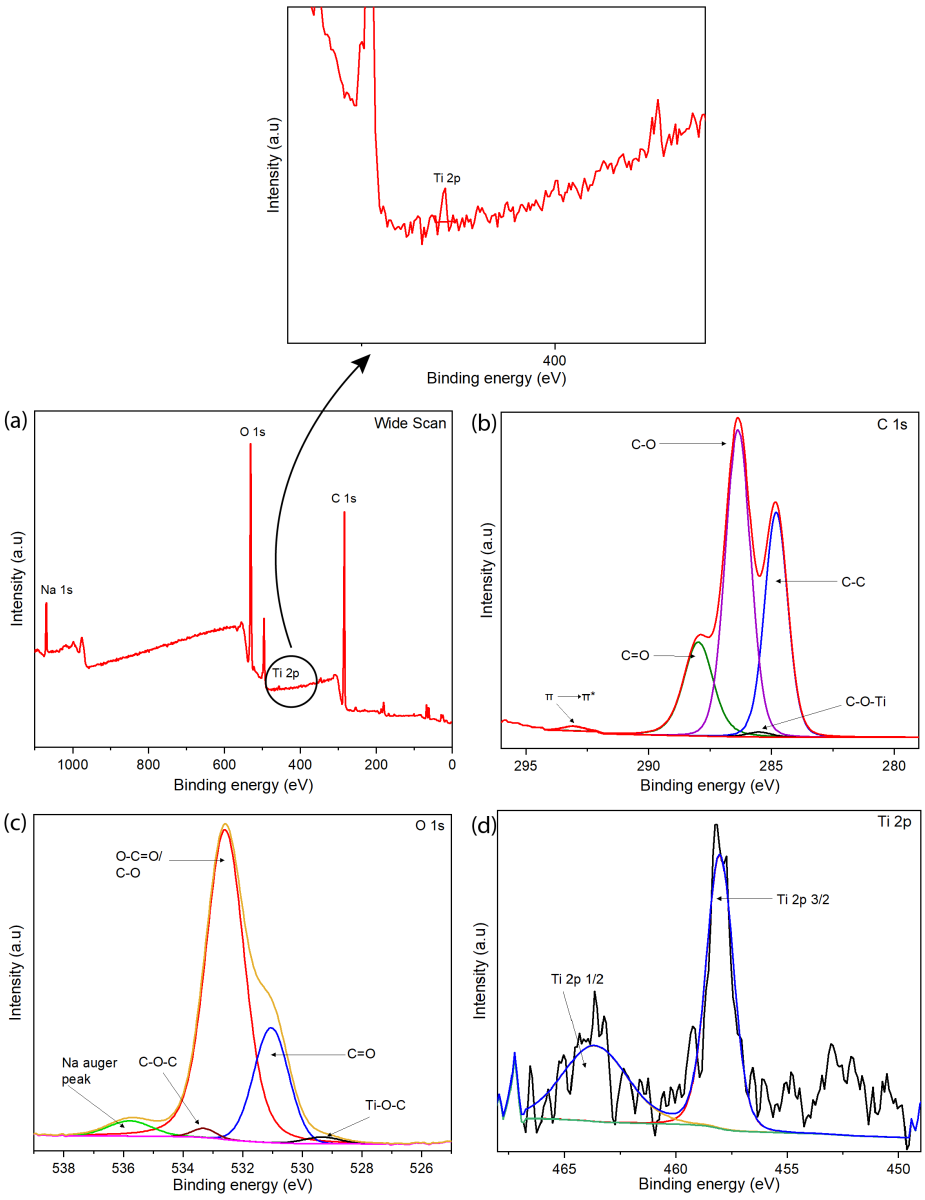

Figure 3.9 XPS profiles of CKT foam, (a) wide scan, (b) high resolution C1s, (c) high resolution O1s, and (d) high resolution Ti2p.

3.3.3.4 Thermogravimetric Analysis (TGA)

TGA is a technique that provides the information about the stability of a compound under a certain temperature range through the process of weight loss upon heating. This research aims

to utilize TGA)to assess the thermal stability of the resultant CKT foam. Understanding this stability is crucial for evaluating the material's viability in wastewater treatment applications, particularly under diverse conditions like elevated temperatures.

TGA curves (Figure 3.10) give an indication of the thermal stability of CMC powder and the prepared samples. The first stage transition at 45-120 ºC is due to the loss of physically adsorbed water - about 3% w/w in foams and 6-7% w/w in CMC.[257] Since all the foams were prepared by freeze drying, it was expected to remove all the free water but it has been reported, polysaccharides can contain some amount of water – likely a form of structural water - while appearing to be dry[296], and of course can absorb moisture from the air through preparation. Redrying the foams leads to hard and brittle samples. The second stage of heating at 200–300 ºC sees further weight loss of approx. 45% in all cases, attributable to degradation of saccharide rings of CMC and evolution of CO_2 from the polysaccharide chain. The last stage of weight loss above 300 ºC is due to the further breaking of − C− O− C bonds in CMC and a charring of the sample.[162] This is roughly 30-40% of the loss.

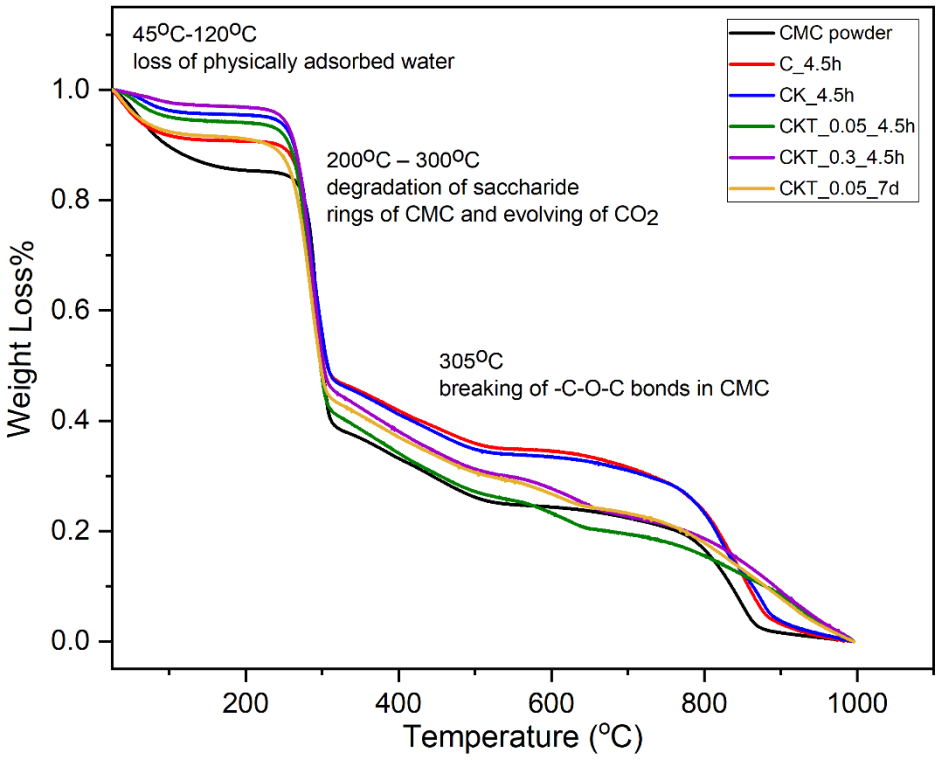

Figure 3.10 TGA curves of CMC powder and prepared samples

3.3.3.5 Scanning Electron Microscopy (SEM)

SEM is a method that uses a finely focused electron beam and reveals the information on topography of a samples such as, particle size, size distribution, particle shape and surface morphology. This study aims to employ SEM analysis to discern changes in the morphology of CKT foam concerning its constituent materials; CMC and TiO_2. This analysis seeks to characterize variations in particle shapes and sizes within the CKT foam compared to its individual raw materials.

As shown in SEM images (Figure 3.11), CMC powder has a rod like structure, but the foams have sheet like structures at the micrometre scale. According to literature, freeze drying techniques can result in both sheet like or network structure with pores.[156] The foam with only CMC and the foam with both CMC and KBr seem to have similar morphologies. Contrary, the foam which has all CMC, KBr and TiO_2, exhibited some small particles on the sheet which can be assumed as TiO_2 crystallites on CMC polymer sheets.

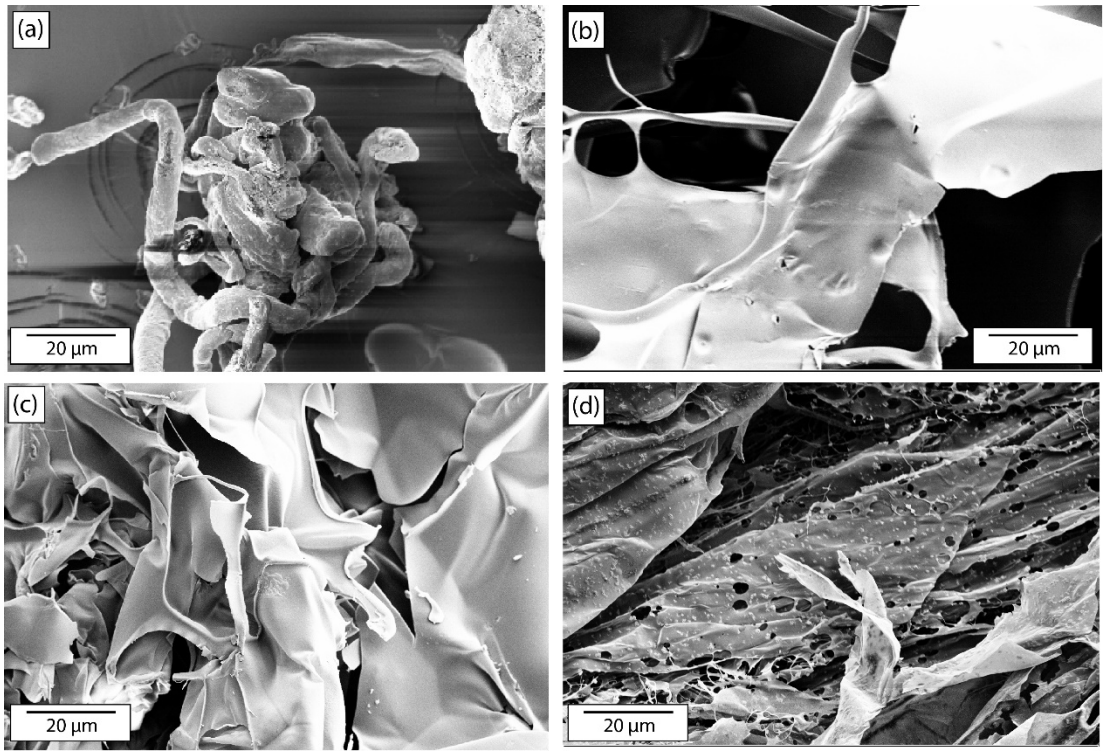

Figure 3.11 SEM images of (a) CMC powder showing rod-like structures, (b) C_4.5h, (c) CK_4.5h, and (d) CKT0.05_4.5h, all showing a more sheeted structure.

3.3.3.6 Energy-Dispersive X-Ray (EDX) Spectroscopy and Elemental Mapping

EDX is a method designed to analyse the elemental composition of a sample. Elemental mapping allows us to visualise the spatial distribution of elements in a particular sample. This study aims to utilize EDX and elemental mapping analysis to characterize the distribution of TiO_2 within the polymer matrix.

The element distribution of the foam with all CMC, KBr and TiO_2 is given in Figure 3.12 and the visualised elements carbon, oxygen, sodium, potassium and titanium have a homogeneous spatial distribution. The elements, carbon, oxygen, sodium are attributed to CMC that is in its sodium salt form and potassium from KBr. According to the images, carbon, oxygen, sodium has distributed densely rather than potassium and titanium which can be due to the large amount of CMC in the foam. The most important fact obtained from this analysis is that TiO_2 has distributed homogeneously and uniformly. By analysing all the results, it can be assumed that the charges on the surface might be the reason behind the homogeneous distribution of TiO_2 and this will be explained elaborately along with zeta potential.

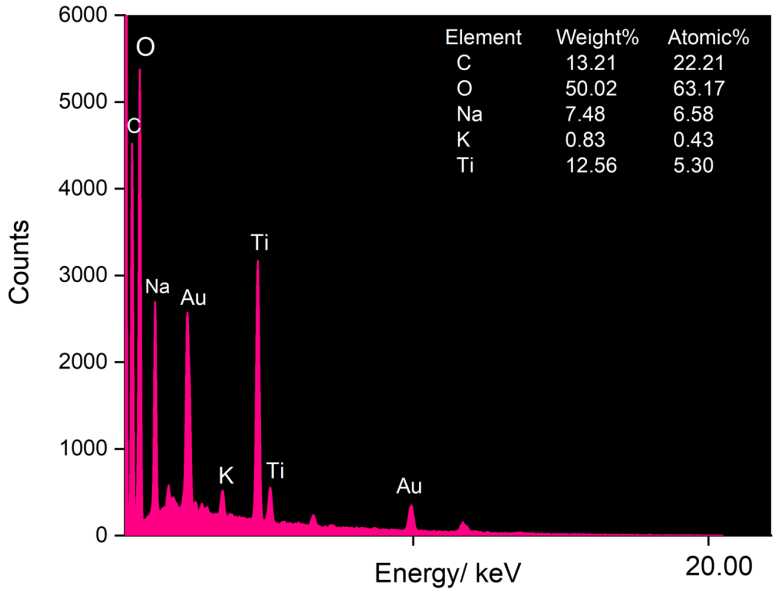

Figure 3.13 confirms the EDX mapping for the foam, indicating the elements present are consistent with the composition. The gold peaks are a result of the coating needed for the technique.

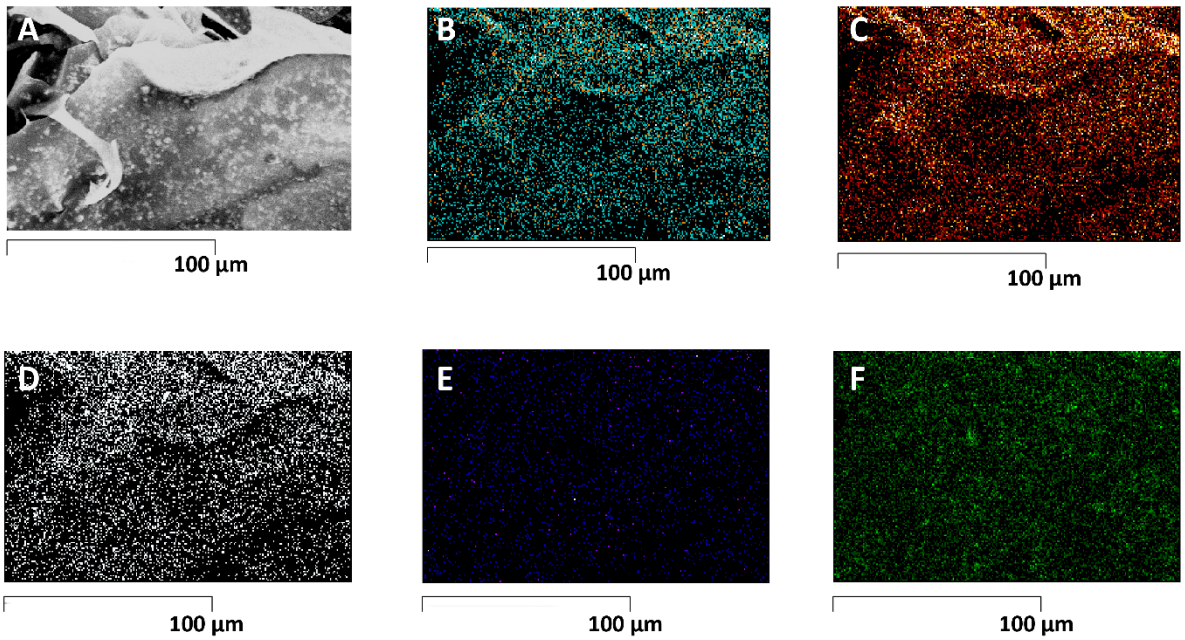

Figure 3.12 Elemental mapping of the foam with CMC/KBr/TiO_2 (A) CKT0.05_4.5h; (B) C; (C) O; (D) Na; and (E) K

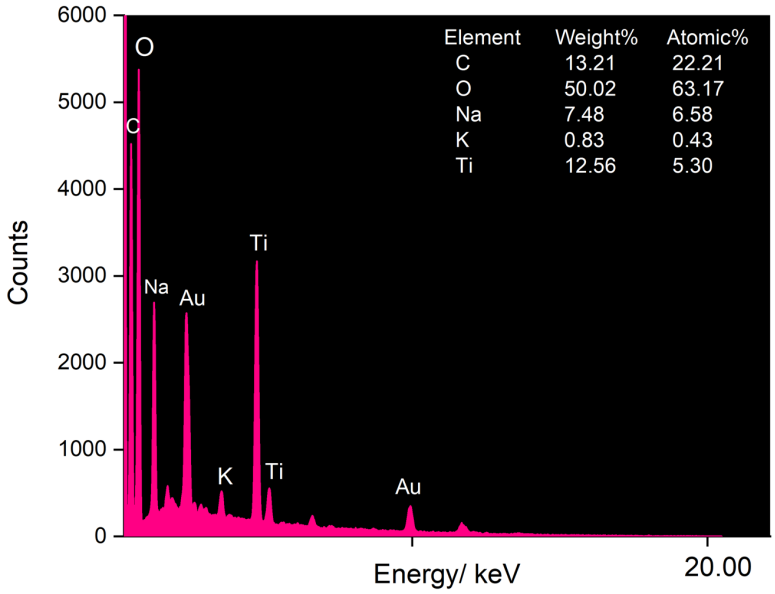

Figure 3.13 EDX plot for the foam with CMC/KBr/TiO_2

3.3.3.7 Zeta Potential Analysis

Zeta potential gives an implication about the surface charge and the potential stability of the suspension. This study aims to employ zeta potential analysis to ascertain the surface charges

and evaluate the stability of the CKT suspension in an aqueous medium. This analysis holds significance in ensuring efficient adsorption and photocatalytic capabilities.

As shown in Table 3.4, the samples with all CMC, KBr and TiO_2 has the highest magnitude of zeta potential, following KBr/TiO_2 suspension the second and the TiO_2 suspension, the lowest. When the magnitude is high, the stability of a compound in a certain solvent is high, which means that compound does not tend to agglomerate. Therefore, the stability of CKT foam in water can be explained in detail as follows. TiO_2 nanoparticles tend to agglomerate rather instantly due to its high surface are which causes the high surface energy. This agglomeration reduces the surface area and the photocatalytic activity. Agglomeration occurs due to the Van der Waal's attraction among particles, but this can be counterbalanced by electrostatic and steric stabilisation, which gives the term, 'electrosteric stabilisation'.[309] Electrostatic stabilisation can be obtained by adding a charge to the nanoparticles as they can repel each other while steric stabilisation can be achieved by adsorbing a thin layer of a polymer on the surface of nanoparticles to prevent them getting closer to each particle. With a polyelectrolyte like CMC, electrosteric stabilization can be obtained easily. The polyelectrolyte can adsorb on the particle surface and neutralize the charge.[310]

Table 3.4 Zeta potential values for different suspensions of tested samples.

Sample	**Zeta potential (mV)**
TiO_2 suspension	-17.6
KBr + TiO_2 suspension	-23.2
Sample C with CMC + KBr + TiO_2	-71.5

According to the results, the magnitude of the zeta potential of the TiO_2 suspension has increased slightly by the addition of KBr because KBr is an electrolyte, yet it is not that strong to separate TiO_2 particles and stabilize the suspension in better way. But the addition of CMC has increased the magnitude of the zeta potential for KBr/TiO_2 suspension three-fold making the suspension more stable. Previous research indicates that higher the magnitude of the zeta potential, higher the stability of the suspension.[311] This drives homogeneity of the dispersion/distribution of TiO_2 which is supported by the elemental mapping (Figure 3.12). By considering all the above facts and literature data, we can assume that there's thin layer of CMC adsorbed on TiO_2 particles as in Figure 3.14.[294, 312]

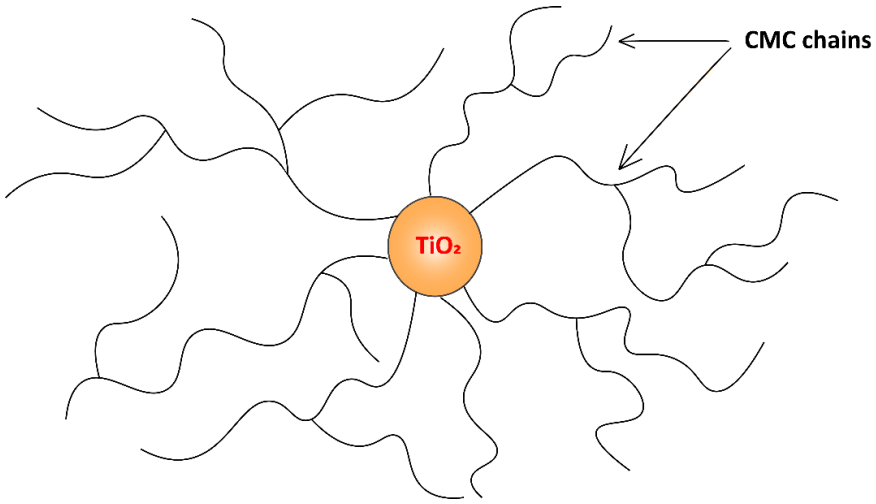

Figure 3.14 Schematic diagram of CMC adsorbed on TiO_2 particles.

3.3.3.8 Brunauer–Emmett–Teller (BET) Analysis

BET analysis is important characterisation technique to measure some unique properties of a solid sample such as surface area, pore volume, pore size distribution and also adsorption desorption isotherms can give a relative idea on the structure. BET occurs by physical adsorption of N_2 gas on to the sample and the specific surface area is determined by calculating the amount of adsorbate gas molecules corresponding to the monolayer surface of the sample at the given pressure and the temperature. This study aims to utilize BET analysis to assess the surface area and pore volume of CKT foam. These parameters are critical for optimizing pollutant adsorption efficacy.

The main characterisation parameters obtained using N_2 adsorption-desorption isotherms are shown in Table 3.5.

Table 3.5 The main characterisation parameters obtained from BET analysis.

Sample	**Surface area m^2/g**	**Average Pore volume cm^3/g**	**Average pore size /A**
CMC powder	23	0.02	41
TiO_2 (P25) powder	115	0.1	44
CKT0.05_4.5h	11	0.2	40

All the prepared samples have comparably high calculated surface areas and pore sizes. Pore size is important in waste water treatment because if the pore size is too large, the filtration

efficiency is poor. Size of pores depends on different facts including materials used, synthesis process and drying method.[313] Therefore, it can be assumed that freeze drying has caused accessible pores in the foams prepared. When freezing prior to the drying, growth of ice crystals takes place. These ice crystals are removed during the drying process via sublimation, resulting the pores where the ice crystals are. It is unclear whether the reason behind the large area is the drying method or the well dispersion.[303, 314]

3.3.4 Methylene Blue (MB) Degradation Test for Foams

This set of experiments was conducted to investigate the photocatalytic activity of the prepared samples through the degradation of MB via a simple UV-Vis study.

3.3.4.1 Adsorption Kinetics

Adsorption is an important process in any catalytic process, but especially wastewater treatment, because it is the adsorbed molecules that are degraded via photocatalytic activity generating more vacant sites for further reaction. This process as seen with foams and MB are shown in Figure 3.15. Initially, the MB is adsorbed onto the composite in the dark to some level. The higher the adsorption, the better. Once stabilised, irradiation of the solution allows the photocatalytic process to begin. Clearly, decomposition products form which are colourless, allowing further adsorption to occur. This ultimately leads to a reduction in optical absorption over time.

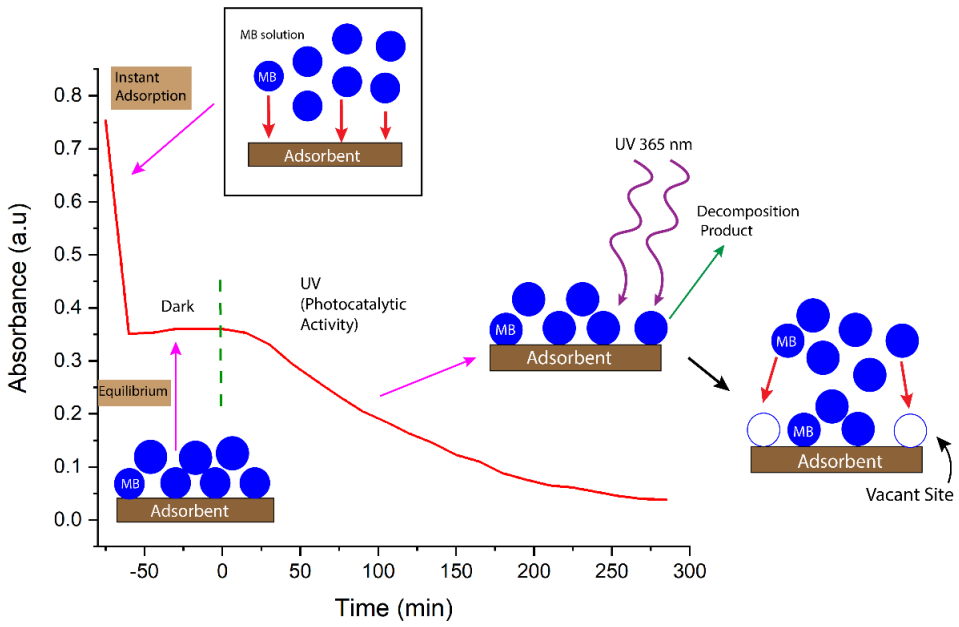

Figure 3.15 Suggested MB Adsorption-degradation mechanism. The green dotted line serves to distinguish between the dark and photocatalytic processes. This division clarifies that ample time is allotted for dye absorption to reach equilibrium in the dark process before the initiation of the photocatalytic phase.

Adsorption of MB on to the photocatalyst prior to the degradation is a major step to ensure that any decrease in absorbance was due to photocatalytic degradation and not because of adsorption of the dye (the green dotted line in Figure 3.15).[315] In that case, all photocatalyst/dye mixtures were initially left in the dark until adsorption was deemed complete before the samples were irradiated. In this project, all samples were kept in dark for 75 minutes (with this sample, MB reached its adsorption-desorption equilibrium within 75 minutes) until the adsorption-desorption equilibrium and CKT foam showed the highest adsorption (52.99%) during that period. As seen in

Figure 3.16, CMC powder shows a high adsorption rate while TiO_2 doesn't, implying that carboxyl groups play a vital role in adsorbing MB.[316] Since CMC has more negative charges, as a result of the exchange of proton between carboxylic acid and its conjugate base, it can easily attract cationic MB dye molecules. Even if TiO_2 powder itself doesn't show a good adsorption, CKT 0.05 foam has a higher adsorption rate than CMC powder indicating that TiO_2 powder also has a contribution towards adsorption when in the composite.

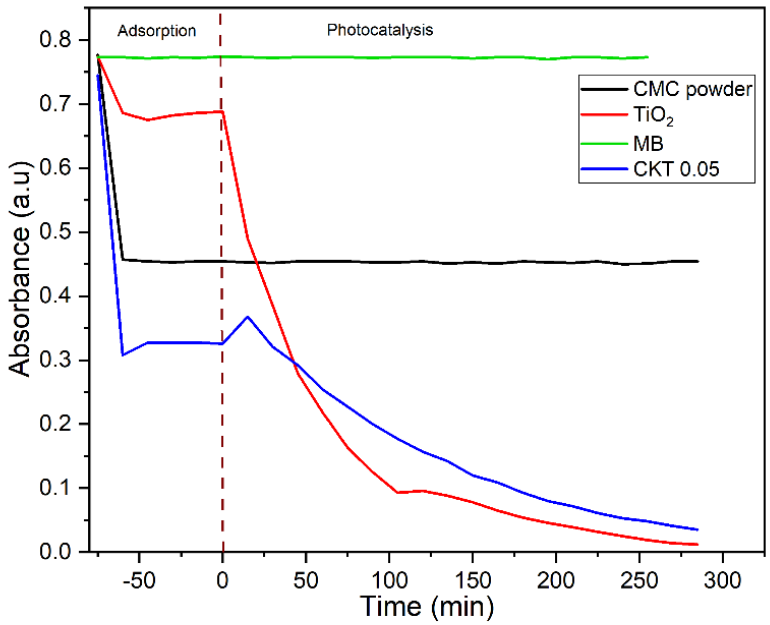

Figure 3.16 MB degradation under UV irradiation.

The adsorption kinetics were investigated using both *pseudo* first and second order kinetics model:[317]

Pseudo first order kinetics model: $\ln(Qe - Qt) = \ln Qe - kt$ Equation 3.2

Pseudo second order kinetics model: $\frac{t}{Qt} = \frac{1}{kQe^2} + \frac{t}{Qe}$ Equation 3.3

Where,

Q_e – Adsorption capacity at equilibrium (mg/g)
Q_t – Adsorption capacity at a given time (t)
K – adsorption constant ($gmg^{-1}min^{-1}$)
T – time (s)

Adsorption capacity at a given time can also be calculated using:[318]

$$Q = \frac{(Co - Ct)V}{m}$$ Equation 3.4

Where,
C_0 – initial concentration (mg/L)
C_t – Concentration at a given time
V – volume of the solution (mL)
M – mass of the sorbent (g)

And the adsorption rate percent calculated using the formula:

$$\text{Adsorption rate\%} = \frac{(Co - Ct)100}{Co}$$ Equation 3.5

Where,
Co – initial concentration
Ct – concentration at time t

Figure 3.17 shows the calculated *pseudo* second order graphs of CMC powder, TiO_2 powder and CKT foam. The adsorption capacity at equilibrium was calculated using the slope of the graph while adsorption rate constant was determined using the intercept.

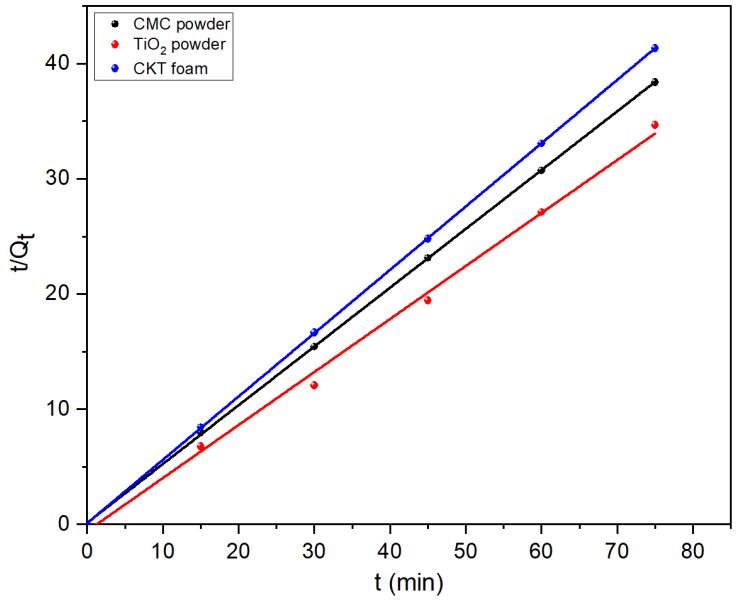

Figure 3.17 *Pseudo* second order kinetics plot of the absorption characteristics.

Table 3.6 summarises the results obtained from *pseudo* first order and second order calculations which depicts that the adsorption of MB on these adsorbents follows *pseudo* second order kinetics model. Furthermore, to substantiate this conclusion, it is evident that the theoretical adsorption capacities at equilibrium derived from *the pseudo* second order kinetics align more closely with the experimental parameters. Since MB system was kept in dark for 75 minutes to make sure it had reached adsorption-desorption equilibrium, adsorption rate after 75 minutes was calculated for each sample. According to the results, CKT 0.05 foam has the highest removal% of MB (53%) while TiO_2 powder has the least (11%). Moreover, removal % of MB by CMC powder is 41.5 %.

Table 3.6 Adsorption kinetics data obtained from MB testing.

Parameters	**CMC powder**	**TiO_2**	**CKT foam**
Experimental Q_e (mg/g)	1.895	2.239	1.814
MB removal by adsorption %	41.50	11.63	52.99
***Pseudo* first order**			

Theoretical Q_e (mg/g)	0.323	1.126	0.928
K (min^{-1})	0.07	0.03	0.07
R^2	0.6899	0.7040	0.7589
***Pseudo* second order**			
Theoretical Q_e (mg/g)	1.958	2.418	1.818
K (g/mgmin)	2.19	0.24	3.25
R^2	0.9996	0.9948	0.9999

3.3.4.2 Intra-particle Diffusion Mechanism

In the adsorption process, investigation of diffusion and mass transfer steps will help to understand the adsorption mechanism. As reported in the literature, the adsorbate (MB molecules) diffuses to the film surrounding the adsorbent through the bulk of the solution, then through micro- and macro-pores, ending up with adsorption.[319] This process of transportation of MB molecules in to the adsorbent can be identified as four steps (Figure 3.18):

- Bulk,
- Film,
- Intra-particle diffusion, and
- Adsorption.

Since bulk/mass movement and adsorption are fast processes they are not considered in adsorption kinetics and also, they are still under further investigation when it comes to heterogeneous adsorption.[320] Therefore, only film diffusion and intra-particle diffusion are taken into kinetics calculations. Film diffusion is mainly based on slow transference of MB molecules to the surface of adsorbent from the boundary layer and this is also called external diffusion. Intra-particle diffusion is mainly about pore diffusion and this is also named as internal diffusion.[321]

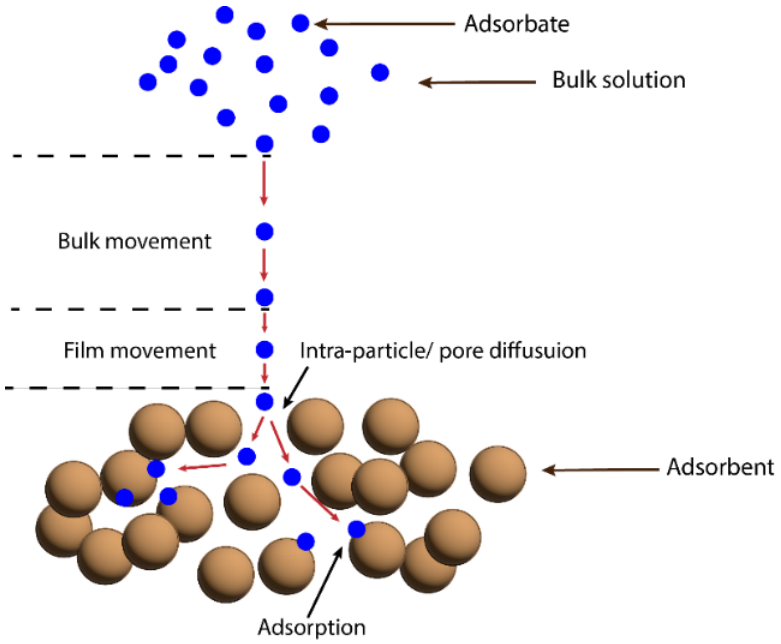

Figure 3.18 Schematic diagram illustrating potential steps of transportation of adsorbent to adsorbate from bulk solution.

Therefore, to identify the adsorption process of a heterogeneous system from a mechanistic point of view Web-Morris model was used:

$Q_t = \mathrm{Ki} * \mathrm{t}^{0.5}$ Equation 3.6

Where,
Q_t – adsorption capacity at time t
K_i – intra-particle diffusion rate constant (mg/gmin$^{0.5}$)

According to this model, the plot of Qt vs $t^{0.5}$ should pass through origin without an intercept, indicating intra-particle diffusion is the rate-limiting step. While a useful guide, it has been proved that not all adsorption systems follow Web-Morris model, but some systems give a plot with an intercept, expressing both film diffusion and intra-particle diffusion participate in diffusion mechanism. Thus, the following new equation has been introduced as the *Intra-particle diffusion model*.[322]

$\mathrm{Q_t} = \mathrm{Ci} + \mathrm{Ki} * \mathrm{t}^{0.5}$ Equation 3.7

Where C_i – constant related to boundary layer thickness

The plot of Qt vs $t^{0.5}$ was plotted for the three samples used (Figure 3.19) and the data is also shown in Table 3.7.

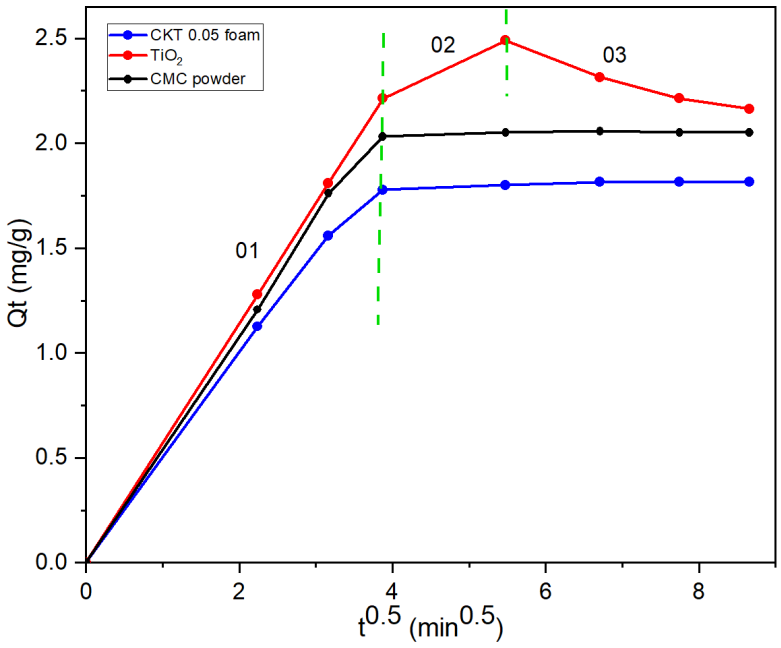

Figure 3.19 Intra-particle diffusion plot of CKT0.05 foam, TiO_2 and CMC powder.

Table 3.7 Kinetics data calculated from using the Intra-particle diffusion model

Sample	**Ki (mg/gmin$^{0.5}$)**			**Ci (mg/g)**		
	Section 01	**Section 02**	**Section 03**	**Section 01**	**Section 02**	**Section 03**
CMC powder	0.4877	-	0.0123	-	-	1.85
TiO_2 powder	0.5718	0.1726	0.1035	-	1.54	3.03
CKT 0.05 foam	0.4593	-	0.0076	$2x10^{-16}$	-	1.75

Plots of both CMC powder and CKT0.05 foam showed the same curve shape, known as a von Bertalanffy curve, with two main features – a regular linear section which is attributed to film diffusion, followed by a asymptote characteristic of the system reaching its adsorption-desorption equilibrium. In contrast, TiO_2 powder shows a more complicated relationship that appears at first glance to be biphasic. While von Bertalanffy curve features exist, a second process can be described as the slow diffusion of solutes into pores or intra-particle diffusion occurs attenuating the curve similar asymptotes to those of CMC powder and the composite.[323]

3.3.4.3 Effect of Initial pH on Adsorption of MB on CMC

Initial pH is a critical factor in adsorption because it can control the protonation/deprotonation of functional groups.[324] A simple adsorption experiment was carried out with CMC powder to

observe how the initial pH value of MB solution affects on the adsorption of MB on CMC powder and the kinetics data received from *pseudo*-second order plot have been tabulated in Table 3.8. According to the observed data, pH 3 has the lowest adsorption rate and capacity because the acidic medium tends to protonate carboxylate groups, thus acquiring more neutrality to positive charge through hydroxonium ion interaction.[325] Since MB is also positively charged, a repulsion takes place between MB and CMC at lower pH which reduces the adsorption.[326] On the contrary, increasing pH leads to increasing adsorption due to more carboxylate groups at higher pH value, facilitating more interactions between MB and CMC.

Table 3.8 Pseudo-second order kinetics data for CMC powder at different pH

	pH = 3.00	**pH = 6.32**	**pH = 10.30**
Amount of dye adsorbed at equilibrium (mg/g)	1.06	1.96	2.05
Adsorption rate constant ($gmg^{-1}min^{-1}$)	0.45	2.19	12.03
Removal of MB by adsorption %	22.65	41.50	42.02

Figure 3.20 shows a plot of adsorption capacity over 110 minutes for CMC at different pH to obtain stable readings. An interesting feature occurs above the pKa of the carboxylic acid, from pH 6 to 10, where a slight increase in adsorption capacity at a given time is seen. We postulate that when the concentration of OH^- is increasing in the system, hydroxyl ions can combine with MB molecules and for hydroxylated MB which causes decreasing adsorption.[325]

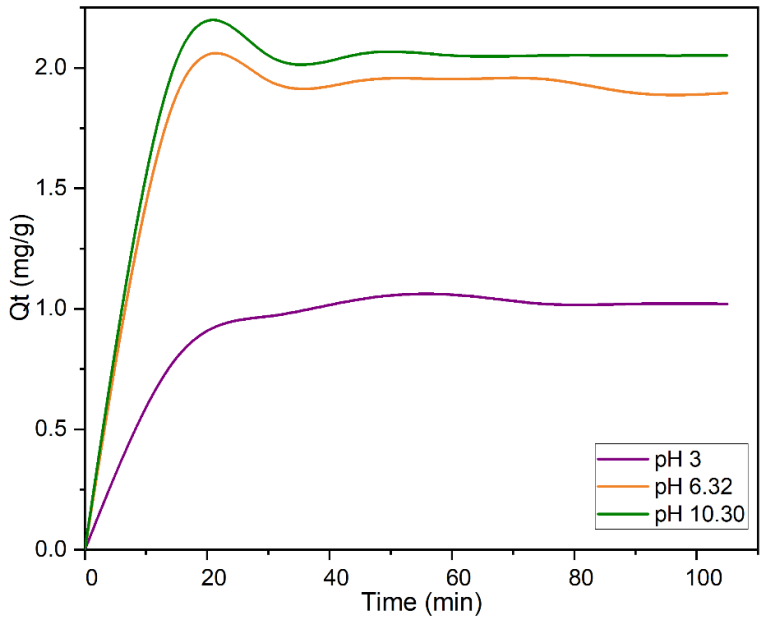

Figure 3.20 Adsorption capacity over time of CMC powder at different pH.

3.3.4.4 Adsorption Isotherms

An adsorption isotherm describes the co-relation between the adsorbent and the adsorbate including how the adsorbate molecules are attached on to the adsorbent surface when the system reached its equilibrium. Based on the nature of the adsorbent and the interactions between the adsorbent and the adsorbate, the system can follow different mathematical functions such as, Langmuir, Freundlich and Linear.[327] In this study, Langmuir and Freundlich studies were employed to explain the affinity of MB towards CKT foam.

Langmuir adsorption, occurs on a homogenous adsorbent is considered as the monolayer adsorption whereas the Freundlich model is based on the heterogeneous adsorption for a surface with a non-uniform heat of adsorption over the surface. The models can be expressed using following equations.

Langmuir adsorption isotherm $$\frac{1}{Q_e} = \frac{1}{Q_m} + \frac{1}{K_L Q_m}\frac{1}{C_e}$$ Equation 3.8

Freundlich adsorption isotherm $$\ln Q_e = \ln K_f + (1/n) \ln C_e$$ Equation 3.9

Where, Q_e is the adsorption capacity at equilibrium (mg/g) and C_e is the equilibrium concentration (mg/L).

In Langmuir model, Q_m is the saturation/maximum monolayer adsorption capacity (mg/g) and K_L is the Langmuir isotherm constant (L/mg). From the intercept and the slope of the plot $\frac{1}{Q_e}$ vs $\frac{1}{C_e}$ given in figure 3.2.1, Q_m and K_L can be calculated respectively. Furthermore, another important, dimensionless term based on Langmuir model is separation factor, R_L, stated by following equation, describes the favorability of MB adsorption on to the CKT foam.

$$R_L = \frac{1}{1+(K_L * C_o)}$$ Equation 3.10

Co is the highest studied initial concentration (mg/L). As stated in the literature, the adsorption is favourable when $0 < R_L < 1$, irreversible when $R_L = 0$, linear when $R_L = 1$ and unfavorable when $R_L > 1$.[328]

In Freundlich model, K_f is the Freundlich constant related to maximum adsorption capacity $[(mgg^{-1})(Lmg^{-1})^{1/n}]$, 1/n is the heterogeniety factor and n is an indication of the intensity of the

adsorption process. K_f and n can be obtained from the graph of ln Q_e vs ln C_e as given in Figure 3.21.

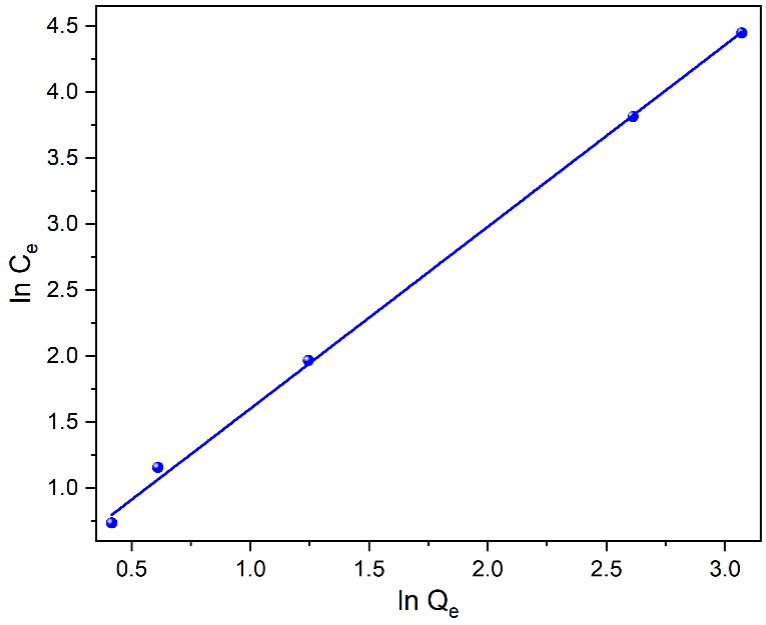

Figure 3.21 Freundlich adsorption isotherm plot of CKT 0.05 foam

The results as shown in Table 3.9 reveal that the adsorption of MB on to the CKT foam is well-fitted using the Freundlich model (from R^2 values), indicating that multi-layer adsorption is favorable. The calculated value for 1/n is higher than 1 which implies that the adsorption is a favorable physical process.[329] Moreover, as mentioned in the literature, when n < 1, the molecules adsorb on to the surface with a horizontal position via multi-layer adsorption.[330]

Table 3.9 Adsorption isotherm data obtained from MB adsorption on CKT foam.

Adsorption model	**Langmuir Isotherm**				**Freundlich Isotherm**		
Parameters	Q_m (mg/g)	K_L (L/mg)	R_L	R^2	K_f	1/n	R^2
Values	19.925	0.063	0.136	0.9313	1.168	1.4017	0.9988

3.3.4.5 Photocatalytic Activity and Kinetics of Composite

Methylene Blue is the gold standard in photocatalytic reactions, as the by-products from the degradation are usually colourless, meaning absorption spectroscopy is a simple and effective way to monitor reaction progress over time, through the diminution of absorption measured at

665 nm. The photocatalytic activity of the prepared CKT 0.05 foam was investigated under UV as shown earlier in the Figure 3.16. Results indicates that MB solution alone showed no effect from the UV light without the photocatalyst, as evidenced by the absorption integrity over time. Similarly, CMC powder alone, after adsorption, did not show any effect on MB under UV, confirming that it is the action of the TiO_2 needed to have photocatalytic activity. In comparison of the photocatalytic effect on degradation of anatase TiO_2 and CKT 0.05 foam, MB degradation rate is lower in CKT0.05 foam than that of TiO_2 powder itself. In line with previous studies, it can be hypothesized that, CMC has adsorbed and formed a thin layer on TiO_2 particles, as discussed in zeta potential analysis, and the photo-generated radicals need to come to the surface to degrade MB, but this layer might impede the generated radicals reaching MB. Also, it is reasonable to consider that these radicals are highly reactive and transient, meaning they wouldn't last until they reach the surface of the micelle. On the other hand, the low rate of degradation might be ascribed by prevention of forming hydroxyl radicals because of the Coulombic repulsion between the anionic surface charge and the hydroxyl anions.[331,332]

In order to determine the kinetics of removal of MB via photocatalysis, the Langmuir-Hinshelwood (L-H) model, as a first order reaction model was applied to the results. The L-H model is a modification of Langmuir model because, in photocatalysis, both adsorption and degradation are taking place under UV.[333]

$$\ln\left(\frac{C_o}{C}\right) = K_{app} * t \qquad \text{Equation 3.11}$$

Where,
C_o – initial concentration of MB
C – concentration of MB at time t
K_{app} – apparent rate constant

The apparent rate constant (K_{app}) can easily be calculated from the graph of ln (Co/C) *vs* t as in Figure 3.22. All the kinetic data calculated is given in Table 3.10.

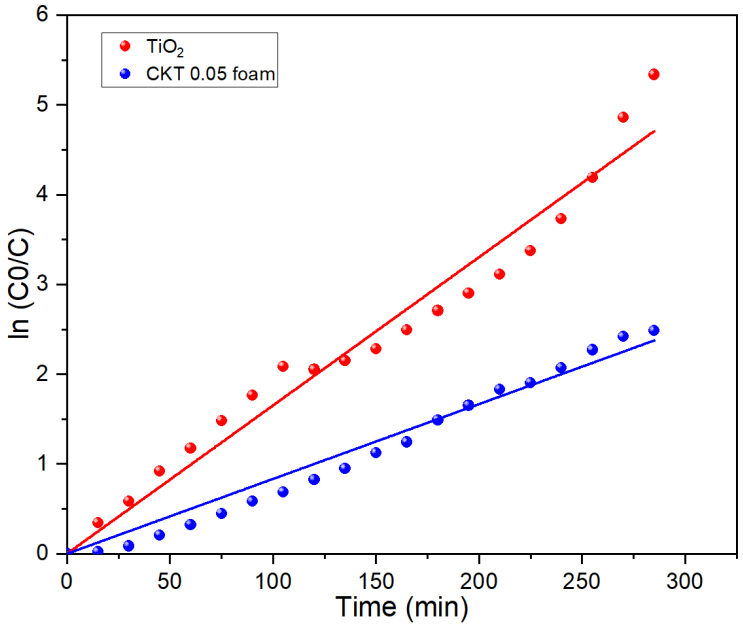

Figure 3.22 *Pseudo*-first order kinetics plot for the degradation of MB using CKT0.05 foam and TiO_2 powder.

Kinetics data supports initial evidence that the photocatalytic rate of TiO_2 is higher than the foam. Also, in TiO_2, two sections can be seen in the graph, indicating a two-stage oxidation of MB. During the first 105 minutes degradation rate was intense with a good linear coefficient of 0.999, after which rate changes. The second stage postulated to be due to the formation of intermediates and their binding to the photocatalytic surface, reducing necessary surface area for MB molecules to bind before removal and a more exponential growth curve develops. The formed intermediates block the active vacant sites and thus, lower the photocatalytic rate. Another reason for that can be low adsorption capacity of TiO_2.[334] Compared to that, CKT0.05 foam significantly shows only one type of behaviour which highlights that even with intermediates, it has a good adsorption capacity (Table 3.10).

Table 3.10 Kinetics data for photocatalytic activity of TiO_2 powder and CKT0.05 foam

	TiO_2		**CKT0.05 foam**
	Section 01	**Section 02**	
R^2	0.9992	0.9347	0.9955
Kapp (min^{-1})	0.0196	0.0912	0.0094
% Removal of MB by photocatalysis	99.51		91.66
Total % removal after 6 h	99.57		96.11

3.3.4.6 Effect of Photocatalyst Dosage

The effect of photocatalyst dosage on MB removal was investigated by using 0.5 g/L, 0.95 g/L, 1.4 g/L and 1.9 g/L adsorbent using 10 ppm of MB solution and were performed in duplicate. All the data are presented in Table 3.11 and Figure 3.23. The highest adsorption is given with 0.5 g/L and 0.95 g/L and with the increase of the catalyst dosage, the rate of MB removal by adsorption was found to decrease. This can be mainly rationalised because of overcrowindg of adsorbent particles which can cause overlaping of adsorption sites.[335]

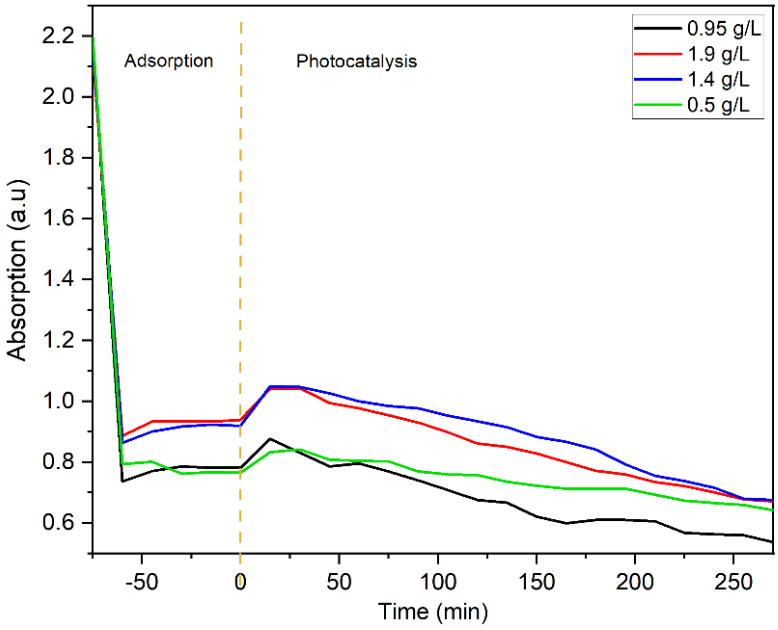

Figure 3.23 Photocatalytic degradation of MB with different amounts of photocatalyst in the system.

When it comes to photocatalytic activity, the 0.5 g/L solutions showed the lowest photocatalytic rate due to the low amount of photocatalyst in the medium. Similar to the adsorption scenario, the photocatalytic rates of 1.4 g/L and 1.9 g/L are lower than that of 0.95 g/L due to the decrease of the efficiency of the photo-Fenton system.[336] In a system with an excess amount of photocatalysts, the active sites can be blocked, catalysts can be clumped together, which can act as a light screen and moreover excess catalysts can make the solution cloudy making it difficult to penetrate light through the solution. Moreover, excessive formation of hydroxyl radical can led to self-scavanging reactions.[337] Therefore, considering all the facts, 0.95 g/L was taken as the most suitable amount of catalyst for this experiment.

Table 3.11 Kinetics data for different amounts of catalytic dosage.

	0.5 g/L	**0.95 g/L**	**1.4 g/L**	**1.9 g/L**
Adsorption rate constant ($gmg^{-1}min^{-1}$)	0.24	0.65	0.65	1.17
Adsorption % after 75	67	66	59	58
Photocatalytic rate constant (min^{-1})	0.001	0.0021	0.002	0.0019
Photocatalytic removal% after 6 h	73.12	78.68	71.24	71.06

3.3.4.7 Effect of Amount of TiO_2 in the Adsorbent on Removal of MB

Degradation of MB is mainly driven by TiO_2 as a photocatalyst. The optimum amount of TiO_2 in the adsorbent is an important parameter in industry. To determine how the amount of TiO_2 in the adsorbent affects the removal of MB, CKT foams were prepared as given in the Table 3.12 below. All adsorption and photocatalysis kinetics data are presented in Table 3.13.

Table 3.12 Prepared CKT foams with different amount of TiO_2

	CMC (g)	**KBr (g)**	**TiO_2 (g)**
CKT 0.025 foam	0.2	0.01	0.25
CKT 0.05 foam	0.2	0.01	0.05
CKT 0.1 foam	0.2	0.01	0.1
CKT 0.5 foam	0.2	0.01	0.5

The outcomes illustrate that the augmentation of TiO_2 quantity has exclusively impacted the adsorption process. Even though the individual adsorption efficacy of TiO_2 powder appears marginal, its role becomes prominent as part of the CMC composite, creating more available sites for MB adsorption. Notably, the foam containing 70% w/w (CKT 0.5 foam) of TiO_2 exhibited the highest adsorption, while the foam containing 10% w/w (CKT 0.025 foam) of TiO_2 demonstrated the lowest. The consequential finding is that the foam with the lowest TiO_2 content showcased the highest photocatalytic activity as shown in Figure 3.24 and Table 3.13.

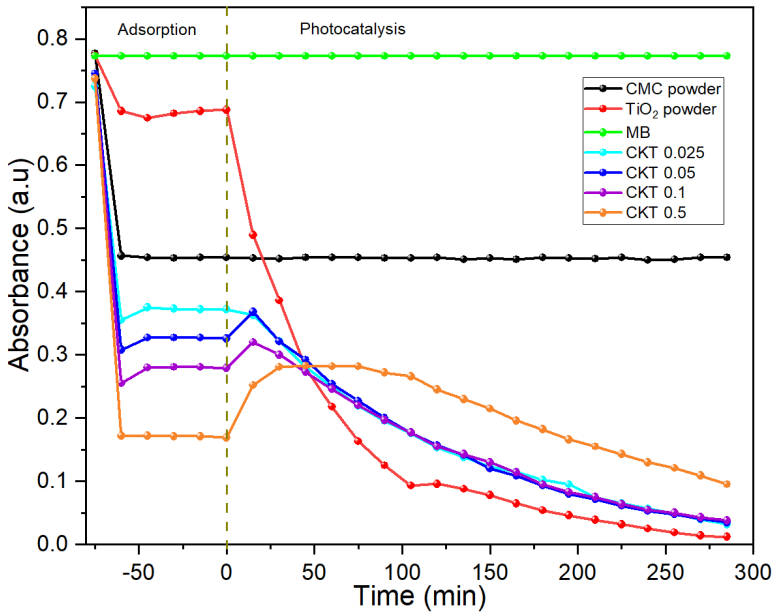

Figure 3.24 Removal of MB by CKT foams with different amount of TiO_2.

Table 3.13 Kinetics data for MB removal by different CKT foams.

	CKT 0.025 foam	**CKT 0.05 foam**	**CKT 0.1 foam**	**CKT 0.5 foam**
Amount of adsorbed at equilibrium (mg/g)	1.75	1.82	2.26	2.81
Adsorption rate ($gmg^{-1}min^{-1}$)	3.03	3.25	1.29	4.86
Removal of MB by adsorption %	49.28	52.99	62.61	77.99
Photocatalytic rate constant (Kapp) (min^{-1})	0.092	0.094	0.085	0.035
Removal of MB by photocatalysis %	93.56	91.66	89.25	49.17
Total removal of MB	96.75	96.11	95.98	88.15

The rationale for the declining photocatalytic rate with increased TiO_2 content mirrors a comparable scenario to the impact of adsorbent dosage on MB removal. Elevated TiO_2 content in the adsorbent can lead to greater leaching of TiO_2 into the solution, resulting in turbidity. Consequently, UV light penetration through the solution becomes challenging, impeding TiO_2 irradiation and thereby diminishing the photocatalytic activity rate. Simultaneously, it can be inferred that TiO_2 might aggregate within the solution, contributing to the reduced

photocatalytic rate.[338]This experiment revealed another unusual observation. In region A and B in Figure 3.25, desorption has been dominated in the adsorption-desorption equilibrium. Even if this scenario has not been deeply investigated, it is believed that this can be due to self-aggregation of MB in the solution. MB molecules generally tends to form dimers, trimers or H-type aggregates and the bonds that hold MB molecules together are believed to be hydrophobic interactions, H-bonds and van der Waal's forces.[339] When the bonds among MB molecules are stronger than the bonds between MB molecules and adsorbent, desorption can take place until the system reaches a new equilibrium. In addition, it is assumed that when UV irradiation occurs, the local pH of the system can be changed with formed products of MB degradation and this change can lead to changing charges and interactions within the system. Therefore, desorption can take place during that period. But as degradation continues, more vacant sites are created and the system starts moving forward with more adsorption. It is clear this hypothesis needs to be further studied as this has not been reported greatly in the literature.[340]

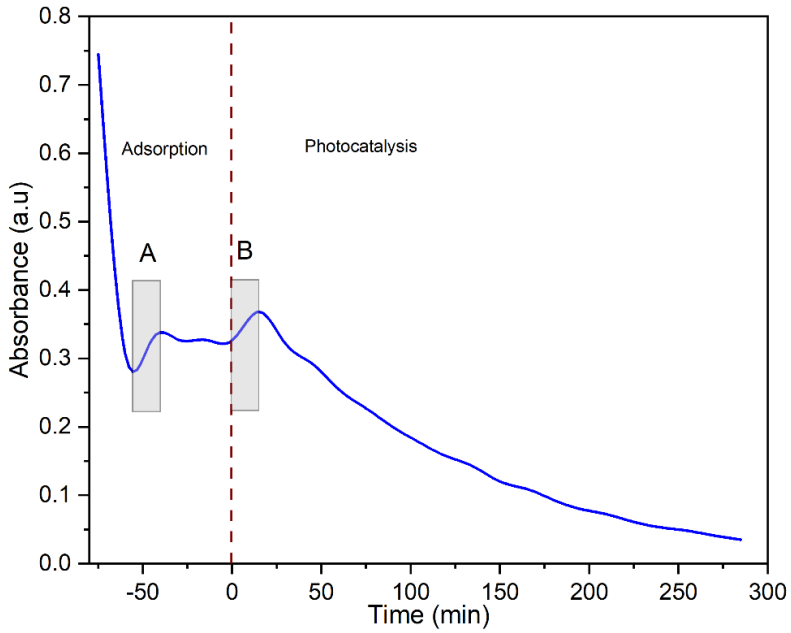

Figure 3.25 Different regions observed in MB removal mechanism.

3.3.4.8 Effect of Initial pH

The pH value of the solution is a critical factor in dye removal as it can affect the process in both adsorption-desorption and photocatalytic activity as it can impact on the surface characteristic including protonation of the functional groups and the generation of the radicals.[341] The effect of initial pH on both dark and UV activities was studied seperately. Figure 3.26 presents a distinct pattern, illustrating that the efficiency of dye removal through

adsorption on TiO_2 powder exhibited enhancement until pH 8, followed by a decline and subsequent rise at pH 10 and 12, respectively. Conversely, when observing CMC powder, a similar upward trend was noticeable until pH 8. However, CKT 0.05 foam demonstrated a reduction in adsorptive removal after reaching a pH of 10.. CKT 0.05 foam showed a decrease in adsorptive removal after pH 10. In the case of photocatalysis, both TiO_2 and CKT foam showed an upward trend with the increase of pH. All these results can be explained using ionisation of the adsorbent/photocatalyst upon point of zero charge (PZC).

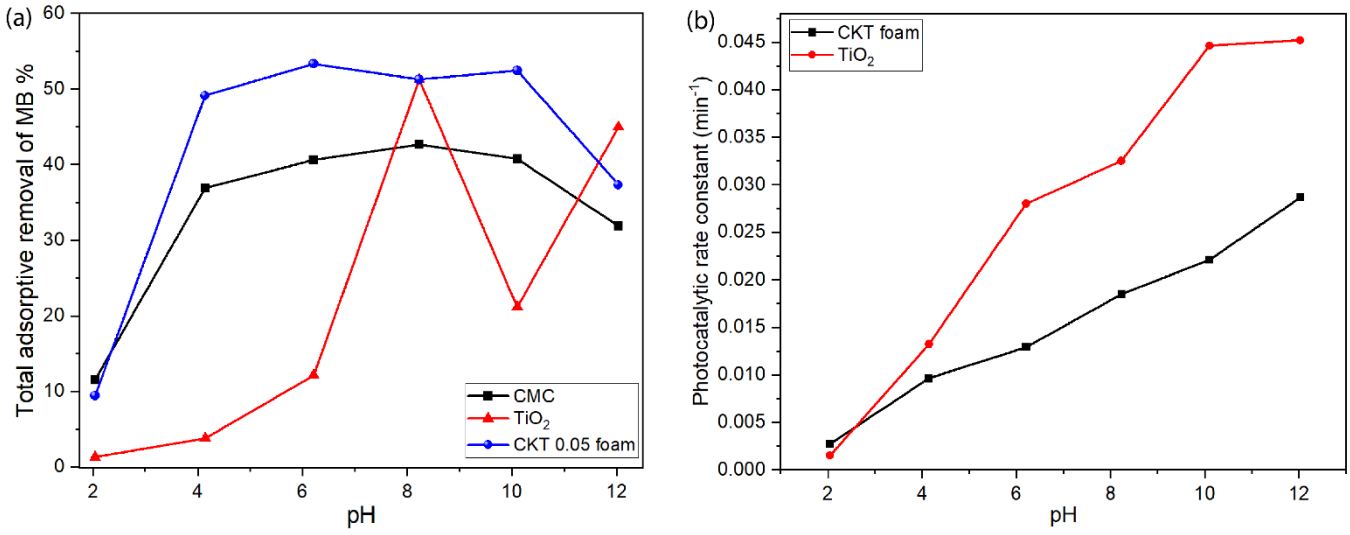

Figure 3.26 Removal of MB at different pH values (a) total adsorptive removal % of MB using CMC, TiO_2 and CKT 0.05 foam and (b) photocatalytic rate constants of TiO_2 and CKT 0.05 foam.

As reported in the literature the PZC of CMC is around pH 3.5-5. Therefore, when pH < PZC, specially in the strong acidic medium both hydroxyl and carboxyl groups tend to get protonated, ($-OH^{2+}$ and $-COOH^{2+}$) thus acquire more positive charges. Since MB is also positively charged, a repulsion takes place between MB and CMC at lower pH which reduces the adsorption.[326] Moreover, higher H^+ in the medium can create a competition between H^+ and MB ions towards CMC.[325] On the contrary, increasing pH has led to increasing adsorption due to more dissociation of carboxyl groups when pH > PZC, facilitating more electrostactic interactions between MB and CMC. But after pH 8, the results showed a decrease in adsorption with the increase of pH. It is assumed that when the amount of OH^- is getting increased in the system, hydroxyl ions can combine with MB molecules and hydroxylated MB causes a decrease in adsorption.[325] The same trend can be seen with CKT foam in the adsorption process as well. Likewise, the PZC of P25 found to be pH 5.5 and this indicates that when pH is less

than PZC, TiO_2 posseses a positive charge on the surface and and when pH is higher than PZC, it is a negative charge on TiO_2 surface.[342] This is supported by the continuous increase of the adsorption towards higher pH values.

$pH < PZC$; $Ti\text{-}OH + H^+ \rightleftharpoons Ti\text{-}OH_2^+$ Equation 3.12

$pH > PZC$; $Ti\text{-}OH + OH^- \rightleftharpoons TiO^- + H_2O$ Equation 3.13

Considering the photocatalytic activity, the deprotonation of Ti-OH with high pH values has led to a higher MB degradation rate. Aditionally, the above mentioned results prove that TiO_2 also plays a considerable role in adsorption process.

3.3.5 Anti-Bacterial Activity Evaluation

The impact of the prepared samples on bacteria was assessed in the presence of UV A light, and a negative control test was conducted simultaneously in the absence of UV light. Regarding the outcomes, unfortunately no notable difference was observed in the measured values across various experimental conditions as summarised in Table 3.14 and Table 3.15 and illustrate in Figure 3.27.

Table 3.14 Results of antibacterial tests against *E.coli.*

sample	**CFU/mL (*E. coli*)**	
	With UV	**Without UV**
Control (bacteria solution only)	16.1×10^6	17.0×10^6
Degussa p25	1.0×10^6	16.0×10^6
Sample A (CMC foam)	11.9×10^6	12.8×10^6
Sample B (CMC+KBr)	10.5×10^6	12.2×10^6
Sample C (CMC+KBr+TiO_2)	9.1×10^6	11.3×10^6

Table 3.15 Results of antibacterial test against *S. aureus.*

sample	**CFU/mL (*S. aureus*)**	
	With UV	**Without UV**
Control (bacteria solution only)	4×10^6	4.4×10^6
Degussa p25	2.5×10^6	3.7×10^6
Sample A (CMC foam)	6.8×10^6	8.7×10^6
Sample B (CMC+KBr)	6.5×10^6	5.1×10^6
Sample C (CMC+KBr+TiO_2)	5.9×10^6	6.0×10^6

UV light, and these radicals have the potential to neutralize or eliminate bacteria. Moreover, the surface characteristics, including the surface charge, of both bacteria and the compound play a crucial role in this process. In most bacterial cases, the net surface charge tends to be negative, which is quantified by zeta potential. Researchers such as Halder et al. have identified that a compound with a more positive surface charge can effectively interact with bacterial cell walls, influencing cell permeability and ultimately causing cell demise. Hence, there is uncertainty whether the prepared sample consisting of CMC, KBr, and TiO_2 (-71.5 mV) could interact favorably with E. coli (-44.2 mV) and S. aureus (-35.6 mV), potentially leading to limited antibacterial properties.[343] Conversely, as stated in available literature, an increased carbon content in the sample could hinder the photocatalytic activity by obstructing the active sites in TiO_2. A similar scenario has been discussed in the context of the MB test, warranting further investigation in this area. Additionally, the physical distance between bacterial cells and TiO_2 during photocatalysis may hinder effective interaction and necessitate a higher radical concentration. But this line of research was not taken further.

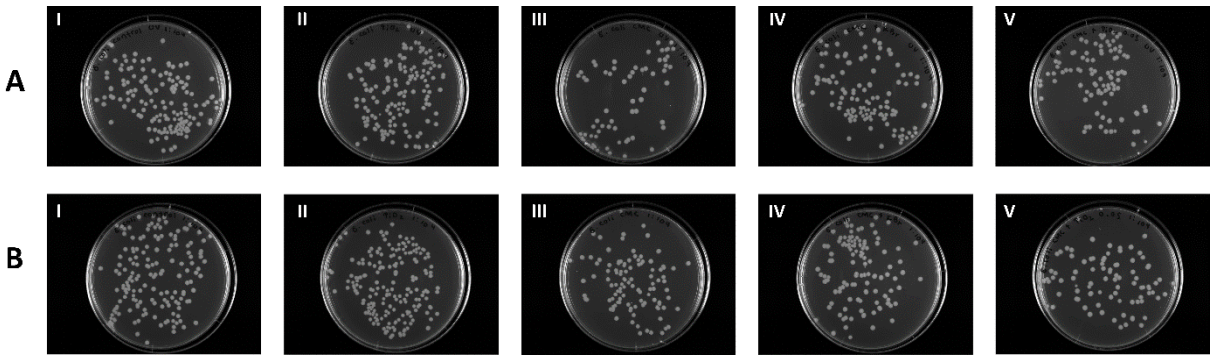

Figure 3.27 Photographs of the agar plates onto which *E. coli* bacteria were recultivated after keeping them in contact with samples. (A) With UV; (B) without UV; (I) control (no sample, bacteria only); (II) bacteria with Degussa P25; (III) bacteria with CMC powder.

CHAPTER 4

In-situ Synthesis of TiO_2 on CMC

4.1 Introduction

The previous Chapter indicated that TiO_2 was potentially leeching from the CKT foam, the next step was to work on solutions to immobilise TiO_2 in the polysaccharide matrix. If successful, this will improve all aspects of the process from separating the TiO_2 slurry from treated water.[344] To achieve this, attempts to synthesise TiO_2 *in-situ,* on CMC, were explored as the *in-situ* synthesis of inorganic semiconductors such as ZnO, TiO_2, CdS and PbS on various substrates including polymers, glass and natural fibres has gained attention recently due to the promising properties of the composite.[345] These properties are enhanced by the strong bond formation between the polymer membrane and the inorganic material due to the on-site formation the nanomaterial. This *in-situ* synthesis process has been carried out in two different ways.

1. Synthesis of the inorganic nanomaterial using an alkoxide and then modification of the substrate using the synthesised nanomaterial.
2. Modification of the substrate directly via *in-situ* synthesis of the nanomaterial on the substrate.

The second method has been found to be more cost and time effective as it reduces the number of reaction steps.[346] There are number of methods such as sol-gel, solvothermal, hydrothermal, microwave-assisted synthesis and microemulsion used to synthesise nanostructured materials. Among the aforementioned methods, sol-gel method has been identified as the highly used method as it is very simple, low temperature and low pressure method but the structure of the nanomaterial produced is amorphous and it requires an extra step with high temperature for annealing and crystallisation.[347] Even if the hydrothermal method had been listed as a high temperature method in the early stages, recently it has been identified as one of the most versatile methods to be undertaken at low temperatures. For example, according to literature, crystalline TiO_2 has been synthesised *via* hydrothermal methods at low temperatures including 60^{o}C, 80^{o}C, 90^{o}C, 130^{o}C, 150^{o}C and so on.[348,349,350,351,352] Literature reports that this method is capable of obtaining homogeneous, highly crystalline and different types of nanostructures. Hydrothermal methods use water in its vapour form as a catalyst to prepare nanocrystals in a sealed vessel named autoclave in the oven.[353] Moreover, hydrothermal processes are cost effective as they eliminate the sintering process at high temperature by producing nanocrystals

at a high pressure but at a lower temperature in an autoclave.[354] As discussed in the Chapter 2, combined systems for synthesising inorganic materials have been emerged to minimise the drawbacks caused by single methods. Out of those combined systems, sol-gel/hydrothermal method has gained the priority as it provides many advantages including, homogeneous distribution of the particles, a better control over properties like crystallinity, morphology and particle size, high purity, environmentally friendliness due to the use of water as the solvent, cost effectiveness, being able to scale up the process and many more.[355,356]

In-situ synthesis of inorganic particles can encounter another drawback of rapid agglomeration. To prevent this issue, surfactants have been used to get a homogeneous distribution of the nanomaterial. In this scenario, substrates like cellulose and CMC can act as surfactants and help in homogeneous distribution of the nanoparticles through electrosteric stabilisation process as discussed in Chapter 3.[357] Additionally, substrates such as CMC are hydrophilic substrates which help in nucleation and growth of nanoparticles. According to the previous research, the monomeric precursor groups of the inorganic material can chemically bind to the reactive groups of the cellulosic material (hydroxyl and carboxylic groups of CMC) and undergo hydrolysis and condensation generating inorganic nanoparticles and reactive organic groups.[358] Furthermore, the polymer substrate can change the particle size through the way it covers/binds with nanoparticle. Nevertheless, there are some drawbacks of having a polymer substrate. The strong bond formation between the inorganic precursor monomer units and the active groups of the polymer can create solubility differences and prevent ions from diffusion for further crystallisation. Moreover, it is possible to have unreacted precursor units, undesired side reactions and by products which can alter the properties of the nanocomposite.[359]

This chapter describes the immobilisation of TiO_2 on CMC via hydrothermal assisted sol-gel method at a low temperature. As far as our understanding goes, no prior research has investigated the immobilization of TiO_2 using CMC. Consequently, this chapter delves into a distinctive and significant research domain.

4.2 Methodology

4.2.1 Materials and Reagents

Sodium carboxymethyl cellulose (degree of substitution = 0.7, average Mw = 250,000), titanium isopropoxide (99.99%) were purchased from Sigma Aldrich, Australia. Absolute ethanol and isopropanol were purchased from Chem Supply, Australia and used as is.

4.2.2 Synthesis of CMC-CTTIP (CTTIP) Composite

CTTIP composites were synthesised varying different parameters as indicated below.

1. The first CTTIP sample was synthesised at 80^{o}C with a total volume of 180 mL inside the autoclave (CTTIP_80)
2. To investigate the effect of temperature, the second sample was synthesised at 110^{o}C, with the same amount of total volume; 180 mL. (CTTIP_110)

In order to see the effect of the pressure inside the autoclave on the synthesis of nanocrystals, three different samples were prepared, varying the total volume of the solution in the autoclave (

Table 4.1)

Table 4.1 : Samples prepared varying the total volume of the autoclave at 110^{o}C.

Sample name	**Total volume (mL)**
CTTIP_110_163	163
CTTIP_110_180	180
CTTIP_110_200	200

The general synthesis procedure can be described as follows: CMC was dissolved in milli Q water and after the CMC has completely dissolved, ethanol was added and the solution stirred for 2 h. A TTIP solution was prepared by dissolving TTIP, in 2-propanol (amount of TIIP - to maintain the same equivalence in the CKT foam). The quantities of solvents employed were calculated using the total volume inside the autoclave, and the volume ratio was consistently maintained across all three pressures. The TTIP solution was added to the CMC aqueous ethanol system dropwise and the whole system was vigorously stirred for 2 h at ambient temperature. The suspension was transferred to an autoclave and hydrothermally treated in an oven for 24 h. The suspension was then cooled naturally, and the solid product separated, washed with cold ethanol and water for 4 times and dried at 60^{o} for 24 h. The ratios among each reactant remained constant across all three different samples.

4.2.3 Characterisation

4.2.3.1 X-ray Diffraction (XRD)

A Bruker X- ray diffractometer (XRD) D8 advance with a CuKα sealed tube (1.5418 ºA) and Lynxeye detector was used for XRD analysis. The samples were scanned between 2 theta= 5° and 80° which focuses on the in-situ synthesis of TiO_2 on CMC and its photocatalytic activities. XRD could provide deeper insights into how the observed amorphous state of TiO_2 affects the composite's stability and effectiveness. The tube current and voltage were 40 mA and 40 kV respectively.

4.2.3.2 Attenuated Reflectance Fourier Transform Infrared (ATR FTIR) Spectroscopy

FTIR spectrum of the prepared samples were recorded using a Thermoscientific Nicolet iD5 spectrophotometer. The functional groups of the samples were identified by spectroscopic analysis with the standard characterisation detection range from 800 to 4000 cm^{-1} to characterise the composite over components.

4.2.3.3 X-Ray Photoelectron Spectroscopy

The elemental compositions of the fabricated materials were examined through X-ray photoelectron spectroscopy (XPS) spectra using NEXSA XPS instrument from Thermo Fisher Scientific to indicate elemental composition and its alignment with composite stability and effectiveness. The X-ray source used was Al Kα at 75 W. Subsequently, the acquired data was subjected to analysis through the casaXPS software.

4.2.3.4 Thermogravimetric Analysis (TGA)

The thermal stability of the synthesised materials was investigated using Q500-0341 TGA instrument. TG curve represents the evolution of the mass as a function of the temperature. The sample was heated from room temperature to 1000°C under a nitrogen atmosphere at a heating rate of 10°C/min. TGA gives information on thermal stability which informs on composite viability.

4.2.3.5 Scanning Electron Microscopy (SEM) and Energy Dispersive X-ray (EDX) Analysis

A Hitachi S-4800 scanning electron microscope with a field emission gun was used to analyse the surface morphology and structure of the samples as an indication of surface roughness, porosity and surface area. The samples were gold coated using a sputter coated before observation.

4.2.3.6 Zeta Potential Analyser

Zeta potential analysis of TiO_2 and CTTIP suspensions were carried out using a Malvern Zetasizer Ultra zeta potential instrument. Measurements were performed on a dilute suspension at native pH to determine overall charge of composite particles.

4.2.4 Photocatalytic Activity

This procedure was undertaken to assess the photocatalytic effectiveness of the synthesized samples against both cationic and anionic dyes and phenols. The primary aim was to determine the potential stabilization of TiO_2 within the polymer matrix using this approach.

4.2.4.1 Degradation of Dyes

Methylene blue (MB) and methyl orange (MO) were used as the model dye samples and the concentrations were monitored by a Shimadzu UV Visible spectrometer at 665 nm and 465 nm respectively. A 50 mL volume of the solution with 0.87 g/L of the CTTIP powder was first kept in the dark for 75 minutes until it reached adsorption equilibrium and then exposed to the UV light source over 4 h, under stirring. Samples were taken every 15 min. The suspension was centrifuged out using an Eppendorf Minispin Centrifuge at 13,000 rpm for 10 min.

Two parallel experiments were conducted, one in dark and the other one under UV A (365 nm). Both MB-sample mixtures were kept in the dark for 75 min until they reach their adsorption-desorption equilibrium. Once reached, one of the samples was irradiated with UV (365nm, 1W) and other was kept in the dark. The same method was followed with TiO_2 powder (9 mg) and CMC powder (36 mg). These masses were obtained by a back calculation. The degradation of the dyes under sunlight with CTTIP composite was conducted for 2 h, according to aforementioned method on a sunny day with a temperature of 35^{o}C.

4.2.4.2 Liquid Chromatography – Mass Spectroscopy (LCMS) Analysis

The LC-MS analysis was carried out to identify the intermediates during the process and the degradation mechanism. Samples were analysed using high resolution mass spectrometry on an Agilent 6510 quadrupole time-of-flight mass spectrometer operated in positive mode. Flow injections of 10 ul were delivered using an Agilent 1290 Infinity liquid chromatography system, with a total flow of 0.3 ml /min and [ultra-pure water; ACN] used as the mobile phase.

4.2.4.3 Degradation of Phenol

A 100 mL of 25 ppm phenol solution with 0.87 g/L of CTTIP_200 was kept in the dark for 1 h until it reached the adsorption equilibrium and then exposed to the UV light source (665nm) until phenol completely degrades, under stirring. Samples were taken every 15 minutes during rapid change extending to 1 h when little further change was recorded. The suspension was centrifuged out using an Eppendorf Minispin Centrifuge at 13,000 rpm for 10 min. The disappearance of phenol was observed using Shimadzu UV Visible spectrometer at 270 nm.

4.3 Results and Discussion

4.3.1 Analysis of CTTIP_80

4.3.1.1 X-ray Diffraction (XRD)

XRD profiles of CMC and CTTIP_80 are shown in Figure 4.1. The broad diffraction peak at 21.83^0 in the CMC profile is attributed to the amorphous nature of CMC.[278] Nevertheless, only a broad peak could be observed in CTTIP XRD spectrum, and that peak could be assigned to amorphous TiO_2.[360] This indicates that the temperature used might not be enough for the crystallisation process. Moreover, no CMC peak could be seen in CTTIP graph, showing that formed amorphous TiO_2 and CMC phases could have been mixed well.

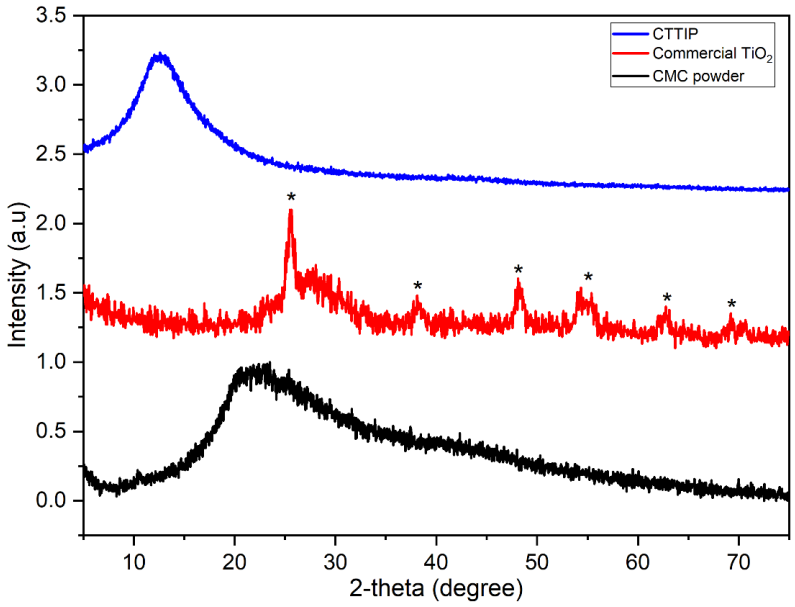

Figure 4.1 XRD patterns of raw materials and CTTIP_80

4.3.1.2 Brunauer–Emmett–Teller (BET) Analysis (BET)

Surface area analysis is a very important characterisation method when it comes to preparation of adsorbents. BET surface area of CTTIP is 35.42 m^2/g which is about 70 times higher than CMC powder itself. This supports the premise that *in-situ* synthesis of TiO_2 on CMC using hydrothermal assisted sol-gel synthesis pathway can increase the surface area of final composite.[195] While the BET analysis underscores the increased surface area it could be more directly related to the composite's photocatalytic efficacy as a result.

4.3.1.3 X-ray Photoelectron Spectroscopy (XPS)

X-ray Photoelectron Spectroscopy (XPS) was again employed for the characterization of the synthesized composite (

Figure 4.2). Notably, Ti peaks were detected at 458.46 eV (Ti^{4+} 2*p* 3/2) and 464.26 eV (Ti^{4+} 2*p* 1/2), providing clear evidence of the presence of TiO_2 in the synthesised material as the major objective. Moreover, the Ti 2*p* profile revealed the occurrence of titanium oxohydroxide ($TiO(OH)_2$), which is a plausible product formed during the hydrothermal synthesis process.[361] The presence of Ti in the composite was further corroborated by the Ti-O-C peak evident in both the C1*s* and O1*s* spectra, with binding energies cantered at 285.96 eV and 529.76 eV, respectively.[362] Additionally, the general C peaks were observed at 284.76 eV (C-C), 286.46 eV (C-O), 287.96 eV (C-O-C), and 289.16 eV (C=O), while the peaks from the O1s profile were identified at 531.10 eV (C=O), 532.76 eV (C-O), 532.96 eV (O-H), and 536.06 eV (Na auger peak).[363,364] Remarkably, no significant peak shifts were discernible in this context when comparing the spectra to those of CMC powder.

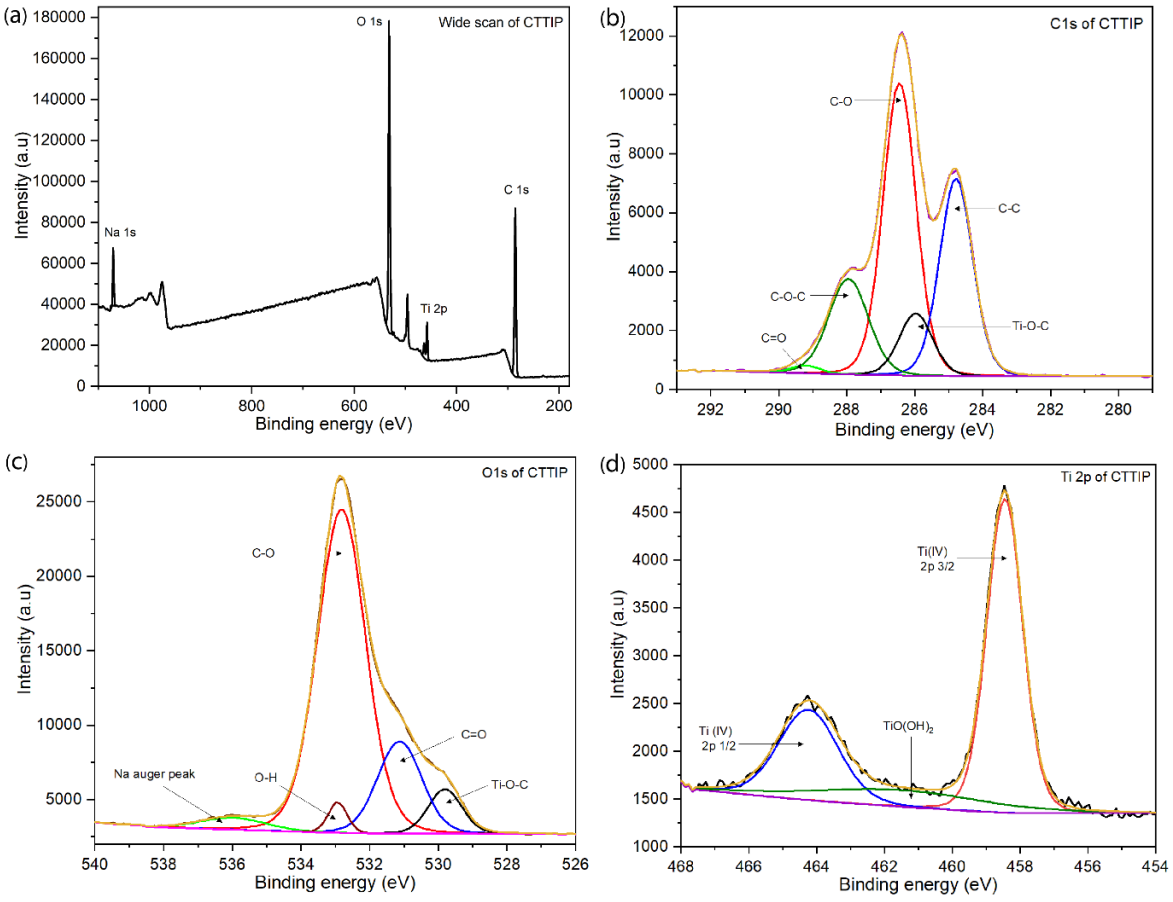

Figure 4.2 : XPS analysis of CTTIP_80 (a) wide scan of CTTIP, high resolution spectra of (b) C1s, (c) O1s, (d) Ti2p.

4.3.1.4 Thermogravimetric Analysis (TGA)

The stability of the crosslink formation in this process was assessed by TGA analysis and compared to CMC powder (

Figure 4.3). The first stage from 40–200°C is attributed to the removal of water in the form of both physically adsorbed and trapped water, and the weight loss is approximately 15%. This stage is commensurate for CMC. Next stage from 200 – 370°C is attributed to degradation of saccharides rings and evolution of CO_2. In this stage the weight loss is around 23%. The third stage from 390°C could be assigned to the breaking of C-O-C bonds and carboxyl groups[365] and the weight loss is about 18%. The residue of CTTIP after heating up to 1000°C is approximately 37.5% which indicates stability of CTTIP is higher compared to CKT foam 14%, and represents mostly carbonaceous and metal-based residue as compared to CMC powder.

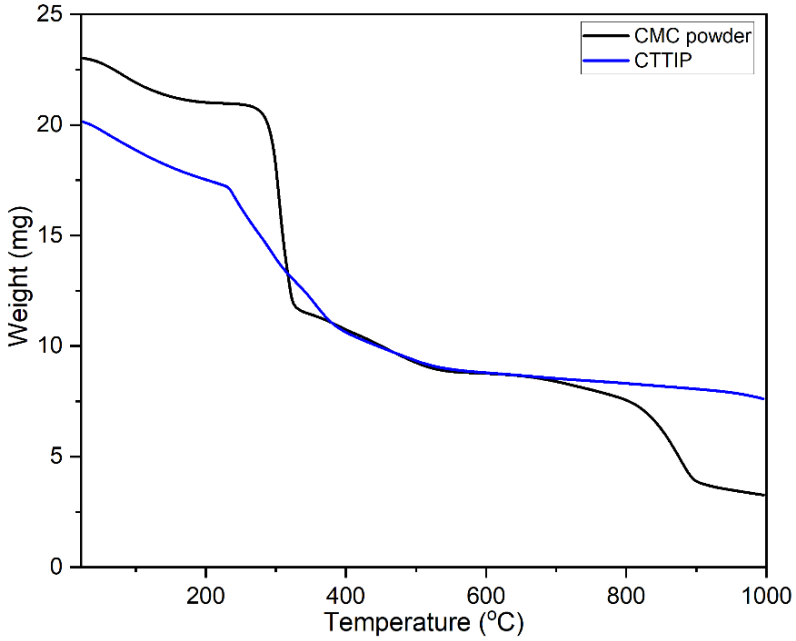

Figure 4.3 TGA curves of CMC powder and CTTIP_80.

4.3.1.5 Methylene Blue Degradation

Methylene blue testing was carried out using a 3 ppm solution to investigate adsorption and photocatalytic activity of newly prepared CTTIP sample (0.0872 g/L) against the degradation of MB's distinctive blue colour (λ_{max} = 665 nm). In the dark reaction time, the system reaches the equilibrium in 15 minutes with a total dye removal of 93%, indicating this new material possesses a ***high adsorption capacity*** for MB. According to the literature, the formation of crosslinks increases the surface area and adsorption due to what is described as a lower wrinkling of cellulose chain.[366] The zeta potential value of CTTIP was calculated as -47.8mV indicating, the material is highly negative which helps in formation of electrostatic bonds with cationic MB molecules. On the other hand, this zeta potential value is less than that of CKT0.05 foam (-69.6mV). From this, we assume that surface area and crosslinks might play a cooperative role in adsorption alongside surface charges. From a practical standpoint, CTTIP needs to be stirred constantly in the aqueous solution to have a homogeneous mixture, as otherwise the composite tends to agglomerate. Figure 4.4 shows the fast removal of MB by CTTIP as indicated by the removal of the blue colour from solution. No observable changes could be observed when MB solution with CTTIP was exposed to UV (Figure 4.5). Despite the identification of TiO_2 and $TiO(OH)_2$ through XPS analysis, the morphology may still be in the amorphous state, as indicated by XRD analysis. According to literature, there are also two

problems arising in TiO_2 immobilisation[344]: The low accessibilty of formed radicals to the photons and the adsorbate because TiO_2 has embedded in the network; Resistance of the mass transfer at low fluid rate as a result of high diffusion.

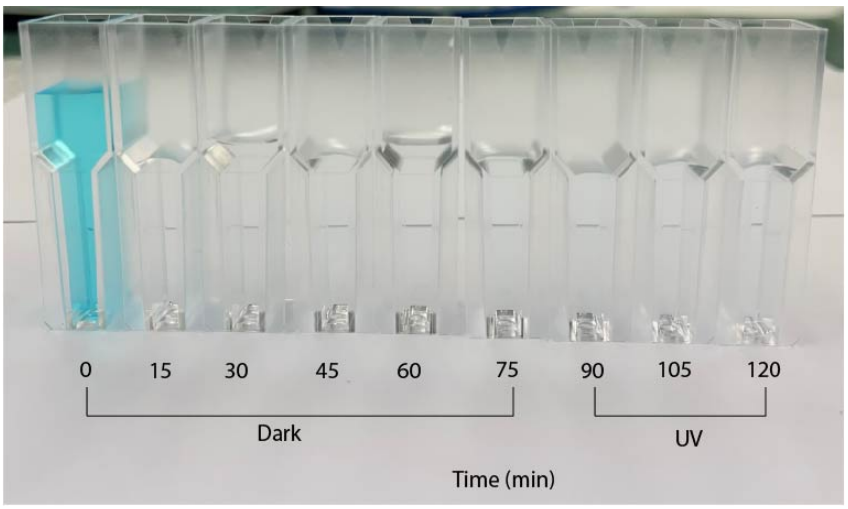

Figure 4.4: Removal of MB over the time.

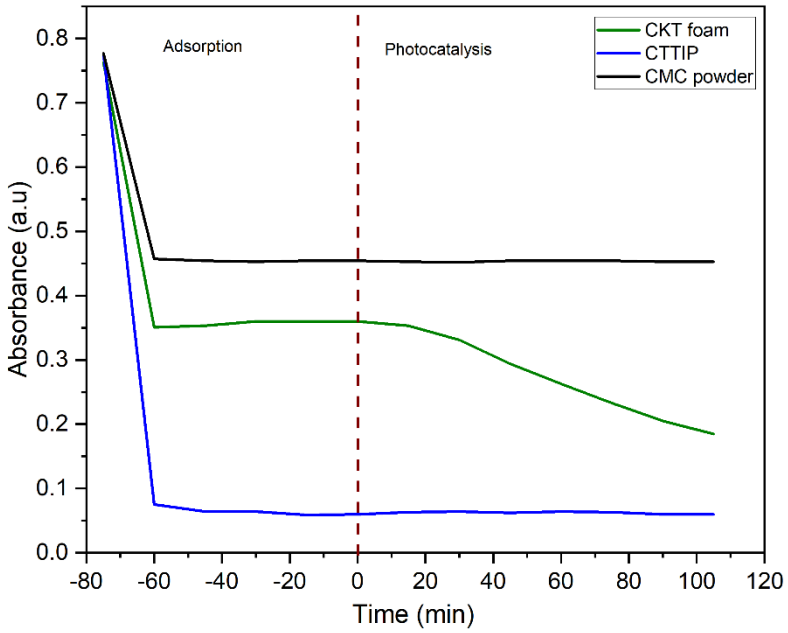

Figure 4.5 : A comparison of adsorption of MB on to different materials indicating the high absorption of MB on CTTIP.

The correct ratio between CMC and TiO_2 is a crucial factor. The findings from Chapter 3 and Chapter 4 indicate that a higher quantity of CMC hinders the photocatalytic activity, while a higher amount of TiO_2 tends to separate from the composite and leech out during the process.

These outcomes present a disadvantage in industrial applications. Therefore, our next objective was to immobilise TiO_2 in CMC, as the composite exhibited a good photocatalytic activity.

4.3.2 Analysis of CTTIP_110

As a strategy to enhance the photocatalytic activity of CTTIP samples based on obtained results, it was decided to increase the reaction temperature to 110°C to complete the reaction. The selected temperature was determined based on its maximum value achievable without causing degradation to CMC, as indicated by TGA analysis. Interestingly, as shown in Figure 4.6, the XRD analysis of this newly prepared sample revealed the presence of anatase peaks, indicating the advantage of elevated temperature.

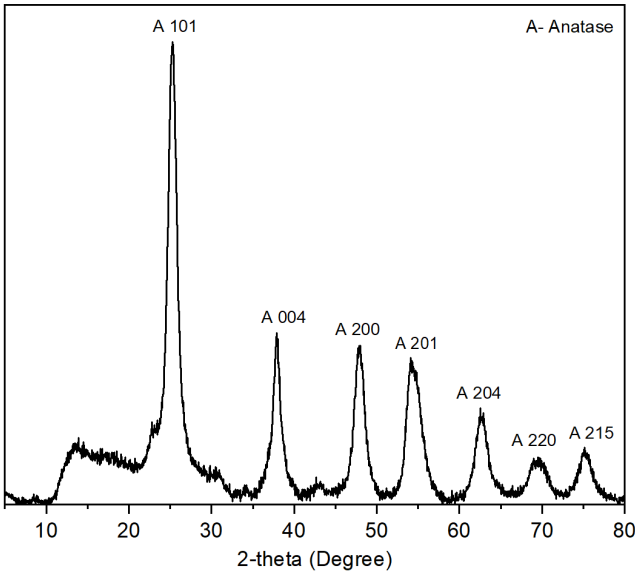

Figure 4.6 : XRD graph of synthesised CTTIP_110 sample.

Consequently, as the next step to examine the influence of autoclave pressure on crystal formation, three distinct samples were prepared, as shown in Table 4.1, with variations in the total volume within the autoclave to modify the headspace volume. All the prepared samples were analysed using the techniques specified in the upcoming subsections.

4.3.2.1 X-Ray Diffraction (XRD)

As mentioned earlier, XRD analysis played an important role in this research to confirm the success or failure of the modification steps taken. Based on the diffraction patterns observed, the crystalline peaks of TiO_2 were clearly seen with higher temperature procedures, and no peak corrosponding to CMC was observed in XRD spectra of all three composites, indicating

CMC is dispersed uniformly in TiO_2 matrix.[367] The only phase of TiO_2 present in substantial quantities within the samples was determined to be anatase - the 2θ peaks at 25.5, 38.1, 48.1, 54.35, 55.4, 62.75 are corresponded to the crystal planes of 101, 004, 200, 201, 211, 204 for anatase, respectively (Figure 4.7). No any additional crystalline or amorphous phases of TiO_2 were detected from XRD results. It can be assumed that the CMC network may have controlled the mobility of cations, thus the formation of other TiO_2 phases or converting anatase to other phases.[368] Previous studies have reported the synthesis of anatase TiO_2 at lower temperatures ranging from room temperature to 160°C. However, most of them were unable to obtain a good crystalline phase until they went through calcination at a higher temperature. Nonetheless, there are some documented examples of successfully synthesizing TiO_2 in the anatase phase at even lower temperatures (T ≤ 130°C) which further supports this research outcome.[369,370] Table 4.2 summarises a few examples of such cases.

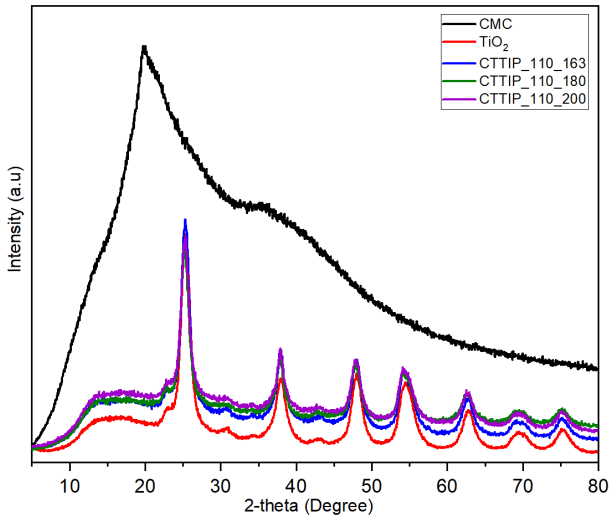

Figure 4.7 : A comparison of XRD patterns of CMC and synthesised samples.

To understand more about the role of CMC, TiO_2 was synthesised under the same conditions without CMC, as a control. As depicted in Figure 4.7, this step proves anatase nanoparicles can be synthesised at lower temperatures in the absence of CMC. Crystallite sizes have been calculated using XRD data related to (101) crystal plane of anatase using Scherrer equation[371] and the results are summerised in Table 4.3. These results imply that CMC may have played a cooperative role in the synthesis of these crystalline phases.

Table 4.2 : Literature examples for low temperature synthesis of TiO_2.

Research Process	**Synthesis temperature**	**Reference**

Synthesis of anatase using poly acrylic acid	ambient temperature	[372]
Synthesis of anatase	ambient temperature	[373]
Synthesising TiO_2 nanoparticles of polyethersulfone and polyvinylidine fluoride	110°C	[353]
Synthesis of TiO_2 nanoparticles on wool	Hydrolysis at 65°C and curing at 120°C	[347]
Synthesis of TiO_2 on polyethylene glycol	Room temperature	[374]
Synthesis of TiO_2 on polyurathane	90°C	[359]
Synthesis of TiO_2 on cellulose	80°C	[357]

$$D = \frac{K * \lambda}{\beta cos\theta}$$ Equation 4.1

Where, D – crystallite size in nm

K – a constant which depends on the method used, and varies between 0.5 and 1, but usually taken as around 0.9

λ – X-ray wavelength

θ – diffraction angle of the peak in radians

β – broadening due to particles

Table 4.3: Crystallite sizes calculated for samples.

Sample	**Crystallite size (nm)**
TiO_2	57.6
CTTIP_110_163	85.2
CTTIP_110_180	78.0
CTTIP_110_200	84.9

The tabulated results clearly show that crystallite sizes are considerably larger than in some publications.[375,376] It has been mentioned that high temperatures and longer reaction time can produce large crystals due to sintering of TiO_2.[372] As indicated in the mechanism, TiO_2 precursors and formed TiO_2 can bind to functional groups within the CMC, and thus CMC can cover TiO_2 like a micelle where formation of TiO_2 can take place inside.[377] A thorough explanation of the mechanism will be explored later in this Chapter.

4.3.2.2 Scanning Electron Microscopy (SEM)

The morphology of prepared samples was explored by SEM analysis. As shown in the Figure 4.8, CMC powder has a rod like structure, while the synthesised TiO_2 powder has the regular crystalline anatase morphology with smooth surfaces and sharp edges.[378] The morphology of composite samples appear as a mixture of particles with regular crystalline structure and irregular, rougher structures. This may be due to the presence of CMC as a surfactant and its influence on the growth rate in specific directions with high surface energy, resulting in the formation of a wide variety of nanocrystal shapes.[379] Moreover, the round edges of the crystals align with previously published data and according to literature this can be another effect of having CMC in the system..[380] No distinct differences could be identified among all three CTTIP_110 samples.

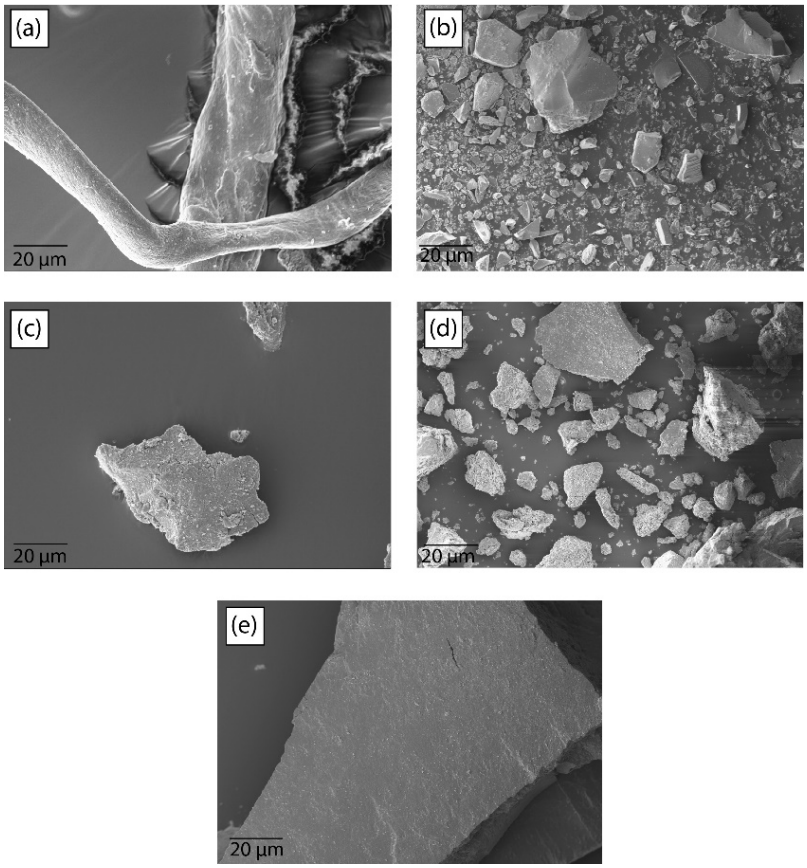

Figure 4.8 : SEM images of (a) CMC powder; (b) synthesised TiO_2 powder; (c) CTTIP_110_163; (d) CTTIP_110_180; (d) CTTIP_110_200.

4.3.2.3 Attenuated Reflectance Fourier Transform Infrared (ATR FTIR) Spectroscopy

ATR-FTIR analysis was conducted to identify the functional groups and the interactions between CMC and the formed TiO_2 composite (Figure 4.9). FT-IR spectrum of CMC is as same as characterised in Chapter 3. The FT-IR spectrum of synthesised TiO_2, revealed peaks at 3163,1739, 1367 and 1217 cm^{-1} corresponding to −OH stretching, −C=O stretching, −OH bending and −C−O stretching respectively.[381] These C peaks might have come from the residue of the precursors used to synthesise TiO_2. Moreover, according to the literature, the wide broad band in the range of 1000-400 cm^{-1} is attributed to Ti−O and O−Ti−O bonds.[382] With correspond to the prepared composites, a distinguishable change in peak intensities could be observed between CTTIP_110_163 and CMC powder, indicating; (i) the well formed interactions between CMC functional groups and formed TiO_2; (ii) the interactions between CMC and other chemicals (ethanol, isopropanol and TTIP) in the system; and (iii) the shielding effect of TiO_2 on the underlying CMC.[383]

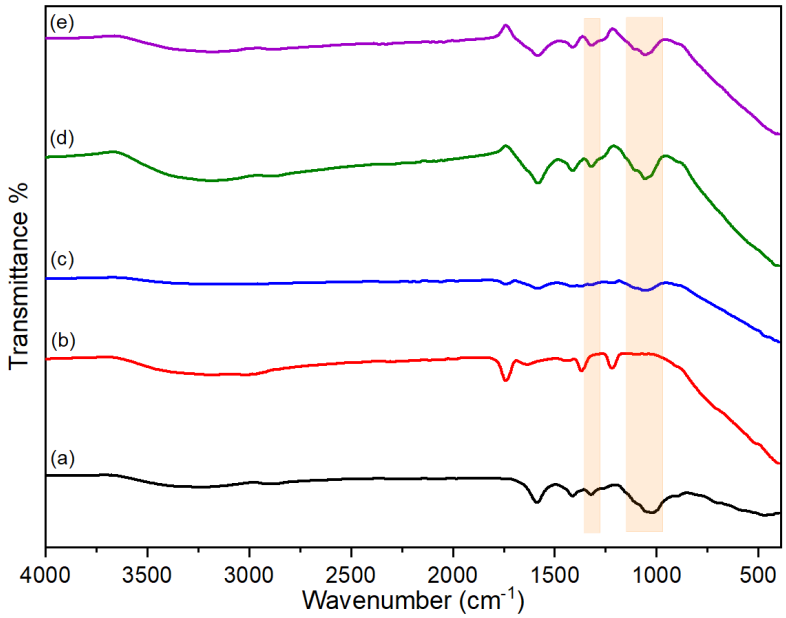

Figure 4.9 : ATR-FTIR spectra of (a) CMC powder (b) TiO_2 (c) CTTIP_110_163 (d) CTTIP_110_180 (e) CTTIP_110_200. (The coloured areas; 1367 cm^{-1} – OH bending and 1367 cm^{-1} C-O stretching)

4.3.2.4 X-ray Photoelectron Spectroscopy (XPS)

In this study, X-ray Photoelectron Spectroscopy (XPS) was conducted to explore the composition and chemical bonding characteristics of CMC powder and various synthesized samples (Figure 4.10). The results including fitting parameters are shown in Table 4.4.

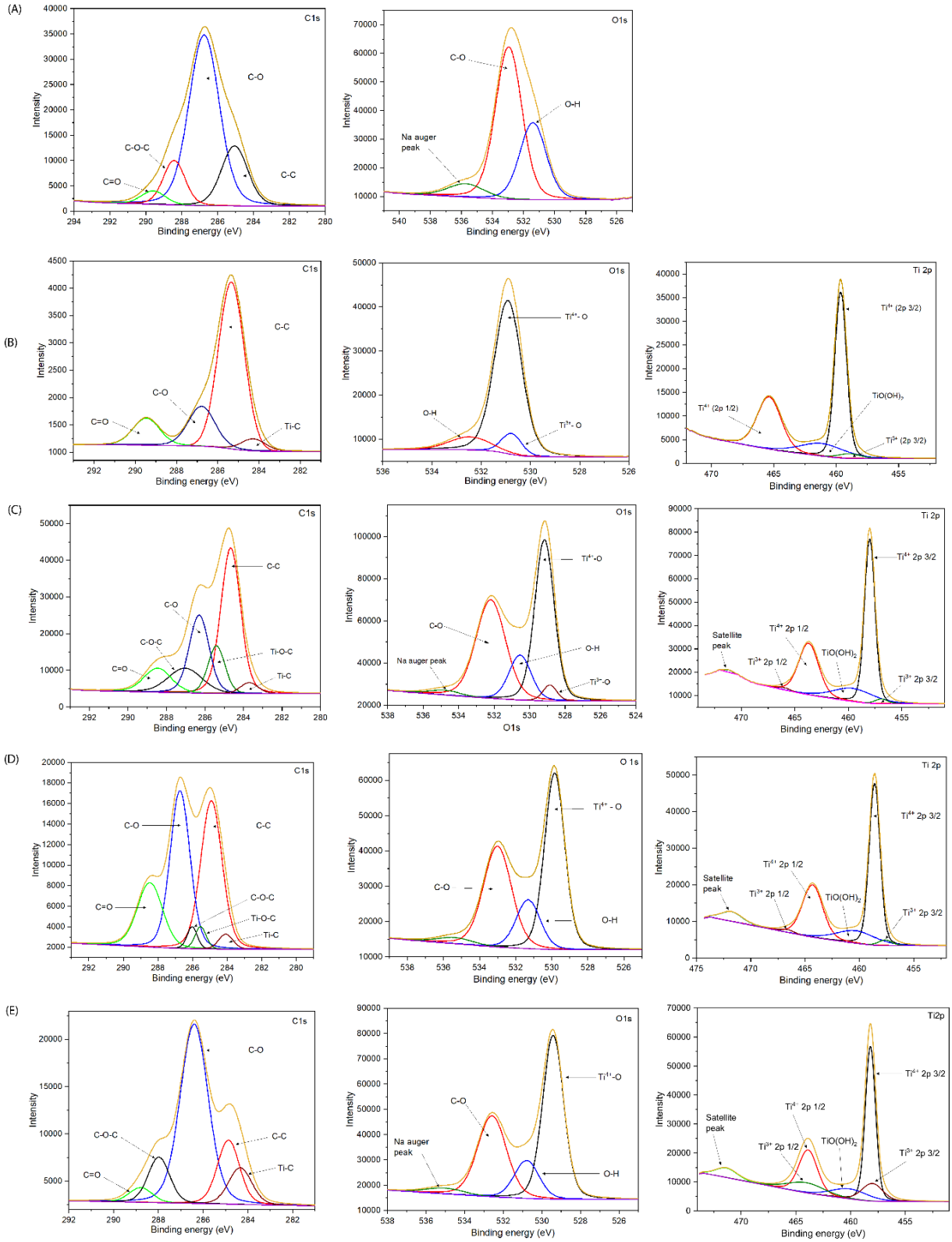

Figure 4.10 High-resolution XPS profiles of (A) CMC powder, (B) synthesised TiO_2 powder, (C) CTTIP_110_163, (D) CTTIP_110_180, (E) CTTIP_110_200.

The high-resolution Ti 2p XPS profiles revealed the presence of both Ti^{4+} and Ti^{3+} oxidation states of titanium in all the synthesized TiO_2 and CTTIP_110 samples. Notably, the formation of Ti^{3+} oxidation state was attributed to the relatively low synthesis temperature employed.[384] In the C1s XPS profile of TiO_2 powder, distinctive C peaks, including C-C, C-O, and C=O bonds, were evident. These features were likely induced by the precursors employed during TiO_2 synthesis, with the formation of C=O bond indicating in-situ carbonization as previously reported in the literature.[385] Furthermore, we observed the formation of $TiO(OH)_2$ in all the synthesized samples, which is postulated to arise from the transformation of alkoxide species and the adsorption of other hydroxyl groups present in the system onto the TiO_2 surface.[386]

Table 4.4 XPS fitting parameters of CMC, synthesised TiO_2, CTTIP_110_163, CTTIP_110_180 and CTTIP_110_200.

C1s					
Peaks	**CMC**	**TiO_2**	**CTTIP_110_163**	**CTTIP_110_180**	**CTTIP_110_200**
C-C	285.06	285.34	284.66	284.90	284.88
C-O	286.75	286.78	286.30	286.72	286.40
C-O-C	288.42		287.03	286.02	287.97
C=O	289.58	289.46	288.45	288.46	288.77
Ti-C		284.27	283.75	284.07	284.35
Ti-O-C			285.40	285.52	
O1s					
C-O	532.95		532.19	533.00	534.03
O-H	531.39	532.46	530.53	531.30	530.78
Ti4+-O		530.91	529.16	529.84	529.41
Ti3+-O		530.76	528.85		
Na auger	535.71		534.76	535.36	535.02
Ti 2p					
Ti^{4+} 3/2		459.64	458.00	458.60	458.19
Ti^{4+} 1/2		465.35	463.70	464.30	463.88
Ti^{3+} 3/2		458.59	456.92	457.64	458.01
Ti^{3+} 1/2			465.94	466.62	464.07
$TiO(OH)_2$		461.35	459.53	460.32	460.11
Satellite			471.15	471.75	473.55

The analysis of the binding energy separation between the Ti spin-split components (Ti 2p 3/2 and 1/2) in Ti-containing samples showed an approximate value of 5.71, aligning with the literature values reported for anatase.[387] Notably, the XPS profiles of CTTIP_110 displayed either positive or negative binding energy shifts compared to their precursors (CMC and TiO_2). For instance, the Ti^{4+} peaks in TiO_2 powder exhibited a lower binding energy value in all three CTTIP_110 samples, which can be attributed to the formation of additional suboxides of Ti (Ti3+).[388] Conversely, in the O1s XPS profile of CTTIP_200, a positive shift of 1.08 eV was observed in the C-O peak compared to CMC powder. This observation may be attributed to the formation of strong bonds between the newly formed Ti species and the C-O moiety.

4.3.2.5 UV-Vis Diffuse Reflectance Spectroscopy (DRS)

DRS is a valuable technique to obtain the optical properties of a chemical species. When the light incidents on a sample, the light can undergo scattering in multiple directions within the material. These scattered lights are collected by a detector positioned at a specific angle. This detected light is termed "remitted light".[389] In the context of this research, this technique was utilised to examine the optical characteristics and band gaps of both synthesized CTTIP samples and TiO_2. As shown in absorbance and band gap spectra in Figure 4.11, prepared CTTIP samples possess the ability to absorb the light of both UV region ($\lambda < 400$ nm, $E > 3.0$ eV) and the visible region ($400 < \lambda < 800$ nm, $1.5 < E < 3.0$).The maximum absorption wavelength of all the synthesised samples is beyond 400 nm, indicating the absorption of visible light range.[390]

To confirm this behaviour of the synthesised samples, band gaps were obtained using the Tauc's plot.[391] It is a well known fact that anatase has an indirect band gap, therefore, $(F(R)*h\upsilon)^{1/2}$ vs $h\upsilon$ was plotted for indirect band gaps. Here, 'F(R)' is the Kubelka-Munk function, 'h' is Plank's constant and 'υ' is the frequency of the photon.[392] According to literature, the reported range for the indirect band gap of anatase is typically between 3.0-3.2 eV, with a commonly observed value of around 3.2 eV.[393,394] However, in this project the band gap of synthesised anatase was found to be 3.0 eV. This change can be attributed to the formation of Ti^{3+} during the synthesis process. The presence of Ti^{3+} within the TiO_2 lattice structure contributes to lowering the band gap by creating intermediate energy levels between valence and conduction band and also by limiting the electron-hole recombination.[395] Moreover, it has been reported that Ti^{3+} sites can generate oxygen vacanies which can enhance the absorption of visible light.[396]

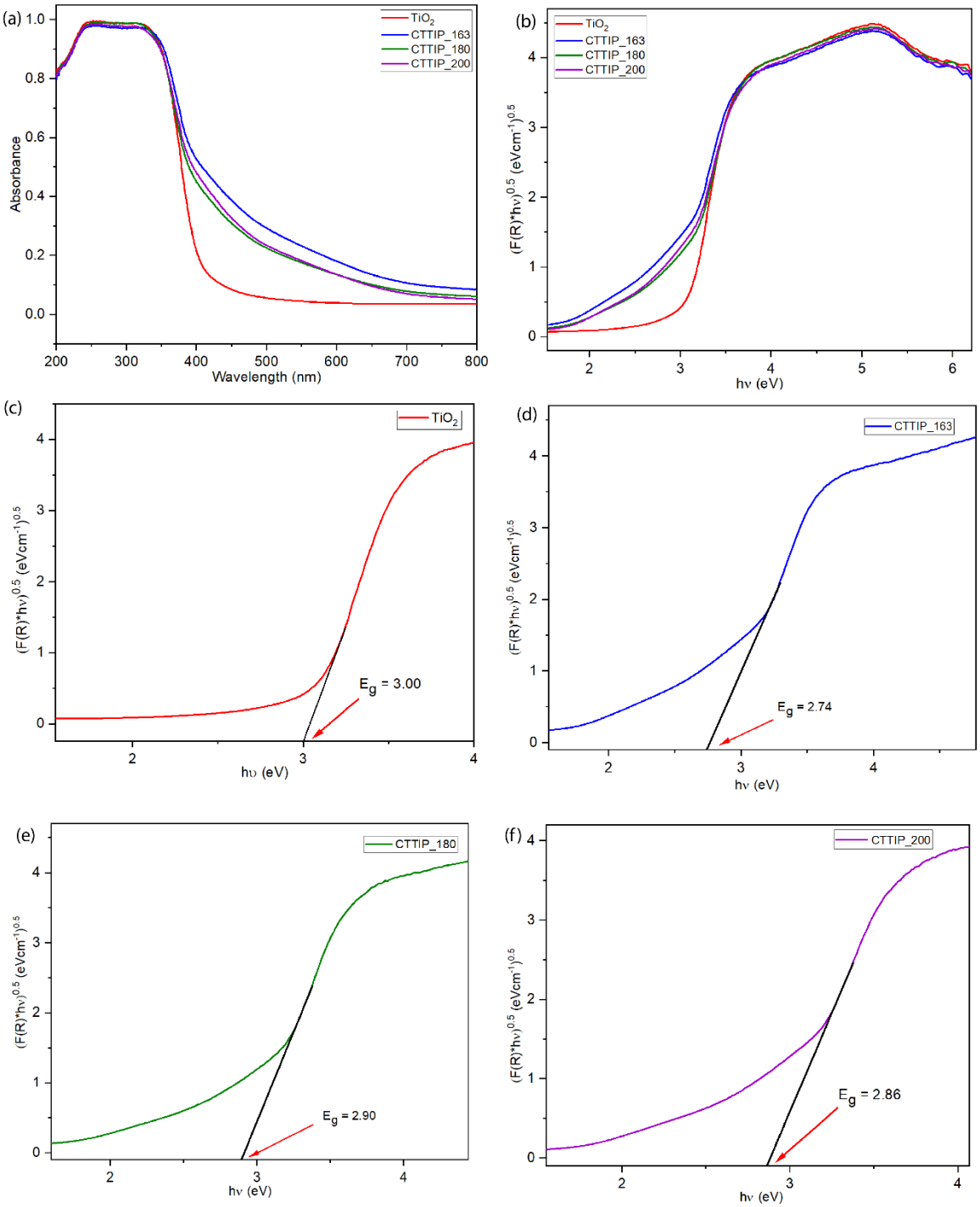

Figure 4.11 (a) absorbance *vs* wavelength spectra of synthesised samples, indirect energy band gap plot ($(F(R)*h\upsilon)^{1/2}$ vs $h\upsilon$) of (b) all synthesised samples for comparison (c) synthesised TiO_2 (c) CTTIP_110_163 (d) CTTIP_110_180 and (e) CTTIP_110_200.

The band gaps of all three CTTIP samples are lower than 3.0 eV, suggesting that these composites possess a good visible light absorption. This can be attributed to having both carbon rich CMC and Ti^{3+} defects in the system. Even if the mechanism by which biopolymers like cellulose, chitosan and CMC contribute to narrowing the band gap has not been extensively

investigated, some studies have revealed that these polymers can create impurity energy levels in between valence and conduction bands, thus new electron transferring pathways.[397,398] Moreover, it has been found out that C−O bonds within a biopolymer/TiO_2 composite can promote the charge separation.[399] When comparing the three CTTIP samples prepared, CTTIP_110_180 showed the highest band gap (2.92 eV), CTTIP_110_200 is 2.86 eV while the lowest band gap is owned by CTTIP_110_163 (2.74 eV). These variations can be due to the differences of crystallite size as demonstrated by XRD analysis. It is known that higher the crystallite size, the lower the band gap, and higher the photocatalytic activity.[400,401]

4.3.2.6 Zeta Potential Analysis

Zeta potential is an important analysis to assess the colloidal behaviour, dispersion and the stability of the nanomaterial suspension as well as provide information about the surface charges and their distribution.[402] The zeta potential of all prepared samples are presented in Table 4.5. Synthesised TiO_2 showed a positive zeta potential value while all three samples with CMC displayed negative zeta potential values, attributed to the carboxylic groups of CMC.[403] In contrast to CKT foams, the magnitude of the negative zeta potential values of CTTIP samples were comparatively low. Generally, nanoparticles with zeta potential values above +30 mV and below -30 mV are considered as strongly cationic or anionic respectively indicating high stablity in its suspended state.[311] Moreover, it can be assumed that the low magnitude of the negative values may be caused by improved interactions between TiO_2 and carboxylic and hydroxyl groups in CMC.

Table 4.5 : Zeta potential values of TiO_2 and CTTIP_110 composites

Material	**Zeta Potential (mV)**
TiO_2	23.4
CTTIP_110_163	-7.64
CTTIP_110_180	-15.5
CTTIP_110_200	-11.2

4.3.3 Removal of Dyes

Two types of organic dyes, cationic (MB) and anionic (MO) dyes were utilized to explore the adsorptive and photocatalytic characteristics of synthesised CTTIP samples. MB is a well-

known cationic dye which has been highly utilised as a model dye in research focused on wastewater treatment.

4.3.3.1 Adsorption Kinetics

The unique characteristic of immobilizing TiO_2 in a CMC matrix is that the resulting composite exhibits a high surface area which results in outstanding adsorption properties even at high concentrations.[190] Even if the zeta potential values are lower than those of CKT foam, the adsorption properties of CTTIP_110 composites surpassed those of CKT foams. This suggests that the high surface area, pore volumes, and availability of active sites in CTTIP composites contribute to their excellent adsorption capability. Figure 4.12a illustrates, the adsorption of MB to CMC, synthesised TiO_2 and CTTIP composites.

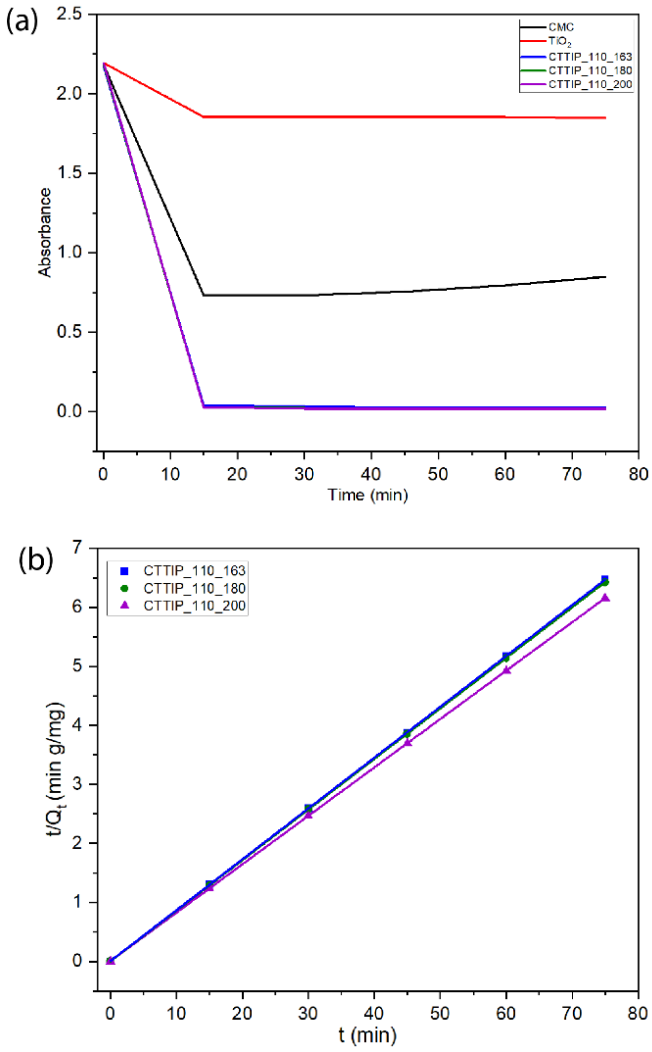

Figure 4.12 : (a) Adsorption of MB on to different samples and (b) Graph of pseudo second order adsorption kinetics

Synthesised TiO_2 shows a very small adsorption which is similar to the results obtained using commercial TiO_2 used in Chapter 3. In contrast, the adsorption of CTTIP composites are considerably higher than CMC powder and CKT foam, proving *in-situ* synthesis of TiO_2 on CMC has increased the properties of both CMC and TiO_2. Moreover, there is no significant difference in the percentage of adsorptive removal of MB observed among three CTTIP_110 composites during the 75-minute dark reaction. The adsorption kinetics of all three CTTIP_110 composites was studied using both the pseudo-first and *pseudo*-second order kinetics models, as described by the equations provided in Chapter 3 (Equation 3.3).[317] The results of the pseudo-second order calculations are summarised in Table 4.6. The data indicates that the adsorption of MB on these adsorbents follows the pseudo-second order kinetics model. Figure 4.12b illustrates the *pseudo*-second order graphs for CMC powder, TiO_2 powder, and CTTIP_110 samples. The adherence to pseudo-second order adsorption kinetics indicates that the adsorption process is primarily controlled by chemisorption.[404] These results conclude that both the surface area and the presence of negative charges within the composite (zeta potential) significantly influence the adsorption process.

Table 4.6 : Kinetics data obtained from *pseudo*-second order adsorption kinetics

Parameters	**CCTIP_110_163**	**CCTIP_110_180**	**CCTIP_110_200**
Experimental Q_e (mg/g)	11.56	11.67	12.18
Theoretical Q_e (mg/g)	11.60	11.68	12.19
K (min^{-1})	1.42	2.52	2.24
R^2	0.9999	0.9999	1.000
MB adsorption % after 75 minutes	98.40	>99	>99

4.3.3.2 Adsorption Isotherms

To determine the relationship between the adsorbent and the adsorbate, including the manner in which adsorbate molecules attach to the surface of the adsorbent when equilibrium is attained, the two isothermal models - namely Langmuir and Freundlich - were utilised. As explained in Chapter 3, the Langmuir isotherm model represents monolayer adsorption, while the Freundlich model is based on heterogeneous adsorption involving multiple layers.[405] All the equations used (Equation 3.8 and 3.9) in this study can be found in Chapter 3.

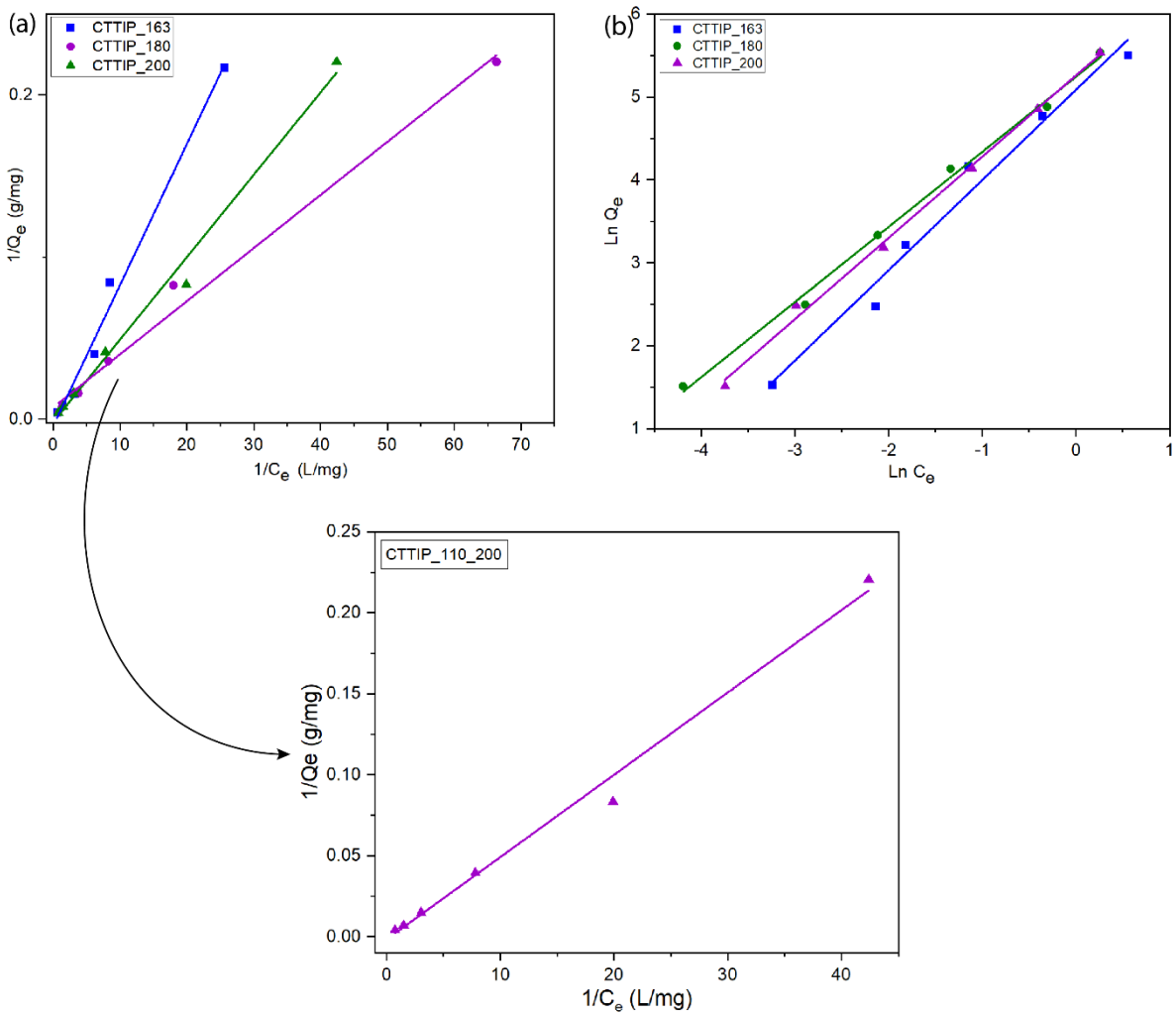

Figure 4.13 : Plots of (a) Langmuir adsorption isotherm, (b) Freundlich adsorption isotherm.

Based on the linear regression values obtained from the analysis of the adsorption isotherm in Figure 4.13 it is evident that CTTIP_110_163 follows a Langmuir adsorption isotherm while CTTIP_110_180 and CTTIP_110_200 follow a Freundlich adsorption isotherm. However, a closer examination suggests that CTTIP_110_200 samples exhibit characteristics of Langmuir adsorption isotherms at higher concentrations. It is important to note that maximum adsorption capacity from the Langmuir and Freundlich isotherms cannot be directly compared despite having the same units because the Freundlich constant does not predict the maximum adsorption.[406] Additionally, for both CTTIP_110_180 and CTTIP_110_200, the samples that facilitate multilayer adsorption, the heterogeneity factor is lower than 1, indicating that the adsorption is a favourable chemical process.[329] According to the literature, when the value of "n" is less than 1, the molecules tend to adsorb onto the surface in a horizontal orientation through multilayer adsorption.[330] The summarised results are shown in Table 4.7.

Table 4.7 : Adsorption isotherm data for the three composites.

	CTTIP_110_163	CTTIP_110_180	CTTIP_110_200
Langmuir adsorption isotherm			
Maximum adsorption capacity (mg/g)	232.55	138.88	555.55
Langmuir constant (L/mg)	0.49	2.18	2.83
R^2	0.9986	0.9900	0.9903
Freundlich adsorption isotherm			
Freundlich constant (mg/g)	162.06	303.03	192.63
Heterogeneity factor	1.08	0.90	0.09
R^2	0.9777	0.9962	0.9968

4.3.3.3 Effect of Initial Dye Concentration on Removal of MB

To determine the impact of initial dye concentration, a range of concentrations of MB (4 – 200 ppm) was used. It was observed that the adsorption capacity increased as the initial concentration of the dye increased, and this can be attributed to the enhanced mass transfer of MB molecules to the adsorbent.[319] Remarkably, from 4 ppm until 200 ppm the percentage removal of MB exceeded 99%, indicating the remarkable adsorption properties of the adsorbent, which provides abundant vacant and accessible sites for MB molecules. Additionally, at higher concentrations, the competition among MB molecules becomes significantly low due to the availability of more vacant sites. MB is also known not only to exist as a monomer in solution, but also dimer meaning the observed adsorption can occur by more than one mechanism.

Importantly, our observations suggest this high concentration of MB has a negative impact on dye degradation. The efficiency of MB degradation decreases as the active sites on the adsorbent surface become covered by adsorbed dye molecules, resulting in a low production of radicals. Furthermore, the penetration of light to reach the target photocatalysts becomes difficult at high concentrations of dye solutions. These factors collectively contribute to the decrease in MB degradation efficiency at higher concentrations.[407]

4.3.3.4 Photocatalytic Degradation of MB

To explore the photocatalytic degradation of cationic MB, all prepared samples were exposed to both UV and sunlight. In this context, a UV lamp was employed to replicate approximately

7% of the solar UV light present in natural sunlight. CMC powder alone did not show any photocatalytic activity under UV light while synthesised TiO_2 and CTTIP_110 composites exhibited useful photocatalytic activity (Figure 4.14). Table 4.8 reveals that CTTIP_110_200 exhibited the highest photocatalytic rate under UV while CTTIP_110_180 possesses the lowest of all. Moreover, as discussed in 3.3.4.1 it can be assumed that strong adsorption capability has facilitated the high photocatalytic activity of all CTTIP samples. However, it should be highlighted that all three CTTIP_110 samples displayed useful photocatalytic performance even with a UV A lamp of 1W which comparably lower in power than what has been reported in literature (Table 4.9).[55-59]

Table 4.8 : Summary of photocatalysis kinetic data for samples evaluated in this chapter.

	TiO_2	**CTTIP_110_163**	**CTTIP_110_180**	**CTTIP_110_200**
Photocatalytic rate constant (min^{-1})	0.0135	0.0539	0.0585	0.1239
Photocatalytic degradation %	95.91	89.54	87.68	> 99
Desorption %		71.14	75.52	13.19

Table 4.9 : Summary of photocatalytic activity of different samples based on the power of the UV lamp used.

Material	**Dye concentration (ppm)**	**Photocatalyst Amount (g/L)**	**Power of UV light source (W)**	**Rate (%)[a]**	**Irradiation time**	**Reference**
$MnTiO_3$	16	0.1	UVA - 100 W	15	5 h	[408]
0.5% Pd-TiO_2	20	1	UVA 100 W	99.4	120 min	[409]
PANI-TiO_2 (3%)	10	0.5	UV C – 32 W	99.6	60 min	[410]
TiO_2/Ti_3C_2	60	0.5	UV A – 500 W	96.4	60 min	[336]
Silane/ TiO_2	10	0.01	UV C – 24 W	65	5 h	[411]

[a] Rate % = photocatalytic degradation amount.

Although this phenomenon has not been extensively studied, it is hypothesised that the observed behaviour may be attributed in part to the self-aggregation of methylene blue (MB) molecules in the solution as described above. MB molecules have a tendency to form dimers, trimers, or H-type aggregates, with the bonding between these molecules believed to involve hydrophobic interactions, hydrogen bonds, and van der Waals forces. When the bonds among MB molecules are stronger than the bonds between MB molecules and the adsorbent, desorption can occur until the system reaches equilibrium. Furthermore, it is speculated that when the UV light is turned on, the localised pH of the system may change due to the formation of degradation products from MB – a phenomena we explore later one. This pH change can result in altered charges and interactions within the system, potentially leading to desorption during this period. However, as the degradation process continues, more vacant sites are created, enabling the system to progress towards increased adsorption onto the adsorbent.

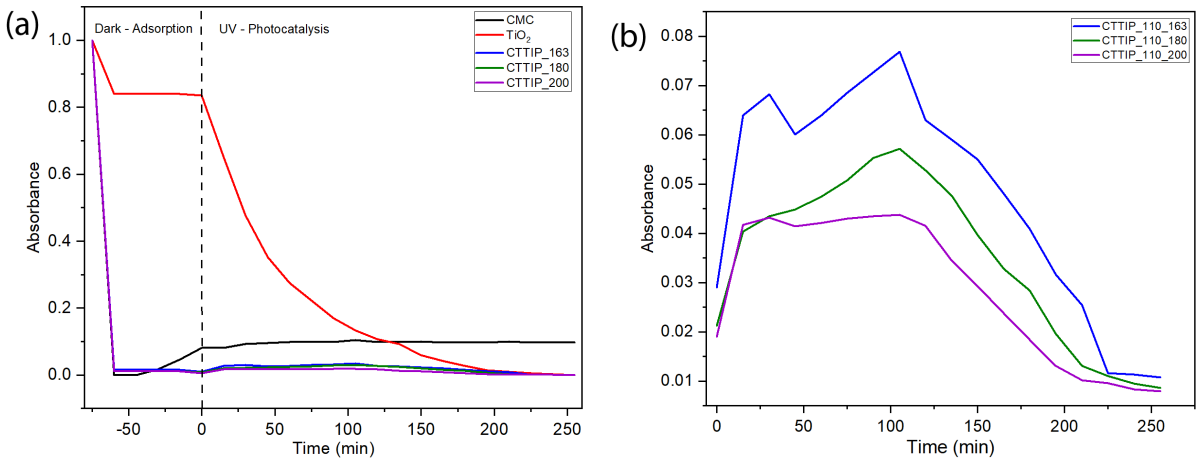

Figure 4.14: (a) Photocatalytic degradation of MB assisted by adsorption (b) a representation of Photocatalytic degradation of MB by CTTIP_110 composites only to show the areas where the desorption is prominent.

The spectrum of primary MB molecules displays a major peak at 665 nm, which is associated with the MB monomer and its n-π* transition.[412] Additionally, a shoulder peak is observed at 613 nm. There are different explanations in the literature regarding the origin of this peak at 613 nm. Some reports suggest that it is due to MB dimers,[413] while others propose that it is a result of a π-π* transition.[414] For completeness, MB also exhibits a strong absorption band at 291nm which is attributed to the substituted benzene rings.[415]

Figure 4.15 illustrates the results of the degradation pathway of methylene blue (MB) over time. It is evident that from 15 minutes to 120 minutes, there is a noticeable increase in the intensities of peaks at 577-580 nm. This indicates a blue shift in the absorption band of MB, moving from 610-570 nm to the range of 577-653 nm. This blue shift phenomenon can be attributed to the self-association of MB, as peaks around 577-580 nm are known to be associated with trimers.[416,417] The intensity of these peaks increases from 15 minutes to 120 minutes before subsequently decreasing. This provides the evidence that UV light stimulates the desorption and formation of MB trimers. Careful examination of the UV-Vis spectroscopy data also shows significant absorption at 650 nm and 607 nm was observed, which can be attributed to specific monomer mesomers and dimers of the methylene blue (MB), respectively.[418] However, these peaks are not prominently visible in the UV spectrum as their intensities are considerably lower compared to the major peaks. Additionally, it has been reported that absorptions between 585 nm and 605 nm are associated with 'multipers', although the exact positions of these peaks can vary depending on factors such as pH, solvent type, MB concentration, and the light sources employed for photodegradation.[419] Furthermore, it has been documented that MB has a tendency to self-aggregate, particularly at higher concentrations.[420]

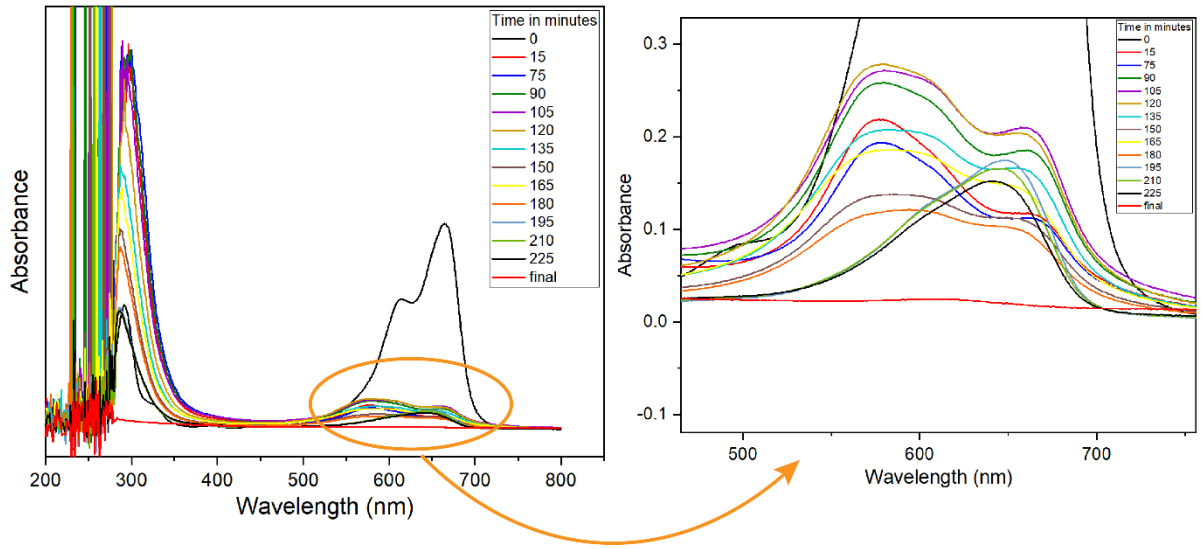

Figure 4.15: Absorption spectrum of MB aqueous solution (10 ppm) over time in the presence of a photocatalyst.

According to the data presented in Table 4.8, CTTIP_110_200 demonstrates the lowest percentage of desorption, whereas CTTIP_110_180 exhibits the highest. This could be attributed to structural modifications occurred during the synthesis process. Consequently,

further characterisation is necessary for a more comprehensive analysis of the chemical structure of CTTIP samples.

4.3.3.5 Photocatalytic Degradation Under Direct Sunlight

The band gap results of the synthesised samples were validated by analysing the photocatalytic activity of the synthesised samples under UV and direct sunlight through degradation plots of C/C_o *vs* time (Figure 4.16). The degradation of dyes in the presence of photocatalysts was observed to be more rapid under direct sunlight compared to UV light.

Several interesting observations have emerged from this analysis. Firstly, a considerable self-degradation of MB (in the absence of a photocatalyst) which is called 'photolysis' could be observed over the time. The bandgap of methylene blue (MB) is measured to be 2.43 eV, allowing it to absorb visible light photons and MB is capable of absorbing light in the wavelength range of 500–700 nm. This absorption leads to the formation of singlet and triplet species through electronic transition and intersystem crossing processes and undergo self-decomposition to a certain degree. In this visible-light-driven self-decomposition of MB, it demonstrates self-photosensitizing properties, especially in applications including phototherapy and water photo-splitting.[420,421]

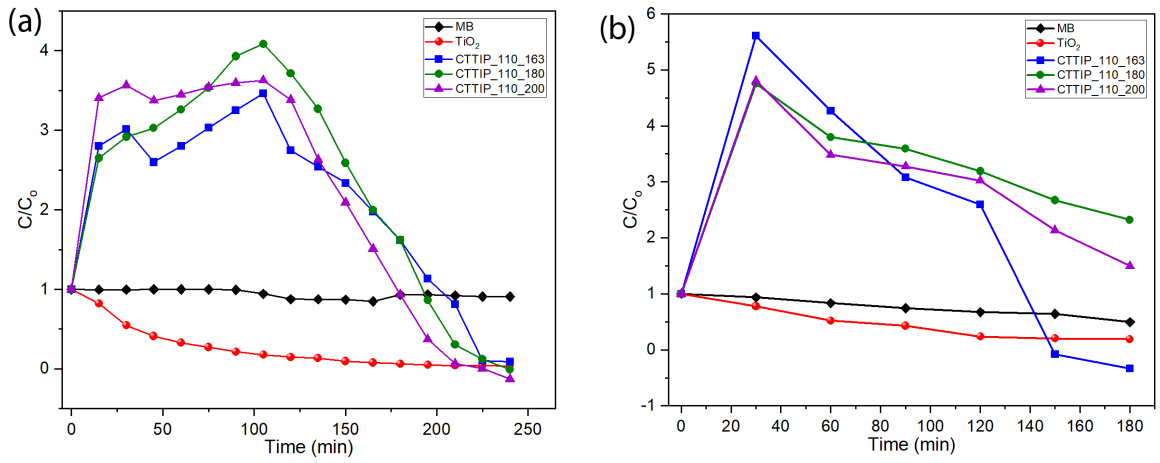

Figure 4.16 : Comparison of degradation rate of MB (a) under UV, (b) under direct sunlight.

Two processes can take place in this photolysis phenomenon;

I. Partial decomposition of MB:[422]

2 $C_{16}H_{18}N_3SCl + 25\ O_2 \longrightarrow 2\ HCl + 2\ H_2SO_4 + 6\ HNO_3 + 16\ CO_2 + 12\ H_2O$

II. Complete decomposition of MB – As documented in the literature this process depends on few factors such as pH of the system, light intensity, MB concentration and available O_2 amount. Moreover, the complete photolysis is prominent in alkaline pH. In alkaline conditions, hydroxyl radicals (˙OH) are generated through the monoelectronic reduction of MB^+ radicals by OH^-. The ˙OH radicals can then undergo reactions with each other, leading to the production of hydrogen peroxide (H_2O_2), which is a crucial active species in degradation processes. Similarly, when O_2 interacts with excited MB* radicals, it forms superoxide radicals ($O_2^{\bullet-}$). These photolysis reactions of MB can be summarised by the following Equations: [412]

$$MB^+ + OH^- \longrightarrow MB^{\cdot} + OH^{\cdot}$$
$$2\ OH^{\cdot} \longrightarrow H_2O_2$$
$$MB^{\cdot} + O_2 \longrightarrow MB^+ + O_2^{\bullet-}$$

In this project, the pH of the MB solution was not adjusted and the initial pH of the MB solution was measured to be 6.5. This can be considered a neutral value, however a considerable degradation of MB (43.0% in 3 h and 60.7% in 4 h) was obtained at this pH. This could be due to the high intensity of the direct sunlight on the particular test day. At around neutral pH conditions, MB exhibits photobleaching which occurs upon the absorption of light induces structural modifications in the MB molecule, causing a reduction in colour intensity. This can include the formation of MB oligomers, as well as the change of the dielectric constant of water, leading to changes in the distribution of electron charges within the MB monomer and impacting the photolysis process.[423,424] Another intriguing finding is that the synthesized TiO_2 powder exhibited a significant photocatalytic activity under visible light, with a degradation percentage of 81.1%. This can be attributed to the presence of Ti^{3+} in the synthesized TiO_2, which contributes to a lower band gap compared to commercial TiO_2 powder. This scenario is proven by Figure 4.11 as TiO_2 powder absorbed light above 400 nm, with a maximum of 412 nm.

When considering the three CTTIP_110 samples, their photocatalytic rates under direct sunlight correlated with their respective band gap values. CTTIP_110_163 demonstrated the highest photocatalytic rate, with a total removal of over 99% of MB within 2.5 hours. On the other hand, CTTIP_110_180 exhibited the slowest rate, resulting in a total MB removal of 98.2% within 3 hours. CTTIP_110_200, meanwhile, achieved an approximate 99% total MB removal within 3 hours. These results prove that CMC in the system had played a major role

in bringing the absorption of CTTIP_110 to the visible light region. As reported in the literature, biopolymers like CMC are rich in oxygen containing functional groups like hydroxyl ions and carboxylic groups. These groups can capture the generated holes and lower the electron-hole recombination, thus increase the photocatalytic activity under direct sunlight.[425,426] Figure 4.17 provides a clear representation of how various synthesized samples react under direct sunlight.

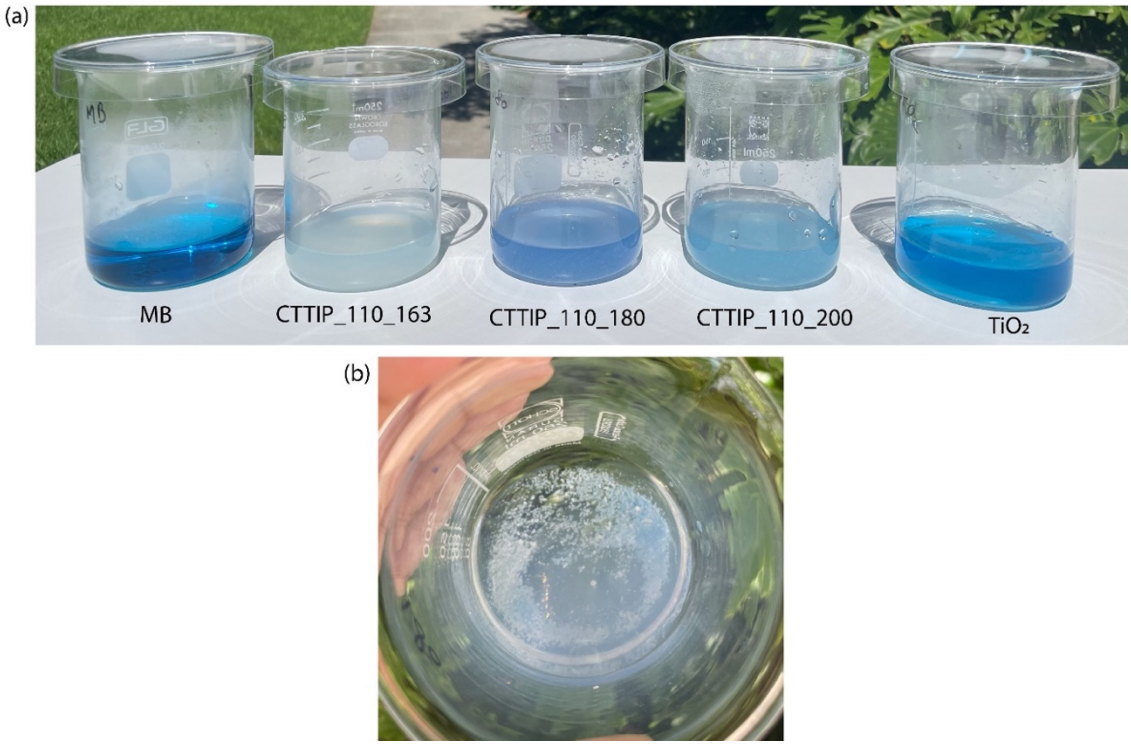

Figure 4.17 : MB degradation under sunlight (a) after 2 h of exposing to direct sunlight (b) the disappearance of the blue colour of the MB.

4.3.3.6 MB Degradation Pathway

The LC-MS technique was used to analyse the formation of intermediates during the photodegradation of MB under UV light. Figure 4.18 displays the LC-MS findings of the MB parent solution both before undergoing adsorption and degradation and after being exposed to irradiation for 240 minutes. Those results reveal a noticeable reduction in the intensity of the primary MB peak at *m/z* 284.1 over time, followed by the emergence of new peaks attributed to the generation of novel molecules. After 75 minutes no signal corresponding to *m/z* 284.1 exists. These observations indicate that nearly all the MB molecules had been removed from solution. After the adsorption process, two additional noticeable peaks emerged in the spectrum at *m/z* 105.0 and 274.2, which can be attributed to fragments of the CMC matrix.

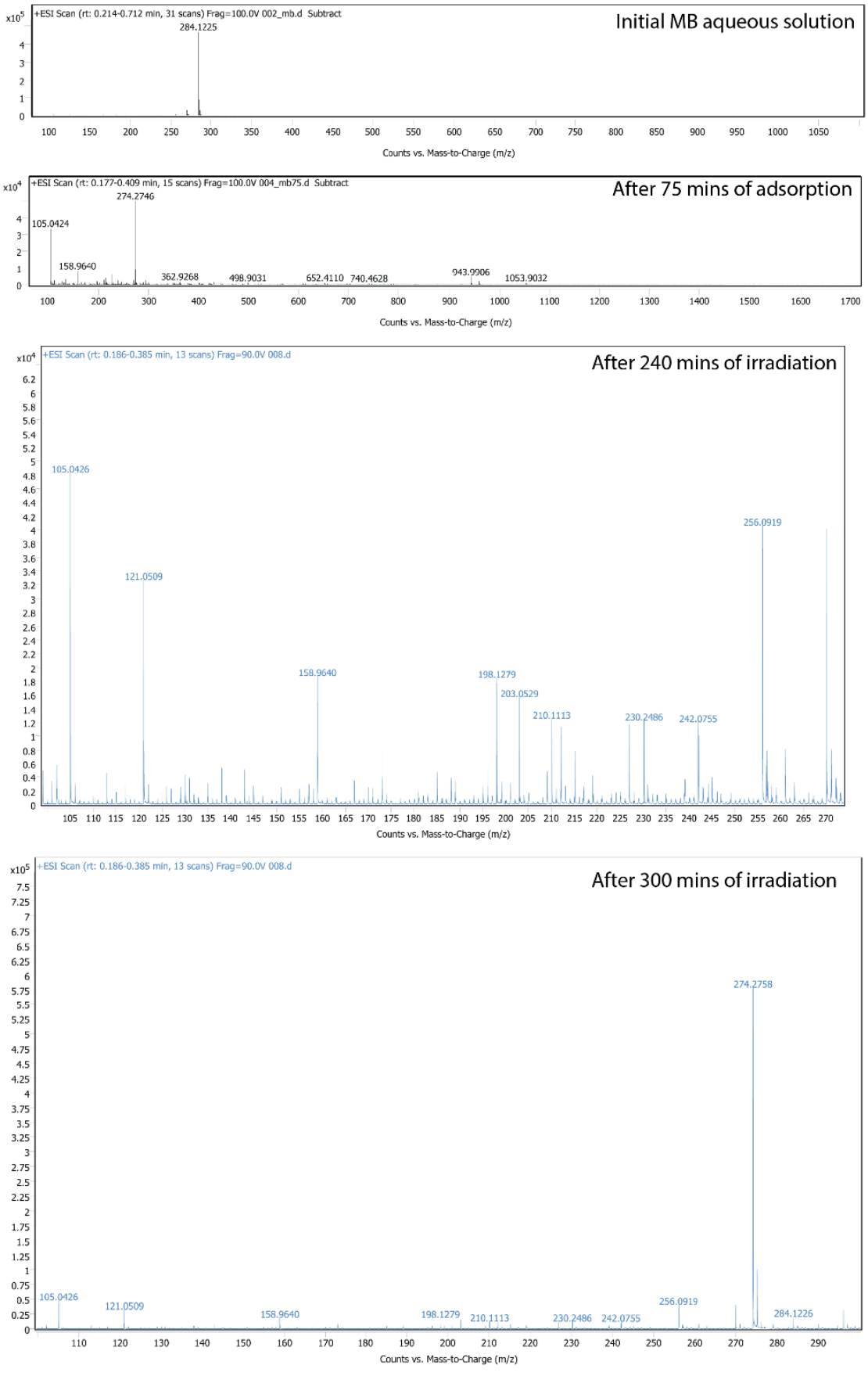

Figure 4.18 : LC-MS profile of the parent MB sample and after UV irradiation.

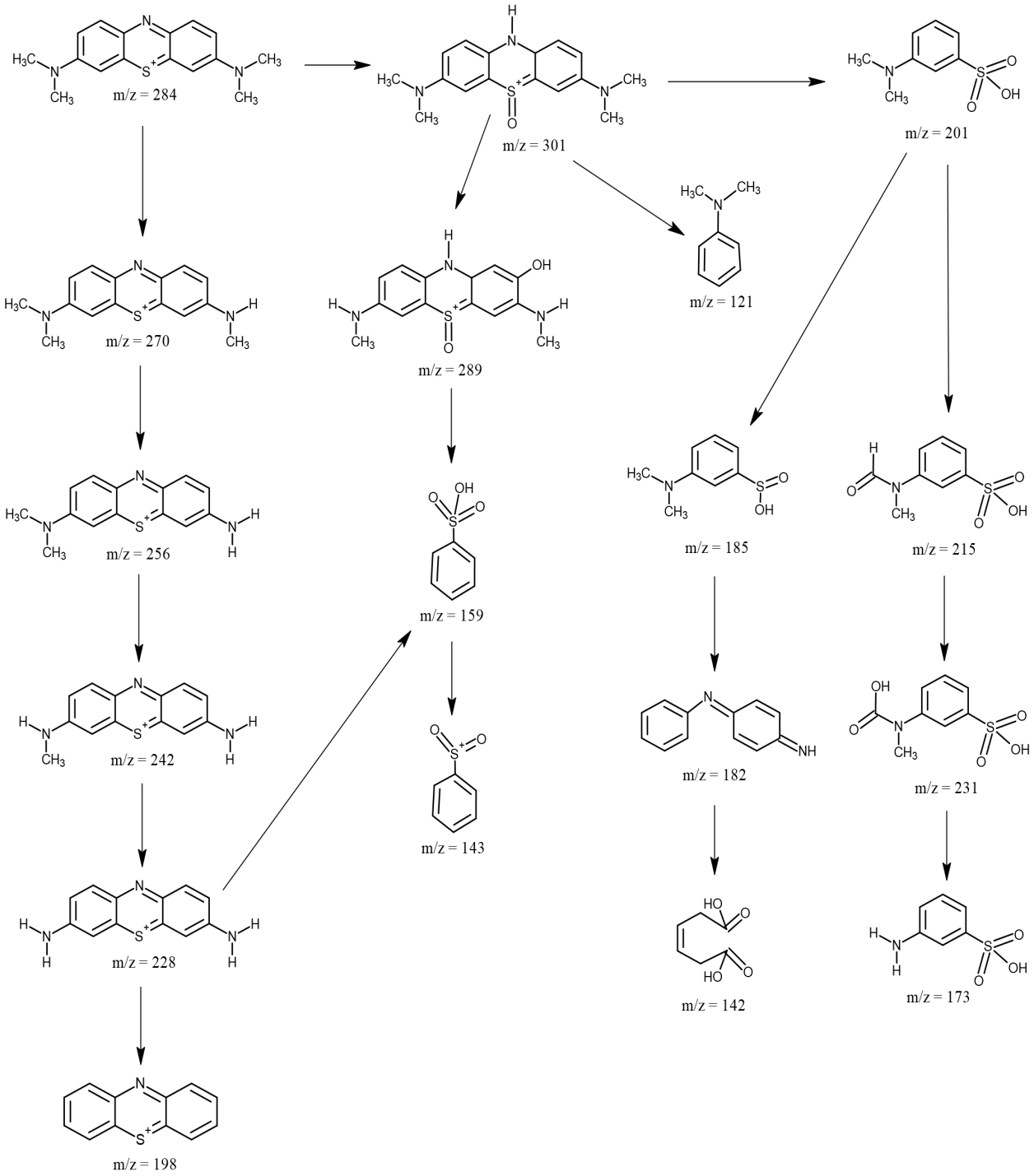

Figure 4.19 : Proposed mechanism of MB degradation under UV as evidenced by mass spectrometry.

After 240 minutes of UV irradiation several intermediate peaks were observed at different *m/z* values, including major peaks detected at 121.0, 158.9, 198.1, 203.0, 230.0, 242.0, and 256.1. Furthermore, during the photocatalytic degradation process in the presence of CTTIP_110 composites, additional intermediate peaks were detected at m/z 228.0, 270.9, 201.1, 201.0, 290.2, 143.0, 226.9, and 173.0. Based on the LC-MS results, the compounds corresponding to

the intermediate peaks and their structural formulas have been determined and a proposed photocatalytic degradation pathway for the MB dye has been developed in Figure 4.19. The pathways occurred via both oxidation and demethylation processes. These products and pathways are consistent with previous reports in the literature.[427,428,429] In order to validate these pathways, UV absorption bands were detected at 633.6 nm and 649.0 nm (648-655 nm), associated with Azure A and Azure B respectively, as in Figure 4.15.[430,431]

4.3.4 Methyl Orange (MO) Test

MO, a well-known anionic dye, was used to investigate the impact of CTTIP_110 samples on the elimination of anionic dyes. Throughout the adsorption duration, there was no observed adsorption of MO with any of the three CTTIP_110 samples. This can be attributed to the electrostatic incompatibility as a result of negative charges in both MO and CTTIP_110 samples. To examine the photocatalytic degradation of Methyl Orange (MO), only the CTTIP_110_200 sample was used due to its superior photocatalytic activity under UV conditions. It is worth noting that MO itself did not exhibit any degradation when exposed to UV radiation.

As depicted in Figure 4.20, the photodegradation of MO in the presence of CTTIP_110_200 under UV irradiation exhibits a notably low efficiency. There are several possible reasons for this behaviour. Firstly, the limited adsorption of MO onto the photocatalyst can be attributed to the repulsive forces between the photocatalyst and MO molecules as the adsorption process plays a vital role in photocatalysis, and the reduced adsorption can hinder the degradation process. Secondly, the type and wavelength of the UV light used can significantly impact photocatalysis. According to literature reports, when the wavelength decreases, TiO_2 is capable of generating more potent oxidative species. Typically, TiO_2 can only absorb a certain portion of the photons emitted by the UV A lamp.[432] Consequently, TiO_2 under UV C exhibits better photocatalytic activity compared to UV A.[433,434] In our case, the combination of relatively weaker oxidative species generation and low adsorption may contribute to the observed lower photocatalytic activity. Nevertheless, MO is clearly degraded (25%) in the presence of the CTTIP composite over 400 minutes.

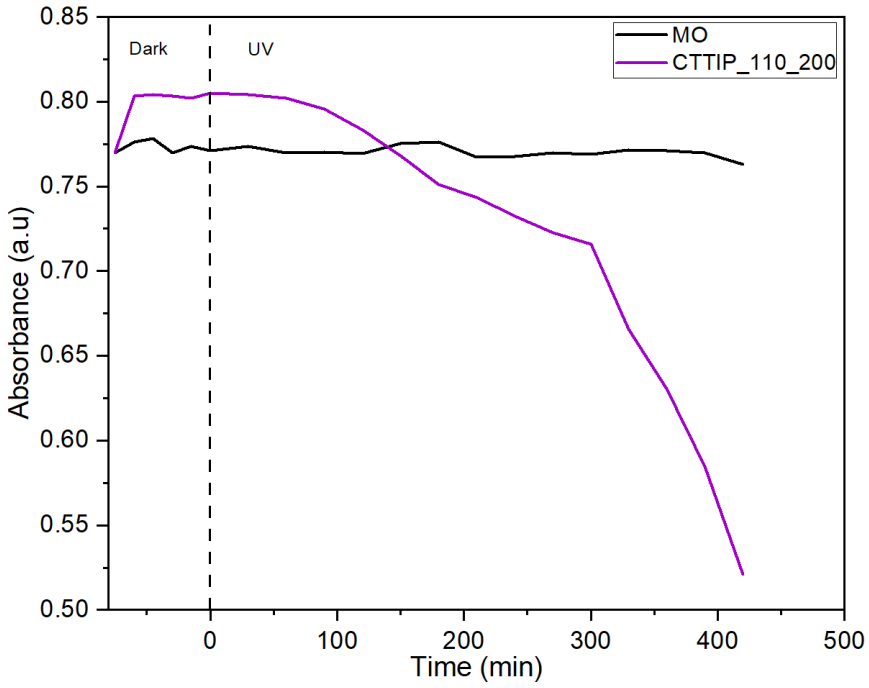

Figure 4.20 : Degradation of MO under UV in water monitoring at 465 nm.

4.3.4.1 Removal of MO Under Direct Sunlight

Figure 4.21 demonstrates the photodegradation of MO in the presence and absence of synthesized photocatalysts under direct sunlight. The control experiment performed in the absence of a photocatalyst showed a negligible amount of MO dye degradation. TiO_2 powder exhibited a slower photocatalytic rate for MO compared to MB. However, all three CTTIP_110 composites displayed superior performance in degrading MO compared to MB under direct sun light. The three composites achieved total degradation rates of 98-99% within 2.5 hours. These results suggest that the lower degradation rate observed under UV light might be attributed to the specific type and intensity of UV radiation used. Since solar light encompasses the entire range of wavelengths, including all types of UV radiation, exposure to direct sunlight leads to the generation of potent oxidative agents for MO. Figure 4.22 demonstrates the decolourisation MO through this experiment in real terms.

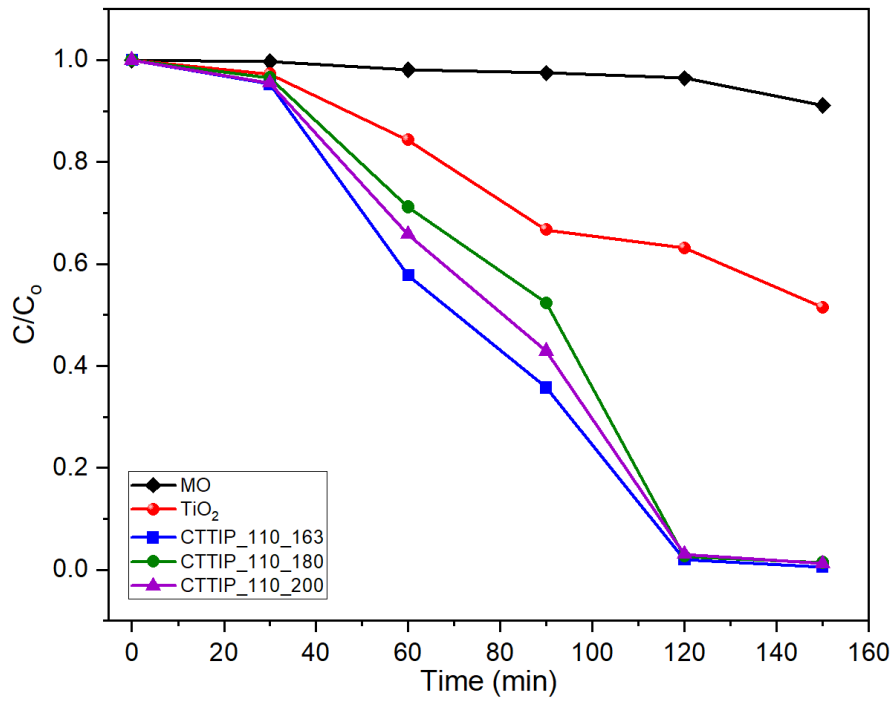

Figure 4.21 : Photocatalytic degradation MO in water under direct sunlight.

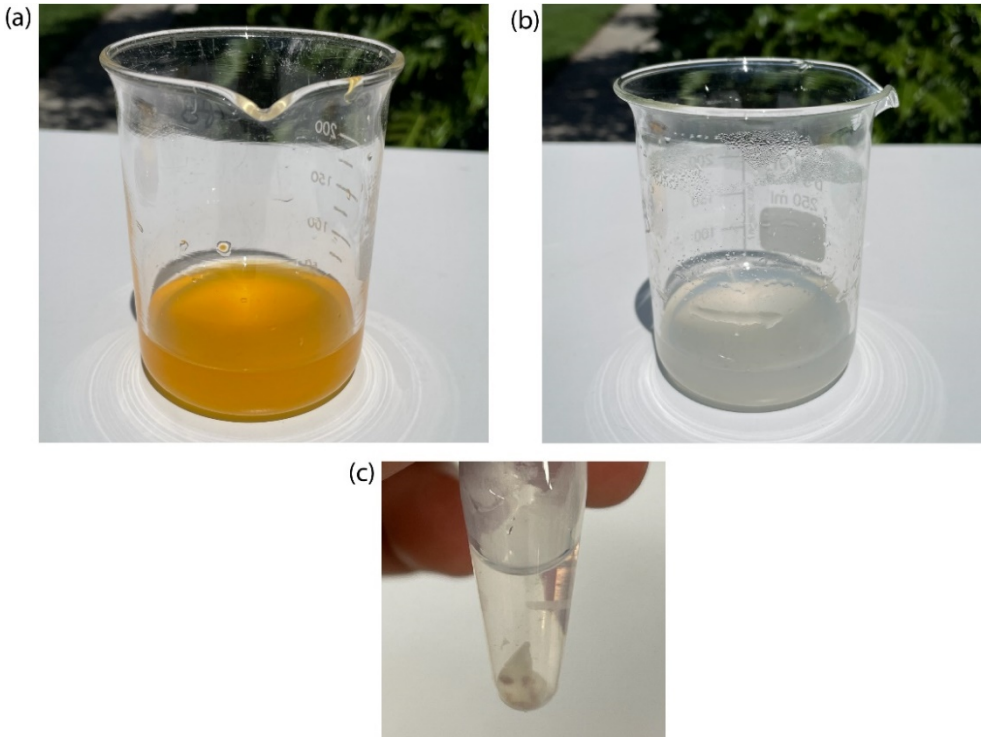

Figure 4.22 : Complete degradation of MO under direct sunlight (a) t = 0 (b) t = 120 min (c) photocatalyst collected by centrifuging the final MO sample again shows little colour.

4.3.4.2 MO Degradation Pathway

The degradation mechanism of MO under the direct sunlight in the presence of CTTIP_110_163 was again studied using LC-MS technique and the proposed mechanism is illustrated in Figure 4.23.

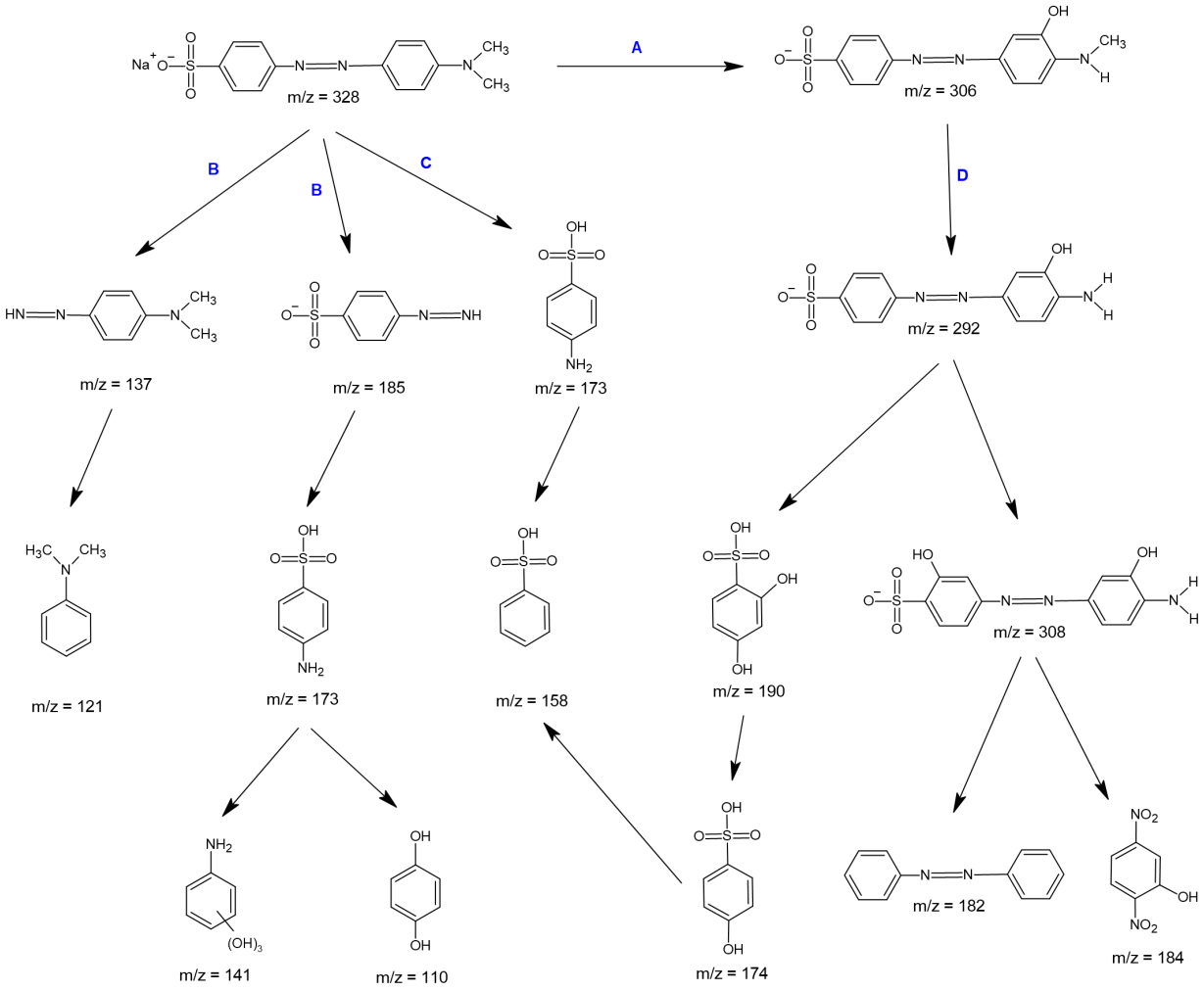

Figure 4.23 : Proposed mechanism for MO degradation under direct sunlight.

The parent MO compound provides a peak at *m/z* 328 and its degradation involves in three main pathways; labelled A-D. Pathway 'A' corresponds to the addition of an additional hydroxyl group the MO parent molecule and formation of a monohydroxylated molecule which gives the rise to the peak at m/z 306.[435] This is followed by path 'D', a loss of methyl group due to the heterolytic cleavage of N-C bond which is called demethylation.[436] Pathways B and C relate to cleavage across the azo linkage, leading to benzenesulfonic acid and *N,N*-dimethylaniline fragments which produce the peaks at *m/z* = 137 and *m/z* = 185 respectively.[437] Path 'C' involves in the cleavage of N=N bond by the attack of active species.[438] The LC-MS data from the final sample reveals the disappearance of the above intermediate peaks. A very

small number of by-products is present in the final system and majority is from the photocatalyst used. As reported in many publications,[439,440] the degradation pathway through direct demethylation of the parent MO molecule was not observed in this analysis.

4.3.5 Removal of Phenol

The photocatalytic removal of phenol in the presence of CTTIP_110_200 under UV was investigated and the change of absorbance over the time is illustrated in Figure 4.24. The findings showed an initial increase in the intensity of the peak within the first 180 minutes after the UV light was switched on. A similar observation was made by Farid and his research group, attributing it to the UV-induced oxidation and polymerization of phenols.[87] Through ESI-MS analysis, they identified the formation of higher molecular weight compounds, which exhibited the same absorption peak as the original phenolic compounds.[441] To understand the significance of the photocatalyst, a control analysis was conducted using only phenol under UV light, without the presence of a photocatalyst. The increase in absorption peak intensity in this control analysis was negligible compared to the system where both phenol and the photocatalyst were present under UV light. This difference can be attributed to the type of UV wavelength used. According to the literature, the self-oxidation of phenol under UV A is insignificant compared to that under UV B and UV C. This is because the maximum absorption of UV A overlaps with the low point in the phenol absorption curve, preventing phenol from absorbing photons emitted by the UV A lamp.[442] This confirms that the presence of TiO_2 enhances the oxidation of phenol under UV A.

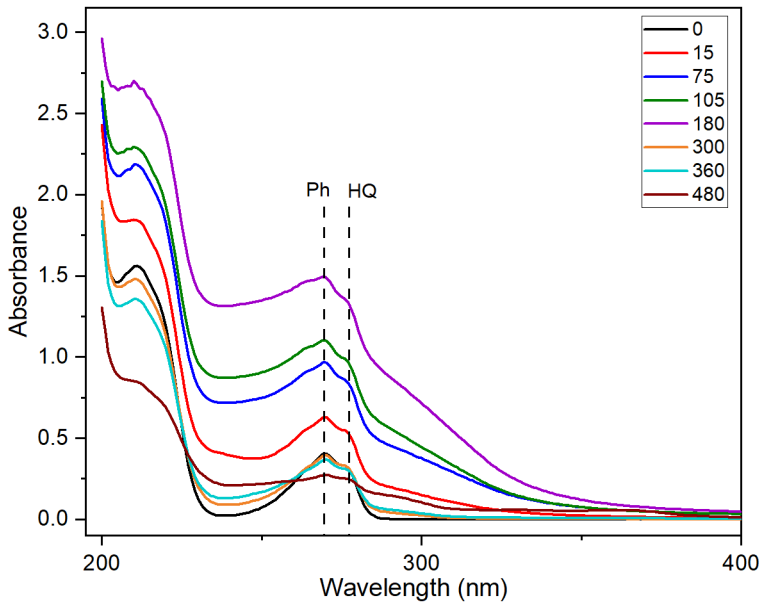

Figure 4.24 : UV-Vis absorbance profile illustrating the removal of phenol over minutes.

This oxidation and polymerisation processes entail the formation of intermediates such as hydroquinones and benzoquinones and chain reactions of them. This can happen through pathways such as those shown in Figure 4.25.[443]

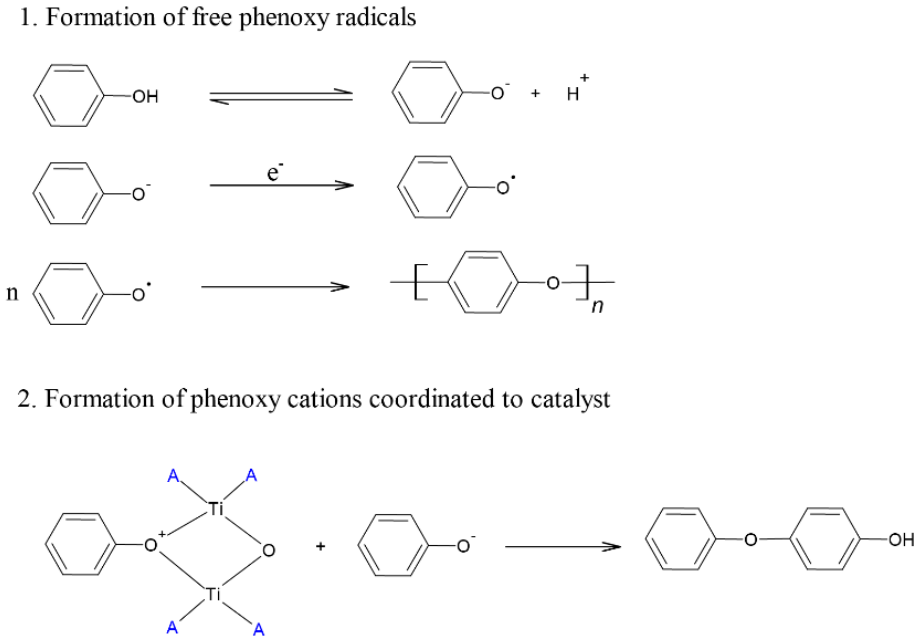

Figure 4.25 Proposed mechanisms for polymerisation of phenol

The formation of intermediates is evidenced by Figure 4.24. The initial spectrum shows a prominent absorption peak of phenol (Ph) at 270 nm. However, after 15 minutes of UV irradiation, a new peak emerges at 276 nm, which can be attributed to the presence of hydroquinone (HQ).[444] When TiO_2 is irradiated, excited electrons are produced, which can trigger the formation of free phenoxy radicals. Additionally, according to existing literature, the reactions involving phenoxy radicals may also lead to the formation of catechol and resorcinol compounds. The formed hydroquinone and catechol compounds can be oxidised in to p-benzoquinone and o-benzoquinone in the presence of O_2 as shown in Figure 4.26.[445]

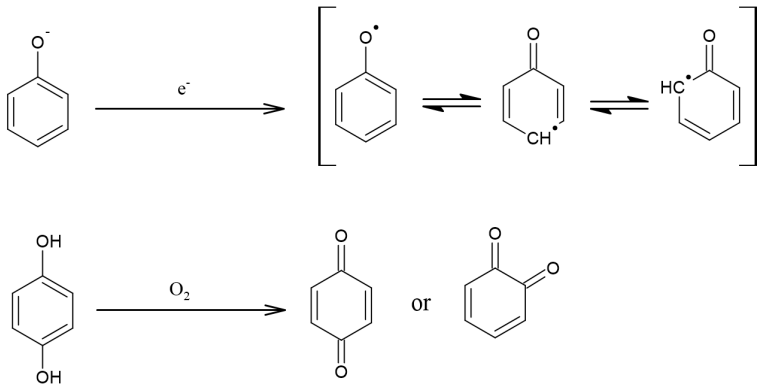

Figure 4.26 : Oxidation of phenols leading to hydroquinones.

After 180 minutes duration, the degradation of phenol slowers rate. Existing literature suggests that the presence of TiO_2 facilitates the generation of superoxide radicals, which enhances the degradation process.[446] The disappearance of both Ph and HQ peaks are clearly seen at later times (>180 min) in Figure 4.24. This process may involve a ring opening mechanism.[447] To gain further understanding into the intermediates formed and the specific degradation pathway of phenol, a mass spectroscopy analysis is necessary.

4.3.5.1 Plausible Mechanism of CTTIP Synthesis

After taking all the above results into consideration, the following mechanism of CTTIP synthesis was developed. The formation of TiO_2 takes place via hydrolysis and condensation of a titanium precursor as in Figure 4.27. Various Ti precursors including titanium isopropoxide (TTIP), titanium butoxide, (TBO), tetrabutyl titanate (TBOT), titanium ethoxide (TEO), titanium halides ($TiCl_4$, TiF_4), and titanium sulfate ($Ti(SO_4)_2$) have been used to achieve the different TiO_2 phases under different reaction conditions.[448] These precursors are Lewis acids and are highly reactive and moreover, they possess a very good coordination chemistry.[359]

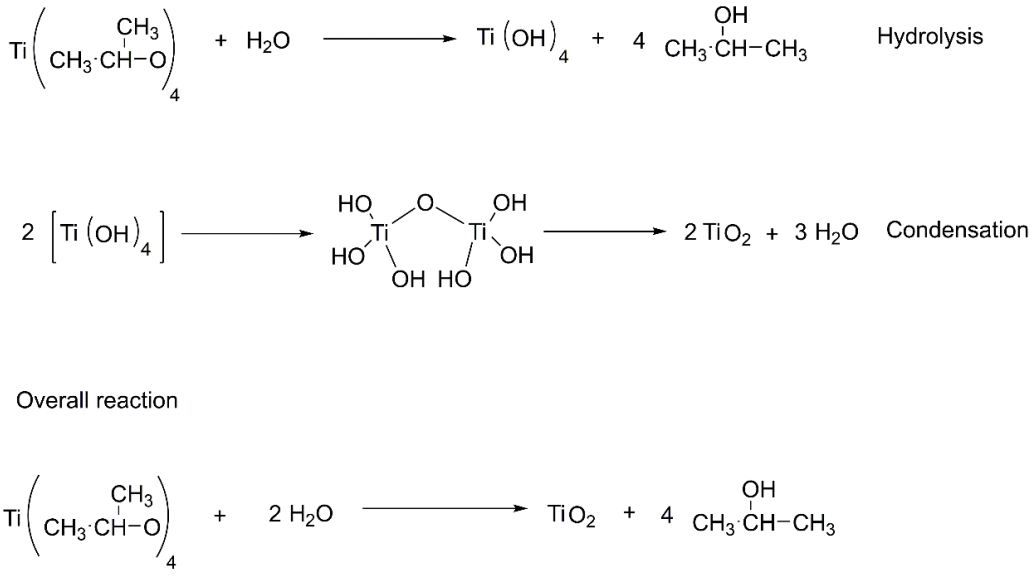

Figure 4.27: Mechanism of *in-situ* synthesis of TiO_2.

In hydrolysis, the very first step of the mechanism, alkoxide groups are replaced by hydroxyl groups through a nucleophilic attack of the oxygen atom of the water molecule. This produces titanium hydroxide and an alcohol. Due to the high reactive nature of alkoxide molecules, they

can readily react with water as soon as water is added and this can cause sudden agglomeration of TiO_2. To prevent this happening, few steps were taken such as, adding ethanol to the system and adding TTIP as a solution (in isopropanol) as these steps can control the hydrolysis rate.[449] Moreover, some researchers have used a surfactant or other compounds like acetic acid to control the hydrolysis rate, but in our method, CMC appears is capable of doing the same. Ti is known for 6 coordinate bonds, thus, it is reported to form octahedral $Ti(OH)_6$ which is considered as the primary monomer. During condensation these primary monomers can produce TiO_6 octahedra, known as the secondary monomer units.[347]

In a system containing an alien molecule such as CMC, this mechanism can deviate from the original routine. It has been suggested that TTIP can form bidentate ligands with carboxylic groups and form a 6-coordinate chelating complex.[450] This is highly possible when the number of carboxylic groups in the system is higher than that of TTIP molecules. These formed complexes can act as new precursors for crystalline TiO_2 and it can facilitate the formation of anatase through helping the octahedral to grow at necessary edges.[179] However, these complexes can be highly stable and it can lower the phase transition (amorphous to crystalline), but the proper phase transition can be achieved with suitable reaction conditions including temperature, reaction time and using proper solvents and correct ratios. For example, introducing a low molecular weight alcohol like ethanol can control the formation of octahedra with carboxylic groups. Even if this preventing mechanism is not yet deeply studied, it has been assumed that ethanol can cover Ti particles and compete with carboxylic groups. In our system, we believe both types of monomer/precursor units can be formed with both carboxylic groups and ethanol.[451] After all, these types of formed precursors are the building blocks for both amorphous and crystalline TiO_2.

Formation of anatase takes place through the rearrangements of these octahedra (TiO_6 in a conventional synthesis) and in a hydrothermal process, this step happens in an autoclave under the pressure of water vapour as a catalyst.[452] This rearrangement step is known as dissolution-crystallisation process, as in here randomly distributed TiO_6 /newly formed precursors can be rearranged with the assistance of water. If these precursor units combine with each other sharing the same edge, it can lead to formation of anatase, but if the precursor units share same corner, it will end up with rutile phases. Formation of anatase or rutile depends not only on temperature, but also other factors such as types of solvents, solvent ratio and amount of hydroxyl groups in the reaction system.[449]

In hydrothermal synthesis, a solid-gas reaction takes place since the solvents can be vaporised with high temperature and that vapour can catalyse the crystalline TiO_2 formation. According to the literature, a layer of soli-liquid-gas forms inside the autoclave where TiO_6/new precursors dissolve in water to form TiO_6^{2-} and these units recrystallise via dissolution-precipitation process.[449]

Solvents can act as a medium for mass and energy transferring, a modifier micro-topography of precursors and a regulator to control reactants concentrations.[453] The common solvents used are water, ethanol, methanol, propanol and acetic acid. Xu *et al*. had synthesised TiO_2 using a range of solvents including acetone, methanol, toluene, chloroform and some more to investigate the solvent effect on the synthesis process and they were able to identify that the dielectric constant of a solvent plays a major role in this scenario.[454] In hydrothermal synthesis, water is the main solvent used. The properties of water can be changed with high temperature and this can help the nucleation and growth process of TiO_2 crystals.[455] At a high temperature, the dielectric constant of a solvent decreases, this leads to the loss of solvent properties and in a hydrothermal reaction it is more about formation of more ions. According to the Arrhenius equations, at a high temperature, the reaction rate increases, thus the formation of ions and ionic products increases at high temperature and pressure. Moreover, the viscosity of water decreases with the density and this increases the mobility of all types of molecules (ions and precursors) in water.[456] The vapour phase of all solvents in the autoclave can create a high pressure on the solid-liquid phase inside the autoclave with high temperature. High pressure can increase the rate of mass end energy transfer in the system which will eventually lead to higher formation of nuclei and then to their growth. Additionally, having a large hydroxyl ion concentration in the medium can enhance the anatase formation.[457]

It has been identified that the water: precursor ratio is one of the principal factors to consider in the synthesis of TiO_2. According to the previous reports if this is 'ratio $\geq$ 30' the system can be led to a complete hydrolysis for a better crystalline phase. Yet, excess water can enhance the development of polymetric Ti-O-Ti chains and to have large crystallite size.[458] Lastly, the stirring rate is another important fact because it has been advised to stir vigorously to maintain a homogeneous mixture and to prevent agglomeration of TiO_2 particles. But, Kim, Tae-Hoon and the team has revealed that about 400 rpm can create large crystallites. This is because, when there are particles below the critical nucleus, they can collide with each other and form new nuclei in the direction of large particles.[459]

In this research, *in-situ* synthesis of TiO_2 on CMC has proven to act as an excellent photocatalyst even under sunlight. In accordance with the above plausible mechanism, the use of all three water, ethanol and 2-propanol has become a good decision as it has been a driving force to have a good crystalline phase of TiO_2. The described mechanisms for dye removal illustrate that CTTIP undergoes photodegradation, resulting in the formation of certain stable by-products. Whatever the mechanism, this approach is repeatable and shows excellent activity.

CHAPTER 5

Applying our Knowledge to Batik Dyes

5.1 Introduction

This chapter focuses on cultural preservation through a scientific approach. It is a well-known fact that the environment is mostly threatened by the previous approaches of the textile industry, including the batik industry.[460] The aim of this chapter is to investigate the effectiveness of novel CTTIP composite for removal of dyes used in Batik industry. Batik is a traditional textile design which originated in Indonesia and is now a technique that has spread throughout South and Southeast Asian countries including Malaysia, India, Sri Lanka and Thailand. In 2009, UNESCO recognised Indonesian batik as an Intangible World Heritage and Batik products are attractive to the international market due to its unique patterns, designs and eye-catching colours.[461] The majority of the batik industry comprises small-to-medium enterprises operated as home-based/ cottage-based businesses. There are several types of batik techniques including hand-written, stamped, printed and a combination of hand-written and stamped. Out of them, hand-written batik technique is common and expensive as it requires a lot of time and patience to gain the beautiful results.[462] In this process (Figure 5.1), the hot melted wax is applied on to a cotton or silk fabric using a metal object called canting to make fine art on the fabric. Then the fabric is dyed in a dye bath which is prepared using other chemicals depending on the type of the dyes used. In this process, the areas covered with wax do not absorb the dyes, therefore, batik is known as a process of wax-resist dying. The dyed fabric is subsequently dried and then boiled to remove wax. Following that, the coloured fabric is washed well with washing powder and then let dry completely in the direct sunlight.[463] Each step of this batik process, except the wax application step, generates a huge amount of toxic effluents which consists of dyes and other chemicals including caustic soda, soda ash, wax, alum sulphate, calcium oxides, ferric sulphate and hydrogen peroxide depending on the types of the dying process utilised. Moreover, washing and boiling steps use a large quantity of water.[464,465]

The majority of dyes utilized in the batik industry are synthetic dyes. These synthetic dyes can be classified into two primary groups, namely azo and non-azo dyes, as explained in Chapter 2. In the batik industry, the selection of dyes is primarily based on the desired colour and

intensity in the final product. Consequently, naphthol, reactive, and vat dyes are the most commonly used types of dyes for this particular process.[466] These dyes are highly toxic, carcinogenic and contain heavy metals such as Cd, Cu, Pb, Cr and Ni.[467]

Figure 5.1: Steps of batik process and the final art produced. (a) drawing the design on the fabric using hot melted wax; (b) dyeing the fabric; (c) boiling the fabric to remove wax; (d) final garments are bright and colourful

Gaining from my personal experience as an entrepreneur in the field of batik, it is evident that many individuals involved in the batik industry are with less awareness regarding the toxicity of the dyes and chemicals used in their processes. Consequently, these individuals are exposed to harmful chemicals through various routes such as inhalation, ingestion, and dermal contact. The lack of basic knowledge contributes to the release of batik effluents into water streams, resulting in severe environmental threats (Figure 5.2)

Figure 5.2 Dye waste flowing into natural water streams.

The chemicals present in batik effluents (Table 5.1) can significantly elevate the levels of chemical oxygen demand (COD) and biochemical oxygen demand (BOD) in water, leading to water pollution. Additionally, the batik sludge, which is a by-product of the batik process, serves as a favourable substrate for the growth of microorganisms. This further aggravate the environmental impact of batik waste.[468]

Table 5.1 Examples for some common dyes used in commercial batik

Dye name	Chemical structure	Chromophore	Reference
Acid Yellow 17	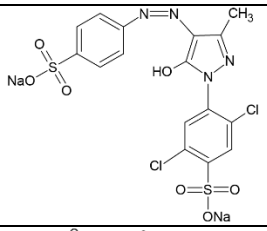	Azo	469
Reactive Blue 19	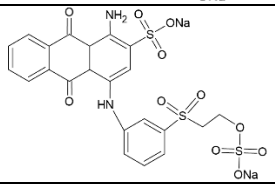	Anthraquinone	470
Sulphur Brilliant Green G	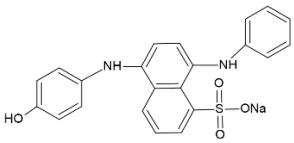	Naphethalene	471
Reactive Orange 122	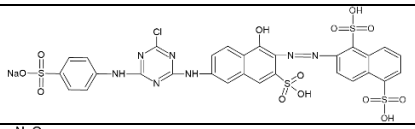	Azo	472
Reactive Black	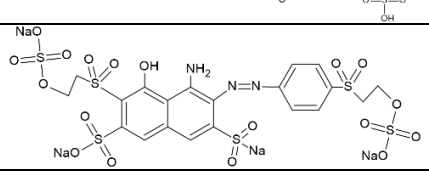	Azo	473
Tyrian Purple	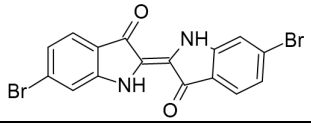	Polymethine	274

Furthermore, based on my personal experiences within my family company, it is evident that the workers in the batik industry lack adequate support from relevant stakeholders in terms of raising awareness about proper waste management practices and providing necessary resources and financial assistance for waste management. For instance, in Sri Lanka, a significant number of batik workers do not have a proper system in place to dispose of batik effluents. There are certain chemicals available for adding to the wastewater, but there is a lack of knowledge regarding their composition. Moreover, these waste treatment materials are highly expensive. In terms of batik sludge, it is often collected by cement plants for disposal. As researchers, it becomes our responsibility to seek effective, environmentally-friendly, and cost-effective methods for managing waste in the batik industry. By doing so, we can contribute to the development and advancement of this world heritage fabric-making technique to a higher level. Hence, the primary objective of this chapter is to evaluate the efficacy of CTTIP compounds in the elimination of batik dyes. This novel CTTIP compound is emphasized for its environmental friendliness and cost-effectiveness.

5.2 Experimental

5.2.1 Materials and Reagents

Three different reactive dyes were obtained by our family batik business in Sri Lanka. The dyes were procured from the Indian dye importer Dye Chem, selected specifically for their high-water solubility. Although they were provided with commercial names, the specific chemical structures of these well-established dyes were confirmed by existing scientific literature. The reactive dyes obtained were named and their structures are shown in Figure 5.3.

5.2.2 Removal of Dyes

Initially, 50 mL solutions of 20 ppm of the above dyes were used in the presence of 0.87 g/L of CTTIP_110_200 for adsorption experiment in the dark under constant stirring. The concentration of the dye solution was deliberately selected to enable the observation of both adsorption and photocatalytic activity of the CTTIP_110_200 sample within the visible range. The quantity of photocatalyst was determined as the optimized amount for this purpose. Based on the adsorption results, all three of the dye samples are anionic. Therefore, only Scarlet LC GN dye was chosen for the photocatalytic activity with CTTIP_110_200 under UV A light. Samples were taken every 30 minutes. The suspension was centrifuged out using an Eppendorf Minispin Centrifuge at 13,000 rpm for 10 min. The concentrations were monitored by a

Shimadzu UV-visible spectrometer. Two parallel experiments were conducted; one in dark and the other one under UV A.

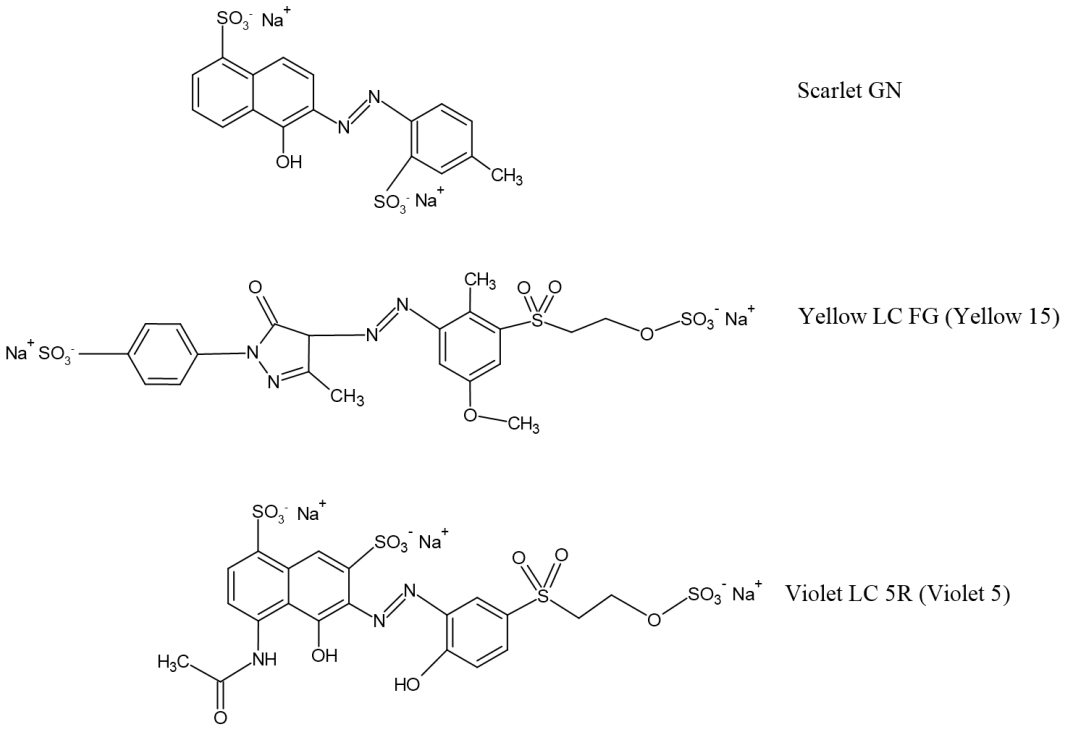

Figure 5.3 Chemical structures of the reactive dyes used within the batik samples.

5.3 Results and Discussions

Throughout the adsorption experiments, it was observed that none of the dyes exhibited significant adsorption, suggesting that all the mentioned reactive dyes are anionic in nature. These findings are consistent with the dye structures reported in the literature, which we were able to identify by correlating the chemical structures with the colour index assigned to their commercial names.

Only Scarlet GN dye was chosen to represent to ensemble of azo dyes in Figure 5.3. The UV absorbance of the dye over the degradation period is illustrated in Figure 5.4. The spectra are complicated and characterised by a maximum absorption of Scarlet GN dye at 506 nm, which can be attributed to the chromophoric azo group. The absorption peaks observed at 290 nm, 315 nm, and 385 nm arise from electron transitions occurring in aromatic groups, including benzene rings attached to the azo group, as well as the inductive effect of the azo group.[474] Upon switching on the UV light until 105 minutes, the intensity of the 290 nm peak increased, possibly due to the optimisation of *cis/trans* isomerism within the azo group.

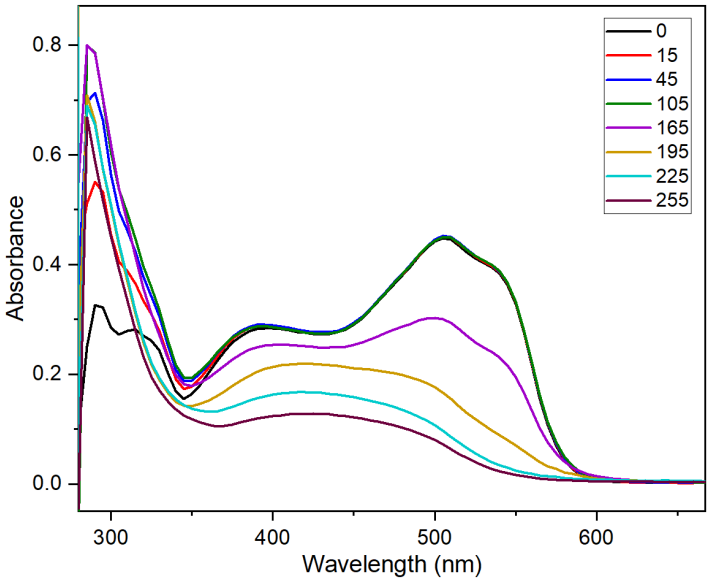

Figure 5.44 Absorption profile of the Scarlet GN dye in water (20 ppm) over 255 min under UVA irradiation.

The degradation of the dye started after 180 minutes of UV light exposure. The observed changes are evident in the gradual reduction of the 506 nm peak over time and the occurrence of a blueshift, signifying the degradation and decomposition of the azo group.[475] The observed changes are evident in the gradual reduction of the 506 nm peak over time and the occurrence of a blueshift, signifying the degradation and decomposition of the azo group. A new broad peak emerged at 345 nm, which is likely attributed to the blue shift of the 385 nm peak caused by the breakdown of the azo group.[476] As time progressed, the appearance of these new peaks disappeared, revealing the degradation of the dye. As a result, it is essential to perform LC-MS analysis to determine the exact degradation pathway, which will be carried out in subsequent studies. The overall degradation percentage of the dye was determined to be 86%, which clearly depicts in Figure 5.5, further confirming that CTTIP_110 materials exhibit effectiveness on both cationic and anionic dyes.

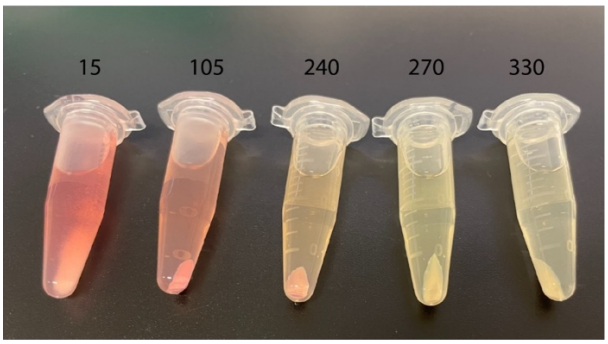

Figure 5.5 : Colour change of Scarlet GN dye over the time.

5.4 Conclusion

In this thesis, the aim was to synthesize a photocatalyst that is not only environmentally friendly and effective but also cost-effective and versatile in its functionality. CMC and TiO_2 were chosen as the main components to achieve this objective. CMC, being a polysaccharide biopolymer with several promising properties such as rich functional groups, cost-effectiveness, environmental friendliness, and abundant availability, was selected to benefit the environment. On the other hand, TiO_2, a well-known and extensively researched photocatalyst, was chosen for its unique characteristics, such as being a good semiconductor, environmentally friendly, low toxicity, and cost-effectiveness.

To create the CMC-TiO_2 bionanocomposite, two methods were employed. In the first method, TiO_2 powder (specifically P25, a mixture of anatase, rutile, and a small amount of amorphous TiO_2) was incorporated into CMC powder using a simple approach. The resulting CMC/TiO_2 composite was freeze-dried to form a foam, which provided the final product with desirable properties, including high porosity. The presence of CMC acted as a surfactant, promoting both steric and electro stabilization, leading to a homogeneous distribution of TiO_2. As a result, the composite exhibited good stability when suspended in water.

The CMC/TiO_2 foam demonstrated a highly negative charge from zeta potential analysis, which facilitated its strong adsorption properties towards MB, a cationic dye. The adsorption of MB dye molecules on the foam followed the Freundlich isotherm, indicative of multi-layer adsorption. Significantly, the CMC/TiO_2 foam was able to remove 53% of MB via adsorption in 75 minutes and over 90% of MB dye via photocatalysis within 4 hours of exposure to UV light. Total removal of MB was recorded as 96% within 6 hours. However, it was observed that the photocatalytic activity of the TiO_2 powder alone (>99%) under UV light was faster compared to that of the prepared foam. This difference may be attributed to the formation of micelles of TiO_2 covered by CMC chains, which could hinder the radicals generated from reaching MB. Additionally, intriguingly, there were certain time periods during UV exposure where desorption of MB became more pronounced than adsorption, possibly due to the formation of MB oligomers in the system.

Additionally, it was observed that increasing the amount of TiO_2 in the composite resulted in more leaching of TiO_2 into the water. As the next step to immobilise TiO_2 within the CMC network, the composite was prepared via in-situ synthesis of TiO_2 on CMC using hydrothermal synthesis at 110°C (CTTIP_110) and three different pressures inside the autoclave. XRD

analysis revealed that all three CTTIP_110 composites and the synthesised TiO_2 powder contained only the anatase phase. Furthermore, the XRD results indicated a well-mixed interaction between CMC and TiO_2 during the synthesis. Notably, XPS results demonstrated the presence of Ti^{3+} in all the synthesized samples, including the TiO_2 powder. Additionally, Ti-C bonds were observed in the prepared CTTIP_110 composites, confirming the successful interactions between CMC and TiO_2. The band gaps were calculated using DRS (diffuse reflectance spectroscopy) technique, showing relatively low band gaps and maximum absorptions in the visible range for all CTTIP_110 composites and TiO_2 powder. The composite prepared at the lowest pressure inside the autoclave exhibited the highest crystallite size and the lowest band gap (2.7 eV) among all the composites.

The CTTIP_110 composites displayed excellent adsorption capacity towards cationic MB dye, even at higher dye concentrations. At 10 ppm dye concentration, nearly 99% of the dye molecules were adsorbed within 75 minutes. However, anionic dyes (MO and SR) did not show significant adsorption. Moreover, all the synthesized composites, including TiO_2 powder, exhibited excellent photocatalytic activity under both UV A and direct sunlight towards both MB and MO dyes. Both types of dyes were degraded under direct sunlight within 2-3 hours. The CTTIP_110 composite prepared at the lowest pressure inside the autoclave (CTTIP_110_163) showed the highest photocatalytic activity under direct sunlight, (>99%) which could be attributed to its low band gap (2.74 eV) and high crystallite size. However, it displayed the lowest photocatalytic activity under UV A, likely due to a wide range of particle sizes in the water system, as indicated by zeta potential analysis showing high polydispersity. Interestingly, the synthesized TiO_2 exhibited good photocatalytic activity under direct sunlight, a characteristic not commonly seen in commercial TiO_2, possibly due to the formation of Ti^{3+} ions during the synthesis process, resulting in a low band gap.

Furthermore, the CTTIP_110 composite demonstrated its versatility in wastewater treatment by effectively degrading phenol under UV A. It was observed that phenol underwent oxidation reaction, which was enhanced by TiO_2, making it useful for deposition purposes. Additionally, the composite effectively degraded scarlet red, a textile dye used in the batik process, within approximately 4 hours of exposure to UV A. Another notable aspect was that the CTTIP_110 composites were activated under UV A even by a UV source with very low power (1W), compared to what has been reported in the literature.

Identifying the limitations of the prepared composites are important to place the research in context. The stability of CKT/TiO_2 foam diminished as the amount of TiO_2 increased, resulting in the leaching of TiO_2 into the system-This will have to be rectified in future development. Disappointingly, the foam did not exhibit notable antibacterial properties under the conditions used. Given the hygroscopic nature of the foam, proper storage precautions are necessary. As for batik dyes, our research was unable to adequately explore stakeholder engagement in wastewater management within the given time constraints.

Based on the above results, it can be concluded that the CMC/ TiO_2 composite is a powerful candidate for wastewater treatment.

5.5 Future Work

Our study has revealed the excellent properties of the prepared CTTIP_110 composites for wastewater treatment applications. As we move forward, our focus will be on understanding the structure-property relationship within these composites to further enhance their capabilities for a wide range of wastewater treatment scenarios.

The utilization of CMC as a bio-polymer with a substantial structure allowed us to form a complex structure with TiO_2. Significantly, ours is the pioneering project that employs CMC to immobilize TiO_2, and we have successfully synthesized a composite with significantly improved adsorption and degradation properties. Hence, it becomes important to gain a profound understanding of the internal structural transformations that occurred during the synthesis process, leading to these remarkable properties. To achieve this, we have planned to obtain Synchrotron beamtimes, as the complexity of the analysis requires finer details on the structure.

Concurrently, our intentions are to delve deeper into working with batik wastes. Having established that the samples are well-suited to degrade anionic dyes, including batik reactive dyes, the next step is to batik wastes directly from batik dye baths, sourced from a Sri Lankan batik workshop. These wastes are known to contain more chemicals, including toxic ones mentioned in Chapter 5, presenting an ideal opportunity for further investigation.

As a promising candidate for wastewater treatment, it is essential to assess the antibacterial properties of the synthesized CTTIP_110 composites and TiO_2 powder. Therefore, we have arranged for antibacterial tests to evaluate their efficacy in tackling bacterial contaminants.

Additionally, our aim is to explore the versatility of CMC/ TiO_2 composites in removing heavy metals and ionic solvents from wastewater, expanding the scope of their applications.

Furthermore, we plan to implement certain modifications in our approach, such as increasing the reaction time, altering solvent ratios, and adjusting the amount of TTIP used, with the objective of enhancing the properties of CTTIP composites even further.

In conclusion, the exceptional performance of the CTTIP_110 composites in wastewater treatment has opened up a new path of research, driving us to investigate their underlying structural attributes and explore their potential in various applications. By continually refining and enhancing their properties, we aim to contribute significantly to the advancement of environment.

5.6 References

(1) Noor, R.; Maqsood, A.; Baig, A.; Pande, C. B.; Zahra, S. M.; Saad, A.; Anwar, M.; Singh, S. K. *Urban Clim.* **2023**, 48, 101413-101442.

(2) Jayaswal, K.; Sahu, V.; Gurjar, B. R. *Water Pollution, Human Health and Remediation*. In *Water Remediation*, Bhattacharya, S., Gupta, A. B., Gupta, A., Pandey, A. Eds.; Springer Singapore, **2018**; pp 11-27.

(3) Yanxun, S.; Yani, W.; Hui, Q.; Yuan, F. *Procedia Environ. Sci* **2011**, 11, 939-944.

(4) Sharma, R.; Kumar, R.; Sharma, D. K.; Sarkar, M.; Mishra, B. K.; Puri, V.; Priyadarshini, I.; Thong, P. H.; Ngo, P. T. T.; Nhu, V.-H. *Environ. Dev. Sustain.* **2022**, 24, 7471-7492.

(5) Kong, X.; Ghaffar, S.; Determann, M.; Friese, K.; Jomaa, S.; Mi, C.; Shatwell, T.; Rinke, K.; Rode, M. *Water Res.* **2022**, 221, 118721-118732.

(6) Okon, A. J.; Inyang, I. B.; Ugbe, U. M.-J.; Ekpenyong, B. N.; Olanrewaju, O. E. *Environ. Monit. Assess.* **2022**, 194, 799-810.

(7) Chen, S.; Ji, C.; Jin, S. *J. Agric. Econ.* **2022**, 73, 541-563.

(8) Ezugbe, E.; Rathilal, S. *Membranes* **2020**, 10, 89.

(9) Zamora-Ledezma, C.; Negrete-Bolagay, D.; Figueroa, F.; Zamora-Ledezma, E.; Ni, M.; Alexis, F.; Guerrero, V. H. *Environ. Technol. Innov.* **2021**, 22, 101504-101529.

(10) Chatterjee, P. *Water Pollutants Classification and Its Effects on Environment*. In *Carbon Nanotubes for Clean Water*, **2018**; pp 11-26.

(11) Ajmal, A.; Majeed, I.; Malik, R. N.; Idriss, H.; Nadeem, M. A. *RSC Adv.* **2014**, 4, 37003-37026.

(12) Santos-Francés, F.; García-Sánchez, A.; Alonso-Rojo, P.; Contreras, F.; Adams, M. *J. Environ. Manage.* **2011**, 92, 1268-1276.

(13) Murray, S. A.; Kohli, G. S.; Farrell, H.; Spiers, Z. B.; Place, A. R.; Dorantes-Aranda, J. J.; Ruszczyk, J. *Harmful Algae* **2015**, 49, 19-28.

(14) La, V. T.; Cooke, S. J. *Reviews fish. sci.* **2011**, 19, 21-33.

(15) Cunningham, S. A. *Disasters* **2005**, 29, 99-128.

(16) Guillot, S.; Charlet, L. *J. Environ. Sci. Health A* **2007**, 42, 1785-1794.

(17) Khurana, D.; Sadashiva, S.; Dey, B.; Guruprasad, K. P.; Bhat, S. N.; Singh, B. N. *Appl. Nanosci.* **2023**.

(18) Lund Schlamovitz, J.; Becker, P. *Int. J. Water Resour. Dev.* **2021**, 37, 278-299.

(19) Mackenzie L. Davis, P. D. P. E. D. E. E. *THE DESIGN AND CONSTRUCTION PROCESSES*. In *Water and Wastewater Engineering: Design Principles and Practice*, First edition. ed.; McGraw-Hill Education, **2010**.

(20) Radcliffe, J. C.; Page, D. *Water Cycle* **2020**, 1, 19-40.

(21) Høibye, L.; Clauson-Kaas J Fau - Wenzel, H.; Wenzel H Fau - Larsen, H. F.; Larsen Hf Fau - Jacobsen, B. N.; Jacobsen Bn Fau - Dalgaard, O.; Dalgaard, O. *Water Sci. Technol.* , 963-968.

(22) Zhang, Y.; Mo, J.; Li, Y.; Sundell, J.; Wargocki, P.; Zhang, J.; Little, J. C.; Corsi, R.; Deng, Q.; Leung, M. H. K.; et al. *Atmos. Environ.* **2011**, 45, 4329-4343.

(23) Mall, I. D.; Srivastava, V. C.; Agarwal, N. K. *J. Hazard. Mater.* **2007**, 143, 386-395.

(24) Sonune, A.; Ghate, R. *Desalination* **2004**, 167, 55-63.

(25) Mo, J.; Zhang, Y.; Xu, Q.; Lamson, J. J.; Zhao, R. *Atmos. Environ.* **2009**, 43, 2229-2246.

(26) Hanaor, D. A. H.; Sorrell, C. C. *J. Mater. Sci.* **2010**, 46, 855-874.

(27) Ohtani, B.; Prieto-Mahaney, O. O.; Li, D.; Abe, R. *J. Photochem. Photobiol. A: Chem.* **2010**, 216, 179-182.

(28) Arun, J.; Nachiappan, S.; Rangarajan, G.; Alagappan, R. P.; Gopinath, K. P.; Lichtfouse, E. *Environ. Chem. Lett.* **2023**, 21, 339-362.

(29) Haider, A. J.; Jameel, Z. N.; Al-Hussaini, I. H. M. *Energy Procedia* **2019**, 157, 17-29.

(30) Mohammed, S.; Shnain, Z.; Abid, M. *Eng. Technol. J.* **2022**, 40, 1-13.

(31) Wu, C.; Tang, Q.; Zhang, S.; Lv, K.; Fuku, X.; Wang, J. *ACS Appl. Mater. Interfaces* **2023**, 15, 30127-30138.

(32) Ren, X.; Yao, H.; Tang, R.; A, R.; Yuan, S.; Wang, W.; Ali, I. M.; Hu, Z.-H. *Environ. Sci. Pollut. Res.* **2023**, 30, 35023-35033.

(33) Rafique, M.; Hajra, S.; Irshad, M.; Usman, M.; Imran, M.; Assiri, M. A.; Ashraf, W. M. *ACS Omega* **2023**, 8, 25640-25648.

(34) Huang, Y.; Ho, S. S.; Lu, Y.; Niu, R.; Xu, L.; Cao, J.; Lee, S. *Molecules* **2016**, 21, 56-75.

(35) An, Y.-C.; Gao, X.-X.; Jiang, W.-L.; Han, J.-L.; Ye, Y.; Chen, T.-M.; Ren, R.-Y.; Zhang, J.-H.; Liang, B.; Li, Z.-L.; et al. *Environ. Res.* **2023**, 223, 115409-115432.

(36) Poonia, K.; Patial, S.; Raizada, P.; Ahamad, T.; Parwaz Khan, A. A.; Van Le, Q.; Nguyen, V.-H.; Hussain, C. M.; Singh, P. *Environ. Res.* **2023**, 222, 115349-115363.

(37) Vatanpour, V.; Pasaoglu, M. E.; Kose-Mutlu, B.; Koyuncu, I. *Ind. Eng. Chem. Res.* **2023**, 62, 6537-6558.

(38) Etale, A.; Onyianta, A. J.; Turner, S. R.; Eichhorn, S. J. *Chem. Rev.* **2023**, 123, 2016-2048.

(39) Ortega Saez, N.; Arno, R.; Marchetti, A.; Cauberghs, S.; Janssens, K.; Van der Snickt, G.; Al-Emam, E. *Herit. Sci.* **2023**, 11, 78-95.

(40) Souzandeh, H.; Wang, Y.; Netravali, A. N.; Zhong, W.-H. *Polym. Rev.* **2019**, 59, 651-686.

(41) Liu, H.; Cao, C.; Huang, J.; Chen, Z.; Chen, G.; Lai, Y. *Nanoscale* **2020**, 12, 437-453. Souzandeh, H.; Johnson, K. S.; Wang, Y.; Bhamidipaty, K.; Zhong, W.-H. *ACS Appl. Mater. Interfaces.* **2016**, 8, 20023-20031.

(42) Heinze, T.; Koschella, A. *Macromol. Symp.* **2005**, 223, 13-40.

(43) Ahmadian, M.; Jaymand, M. *Coord. Chem. Rev.* **2023**, 486, 215152-215173.

(44) Jadeja, N. B.; Banerji, T.; Kapley, A.; Kumar, R. *Water Secur.* **2022**, 16, 100119-100123.

(45) Xue, J.; Wang, Q.; Zhang, M. *Sci. Total Environ.* **2022**, 826, 154146-154158.

(46) Liu, Y.; Li, H.; Cui, G.; Cao, Y. *Sci. Rep.* **2020**, 10, 3012-3026.

(47) Kumar, A.; Sharma, G.; Naushad, M.; Thakur, S. *J. Chem. Eng.* **2015**, 280, 175-187.

(48) Srivastav, A. L.; Ranjan, M. *Chapter 1 - Inorganic water pollutants*. In *Inorganic Pollutants in Water*, Devi, P., Singh, P., Kansal, S. K. Eds.; Elsevier, **2020**; pp 1-15.

(49) Malakar, A.; Snow, D. D. *Chapter 17 - Nanoparticles as sources of inorganic water pollutants*. In *Inorganic Pollutants in Water*, Devi, P., Singh, P., Kansal, S. K. Eds.; Elsevier, **2020**; pp 337-370.

(50) Xia, Y.; Zhang, M.; Tsang, D. C. W.; Geng, N.; Lu, D.; Zhu, L.; Igalavithana, A. D.; Dissanayake, P. D.; Rinklebe, J.; Yang, X.; et al. *Appl. Biol. Chem.* **2020**, 63, 8-21.

(51) Madhav, S.; Ahamad, A.; Singh, A. K.; Kushawaha, J.; Chauhan, J. S.; Sharma, S.; Singh, P. *Water Pollutants: Sources and Impact on the Environment and Human Health*. In *Sensors in Water Pollutants Monitoring: Role of Material*, Pooja, D., Kumar, P., Singh, P., Patil, S. Eds.; Springer Singapore, **2020**; pp 43-62.

(52) Singh, J.; Yadav, P.; Pal, A. K.; Mishra, V. *Water Pollutants: Origin and Status*. In *Sensors in Water Pollutants Monitoring: Role of Material*, Pooja, D., Kumar, P., Singh, P., Patil, S. Eds.; Springer Singapore, **2020**; pp 5-20.

(53) Islam, T.; Repon, M. R.; Islam, T.; Sarwar, Z.; Rahman, M. M. *Environ. Sci. Pollut. Res.* **2023**, 30, 9207-9242.

(54) Lima, I. B.; Boëchat, I. G.; Fernandes, M. D.; Monteiro, J. A. F.; Rivaroli, L.; Gücker, B. *Environ. Sci. Pollut. Res.* **2023**, 30, 27030-27040.

(55) Morin-Crini, N.; Lichtfouse, E.; Liu, G.; Balaram, V.; Ribeiro, A. R. L.; Lu, Z.; Stock, F.; Carmona, E.; Teixeira, M. R.; Picos-Corrales, L. A.; et al. *Environ. Chem. Lett.* **2022**, 20, 2311-2338.

(56) Qasemi, M.; Darvishian, M.; Nadimi, H.; Gholamzadeh, M.; Afsharnia, M.; Farhang, M.; Allahdadi, M.; Darvishian, M.; Zarei, A. *J. Food Compos. Anal.* **2023**, 115, 104870-104879.

(57) Selatile, M.; Sinha Ray, S.; Ojijo, V.; Sadiku, R. *RSC Adv.* **2018**, 8, 37915-37938.

(58) Sarode, S.; Upadhyay, P.; Khosa, M. A.; Mak, T.; Shakir, A.; Song, S.; Ullah, A. *Int. J. Biol. Macromol.* **2019**, 121, 1086-1100.

(59) Saleh, T. A.; Mustaqeem, M.; Khaled, M. *Environ. Nanotechnol. Monit. Manag.* **2022**, 17, 100617-100630.

(60) Crini, G.; Lichtfouse, E. *Environ. Chem. Lett.* **2019**, 17, 145-155.

(61) Peng, H.; Guo, J. *Environ. Chem. Lett.* **2020**, 18, 2055-2068.

(62) Devkota, S.; Ban, S.; Shrestha, R. *J. Environ. Chem. Eng.* **2021**, 105688, 2213-3437.

(63) Wan Nafi, A.; Taseidifar, M. *J. Environ. Manage.* **2022**, 319, 115666-115685.

(64) Chang, L.; Cao, Y.; Fan, G.; Li, C.; Peng, W. *RSC Adv.* **2019**, 9, 20226-20239.

(65) Taseidifar, M.; Makavipour, F.; Pashley, R. M.; Rahman, A. F. M. M. *Environ. Technol. Innov.* **2017**, 8, 182-190.

(66) Kwong, C. W.; Chao, C. Y. H.; Hui, K. S.; Wan, M. P. *Atmos. Environ.* **2008**, 42, 2300-2311.

(67) Wang, J.; Chen, H. *Sci. Total Environ.* **2020**, 704, 135249-135265.

(68) Narayanan, C. M.; Narayan, V. *Sustain. Environ. Res.* **2019**, 29, 33-49.

(69) Aziz, A.; Basheer, F.; Sengar, A.; Irfanullah; Khan, S. U.; Farooqi, I. H. *Sci. Total Environ.* **2019**, 686, 681-708.

(70) Feng, C.; Sugiura, N.; Shimada, S.; Maekawa, T. *J. Hazard. Mater.* **2003**, 103, 65-78.

(71) Ghaffarian Khorram, A.; Fallah, N.; Nasernejad, B.; Afsham, N.; Esmaelzadeh, M.; Vatanpour, V. *Chemosphere* **2023**, 338, 139565-139581.

(72) Fu, R.; Zhang, P.-S.; Jiang, Y.-X.; Sun, L.; Sun, X.-H. *Chemosphere* **2023**, 311, 136993-137003.

(73) Dai, C.; Chen, D.; Wu, J.; Liu, J.; Shi, S.; Zhang, J.; Feng, Y. *Chem. Eng. J.* **2022**, 447, 137505-137517.

(74) Rashid, R.; Shafiq, I.; Akhter, P.; Iqbal, M. J.; Hussain, M. *Environ. Sci. Pollut. Res. Int.* **2021**, 28, 9050-9066.

(75) Caravaca, M.; Vicente-Martínez, Y.; Soto-Meca, A.; Angulo-González, E. *Environ. Res.* **2022**, 211, 113091-113098.

(76) Chai, W. S.; Cheun, J. Y.; Kumar, P. S.; Mubashir, M.; Majeed, Z.; Banat, F.; Ho, S.-H.; Show, P. L. *J. Clean. Prod.* **2021**, 296, 126589-126604.

(77) Al-Ghouti, M. A.; Da'ana, D. A. *J. Hazard. Mater.* **2020**, 393, 122383-122404.

(78) Mozaffari Majd, M.; Kordzadeh-Kermani, V.; Ghalandari, V.; Askari, A.; Sillanpää, M. *Sci. Total Environ.* **2022**, 812, 151334-151361.

(79) Kim, K.-J.; Ahn, H.-G. *Microporous Mesoporous Mater.* **2012**, 152, 78-83.

(80) Sidheswaran, M. A.; Destaillats, H.; Sullivan, D. P.; Cohn, S.; Fisk, W. J. *Build. Environ.* **2012**, 47, 357-367.

(81) Boyjoo, Y.; Sun, H.; Liu, J.; Pareek, V. K.; Wang, S. *Chem. Eng. J.* **2017**, 310, 537-559.

(82) Binas, V.; Venieri, D.; Kotzias, D.; Kiriakidis, G. *Journal of Materiomics* **2017**, 3, 3-16.

(83) Al-Mamun, M. R.; Kader, S.; Islam, M. S.; Khan, M. Z. H. *J. Environ. Chem. Eng.* **2019**, 7, 103248-103264.

(84) Destaillats, H.; Sleiman, M.; Sullivan, D. P.; Jacquiod, C.; Sablayrolles, J.; Molins, L. *Appl. Catal. B* **2012**, 128, 159-170. Siegel, J. A. *Indoor Air* **2016**, 26, 88-96.

(85) Al-Qodah, Z.; Tawalbeh, M.; Al-Shannag, M.; Al-Anber, Z.; Bani-Melhem, K. *Sci. Total Environ.* **2020**, 744, 140806-140819.

(86) Luengas, A.; Barona, A.; Hort, C.; Gallastegui, G.; Platel, V.; Elias, A. *Rev. Environ. Sci. Biotechnol.* **2015**, 14, 499-522.

(87) Sadegh, H.; Ali, G. A. M.; Gupta, V. K.; Makhlouf, A. S. H.; Shahryari-ghoshekandi, R.; Nadagouda, M. N.; Sillanpää, M.; Megiel, E. *J. Nanostructure Chem.* **2017**, 7, 1-14.

(88) Chang, T.; Lu, J.; Shen, Z.; Huang, Y.; Lu, D.; Wang, X.; Cao, J.; Morent, R. *Appl. Catal. B* . **2019**, 244, 107-119.

(89) Guo, H.; Wang, Y.; Yao, X.; Zhang, Y.; Li, Z.; Pan, S.; Han, J.; Xu, L.; Qiao, W.; Li, J.; et al. *Chem. Eng. J.* **2021**, 425, 130614-130630.

(90) Wen, D.; Li, G.; Xing, R.; Park, S.; Rittmann, B. E. *Appl. Microbiol. Biotechnol.* **2012**, 95, 263-272.

(91) Dong, S.; Dong, S.; Tian, X.; Xu, Z.; Ma, D.; Cui, B.; Ren, N.; Rittmann, B. E. *J. Hazard. Mater.* **2016**, 302, 386-394.

(92) Li, G.; Park, S.; Rittmann, B. E. *Biotechnol. Bioeng.* **2012**, 109, 884-893.

(93) Xu, X.; Zhai, Z.; Li, H.; Wang, Q.; Han, X.; Yu, H. *Chem. Eng. J.* **2017**, 323, 520-529.

(94) Naddeo, V.; Secondes, M. F. N.; Borea, L.; Hasan, S. W.; Ballesteros, F.; Belgiorno, V. *Ultrason. Sonochem.* **2020**, 68, 105237-105246.

(95) de Wilt, A.; van Gijn, K.; Verhoek, T.; Vergnes, A.; Hoek, M.; Rijnaarts, H.; Langenhoff, A. *Water Res.* **2018**, 138, 97-105.

(96) Al Hawli, B.; Benamor, A.; Hawari, A. A. *Chem. Eng. Process.* **2019**, 143, 107621-107628.

(97) Zhu, J. R. *Int. J. Electrochem. Sci.* **2021**, 16, 210318-210330.

(98) Al-Rubaiey, N. A.; Albrazanjy, M. G.; Kadhim, W. A. *Egypt. J. Chem.* **2022**, 65, 55-64.

(99) Cao, Y.; Hu, Y.; Sun, J.; Hou, B. *Bioelectrochemistry* **2010**, 79, 71-76.

(100) Wang, A.-J.; Cheng, H.-Y.; Liang, B.; Ren, N.-Q.; Cui, D.; Lin, N.; Kim, B. H.; Rabaey, K. *Environ. Sci. Technol.* **2011**, 45, 10186-10193.

(101) Wang, Q.; Huang, L.; Quan, X.; Li Puma, G. *Appl. Catal. B: Environ.* **2019**, 245, 672-680.

(102) Fazal, T.; Razzaq, A.; Javed, F.; Hafeez, A.; Rashid, N.; Amjad, U. S.; Ur Rehman, M. S.; Faisal, A.; Rehman, F. *J. Hazard. Mater.* **2020**, 390, 121623-121636.

(103) Chkirida, S.; Zari, N.; Achour, R.; Hassoune, H.; Lachehab, A.; Qaiss, A. e. k.; Bouhfid, R. *J. Photochem. Photobiol. A.* **2021**, 412, 113215-113225.

(104) Nadeem, Q. U. A.; Nadeem, Z.; Gill, R.; Shchukin, D. G. *Environ. Sci. Pollut. Res.* **2022**, 29, 46737-46750.

(105) Firouzi, F.; Ebrahimian Pirbazari, A.; Esmaeili Khalil Saraei, F.; Tabatabai-Yazdi, F.-S.; Esmaeili, A.; Khodaee, Z. *J. Environ. Chem. Eng.* **2021**, 9, 106795-106810.

(106) Yu, Y.; Chen, D.; Xu, W.; Fang, J.; Sun, J.; Liu, Z.; Chen, Y.; Liang, Y.; Fang, Z. *J. Hazard. Mater.* **2021**, 416, 126183-126197.

(107) Mohamed, S. K.; Hegazy, S. H.; Abdelwahab, N. A.; Ramadan, A. M. *Int. J. Biol. Macromol.* **2018**, 108, 1185-1198.

(108) Kanakaraju, D.; bin Ya, M. H.; Lim, Y.-C.; Pace, A. *Surf. Interfaces.* **2020**, 19, 100534-100541.

(109) DeCoste, J. B.; Peterson, G. W. *Chem. Rev.* **2014**, 114, 5695-5727.

(110) Mahfoudhi, N.; Boufi, S. *Cellulose* **2017**, 24, 1171-1197.

(111) Sadegh, H.; Shahryari-ghoshekandi, R.; Agarwal, S.; Tyagi, I.; Asif, M.; Gupta, V. *J. Mol. Liq.* **2015**, 206, 151-158.

(112) Jiang, Z. M.; Fang, H. S.; Jin, Z. L.; Wang, M. Y. *Fuller. Nanotub. Carbon Nanostructures* **2015**, 23, 890-898.

(113) A.; Sahraie, R.; Daneshfar, A. *Spectrosc Lett* . **2012**, 45, 500-510.

(114) Zou, W.; Gu, B.; Sun, S.; Wang, S.; Li, X.; Zhao, H.; Yang, P. *Mater. Res. Express.* **2019**, 6, 105624-105633.

(115) Apul, O. G.; Wang, Q.; Zhou, Y.; Karanfil, T. *Water Res.* **2013**, 47, 1648-1654.

(116) Du, Q.; Sun, J.; Li, Y.; Yang, X.; Wang, X.; Wang, Z.; Xia, L. *Chem. Eng. J.* **2014**, 245, 99-106.

(117) Chatterjee, S.; Lee, M. W.; Woo, S. H. *Bioresour. Technol.* **2010**, 101, 1800-1806.

(118) Bina, B.; Amin, D. M.; Rashidi, A.; Pourzamani, H. *Arch. Environ. Prot.* **2012**, 38, 2478-2500.

(119) Dai, R.; Guo, H.; Tang, C. Y.; Chen, M.; Li, J.; Wang, Z. *Environ. Sci. Technol.* **2019**, 53, 13776-13783.

(120) Yu, S.; Pang, H.; Huang, S.; Tang, H.; Wang, S.; Qiu, M.; Chen, Z.; Yang, H.; Song, G.; Fu, D.; et al. *Sci. Total Environ.* **2021**, 800, 149662-149683.

(121) Zhang, X.; Zhao, Y.; Mu, S.; Jiang, C.; Song, M.; Fang, Q.; Xue, M.; Qiu, S.; Chen, B. *ACS Appl. Mater. Interfaces.* **2018**, 10, 17301-17308.

(122) Long, Y.; You, X.; Chen, Y.; Hong, H.; Liao, B.-Q.; Lin, H. *Sci. Total Environ.* **2020**, 703, 135540-135548.

(123) Ma, J.; Wang, R.; Wang, X.; Zhang, H.; Zhu, B.; Lian, L.; Lou, D. *J. Environ. Chem. Eng.* **2019**, 7, 103049-103055.

(124) Huang, J.; Kankanamge, N. R.; Chow, C.; Welsh, D. T.; Li, T.; Teasdale, P. R. *J. Environ. Sci.* **2018**, 63, 174-197.

(125) Peng, B.; Yao, Z.; Wang, X.; Crombeen, M.; Sweeney, D. G.; Tam, K. C. *GEE* **2020**, 5, 37-49.

(126) Souzandeh, H.; Wang, Y.; Zhong, W.-H. *RSC Adv.* **2016**, 6, 105948-105956.

(127) Kadam, V. V.; Wang, L.; Padhye, R. *J. Ind. Text.* **2016**, 47, 2253-2280. Zhang, Y.; Yuan, S.; Feng, X.; Li, H.; Zhou, J.; Wang, B. *J. Am. Chem. Soc.* **2016**, 138, 5785-5788.

(128) Albadarin, A. B.; Collins, M. N.; Naushad, M.; Shirazian, S.; Walker, G.; Mangwandi, C. *Chem. Eng. J.* **2017**, 307, 264-272.

(129) Seera, S. D. K.; Kundu, D.; Gami, P.; Naik, P. K.; Banerjee, T. *Carbohydr. Polym.* **2021**, 256, 117520-117531.

(130) Eltaweil, A. S.; Elgarhy, G. S.; El-Subruiti, G. M.; Omer, A. M. *Int. J. Biol. Macromol.* **2020**, 154, 307-318.

(131) Hosseini, H.; Zirakjou, A.; McClements, D. J.; Goodarzi, V.; Chen, W.-H. *J. Hazard. Mater.* **2022**, 421, 126752-126767.

(132) Eliza, M. Y.; Shahruddin, M.; Noormaziah, J.; Rosli, W. D. W. Carboxymethyl Cellulose (CMC) from Oil Palm Empty Fruit Bunch (OPEFB) in the new solvent Dimethyl Sulfoxide (DMSO)/Tetrabutylammonium Fluoride (TBAF). 2015; Vol. 622, pp 012026-012036.

(133) Metodiev, A. *Electric Properties of Carboxymethyl Cellulose*. In *Cellulose - Fundamental Aspects*, **2013**; pp 197-226.

(134) Wüstenberg, T. *Sodium Carboxymethylcellulose*. In *Cellulose and Cellulose Derivatives in the Food Industry: Fundamentals and Applications*, 01 ed.; Wüstenberg, T. Ed.; Wiley-VCH Verlag GmbH & Co. KGaA, **2015**; pp 387-477.

(135) Pushpamalar, V.; Langford, S. J.; Ahmad, M.; Lim, Y. Y. *Carbohydr. Polym.* **2006**, 64, 312-318.

(136) Haleem, N.; Arshad, M.; Shahid, M.; Tahir, M. A. *Carbohydr. Polym.* **2014**, 113, 249-255.

(137) Adinugraha, M. P.; Marseno, D. W.; Haryadi. *Carbohydr. Polym.* **2005**, 62, 164-169.

(138) Heydarzadeh, H. D., Najafpour, G. D., & Nazari-Moghaddam, A. A. *World Appl. Sci. J.* **2009**, 06, 564-569. Rodsamran, P.; Sothornvit, R. *Journal of Food Processing and Preservation* **2018**, 42, 13762-13770.

(139) Lopez, C. G.; Rogers, S. E.; Colby, R. H.; Graham, P.; Cabral, J. T. *J. Polym. Sci. B Polym. Phys.* **2015**, 53, 492-501.

(140) BeMiller, J. N. *Cellulose and Cellulose-Based Hydrocolloids*. In *Carbohydrate Chemistry for Food Scientists*, **2019**; pp 223-240.

(141) Kanikireddy, V.; Varaprasad, K.; Jayaramudu, T.; Karthikeyan, C.; Sadiku, R. *Int. J. Biol. Macromol.* **2020**, 164, 963-975.

(142) Wang, J.; Somasundaran, P. *J. Colloid. Interface. Sci.* **2005**, 291, 75-83.

(143) Ali, M.; Khan, N. R.; Basit, H. M.; Mahmood, S. *J. Polym. Res.* **2019**, 27, 20-30.

(144) Verma, N.; Pramanik, K.; Singh, A. K.; Biswas, A. *Mater. Technol.* **2022**, 37, 706-716.

(145) Bhatti, H. N.; Safa, Y.; Yakout, S. M.; Shair, O. H.; Iqbal, M.; Nazir, A. *Int. J. Biol. Macromol.* **2020**, 150, 861-870.

(146) Yadollahi, M.; Gholamali, I.; Namazi, H.; Aghazadeh, M. *Int. J. Biol. Macromol.* **2015**, 74, 136-141.

(147) Rahman, M. S.; Hasan, M.; Nitai, A.; Nam, S.; Karmakar, A.; Ahsan, M.; Shiddiky, M. *Polymers* **2021**, 13, 1345-1392.

(148) McClements, D. J. *Food emulsions: principles, practices, and techniques*; CRC Press, **2015**.

(149) Costa, E. M.; Pereira, C. F.; Ribeiro, A. A.; Casanova, F.; Freixo, R.; Pintado, M.; Ramos, O. L. *Appl. Sci.* **2022**, 12, 6560-6575.

(150) Kamel, S. *EXPRESS Polym. Lett.* **2008**, 2, 758-778.

(151) Zhang, Y.; Liu, Y.; Wang, X.; Sun, Z.; Ma, J.; Wu, T.; Xing, F.; Gao, J. *Carbohydr. Polym.* **2014**, 101, 392-400.

(152) Liu, T.; Wu, W.; Liao, K.-N.; Sun, Q.; Gong, X.; Roy, V. A. L.; Yu, Z.-Z.; Li, R. K. Y. *Carbohydr. Polym.* **2019**, 214, 213-220.

(153) Yu, H.; Hong, H.-J.; Kim, S. M.; Ko, H. C.; Jeong, H. S. *Carbohydr. Polym.* **2020**, 240, 116348-116354.

(154) Koushesh Saba, M.; Amini, R. *Food Chem.* **2017**, 232, 721-726.

(155) Miyashiro, D.; Hamano, R.; Umemura, K. *Nanomaterials* **2020**, 10, 186-209.

(156) Long, L.; Li, F.; Shu, M.; Zhang, C.; Weng, Y. *Materials (Basel)* **2019**, 12, 1867-1875.

(157) Lin, Q.; Gao, M.; Chang, J.; Ma, H. *J. Appl. Polym. Sci.* **2017**, 134, 44363-44373.

(158) Han, Y.; Wang, L. *J. Sci. Food Agric.* **2017**, 97, 1295-1301.

(159) Kamal, T.; Ahmad, I.; Khan, S. B.; Ul-Islam, M.; Asiri, A. M. *J. Polym. Environ.* **2019**, 27, 2867-2877.

(160) Abdulkhani, A.; Daliri Sousefi, M.; Ashori, A.; Ebrahimi, G. *Polym. Test.* **2016**, 52, 218-224.

(161) Jin, H.-X.; Xu, H. P.; Wang, N.; Yang, L.-Y.; Wang, Y.-G.; Yu, D.; Ouyang, X.-K. *Materials* **2019**, 12, 942-957.

(162) Basu, P.; Narendrakumar, U.; Arunachalam, R.; Devi, S.; Manjubala, I. *ACS Omega* **2018**, 3, 12622-12632.

(163) Benhalima, T.; Ferfera-Harrar, H. *Int. J. Biol. Macromol.* **2019**, 132, 126-141.

(164) Sathiyanarayanan, S., Karunakaran, R. J., Gomathi, T., & Sudha, P. N. *IJNTPS* **2015**, 5, 36-41.

(165) Association, O. a. C. C. *Titanium Dioxide Pigments*. In *Surface Coatings: Vol I-Raw Materials and Their Usage*, Springer Netherlands, **1983**; pp 305-312.

(166) Maurya, P.; Mukherjee, M. D.; Ranjan, K. R. *Chapter 3 - Role of nanobiotechnology in maintaining a hygienic environment for the livestock*. In *Nanobiotechnology for the Livestock Industry*, Pratap Singh, R., Adetunji, C. O., Singh, R. L., Singh, J., Solanki, P. R., Singh, K. R. B. Eds.; Elsevier, **2023**; pp 61-81.

(167) Reghunath, S.; Pinheiro, D.; Kr, S. D. *APSADV* **2021**, 3, 100063-100097.

(168) Navidpour, A. H.; Abbasi, S.; Li, D.; Mojiri, A.; Zhou, J. L. *Catalysts* **2023**, 13, 232-260.

(169) S. Muniandy, S.; Mohd Kaus, N. H.; Jiang, Z.-T.; Altarawneh, M.; Lee, H. L. *RSC Adv.* **2017**, 7, 48083-48094.

(170) Benčina, M.; Iglič, A.; Mozetič, M.; Junkar, I. *Nanomaterials* **2020**, 10, 1121-1143.

(171) Bickley, R. I., Arreno, T.G., Lees, J.S., Palmisanol,L., & Tilleyd, R.J.D. *J. Solid State Chem.* **1991**, 92, 178-190.

(172) Ma, Y.; Wang, X.; Jia, Y.; Chen, X.; Han, H.; Li, C. *Chem. Rev.* **2014**, 114, 9987-10043.

(173) Jiang, X.; Manawan, M.; Feng, T.; Qian, R.; Zhao, T.; Zhou, G.; Kong, F.; Wang, Q.; Dai, S.; Pan, J. H. *Catal. Today* **2018**, 300, 12-17.

(174) Valencia, S.; Marín, J.; Restrepo, G. *Open Mater. Sci.* **2010**, 4, 9-14.

(175) Bickley, R. I.; Gonzalez-Carreno, T.; Lees, J. S.; Palmisano, L.; Tilley, R. J. D. *J. Solid State Chem.* **1991**, 92, 178-190.

(176) Tan, Z.; Sato, K.; Ohara, S. *Adv. Powder Technol.* **2015**, 26, 296-302.

(177) Jayawardena, S.; Kubono, A.; Rajapakse, R. M. G.; Shimomura, M. *Nano-Structures* **2021**, 28, 100780-100793.

(178) Liang, Y.; Sun, S.; Deng, T.; Ding, H.; Chen, W.; Chen, Y. *Materials* **2018**, 11, 450-461.

(179) Ullattil, S. G.; Periyat, P. *Sol-Gel Synthesis of Titanium Dioxide*. In *Sol-Gel Materials for Energy, Environment and Electronic Applications*, Pillai, S. C., Hehir, S. Eds.; Springer International Publishing, **2017**; pp 271-283.

(180) Qamar, O. A.; Jamil, F.; Hussain, M.; Bae, S.; Inayat, A.; Shah, N. S.; Waris, A.; Akhter, P.; Kwon, E. E.; Park, Y.-K. *Chem. Eng. J.* **2023**, 460, 141734-141754.

(181) Jitan, S.; Garlisi, C. *Catalysts* **2020**, 10, 227-256.

(182) Yang, Z.; Wang, B.; Cui, H.; An, H.; Pan, Y.; Zhai, J. *J. Phys. Chem. C* **2015**, 119, 16905-16912.

(183) Ding, K.; Miao, Z.; Liu, Z.; Zhang, Z.; Han, B.; An, G.; Miao, S.; Xie, Y. *J. Am. Chem. Soc.* **2007**, 129, 6362-6363.

(184) Miditana, S. R.; Tirukkovalluri, S. R.; Imandi, M. R.; A, B. B.; A, R. B. *J. Water Environ. Nanotechnol.* **2022**, 7, 218-229.

(185) Imoisili, P. E.; Jen, T.-C.; Safaei, B. *Nanotechnol. Rev.* **2021**, 10, 126-136.

(186) Rashid, H.; Yu, K.; Muhammad Naveed, U.; Anjum, M.; Khan, K.; Ahmad, N.; Jan, M. *Rev. Adv. Mater. Sci.* **2015**, 40, 235-248.

(187) Yu, J.; Lei, J.; Wang, L.; Zhang, J.; Liu, Y. *J. Alloys Compd.* **2018**, 769, 740-757.

(188) Gedanken, A. *Ultrason. Sonochem.* **2004**, 11, 47-55.

(189) Kaviyarasan, K.; Vinoth, V.; Sivasankar, T.; Asiri, A. M.; Wu, J. J.; Anandan, S. *Ultrason. Sonochem.* **2019**, 51, 223-229.

(190) Kong, Y.; Shen, X.; Cui, S.; Fan, M. *Green Chem.* **2015**, 17, 3436-3445.

(191) Yang, Y.; Jiang, L.; Tang, Q.; Li, M.; Xu, P.; Chen, D.; He, J.; Chen, Y.; Wang, J. *Water Air Soil Pollut.* **2022**, 233, 61-74.

(192) Alsamet, M. A. M. M.; Burgaz, E. *Electrochim. Acta* **2021**, 367, 137530. Ding, X.-K.; Liu, J.; Zhang, L.-L.; Yang, X.-L. *Ionics* **2019**, 25, 2057-2067.

(193) Qian, X.; Han, H.; Chen, Y.; Yuan, Y. *J. Sol-Gel Sci. Technol.* **2018**, 85, 394-401.

(194) Hu, H.; Sun, L.; Gao, Y.; Wang, T.; Huang, Y.; Lv, C.; Zhang, Y.-F.; Huang, Q.; Chen, X.; Wu, H. *J. Hazard. Mater.* **2020**, 387, 121670-121680.

(195) Natarajan, T. S.; Natarajan, K.; Bajaj, H. C.; Tayade, R. J. *J. Nanoparticle Res.* **2013**, 15, 1669-1686.

(196) Zhang, B.; Mei, M.; Li, K.; Liu, J.; Wang, T.; Chen, S.; Li, J. *J. Clean. Prod.* **2022**, 381, 135210-135220.

(197) Diebold, U. *Surf. Sci. Rep.* **2003**, 48, 53-229.

(198) Markov, S.; Vidakovic, A. *Acta Period. Technol.* **2014**, 141-152.

(199) Kang, X.; Liu, S.; Dai, Z.; He, Y.; Song, X.; Tan, Z. *Catalysts* **2019**, 9, 191-223.

(200) Liu, G.; Yang, H.; Pan, J.; Yang, Y.; Lu, M.; Cheng, H.-M. *Chem. Rev.* **2014**, 114, 9559–9612.

(201) Guo, Q.; Ma, Z.; Zhou, C.; Ren, Z.; Yang, X. *Chem. Rev.* **2019**, 119, 11020-11041.

(202) Lettieri, S.; Pavone, M.; Fioravanti, A.; Santamaria Amato, L.; Maddalena, P. *Materials* **2021**, 14, 1645-1701.

(203) Kordouli, E.; Bourikas, K.; Lycourghiotis, A.; Kordulis, C. *Catal. Today* **2015**, 252, 128-135.

(204) Amano, F.; Nakata, M.; Yamamoto, A.; Tanaka, T. *Catal. Sci. Technol.* **2016**, 6, 5693-5699.

(205) Binas, V.; Venieri, D.; Kotzias, D.; Kiriakidis, G. *J. Materiomics* **2017**, 3, 3-16.

(206) Sun, B.; Vorontsov, A. V.; Smirniotis, P. G. *Langmuir* **2003**, 19, 3151-3156.

(207) Franch, M. I.; Peral, J.; Domènech, X.; Ayllón, J. A. *ChemComm* **2005**, 1851-1853.

(208) Basera, P.; Saini, S.; Arora, E.; Singh, A.; Kumar, M.; Bhattacharya, S. *Sci. Rep.* **2019**, 9, 11427.

(209) Tang, X.; Xue, Q.; Qi, X.; Cheng, C.; Yang, M.; Yang, T.; Chen, F.; Qiu, F.; Quan, X. *Vacuum* **2022**, 200, 110972-110983.

(210) Parida, K. M.; Sahu, N. *J. Mol. Catal. A Chem.* **2008**, 287, 151-158.

(211) Vanlalhmingmawia, C.; Lalhriatpuia, C.; Tiwari, D.; Kim, D.-J. *Environ. Sci. Pollut. Res. Int.* **2022**, 29, 51732-51743.

(212) Patil, S. B.; Basavarajappa, P. S.; Ganganagappa, N.; Jyothi, M. S.; Raghu, A. V.; Reddy, K. R. *Int. J. Hydrog. Energy.* **2019**, 44, 13022-13039.

(213) Greiner, M.; Lu, Z.-H. *NPG Asia Mater.* **2013**, 5, 55-71.

(214) Asahi, R.; Taga, Y.; Mannstadt, W.; Freeman, A. J. *Phys. Rev. B* **2000**, 61, 854-858.

(215) Prakash, J.; Samriti; Kumar, A.; Dai, H.; Janegitz, B. C.; Krishnan, V.; Swart, H. C.; Sun, S. *Mater. Today Sustain.* **2021**, 13, 100066-100105.

(216) Sun, M.; Liu, H.; Sun, Z.; Li, W. *J. Environ. Chem. Eng.* **2020**, 8, 104168-104225.

(217) Wen, J.; Li, X.; Liu, W.; Fang, Y.; Xie, J.; Xu, Y. *Chinese J. Catal.* **2015**, 36, 2049-2070.

(218) Kumar, S.; Kumar, A.; Kumar, A.; Krishnan, V. *Catal. Rev.* **2019**, 62, 1-60.

(219) Sharma, P. K.; Cortes, M. A. L. R. M.; Hamilton, J. W. J.; Han, Y.; Byrne, J. A.; Nolan, M. *Catal. Today* **2019**, 321-322, 9-17.

(220) Paul, K. K.; Jana, S.; Giri, P. K. *Part. Part. Syst. Charact.* **2018**, 35, 1800198-1800213.

(221) Shabir, M.; Shezad, N.; Shafiq, I.; Maafa, I. M.; Akhter, P.; Azam, K.; Ahmed, A.; Lee, S. H.; Park, Y.-K.; Hussain, M. *J. Ind. Eng. Chem.* **2022**, 105, 539-548.

(222) Sathasivam, S.; Bhachu, D. S.; Lu, Y.; Chadwick, N.; Althabaiti, S. A.; Alyoubi, A. O.; Basahel, S. N.; Carmalt, C. J.; Parkin, I. P. *Sci. Rep.* **2015**, 5, 10952-10961.

(223) He, S.; Meng, Y.; Cao, Y.; Huang, S.; Yang, J.; Tong, S.; Wu, M. *Nanomaterials* **2018**, 8, 983-995.

(224) Tahir, M.; Amin, N. S. *Appl. Catal. B: Environ.* **2015**, 162, 98-109.

(225) Rajaramanan, T.; Shanmugaratnam, S.; Gurunanthanan, V.; Yohi, S.; Velauthapillai, D.; Ravirajan, P.; Senthilnanthanan, M. *Catalysts* **2021**, 11, 690-702.

(226) Khan, M.; Mutee Ur Rehman, H. M.; Tehreem, R.; Saqib, M.; Rehman, M. M.; Kim, W.-Y. *Nanomaterials* **2022**, 12, 2289-2300.

(227) Razali, M.; Noor, A.; Yusoff, M. *Sci. Adv. Mater.* **2017**, 9, 1032-1041.

(228) Mancuso, A.; Sacco, O.; Vaiano, V.; Sannino, D.; Pragliola, S.; Venditto, V.; Morante, N. *Catal. Today* **2021**, 380, 93-104.

(229) Mekprasart, W.; Pavasupree, S.; Jayasankar, C. K.; Ravuri, B. R.; Wattanawikkam, C.; Pecharapa, W. *Crystals* **2021**, 11, 1254-1264.

(230) Chen, D.; Jiang, Z.; Geng, J.; Wang, Q.; Yang, D. *Ind. Eng. Chem. Res.* **2007**, 46, 2741-2746.

(231) Giannakas, A.; Antonopoulou, M.; Daikopoulos, C.; Deligiannakis, Y.; Konstantinou, I. *Appl. Catal. B: Environ.* **2016**, 184, 44-54.

(232) Peiris, S.; de Silva, H. B.; Ranasinghe, K. N.; Bandara, S. V.; Perera, I. R. *JCCS* **2021**, 68, 738-769.

(233) Li, W.; Ding, H.; Ji, H.; Dai, W.; Guo, J.; Du, G. *Nanomaterials* **2018**, 8, 415-426.

(234) Wang, Y.; Lu, N.; Luo, M.; Fan, L.; Zhao, K.; Qu, J.; Guan, J.; Yuan, X. *Appl. Surf. Sci.* **2019**, 463, 234-243.

(235) Lv, Y.-R.; Liu, C.-J.; He, R.-K.; Li, X.; Xu, Y.-H. *Mater. Res. Bull.* **2019**, 117, 35-40.

(236) Kapilashrami, M.; Zhang, Y.; Liu, Y.-S.; Hagfeldt, A.; Guo, J. *Chem. Rev.* **2014**, 114, 9662-9707.

(237) Warnan, J.; Willkomm, J.; Farré, Y.; Pellegrin, Y.; Boujtita, M.; Odobel, F.; Reisner, E. *Chem. Sci.* **2019**, 10, 2758-2766.

(238) Cho, Y.; Choi, W.; Lee, C.-H.; Hyeon, T.; Lee, H.-I. *Environ. Sci. Technol.* **2001**, 35, 966-970.

(239) Patterson, K.; Howlett, K.; Patterson, K.; Wang, B.; Jiang, L. *WER* **2020**, 92, 1152-1161.

(240) Humayun, M.; Khan, A.; Luo, W. *Green Chem. Lett. Rev.* **2018**, 2, 86-102.

(241) Balakrishnan, A.; Gopalram, K.; Appunni, S. *Environ. Sci. Pollut. Res.* **2021**, 28, 33331-33343.

(242) Anaya-Esparza, L. M.; Ruvalcaba-Gomez, J. M.; Maytorena-Verdugo, C. I.; Gonzalez-Silva, N.; Romero-Toledo, R.; Aguilera-Aguirre, S.; Perez-Larios, A.; Montalvo-Gonzalez, A. E. *Materials (Basel)* **2020**, 13, 811-837.

(243) Goudarzi, V.; Shahabi-Ghahfarrokhi, I. *Int. J. Biol. Macromol.* **2018**, 106, 661-669.

(244) Yu, Q.; Wu, P.; Xu, P.; Li, L.; Liu, T.; Zhao, L. *Green Chem.* **2008**, 10, 1061-1067.

(245) Goudarzi, V.; Shahabi-Ghahfarrokhi, I.; Babaei-Ghazvini, A. *Int. J. Biol. Macromol.* **2017**, 95, 306-313.

(246) Zhao, K.; Feng, L.; Li, Z.; Fu, Y.; Zhang, X.; Wei, J.; Wei, S. *RSC Adv.* **2014**, 4, 51321-51329.

(247) Zhang, J.; Li, L.; Li, Y.; Yang, C. *Chem. Eng. J.* **2017**, 313, 1132-1141. Malmir, S.; Karbalaei, A.; Pourmadadi, M.; Hamedi, J.; Yazdian, F.; Navaee, M. *Carbohydr. Polym.* **2020**, 234, 115835-115844.

(248) Afzal, S.; Daoud, W. A.; Langford, S. J. *ACS Appl. Mater. Interfaces* **2013**, 5, 4753-4759.

(249) Chauhan, I.; Mohanty, P. *Cellulose* **2014**, 22, 507-519. Chen, X.; Kuo, D.-H.; Lu, D. *Chem. Eng. J.* **2016**, 295, 192-200. Afzal, S.; Daoud, W.; Langford, S. *J. Mater. Chem.* **2012**, 22, 4083-4088.

(250) Atitar, M. F.; Belhadj, H.; Dillert, R.; Bahnem, D. W. *The Relevance of ATR-FTIR Spectroscopy in Semiconductor Photocatalysis*. In *Emerging Pollutants in the Environment - Current and Further Implications*, **2015**; pp 201-227. Qu, Q.; Geng, H.; Peng, R.; Cui, Q.; Gu, X.; Li, F.; Wang, M. *Langmuir* **2010**, 26, 9539-9546. Hoogendam, C. W.; de Keizer, A.; Stuart, M.; Bijsterbosch, B.; Batelaan, J.; van Der Horst, P. *Langmuir* **1998**, 14, 3825-3839.

(251) Wang, S.; Zhou, Y.; Han, S.; Wang, N.; Yin, W.; Yin, X.; Gao, B.; Wang, X.; Wang, J. *Chemosphere* **2018**, 197, 20-25.

(252) Farshchi, E.; Pirsa, S.; Roufegarinejad, L.; Alizadeh, M.; Rezazad, M. *Carbohydr. Polym.* **2019**, 216, 189-196.

(253) Abdel-Galil, A.; Ali, H. E.; Atta, A.; Balboul, M. R. *J. Radiat. Res. Appl. Sci.* **2019**, 7, 36-43.

(254) Joo, S.; Al-Abed, S.; Luxton, T. *Environ. Sci. Technol.* **2009**, 43, 4954-4959. Han, S.; Wang, T.; Li, B. *J. Appl. Polym. Sci.* **2017**, 134, 44925-44934.

(255) Tanzifi, M.; Tavakkoli Yaraki, M.; Karami, M.; Karimi, S.; Dehghani Kiadehi, A.; Karimipour, K.; Wang, S. *J. Colloid. Interface. Sci.* **2018**, 519, 154-173.

(256) Li, X.; Lv, J.; Li, D.; Wang, L. *Carbohydr. Polym.* **2017**, 169, 398-405.

(257) Ahmadi, R.; Tanomand, A.; Kazeminava, F.; Kamounah, F. S.; Ayaseh, A.; Ganbarov, K.; Yousefi, M.; Katourani, A.; Yousefi, B.; Kafil, H. S. *Int. J. Nanomedicine* **2019**, 14, 3439-3454.

(258) Chang, C.; Wang, Q.; Xue, Q.; Liu, F.; Hou, L.; Pu, S. *Microchem. J.* **2022**, 173, 107037.

(259) Fathi Achachlouei, B.; Zahedi, Y. *Carbohydr. Polym.* **2018**, 199, 415-425.

(260) Ezati, P.; Riahi, Z.; Rhim, J.-W. *Food Hydrocoll.* **2022**, 122, 107104-107114.

(261) Khafaga, M. R.; Ali, H. E.; El-Naggar, A. W. M. *J. Text. Inst.* **2016**, 107, 766-773.

(262) Yemmireddy, V. K.; Hung, Y.-C. *Compr. Rev. Food Sci. Food Saf.* **2017**, 16, 617-631.

(263) Raghunath, A.; Perumal, E. *Int. J. Antimicrob. Agents* **2017**, 49, 137-152.

(264) Frei, A.; Verderosa, A. D.; Elliott, A. G.; Zuegg, J.; Blaskovich, M. A. T. *Nat. Rev. Chem.* **2023**, 7, 202-224.

(265) Banerjee, S.; Gopal, J.; Muraleedharan, P.; Tyagi, A. K.; Raj, B. *Curr. Sci.* **2006**, 90, 1378-1383.

(266) Huang, Y. Y.; Choi, H.; Kushida, Y.; Bhayana, B.; Wang, Y.; Hamblin, M. R. *Antimicrob. Agents Chemother.* **2016**, 60, 5445-5453.

(267) Khezerlou, A.; Alizadeh-Sani, M.; Azizi-Lalabadi, M.; Ehsani, A. *Microb. Pathog.* **2018**, 123, 505-526.

(268) Khaiboullina, S.; Uppal, T.; Dhabarde, N.; Subramanian, V. R.; Verma, S. C. *Viruses* **2021**, 13, 19-33.

(269) Xing, Y.; Li, X.; Zhang, L.; Xu, Q.; Che, Z.; Li, W.; Bai, Y.; Li, K. *Prog. Org. Coat.* **2012**, 73, 219-224.

(270) Wanag, A.; Rokicka, P.; Kusiak-Nejman, E.; Kapica-Kozar, J.; Wrobel, R. J.; Markowska-Szczupak, A.; Morawski, A. W. *Ecotoxicol. Environ. Saf.* **2018**, 147, 788-793.

(271) Faure, M.; Gerardin, F.; André, J.-C.; Pons, M.-N.; Zahraa, O. *J. Photochem. Photobiol. A: Chem.* **2011**, 222, 323-329. Wang, J.; Zhuang, H.; Hinton, A.; Bowker, B.; Zhang, J. *LWT - Food Science and Technology* **2014**, 59, 1009-1017. Yemmireddy, V. K.; Hung, Y.-C. *LWT - Food Science and Technology* **2015**, 61, 1-6.

(272) Chen, D.; Cheng, Y.; Zhou, N.; Chen, P.; Wang, Y.; Li, K.; Huo, S.; Cheng, P.; Peng, P.; Zhang, R.; et al. *J. Clean. Prod.* **2020**, 268, 121725-121738.

(273) Gürses, A.; Açıkyıldız, M.; Güneş, K.; Gürses, M. S. *Dyes and Pigments: Their Structure and Properties*. In *Dyes and Pigments*, Gürses, A., Açıkyıldız, M., Güneş, K., Gürses, M. S. Eds.; Springer International Publishing, **2016**; pp 13-29.

(274) Benkhaya, S.; M' rabet, S.; El Harfi, A. *Inorg. Chem. Commun.* **2020**, 115, 107891-107925.

(275) Su, C. X.-H.; Low, L. W.; Teng, T. T.; Wong, Y. S. *J. Environ. Chem. Eng.* **2016**, 4, 3618-3631.

(276) Li, Q.; Yue, Q.-Y.; Sun, H.-J.; Su, Y.; Gao, B.-Y. *J. Environ. Manage.* **2010**, 91, 1601-1611.

(277) Randorn, C.; Wongnawa, S.; Boonsin, P. *ScienceAsia* **2004**, 30, 149-156.

(278) Thomas, M.; Naikoo, G. A.; Sheikh, M. U. D.; Bano, M.; Khan, F. *J. Photochem. Photobiol. A: Chem.* **2016**, 327, 33-43.

(279) Jiang, Y.; Sun, Y.; Liu, H.; Zhu, F.; Yin, H. *Dyes Pigm.* **2008**, 78, 77-83.

(280) Akpan, U. G.; Hameed, B. H. *J. Hazard. Mater.* **2009**, 170, 520-529.

(281) Norouzi, A.; Nezamzadeh-Ejhieh, A.; Fazaeli, R. *Mater. Sci. Semicond. Process.* **2021**, 122, 105495-105506.

(282) Ajmal, A.; Majeed, I.; Malik, R.; Idriss, H.; Nadeem, M. *RSC Adv.* **2014**, 4, 37003-37026.

(283) Wahid, F.; Zhao, X.-Q.; Cui, J.-X.; Wang, Y.-Y.; Wang, F.-P.; Jia, S.-R.; Zhong, C. *J. Colloid. Interface. Sci.* **2022**, 620, 1-13.

(284) Yaseen, D. A.; Scholz, M. *Int. J. Environ. Sci. Technol.* **2019**, 16, 1193-1226.

(285) Myslak, Z. W.; Bolt, H. M.; Brockmann, W. *Am. J. Ind. Med.* **1991**, 19, 705-713.

(286) Parvin, F.; Islam, S.; Urmy, Z.; Ahmed, S.; Islam, A. *A Study on the Solutions of Environment Pollutions and Worker's Health Problems Caused by Textile Manufacturing Operations*; **2020**.

(287) Dong, H.; Zeng, G.; Tang, L.; Fan, C.; Zhang, C.; He, X.; He, Y. *Water Res.* **2015**, 79, 128-146.

(288) Saber-Samandari, S.; Saber-Samandari, S.; Heydaripour, S.; Abdouss, M. *J. Environ. Manage.* **2016**, 166, 457-465.

(289) Sun, Q.; Xiang, B.; Mu, P.; Li, J. *Langmuir* **2022**, 38, 7067-7076.

(290) Mohammadzadeh Pakdel, P.; Peighambardoust, S. J.; Arsalani, N.; Aghdasinia, H. *Environ. Res.* **2022**, 212, 113201-113217.

(291) Wang, X.; Fan, X.; Xie, H.; Li, X.; Hao, C. *Cellulose* **2022**, 29, 483-501.

(292) Liu, H.; Tian, X.; Xiang, X.; Chen, S. *Int. J. Biol. Macromol.* **2022**, 202, 632-643.

(293) Godiya, C. B.; Cheng, X.; Li, D.; Chen, Z.; Lu, X. *J. Hazard. Mater.* **2019**, 364, 28-38.

(294) Tsai, W.-B.; Kao, J.-Y.; Wu, T.-M.; Cheng, W.-T. *J. Nanomater.* **2016**, 2016, 1-9.

(295) Sugimoto, T.; Zhou, X. *J. Colloid. Interface*

Sci. **2002**, 252, 347-353.

(296) BeMiller, J. N. *Polysaccharides*. In *Carbohydrate Chemistry for Food Scientists*, **2019**; pp 103-157.

(297) Leroux, G.; Neumann, M.; Meunier, C. F.; Fattaccioli, A.; Michiels, C.; Arnould, T.; Wang, L.; Su, B. L. *ACS Appl. Mater. Interfaces* **2018**, 10, 37865-37877.

(298) Ma, S.; Zhang, M.; Nie, J.; Tan, J.; Song, S.; Luo, Y. *Carbohydr. Polym.* **2019**, 208, 328-335.

(299) Kim, U.-J.; Kim, D.; You, J.; Choi, J. W.; Kimura, S.; Wada, M. *Cellulose* **2018**, 25, 2615-2628.

(300) Petzold, G.; Aguilera, J. M. *Innov. Food Sci. Emerg. Technol.* **2013**, 20, 253-258.

(301) Yoon, B.-H.; Choi, W.-Y.; Kim, H.-E.; Kim, J.-H.; Koh, Y.-H. *Scr. Mater.* **2008**, 58, 537-540.

(302) Gutiérrez, M. C.; Ferrer, M. L.; del Monte, F. *Chem. Mater.* **2008**, 20, 634-648.

(303) Buchtová, N.; Budtova, T. *Cellulose* **2016**, 23, 2585-2595.

(304) Maheswari, J. U.; Krishnan, C.; Kalyanaraman, S.; Selvarajan, P. *Phys. B: Condens. Matter* **2016**, 502, 32-38.

(305) Pasikhani, J. V.; Gilani, N.; Pirbazari, A. E. *Solid State Sci.* **2018**, 84, 57-74.

(306) Mahalingam, T.; Selvakumar, C.; Ranjith Kumar, E.; Venkatachalam, T. *Phys. Lett. A* **2017**, 381, 1815-1819.

(307) Wang, W.; Xu, D.; Cheng, B.; Yu, J.; Jiang, C. *J. Mater.Chem. A* **2017**, 5, 5020-5029.

(308) Muñoz, R.; Sánchez-Sánchez, C.; Merino, P.; López-Elvira, E.; Munuera, C.; Gant, P.; López, M. F.; Castellanos-Gómez, A.; Martín-Gago, J. A.; García-Hernández, M. *Appl. Surf. Sci.* **2020**, 504, 144439.

(309) Gibson, R. R.; Armes, S. P.; Musa, O. M.; Fernyhough, A. *Polym. Chem.* **2019**, 10, 1312-1323.

(310) Othman, S. H.; Abdul Rashid, S.; Mohd Ghazi, T. I.; Abdullah, N. *Journal of Nanomaterials* **2012**, 2012, 1-10. Hierrezuelo, J.; Sadeghpour, A.; Szilagyi, I.; Vaccaro, A.; Borkovec, M. *Langmuir* **2010**, 26, 15109-15111.

(311) Clogston, J. D.; Patri, A. K. *Zeta Potential Measurement*. In *Characterization of Nanoparticles Intended for Drug Delivery*, McNeil, S. E. Ed.; Humana Press, **2011**; pp 63-70.

(312) Li, G.; Lv, L.; Fan, H.; Ma, J.; Li, Y.; Wan, Y.; Zhao, X. S. *J. Colloid. Interface. Sci.* **2010**, 348, 342-347.

(313) Zhang, X.; Zhang, W.; Yi, M.; Wang, Y.; Wang, P.; Xu, J.; Niu, F.; Lin, F. *Sci. Rep.* **2018**, 8, 4757-4763.

(314) Nemoto, J.; Saito, T.; Isogai, A. *ACS Appl. Mater. Interfaces* **2015**, 7, 19809-19815.

(315) Jeasmin, A.; Md. Abu, H.; Md. Akherul, I.; Kamal, S.; Jae, H. *Sci. Rep.* **2021**, 11, 9490-9501.

(316) Yan, H.; Zhang, W.; Kan, X.; Dong, L.; Jiang, Z.; Li, H.; Yang, H.; Cheng, R. *Colloids Surf. A Physicochem. Eng. Asp.* **2011**, 380, 143-151.

(317) Li, Y.; Yin, X.; Huang, X.; Tian, J.; Wu, W.; Liu, X. *Appl. Surf. Sci.* **2019**, 495, 143626.

(318) Yu, M.; Li, J.; Wang, L. *Chem. Eng. J.* **2017**, 310, 300-306.

(319) Radjai, M.; Ferkous, H.; Jebali, Z.; Majdoub, H.; Bourzami, R.; Raffin, G.; Achour, M.; Gil, A.; Boutahala, M. *J. Mol. Liq.* **2022**, 361, 119670-119685.

(320) Hwang, K.-J.; Shim, W.-G.; Kim, Y.; Kim, G.; Choi, C.; Kang, S. O.; Cho, D. W. *Phys. Chem. Chem. Phys.* **2015**, 17, 21974-21981.

(321) Fierro, V.; Torné-Fernández, V.; Montané, D.; Celzard, A. *Microporous Mesoporous Mater.* **2008**, 111, 276-284.

(322) Qiu, H.; Lv, L.; Pan, B.-c.; Zhang, Q.-j.; Zhang, W.-m.; Zhang, Q.-x. *J. Zhejiang Univ. Sci.* **2009**, 10, 716-724.

(323) Boparai, H. K.; Joseph, M.; O'Carroll, D. M. *J. Hazard. Mater.* **2011**, 186, 458-465.

(324) Shi, H.; Li, W.; Zhong, L.; Xu, C. *Ind. Eng. Chem. Res.* **2014**, 53, 1108-1118.

(325) Zhao, M.; Zhang, S.; Fang, G.; Huang, C.; Wu, T. *Polymers (Basel)* 12, 2219-2233.

(326) Chen, Y.; Long, Y.; Li, Q.; Chen, X.; Xu, X. *Int. J. Biol. Macromol.* **2019**, 126, 107-117.

(327) Ghazali, A.; Shirani, M.; Semnani, A.; Zare-Shahabadi, V.; Nekoeinia, M. *J. Environ. Chem. Eng.* **2018**, 6, 3942-3950.

(328) Tran, T. H.; Le, A. H.; Pham, T. H.; Nguyen, D. T.; Chang, S. W.; Chung, W. J.; Nguyen, D. D. *Sci. Total Environ.* **2020**, 725, 138325-138334.

(329) Madaeni, S. S.; Salehi, E. *Chem. Eng. J.* **2009**, 150, 114-121.

(330) Khalfaoui, M.; Baouab, M. H. V.; Gauthier, R.; Lamine, A. B. *Adsorpt. Sci. Technol.* **2002**, 20, 33-47.

(331) Awungacha Lekelefac, C.; Czermak, P.; Herrenbauer, M. *Int. J. Photoenergy* **2013**, 2013, 1-9.

(332) Begum, H.; Bin Mahbub, M. K. *Dhaka Univ. J. Sci.* **2013**, 61, 193-198.

(333) Petit, M.; Michez, L.; Raimundo, J.-M.; Malinowski, T.; Dumas, P. *Eur. J. Phys.* **2016**, 37, 065808-065820.

(334) Zawadzki, P.; Kudlek, E.; Dudziak, M. *J. Ecol. Eng.* **2018**, 19, 260-268.

(335) Suhaimi, N.; Kooh, M. R. R.; Lim, C. M.; Chou Chao, C.-T.; Chou Chau, Y.-F.; Mahadi, A. H.; Chiang, H.-P.; Haji Hassan, N. H.; Thotagamuge, R. *Adsorpt. Sci. Technol.* **2022**, 2022, 8245797-8245808.

(336) Zhang, S.; Cai, M.; Wu, J.; Wang, Z.; Lu, X.; Li, K.; Lee, J.-M.; Min, Y. *Catal. Commun.* **2023**, 174, 106594-106602.

(337) Loo, W. W.; Pang, Y. L.; Lim, S.; Wong, K. H.; Lai, C. W.; Abdullah, A. Z. *Chemosphere* **2021**, 272, 129588-129597.

(338) Abdellah, M. H.; Nosier, S. A.; El-Shazly, A. H.; Mubarak, A. A. *Alex. Eng. J.* **2018**, 57, 3727-3735.

(339) Patil, K.; Pawar, R.; Talap, P. *Phys. Chem. Chem. Phys.* **2000**, 2, 4313-4317.

(340) Xu, C.; Rangaiah, G. P.; Zhao, X. S. *Ind. Eng. Chem. Res.* **2014**, 53, 14641-14649.

(341) Rajagopal, S.; Paramasivam, B.; Muniyasamy, K. *Sep. Purif. Technol.* **2020**, 252, 117444-117454.

(342) Zeng, M. *Bull. Korean Chem. Soc.* **2013**, 34, 953-956.

(343) Halder, S.; Yadav, K. K.; Sarkar, R.; Mukherjee, S.; Saha, P.; Haldar, S.; Karmakar, S.; Sen, T. *SpringerPlus* **2015**, 4, 672-685.

(344) Mukherjee, D.; Barghi, S.; Ray, A. K. *Processes* **2014**, 2, 12-23.

(345) Chiang, C.-J.; Lee, Y.-H.; Lee, Y.-P.; Lin, G.-T.; Yang, M.-H.; Wang, L.; Hsieh, C.-C.; Dai, C.-A. *J. Mater. Chem. A* **2016**, 4, 908-919.

(346) Dalod, A.; Henriksen, L.; Grande, T.; Einarsrud, M.-A. *Beilstein J. Nanotechnol.* **2017**, 8, 304-312.

(347) Behzadnia, A.; Montazer, M.; Rashidi, A.; Rad, M. M. *Ultrason. Sonochem.* **2014**, 21, 1815-1826.

(348) Dong, P.; Cheng, X.; Huang, Z.; Chen, Y.; Zhang, Y.; Nie, X.; Zhang, X. *Mater. Res. Bull.* **2018**, 97, 89-95.

(349) Wang, D.; Zhou, Z.-H.; Yang, H.; Shen, K.-B.; Huang, Y.; Shen, S. *J. Mater.Chem.* **2012**, 22, 16306-16311.

(350) Mali, S. S.; Shinde, P. S.; Betty, C. A.; Bhosale, P. N.; Lee, W. J.; Patil, P. S. *Appl. Surf. Sci.* **2011**, 257, 9737-9746.

(351) Ding, J.; Huang, Z.; Zhu, J.; Kou, S.; Zhang, X.; Yang, H. *Sci. Rep.* **2015**, 5, 17773-17779.

(352) Leyva-Porras, C.; Toxqui-Teran, A.; Vega-Becerra, O.; Miki-Yoshida, M.; Rojas-Villalobos, M.; García-Guaderrama, M.; Aguilar-Martínez, J. A. *J. Alloys Compd.* **2015**, 647, 627-636.

(353) Fischer, K.; Grimm, M.; Meyers, J.; Dietrich, C.; Gläser, R.; Schulze, A. *J. Membr. Sci.* **2015**, 478, 49-57.

(354) Prathan, A.; Sanglao, J.; Wang, T.; Bhoomanee, C.; Ruankham, P.; Gardchareon, A.; Wongratanaphisan, D. *Sci. Rep.* **2020**, 10, 8065-8075.

(355) Yeşil Acar, Z.; Asiltürk, M.; Arpaç, E. *Chem. Pap.* **2022**, 76, 4927-4939.

(356) Ding, Y.; Jiang, Z.; Li, Y.; Tang, Y.; Li, J.; Dong, X.; Dan, H.; Yang, Y.; Duan, T. *J. Alloys Compd.* **2018**, 735, 2190-2196.

(357) Chauhan, I.; Mohanty, P. *RSC Adv.* **2014**, 4, 57885-57890.

(358) Li, J.; Yu, H.; Sun, Q.; Liu, Y.; Cui, Y.; Lu, Y. *Appl. Surf. Sci.* **2010**, 256, 5046-5050.

(359) Reid, D. L.; Draper, R.; Richardson, D.; Demko, A.; Allen, T.; Petersen, E. L.; Seal, S. *J. Mater.Chem. A* **2014**, 2, 2313-2322.

(360) Grilli, M. L.; Yilmaz, M.; Aydogan, S.; Cirak, B. B. *Ceram. Int.* **2018**, 44, 11582-11590.

(361) Yao, H.; Toan, S.; Huang, L.; Fan, M.; Wang, Y.; Russell, A. G.; Luo, G.; Fei, W. *Sci. Rep.* **2017**, 7, 2943-2950.

(362) Sallem, F.; Chassagnon, R.; Megriche, A.; El Maaoui, M.; Millot, N. *J. Alloys Compd.* **2017**, 722, 785-796.

(363) Jastrzębska, A.; Szuplewska, A.; Wojciechowska, A.; Chudy, M.; Olszyna, A.; Birowska, M.; Popielski, M.; Majewski, J.; Scheibe, B.; Natu, V.; et al. *2D Materials* **2020**, 7, 025018-025036.

(364) Gautam, A.; Kshirsagar, A.; Biswas, R.; Banerjee, S.; Khanna, P. K. *RSC Adv.* **2016**, 6, 2746-2759.

(365) Al-Ahmed, Z. A.; Hassan, A. A.; El-Khouly, S. M.; El-Shafey, S. E. *Polym. Bull.* **2020**, 77, 6213-6226.

(366) Akhavan Sadr, F.; Montazer, M. *Ultrason. Sonochem.* **2014**, 21, 681-691.

(367) Vijayan, B. K.; Dimitrijevic, N. M.; Wu, J.; Gray, K. A. *J. Phys. Chem. C* **2010**, 114, 21262-21269.

(368) Barakat, N. A. M.; Park, S. J.; Khil, M. S.; Kim, H. Y. *Mater. Sci. Eng. B.* **2009**, 162, 205-208.

(369) Tekin, D.; Birhan, D.; Kiziltas, H. *Mater. Chem. Phys.* **2020**, 251, 123067-123072.

(370) Karthick, S. N.; Prabakar, K.; Subramania, A.; Hong, J.-T.; Jang, J.-J.; Kim, H.-J. *Powder Technol.* **2011**, 205, 36-41.

(371) Nasiri, S.; Rabiei, M.; Palevicius, A.; Janusas, G.; Vilkauskas, A.; Nutalapati, V.; Monshi, A. *Nano Trends* **2023**, 3, 100015-100026.

(372) Ojeda, M.; Kumar, D. K.; Chen, B.; Xuan, J.; Maroto-Valer, M. M.; Leung, D. Y. C.; Wang, H. *ChemistrySelect* **2017**, 2, 702-706.

(373) Behnajady, M. A.; Eskandarloo, H.; Modirshahla, N.; Shokri, M. *Photochem. Photobiol.* **2011**, 87, 1002-1008.

(374) Nawawi, W.; Zaharudin, R.; Ishak, M.; Ismail, K.; Zuliahani, A. *Appl. Sci.* **2016**, 7.

(375) Zhang, J.; Xiao, X.; Nan, J. *J. Hazard. Mater.* **2010**, 176, 617-622.

(376) Qourzal, S.; Assabbane, A.; Ait-Ichou, Y. *J. Photochem. Photobiol. A: Chem.* **2004**, 163, 317-321.

(377) Hu, Q.; Marand, E. *Polymer* **1999**, 40, 4833-4843.

(378) Ali, H. A.; Hameed, N. J. *J. Mech. Behav. Mater.* **2022**, 31, 150-159.

(379) Rezaei, M.; Mirkazemi, S. M.; Alamolhoda, S. *J. Supercond. Nov. Magn.* **2021**, 34, 1397-1408.

(380) Yang, S.; Yang, B.; Wu, L.; Li, Y. H.; Liu, P.; Zhao, H.; Yu, Y.; Gong, X.; Yang, H. *Nat. Commun.* **2014**, 5, 5355-5361.

(381) Alizadeh-Sani, M.; Khezerlou, A.; Ehsani, A. *Ind. Crop. Prod.* **2018**, 124, 300-315.

(382) Praveen, P.; Viruthagiri, G.; Mugundan, S.; Shanmugam, N. *Spectrochim. Acta A Mol. Biomol.* **2013**, 117, 622-629.

(383) Yang, J.; Wang, H.; Liu, X.; Fu, S.; Song, P. *Compos. Sci. Technol.* **2021**, 212, 108884-108892.

(384) Xie, W.; Li, R.; Xu, Q. *Sci. Rep.* **2018**, 8, 8752-8761.

(385) Zhu, Y.; Li, H.; Gu, D.; Wang, H.; Bao, N. *J. Mater. Sci.* **2017**, 52, 6623-6634.

(386) Flores-Caballero, A. A.; Manzo-Robledo, A.; Alonso-Vante, N. *Surfaces* **2021**, 4, 54-65.

(387) Greczynski, G.; Hultman, L. *Prog. Mater. Sci.* **2020**, 107, 100591-100636.

(388) Wu, D.; Ma, J.; Bao, Y.; Cui, W.; Hu, T.; Yang, J.; Bai, Y. *Sci. Rep.* **2017**, 7, 43749-43758.

(389) Lakshmi, B.; Joe Thomas, B.; Gopinath, P. *Adv. Powder Technol.* **2021**, 32, 3706-3716.

(390) Han, K.; Wang, Y.; Wang, S.; Liu, Q.; Deng, Z.; Wang, F. *Chem. Eng. J.* **2021**, 421, 129989-129996.

(391) Landi, S.; Segundo, I. R.; Afonso, C.; Lima, O.; Costa, M. F. M.; Freitas, E.; Carneiro, J. *Phys. B: Condens. Matter* **2022**, 639, 414008-414011.

(392) Mishra, V.; Warshi, M. K.; Sati, A.; Kumar, A.; Mishra, V.; Kumar, R.; Sagdeo, P. R. *SN Appl. Sci.* **2019**, 1, 241-248.

(393) Liao, W.; Zhang, Y.; Zhang, M.; Murugananthan, M.; Yoshihara, S. *Chem. Eng. J.* **2013**, 231, 455-463.

(394) Murphy, A. B.; Barnes, P. R. F.; Randeniya, L. K.; Plumb, I. C.; Grey, I. E.; Horne, M. D.; Glasscock, J. A. *Int. J. Hydrog. Energy* **2006**, 31, 1999-2017.

(395) Colmenares, J. C.; Kuna, E.; Lisowski, P. *Top. Curr. Chem.* **2016**, 374, 59-70.

(396) Karthik, P.; Vinesh, V.; Mahammed Shaheer, A. R.; Neppolian, B. *Appl. Catal. A: Gen.* **2019**, 585, 117208-117216.

(397) Chai, Y. D.; Pang, Y. L.; Lim, S.; Chong, W. C.; Lai, C. W.; Abdullah, A. Z. *Polymers* **2021**, 13, 3530-3550.

(398) Piątkowska, A.; Janus, M.; Szymański, K.; Mozia, S. *Catalysts* **2021**, 11, 144-199.

(399) Wang, W.-K.; Zhu, W.; Mao, L.; Zhang, J.; Zhou, Z.; Zhao, G. *J. Colloid. Interface. Sci.* **2019**, 557, 227-235.

(400) Ummadisingu, A.; Meloni, S.; Mattoni, A.; Tress, W.; Grätzel, M. *Angew. Chem. Int. Ed.* **2021**, 60, 21368-21376.

(401) al, B. S. e. *J. Semicond.* **2014**, 35, 042001-042004.

(402) Rashid, M. M.; Shen, X.; Islam, S. R.; Al Mizan, R.; Hong, Y. *J. Water Process. Eng.* **2022**, 47, 102799-102812.

(403) Czabany, I.; Hribernik, S.; Bračič, M.; Kurečič, M.; Thomas, S.; Stana Kleinschek, K.; Mohan, T. *Nano-Struct. Nano-Objects.* **2020**, 24, 100564-100575.

(404) Munir, M.; Nazar, M. F.; Zafar, M. N.; Zubair, M.; Ashfaq, M.; Hosseini-Bandegharaei, A.; Khan, S. U.-D.; Ahmad, A. *ACS Omega* **2020**, 5, 16711-16721.

(405) Yu, K. L.; Lee, X. J.; Ong, H. C.; Chen, W.-H.; Chang, J.-S.; Lin, C.-S.; Show, P. L.; Ling, T. C. *Environ. Pollut.* **2021**, 272, 115986-115997.

(406) Sparks, D. L. *5 - Sorption Phenomena on Soils*. In *Environmental Soil Chemistry (Second Edition)*, Sparks, D. L. Ed.; Academic Press, **2003**; pp 133-186.

(407) Badvi, K.; Javanbakht, V. *J. Clean. Prod.* **2021**, 280, 124518-124530.

(408) Alkaykh, S.; Mbarek, A.; Ali-Shattle, E. E. *Heliyon* **2020**, 6, e03663-e03668.

(409) Nguyen, C. H.; Fu, C.-C.; Juang, R.-S. *J. Clean. Prod.* **2018**, 202, 413-427.

(410) Zhang, H.; Zong, R.; Zhao, J.; Zhu, Y. *Environ. Sci. Technol.* **2008**, 42, 3803-3807.

(411) Ataabadi, M. R.; Jamshidi, M. *Sci. Rep.* **2023**, 13, 7383-7396.

(412) Khan, I.; Saeed, K.; Zekker, I.; Zhang, B.; Hendi, A. H.; Ahmad, A.; Ahmad, S.; Zada, N.; Ahmad, H.; Shah, L. A.; et al. *Water* **2022**, 14, 242-271.

(413) Shahinyan, G. A.; Amirbekyan, A. Y.; Markarian, S. A. *Spectrochim. Acta A Mol. Biomol.* **2019**, 217, 170-175.

(414) Pahang, F.; Parvin, P.; Ghafoori-Fard, H.; Bavali, A.; Moafi, A. *OSA Contin.* **2020**, 3, 688-697.

(415) Rauf, M. A.; Meetani, M. A.; Khaleel, A.; Ahmed, A. *Chem. Eng. J.* **2010**, 157, 373-378.

(416) Ovchinnikov, O. V.; Evtukhova, A. V.; Kondratenko, T. S.; Smirnov, M. S.; Khokhlov, V. Y.; Erina, O. V. *Vib. Spectrosc.* **2016**, 86, 181-189.

(417) Klika, Z.; Čapková, P.; Horáková, P.; Valášková, M.; Malý, P.; Macháň, R.; Pospíšil, M. *J. Colloid. Interface. Sci.* **2007**, 311, 14-23.

(418) Fernández-Pérez, A.; Marbán, G. *ACS Omega* **2020**, 5, 29801-29815.

(419) Zhang, H.; Xu, L.; Gu, X.; Yu, D.; Li, S. *RSC Adv.* **2023**, 13, 239-250.

(420) Matveev, A. T.; Varlamova, L. A.; Konopatsky, A. S.; Leybo, D. V.; Volkov, I. N.; Sorokin, P. B.; Fang, X.; Shtansky, D. V. *Materials* **2022**, 15, 8169-8188.

(421) Lee, S.-L.; Ho, L.-N.; Ong, S.-A.; Lee, G.-M.; Wong, Y.-S.; Voon, C.-H.; Khalik, W. F.; Yusoff, N. A.; Nordin, N. *Water Air Soil Pollut.* **2016**, 227, 445-452.

(422) Galagan, Y.; Su, W.-F. *J. Photochem. Photobiol. A: Chem.* **2008**, 195, 378-383.

(423) Soltani, T.; Entezari, M. H. *J. Mol. Catal. A: Chem.* **2013**, 377, 197-203.

(424) Wen, D.; Li, W.; Lv, J.; Qiang, Z.; Li, M. *J. Hazard. Mater.* **2020**, 391, 121855-121862.

(425) Li, S.; Hao, X.; Dai, X.; Tao, T. *J. Nanomater.* **2018**, 2018, 8752015-8752027.

(426) Feng, X.; Li, X.; Su, B.; Ma, J. *Colloids Surf. A Physicochem. Eng. Asp.* **2022**, 648, 129114-129129.

(427) Gnaser, H.; Savina, M. R.; Calaway, W. F.; Tripa, C. E.; Veryovkin, I. V.; Pellin, M. J. *Int. J. Mass Spectrom.* **2005**, 245, 61-67.

(428) Ray, S. K.; Dhakal, D.; Kshetri, Y. K.; Lee, S. W. *J. Photochem. Photobiol. A: Chem.* **2017**, 348, 18-32.

(429) Awais, M.; Khursheed, S.; Tehreem, R.; Sirajuddin; Mok, Y. S.; Siddiqui, G. U. *Appl. Catal. A: Gen.* **2022**, 643, 118764-118773.

(430) Zhang, T.; Oyama, T. k.; Horikoshi, S.; Hidaka, H.; Zhao, J.; Serpone, N. *Sol. Energy Mater. Sol.* **2002**, 73, 287-303.

(431) Zhang, T.; Oyama, T.; Aoshima, A.; Hidaka, H.; Zhao, J.; Serpone, N. *J. Photochem. Photobiol. A.* **2001**, 140, 163-172.

(432) Cortés, J. A.; Alarcón-Herrera, M. T.; Villicaña-Méndez, M.; González-Hernández, J.; Pérez-Robles, J. F. *Environ. Prog. Sustain. Energy* **2011**, 30, 318-325.

(433) Chaker, H.; Chérif-Aouali, L.; Khaoulani, S.; Bengueddach, A.; Fourmentin, S. *J. Photochem. Photobiol. A.* **2016**, 318, 142-149.

(434) Nasirian, M.; Mehrvar, M. *J. Environ. Sci.* **2018**, 66, 81-93.

(435) Baiocchi, C.; Brussino, M. C.; Pramauro, E.; Prevot, A. B.; Palmisano, L.; Marcì, G. *Int. J. Mass Spectrom.* **2002**, 214, 247-256.

(436) Tang, J.; Wang, J. *RSC Adv.* **2017**, 7, 50829-50837.

(437) Zhang, X.; Ao, K.; Daoud, W. *Sci. Total Environ.* **2023**, 865, 161126-161136.

(438) Li, W.; Zhang, H.; Chen, P.; Yao, J.; Dong, X. *Fibers Polym.* **2023**, 24, 575-588.

(439) Naeem, A.; Saeed, T.; Sayed, M.; Ahmad, B.; Mahmood, T.; Farooq, M.; Perveen, F. *Process Saf. Environ. Prot.* **2023**, 176, 115-130.

(440) Kokilavani, S.; Alaraidh, I. A.; Okla, M. K.; Chandran, P.; Mohebaldin, A.; Soufan, W.; Al-ghamdi, A. A.; Abdel-Maksoud, M. A.; AbdElgawad, H.; Thomas, A. M.; et al. *J. Alloys Compd.* **2022**, 909, 164703-164712.

(441) Behboodi-Sadabad, F.; Zhang, H.; Trouillet, V.; Welle, A.; Plumeré, N.; Levkin, P. A. *Adv. Funct. Mater.* **2017**, 27, 1700127-1700138.

(442) Eskandarian, M. R.; Choi, H.; Fazli, M.; Rasoulifard, M. H. *Chem. Eng. J.* **2016**, 300, 414-422.

(443) Kobayashi, S.; Higashimura, H. *Prog. Polym. Sci.* **2003**, 28, 1015-1048.

(444) Wang, X.; Xu, H.; Luo, X.; Li, M.; Dai, M.; Chen, Q.; Song, H. *Colloids Interface Sci. Commun.* **2021**, 44, 100476-100487.

(445) Fónagy, O.; Szabó-Bárdos, E.; Horváth, O. *J. Photochem. Photobiol. A: Chem.* **2021**, 407, 113057-113070.

(446) Yuan, D.; Liu, S.; Zhao, C.; He, Z.; Wu, M.; Su, Y.; Pan, Z.; Yang, X.; Huang, L.; Liu, D. *J. Catal.* **2019**, 370, 470-479.

(447) Alapi, T.; Dombi, A. *J. Photochem. Photobiol. A: Chem.* **2007**, 188, 409-418.

(448) Kinoshita, M.; Kamizato, T.; Shimoyama, Y. *J. Supercrit. Fluids* **2018**, 138, 193-199.

(449) Wang, X.; Zhang, D.; Xiang, Q.; Zhong, Z.; Liao, Y. *Nanomicro Lett.* **2018**, 10, 77.

(450) Eremeeva, E. A.; Yakovlev, A. V.; Pidko, E. A.; Vinogradov, A. V. *J. Mater. Chem. C* **2017**, 5, 5487-5493.

(451) Wang, P.; Xie, T.; Peng, L.; Li, H.; Wu, T.; Pang, S.; Wang, D. *J. Phys. Chem. C* **2008**, 112, 6648-6652.

(452) Yu, J.; Dai, G.; Cheng, B. *J. Phys. Chem. C* **2010**, 114, 19378-19385.

(453) Liu, Y.; Chen, X.; Yao, R.; Liao, S.; Chen, W.; Nie, D.; Wang, Y.; Zheng, F. *Int. J. Appl. Ceram. Technol.* **2017**, 14, 474-485.

(454) Xu, S.; Sun, X.; Gao, Y.; Yue, M.; Yue, Q.; Gao, B. *J. Solid State Chem.* **2017**, 253, 167-175.

(455) Ben Smida, Y.; Marzouki, R.; Kaya, S.; Sultan, E.; Zid, M.; Hamzaoui, A. *Synthesis Methods in Solid-State Chemistry*. In *Synthesis-methods-and-crystallization*, IntechOpen, London, UK, **2020**; pp 5-21.

(456) Gupta, T.; Samriti; Cho, J.; Prakash, J. *Mater. Today Chem.* **2021**, 20, 100428-100467.

(457) Yamamoto, D.; Tachibana, S. *ACS Earth Space Chem.* **2018**, 2, 778-786.

(458) Wang, C.-C.; Ying, J. Y. *Chem. Mater.* **1999**, 11, 3113-3120.

(459) Kim, T.-H.; Lim, D.-Y.; Yu, B.-S.; Lee, J.-H.; Goto, M. *Ind. Eng. Chem. Res.* **2000**, 39, 4702-4706.

(460) Ali, N.; Suhaimi, N. *World Appl. Sci. J.* **2009**, 5.

(461) Kusworo, T. D.; Azizah, D. A.; Kumoro, A. C.; Kurniawan, T. A.; Dzarfan Othman, M. H. *Mater. Today Chem.* **2023**, 30, 101493-101516.

(462) Oginawati, K.; Suharyanto; Susetyo, S. H.; Sulung, G.; Muhayatun; Chazanah, N.; Dewi Kusumah, S. W.; Fahimah, N. *Heliyon* **2022**, 8, e08914-e08920.

(463) Zakaria, N.; Rohani, R.; Wan Mohtar, W. H.; Purwadi, R.; Sumampouw, G. A.; Indarto, A. *Water* **2023**, 15, 1339-1362.

(464) Yaacob, M. R.; Zain, N. F. M.; Zakaria, M. N.; Ismail, M. B. *J. econ. sustain. dev.* **2016**, 7, 36-43.

(465) Daud, N. M.; Abdullah, S. R. S.; Hasan, H. A.; Ismail, N. I.; Dhokhikah, Y. *Sci. Total Environ.* **2022**, 819, 152931-152947.

(466) Rashidi, H. R.; Sulaiman, N. M. N.; Hashim, N. A.; Hassan, C. R. C.; Ramli, M. R. *Desalin. Water Treat.* **2015**, 55, 86-95.

(467) Kaewrueng, P.; Siriwong, W.; Siripanich, S. *J. Health Res.* **2013**, 27, 217-223.

(468) Meylani, V.; Surahman, E.; Fudholi, A.; Almalki, W. H.; Ilyas, N.; Sayyed, R. Z. *J. Environ. Chem. Eng.* **2023**, 11, 109503-109510.

(469) Ranjithkumar, V.; Sangeetha, S.; Vairam, S. *J. Hazard. Mater.* **2014**, 273, 127-135.

(470) Lizama, C.; Freer, J.; Baeza, J.; Mansilla, H. D. *Catal. Today* **2002**, 76, 235-246.

(471) Burkinshaw, S. M.; Paraskevas, M. *Dyes Pigm.* **2010**, 87, 225-233.

(472) Santana, M. H. P.; Da Silva, L. M.; Freitas, A. C.; Boodts, J. F. C.; Fernandes, K. C.; De Faria, L. A. *J. Hazard. Mater.* **2009**, 164, 10-17.

(473) Eren, Z.; Acar, F. N. *Desalination* **2006**, 194, 1-10.

(474) Dong, X.; Ding, W.; Zhang, X.; Liang, X. *Dyes Pigm.* **2007**, 74, 470-476.

(475) Begum, S.; Mishra, S. R.; Ahmaruzzaman, M. *Environ. Sci. Pollut. Res.* **2022**, 29, 87347-87360.

(476) Zhang, L.; Gao, X.; Zhang, Z.; Zhang, M.; Cheng, Y.; Su, J. *Sci. Rep.* **2016**, 6, 31797-31810.